Linking cell-matrix adhesions and microtubules:
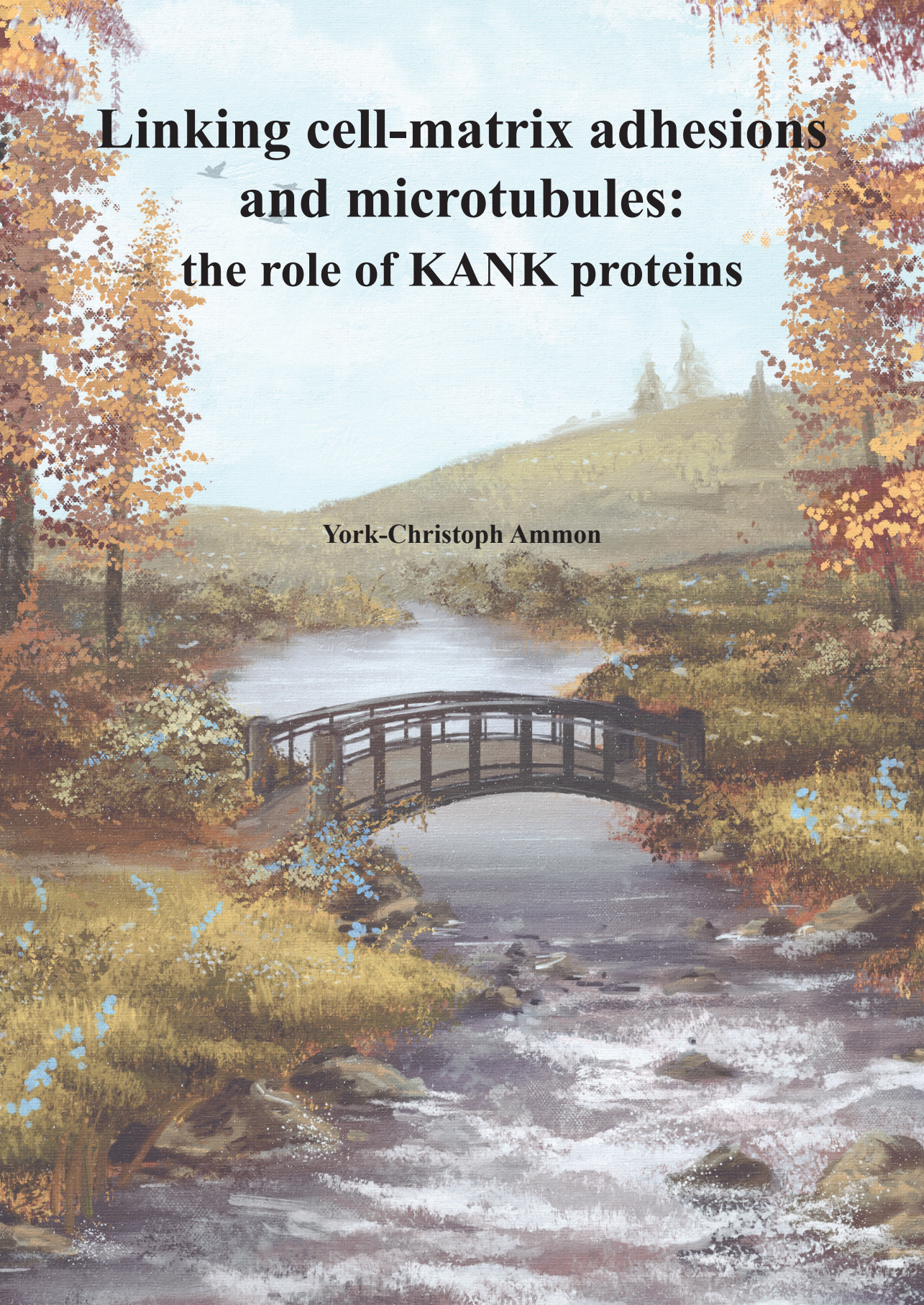## the role of KANK proteins

York-Christoph Ammon

Linking cell-matrix adhesions and microtubules:

the role of KANK proteins

York-Christoph Ammon

Linking cell-matrix adhesions and microtubules: the role of KANK proteins

**Koppeling van cel-matrix aanhechtingen en microtubuli:
de rol van KANK-eiwitten**

(met een samenvatting in het Nederlands)

Proefschrift

ter verkrijging van de graad van doctor aan de
Universiteit Utrecht
op gezag van de
rector magnificus, prof.dr. H.R.B.M. Kummeling,
ingevolge het besluit van het college voor promoties
in het openbaar te verdedigen op

maandag 14 december 2020 des ochtends te 11.00 uur

door

York-Christoph Ammon

geboren op 27 november 1988
te Braunschweig, Duitsland

Promotor: Prof. dr. A.S. Akhmanova

"Success is not final, failure is not fatal: it is the courage to continue that counts."

Sir Winston Churchill

Table of contents

1

General introduction

York-Christoph Ammon[1]

1 Cell Biology, Neurobiology and Biophysics, Department of Biology, Faculty of Science, Utrecht University, Utrecht, The Netherlands

General introduction

Development and homeostasis of multicellular life critically depend on highly versatile connections between the proteins of the extracellular matrix and the intracellular cytoskeleton. These connections, the cell-matrix adhesions, play an essential role in numerous biological processes such as the regulation of tissue integrity, cell migration, wound healing and immune responses. Alterations in these adhesion complexes are often involved in human diseases including cancer, developmental and neurological disorders (Byron et al., 2015; Winograd-Katz et al., 2014).

Focal adhesions

Structure and components of focal adhesions

Focal adhesion (FAs) are mature integrin-mediated cell attachment complexes. These adhesion complexes are macromolecular assemblies, which consist of more than 50 different proteins that form highly organized plaques at the plasma membrane (PM) which link the ECM to the actin cytoskeleton (Burridge and Chrzanowska-Wodnicka, 1996; Geiger and Yamada, 2011; Winograd-Katz et al., 2014; Wolfenson et al., 2009; Zaidel-Bar et al., 2007). FAs have a well-structured 3-dimensional organization with three distinct layers (Kanchanawong et al., 2010) (Figure 1): i) The layer most proximal to the PM is the so-called "integrin signaling layer". It contains proteins such as the heterodimeric α/β integrin receptors, which span through the PM and bind with their N-terminal part to extracellular proteins such as fibronectin or collagen whereas their cytosolic C-terminus binds to FA proteins such as talin (Barczyk et al., 2010; Hynes, 2002). Further, the integrin signaling layer contains also paxillin and focal adhesion kinase (FAK), which relay the integrin-ECM contact into the cell to signaling pathways that control adhesion dynamics or gene transcription (Brown and Turner, 2004; Mitra et al., 2005). ii) The intermediate layer, the so-called "force transduction layer" mainly consists of the two mechanosensitive adaptor proteins talin and vinculin (Kanchanawong et al., 2010). In this layer, talin directly links the integrin receptors to the actin cytoskeleton whereas vinculin binds alongside to stretched talin molecules thereby supporting the integrin-talin-actin connection. Consequently, this layer transmits force either from outside-to-inside or vice versa (Brown et al., 2006; del Rio et al., 2009; Hu et al., 2007; Wang, 2007). iii) The third layer, the "actin-regulatory layer" contains α-actinin, an actin-binding protein that can cross-link actin filaments thereby helping to assemble stress fibers (Otey and Carpen, 2004). Besides, this layer also contains zyxin, a zinc-binding phosphoprotein that together with vasodilator-stimulated phosphoprotein (VASP) helps strengthening the FAs by stimulating actin polymerization and stress-fiber enlargement (Yoshigi et al., 2005).

Assembly, maturation and disassembly of FAs

The formation/life cycle of FAs begins with the previously mentioned heterodimeric α/β integrin receptors (hereafter simply named integrins). Integrins can reversibly switch between low-affinity (inactive) and high-affinity (active) states (Hynes, 2002). This switch can be mediated from "the outside" by binding of extracellular ligands, such as
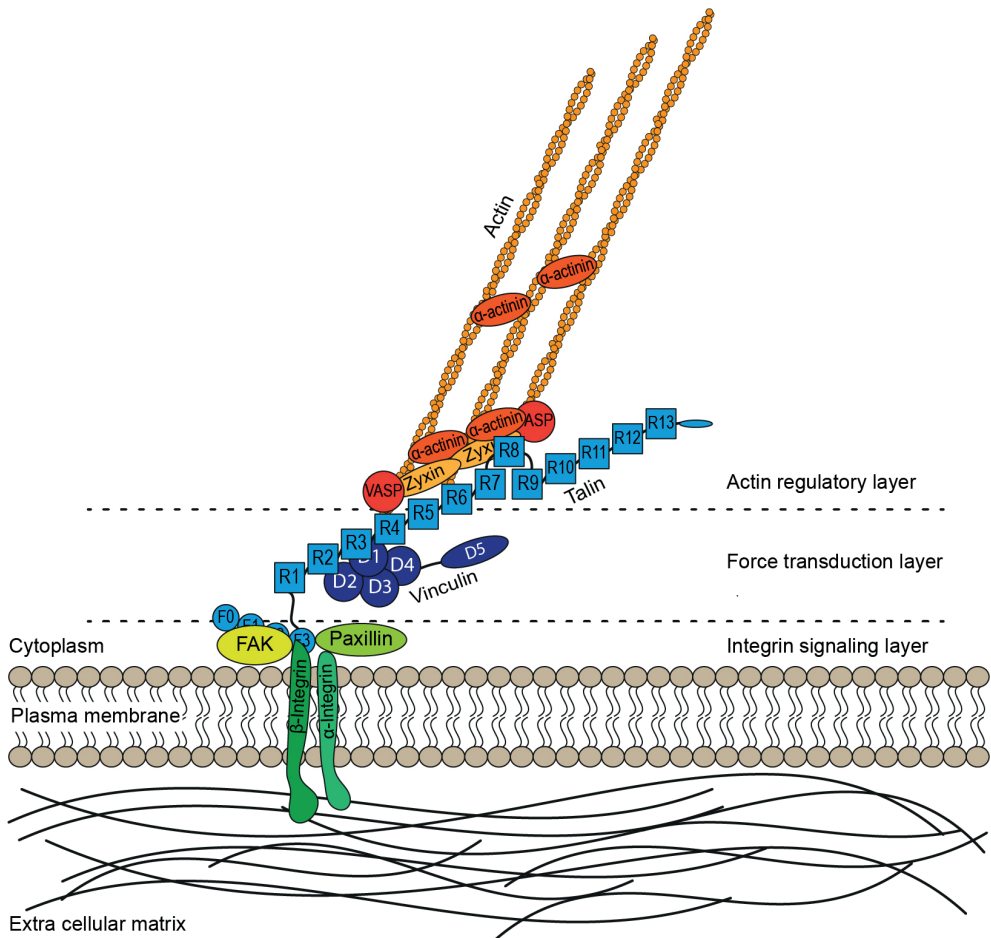
Figure 1. Schematic overview of a focal adhesion with its highly organized three-layered structure
The cytoplasmic tails of the integrins together with paxillin and focal adhesion kinase (FAK) form the integrin signaling layer. The two mechanosensitive adaptor proteins talin and vinculin form the force transduction layer. The actin regulatory layer consists of actin, α-actinin, zyxin and vasodilator-stimulated phosphoprotein (VASP).

fibronectin, to the integrin receptors ("outside – in" activation). The binding of ECM proteins leads to the activation of the cytosolic integrin domains thereby promoting the binding to adaptor proteins such as talin and kindlin, which is, like talin, a FERM domain-containing protein that functions as interaction hub and recruits other proteins to the adhesion complex (Calderwood et al., 2013; Sun et al., 2019). Yet, integrin activation can as well be triggered from "the inside" by binding of the cytosolic adaptor protein talin to the β-integrin tail ("inside – out" activation) which in turn stimulates binding of integrins to ECM components. Overall, integrin activation leads to binding of integrin receptors to ECM proteins and to cytosolic adaptor proteins which link integrins to the actin cytoskeleton consequently leading to the recruitment of further FA proteins (Calderwood et al., 2013; Li and Springer, 2017; Winograd-Katz et al., 2014). Activated integrins can cluster into small short-lived so-called nascent adhesions (NAs) and bind to

ECM components (Bachir et al., 2014). While most of these newly formed NAs quickly disintegrate, a small fraction remains, accumulates more integrins as well as additional adaptor proteins and consequently matures further into bigger so-called focal complexes (FXs) that ultimately develop into FAs, which are connected to stress fibers, contractile bundles of actin and myosin IIA (actomyosin) (Vicente-Manzanares et al., 2007; Wolfenson et al., 2009). Mature FAs, can either disassemble, for example by detaching from actomyosin, releasing the adaptor proteins and clathrin-mediated endocytosis of integrins (Ezratty et al., 2009); or, the FAs can mature further and become elongated fibrillar adhesions (FBs) by retrograde sliding into the cell center (Geiger and Yamada, 2011; Sun et al., 2016).

The role of the microtubules and Rho GTPases in the regulation of FA dynamics
For more than 20 years it has been known that microtubules (MTs) grow towards FAs and that this FA targeting is usually correlated with FA disassembly (Kaverina et al., 1999; Kaverina et al., 1998; Krylyshkina et al., 2003; Rid et al., 2005).
One way how MTs can affect FA dynamics is by modulation of Rho GTPase signaling. Rho GTPases are the major regulators of actin dynamics; yet, they also regulate a wide range of other cellular processes (Hall, 2012; Hodge and Ridley, 2016). Rho GTPases can be in a GTP-bound (active) or a GDP-bound (inactive) state. Guanine nucleotide exchange factors (GEFs), proteins which stimulate the exchange of GDP for GTP, activate Rho GTPases; whereas GTPase-activating proteins (GAPs) inactivate Rho GTPases by stimulating the hydrolysis of GTP to GDP. Moreover, Guanine nucleotide dissociation inhibitors (GDIs), bind to GDP-bound GTPases, thereby preventing the exchange of GDP for GTP as well as the activation of the GTPase; furthermore, GDIs also sequester the Rho GTPase in the cytoplasm and block their translocation to the PM (Hall, 2012; Hodge and Ridley, 2016). The active GTPase RhoA promotes the assembly of contractile actomyosin fibers (Ridley and Hall, 1992). RhoA does this via its two main effectors: mDia, Diaphanous-related formin 1, which stimulates actin polymerization (Watanabe et al., 1997), and Rho-associated kinase (ROCK), which phosphorylates and thereby inactivates myosin light chain phosphatase that in turn activates myosin II (Kimura et al., 1996; Watanabe et al., 1999). The active GTPase Rac1 on the other hand promotes the assembly of an actin meshwork at the cell periphery thereby stimulating the formation of membrane protrusions (Ridley et al., 1992). It does so by activating the actin-polymerizing complex Arp2/3 which promotes formation of a new actin filament from an already existing filament (actin filament branching) (Eden et al., 2002). For cell migration, for example, these processes are required to form membrane protrusions at the leading edge and to form NAs, whereas actomyosin contractility is needed at the cell body for formation of FAs and translocation of the cell (Raftopoulou and Hall, 2004).
It has been shown that drug-induced MT depolymerization (e.g. by nocodazole) leads to elevated RhoA activity, which results in increased cell contractility (via increased actomyosin activity) and FA assembly (Ren et al., 1999). On the other side, MT re-growth (polymerization) after nocodazole-induced MT depolymerization yields rapid FA disassembly (Ezratty et al., 2005). Later it was found that the depolymerization of MTs leads to the release of GEF-H1, a special GEF that is normally bound to MTs and is therefore inactive (Krendel et al., 2002; Ren et al., 1998), consequently GEF-H1 locally

activates RhoA (Chang et al., 2008).

Another way how MTs can influence FA dynamics is by serving as tracks for cargo transport either directed to FAs or away from them. For example, all the traffic between the different subcellular compartments involved in the recycling of endocytosed integrins occurs via MT-dependent transport regulated by Rab GTPases (Caswell et al., 2009; Horgan and McCaffrey, 2011). Direct cleavage of the integrin attachment to the ECM is another potent trigger for FA disassembly. The membrane-type 1 matrix metalloproteases (MT1-MMP) mediates ECM degradation in the vicinity of FAs (Takino et al., 2006; Wang and McNiven, 2012). It was shown by Stehbens et al. that MTs, that are anchored by CLASPs and LL5β containing plaques (the cortical microtubule stabilization complex, CMSC) at the cortex in the vicinity of FAs, function as tracks for transport of MT1-MMP to FAs where they are secreted to cut the ECM (Stehbens et al., 2014).

All in all, MTs play an essential role in regulating the interplay between the actin cytoskeleton and FAs at the cell cortex. Yet, despite the growing knowledge how MTs moderate the dynamics of FAs, there are still many unanswered questions.

Talin: the mechanosensitive FA adaptor protein

Talin was first described as part of adhesion complexes in 1983 (Burridge and Connell, 1983). Later, it was discovered that there are two paralogs: talin1 and talin2 which share 77% homology (Monkley et al., 2001). Of the two talins, which are expressed by two separate genes, talin1 is ubiquitously expressed whereas talin2 is mainly expressed in brain, heart muscle and kidney (Thul et al., 2017). Moreover, it was found that knockout of talin1 in mice is lethal due to perturbed gastrulation (Monkley et al., 2000); whereas
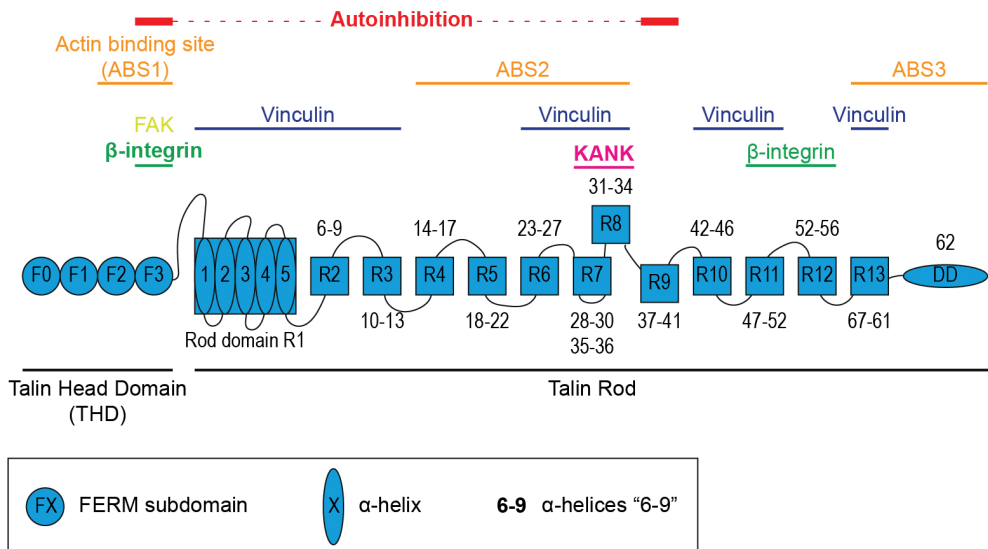
Figure 2. Schematic overview of the FA adaptor protein talin (representative for both talin paralogs)
Talin1 and talin2 both contain a talin head domain (THD). The THD comprises an atypical FERM domain (F0-F3). Via a flexible linker the THD is connected to the talin rod. The rod consists of 62 α-helices that group into 4/5-helix-bundles. Each bundle forms one of the 13 talin rod domains (R1 – 13). Some interaction partners of talins and the regions where they bind to talins are indicated in the upper panel.

talin2-knockout mice are viable (Debrand et al., 2012).

Structure of the talins

Talins are large proteins weighing around 270 kDa which are 2541 (talin1) and 2540 (talin2) amino acids long, sharing a highly conserved structure (Figure 2):

The N-terminal region of talins, the so-called talin head domain (THD) consists of an atypical FERM domain containing four subdomains (F0 - F3) (Elliott et al., 2010). The F2 subdomain can bind to phosphatidylinositol 4,5-bisphosphate (PIP2) and thereby help localizing talin to the PM (Saltel et al., 2009). Talins contain three actin binding sites (ABS1 – 3) (Hemmings et al., 1996), ABS1 is located in the THD (subdomains F2 - 3) and is considered to be involved in blocking actin polymerization (Ciobanasu et al., 2018; Lee et al., 2004). The F3 subdomain has multiple binding partners including focal adhesion kinase (FAK) (Lawson et al., 2012), and Rap1-GTP-interacting adaptor molecule (RIAM), which is important for lifting talin autoinhibition (Yang et al., 2014a). Yet, the most important binding partner of the F3 subdomain is the cytosolic part of β-integrins (Calderwood et al., 1999).

The THD is coupled to the so-called talin rod via an unstructured linker that can be cleaved by the calcium-dependent protease calpain. Calpain-mediated cleavage of talin1 is one way how FA disassembly can be initiated (Franco and Huttenlocher, 2005; Franco et al., 2004).

The talin rod consists of 62 α-helices which are organized into 4-/5-helix-bundles, each bundle forming one of the 13 rod (R1 – 13) domains (Gingras et al., 2008; Goult et al., 2013). The 62nd α-helix is the so-called dimerization domain (DD) which mediates homodimerization of two talin proteins, and so far there has been no report of talin heterodimers (Gingras et al., 2008). The talin rod domains bind to multiple proteins often in a mechanosensitive manner: Rod domains R11 - 12 can interact with integrins (integrin binding site (IBS) 2) which can be important for formation of NAs (Changede et al., 2015; Gingras et al., 2009). Moreover, two of the three actin binding sites (ABS2 and 3) are located in the talin rod: ABS2: rod domains R4 - R8 (Atherton et al., 2015; Hemmings et al., 1996); and ABS3: rod domain R13 and DD (Gingras et al., 2008). ABS3 is thought to mediate the first contact with the actin cytoskeleton (Gingras et al., 2008), which leads to initial force exposure and to unfolding of the mechanosensitive rod domain R3 that in turn allows vinculin binding to talin (Yao et al., 2014). On the other hand, ABS2 is thought to be the tension-bearing actin connection (Atherton et al., 2015; Kumar et al., 2016). Among the various binding partners of talins are also the Kidney ankyrin repeat-containing (KANK) family proteins. KANKs bind to the rod domain R7 of talin and thereby link the FA complex to the cortical microtubule stabilization complex that anchors and stabilizes MTs in close proximity to FAs (Bouchet et al., 2016; Sun et al., 2016). Furthermore, this interaction between KANK and talin R7 is force-regulated (Yu et al., 2019).

In the cytosol, talins acquire an autoinhibited conformation by binding of the THD subdomain F3 to rod domain R9 (Goksoy et al., 2008; Goult et al., 2009). This autoinhibition can be lifted, for example, by RIAM binding to the F3 subdomain (Yang et al., 2014a), thereby activating talin for its function in integrin-mediated adhesions.

Overall, talins are important adaptor proteins, which provide an anchor point for various

FA proteins, and they can respond to mechanical force in a highly flexible manner.

The Kidney ankyrin repeat domain containing protein (KANK) family

A protein family that has recently been closely associated with FA complexes, in particular with the adaptor protein talin, and with the cortical microtubule stabilizing complex (CMSC) is the Kidney ankyrin repeat domain-containing protein (KANK) family. Sarkar et al. were the first to describe this novel protein family when studying cases of renal cell carcinoma (Sarkar et al., 2002). Blast and domain searches as well as phylogenetic analyses revealed that the KANK protein family is highly conserved among animals. Whereas there is only a single KANK ortholog in *C. elegans*, VAB-19 (Ding et al., 2003; Ihara et al., 2011), and in *Drosophila*, dKANK (Clohisey et al., 2014), there are four vertebrate homologs (KANK1 – 4), likely due to two whole genome duplication events around the origin of the vertebrates (Hensley et al., 2016; Zhu et al., 2008). In humans, there exist two isoforms of KANK1 due to alternative splicing of exon1: KANK1-S (short) and KANK1-L (long; note that from here on the term "KANK1" will always refer to the KANK1-L isoform). KANK1-L possesses an additional 158 amino acids at its N-terminus compared to KANK1-S (Wang et al., 2005).

In humans, KANK1 is predominantly expressed in the heart, liver and kidney; KANK2 shows high levels of expression in the cervix, colon, heart, kidney and lung; KANK3 is mainly expressed in the breast, liver, lung, skeletal muscle and kidney; whereas KANK4 is predominantly expressed in the colon, kidney, liver, lung and skeletal muscle (Zhu et al., 2008).
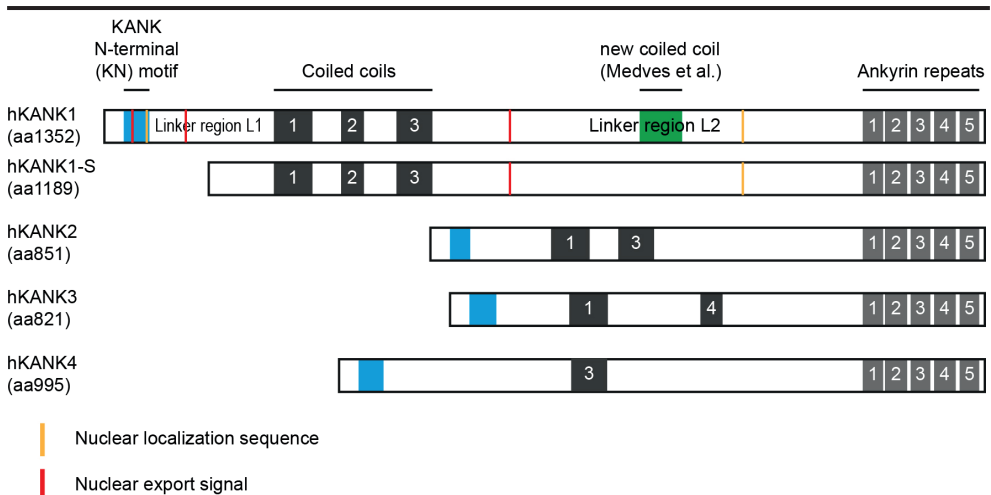
Figure 3. Schematic overview of the four human KANK homologs including the short isoform of KANK1 (KANK1-S)
All four human KANK homologs possess a similar structure with three distinct domains. At the N-terminus, there is the KANK N-terminal (KN) domain (blue), except for KANK1-S which is missing the first 158 amino acids of KANK1, including the KN domain. In the central region there are the coiled coil domains (black). There are four conserved CC domains (CC1 – 4) among the KANK family and their composition and number vary among the family members. At the C-terminus, there is the highly conserved ankyrin repeat domain, which consists of five ankyrin repeats (grey).

Structure of the KANK family proteins

Characteristic for the KANK family proteins is their structure with three distinct domains (Figure 3). At the N-terminus, all KANK proteins possess a highly conserved so-called KANK N-terminal (KN) domain, an α-helix with a leucine-aspartic acid (LD) motif, which mediates binding of KANK1 and 2 to talin (Bouchet et al., 2016; Sun et al., 2016; Yu et al., 2019). For KANK3 and 4 binding to talin has not been shown yet; however, due to the high conservation of the KN domains among the KANK family it is expected that KANK3 and 4 can bind to talin as well. Moreover, all KANKs possess at least one coiled coil domain located in the central region of the protein. In total there exist four different conserved coiled coil domains (CC1 – 4) among the KANK family, the composition of the different coiled coils differs between the four KANK paralogs (Zhu et al., 2008). Van der Vaart et al. have found that KANK coiled coil domain 1 (CC1) mediates binding to liprin-β1, a member of the family of LAR transmembrane tyrosine phosphatase-interacting proteins, at the cell cortex in the vicinity of adhesion complexes (van der Vaart et al., 2013). At their C-terminus all KANK family members contain an ankyrin repeat domain which was shown to bind to the kinesin-4 motor protein KIF21A (Kakinuma and Kiyama, 2009; van der Vaart et al., 2013). Interestingly, the majority of studies reported that the KANK ankyrin repeat domain consists of five repeats of the ankyrin motif (Ankr1 – 5) (Bouchet et al., 2016; Kakinuma and Kiyama, 2009; Sun et al., 2016; van der Vaart et al., 2013; Zhu et al., 2008) whereas other studies mentioned an additional sixth ankyrin repeat (Ankr0) prior to the other five repeats (Guo et al., 2018; Pan et al., 2018; Weng et al., 2018). Moreover, these studies demonstrated through extensive structural analyses that mere 21 amino acids of KIF21A are required for binding to KANK1 or 2; and that KIF21A is recognized by two distinct pockets of KANK1 and 2, which are formed by Ankr1 - 2 and Ankr3 - 4 respectively (Guo et al., 2018; Pan et al., 2018; Weng et al., 2018). Since it seems that the Ankr0 repeat is not essential for binding to KIF21A and because this repeat is not mentioned in the UniProt database, the term "ankyrin repeat domain" will refer to the previously described five repeats (Ankr1 – 5) in the remainder of this chapter/thesis.

In addition to the three well described domains, there are two linker regions (L1 and L2) in KANKs: linker region L1 is located between the KN domain and the coiled coil domains; whereas linker region L2 sits between the coiled coil domains and the ankyrin repeat domain. Not much is known about the functions of these two regions.

Interestingly, Medves et al. described a unique example of a fusion gene generated by translocation between the KANK1 gene and the *platelet-derived growth factor receptor β* (*PDGFRβ*) gene (*KANK1-PDGFRβ*). They showed that either the KANK1-CC1 domain or the N-terminal part of the linker region L2 are required for oligomerization of the KANK1-PDGFRβ fusion protein thus referring to this part of the linker region as KANK oligomerization domain (KOD). Further, they also mentioned a coiled coil domain that is located C-terminally to the KOD region and is also part of the linker region L2. Yet, this new coiled coil domain seems not to be essential for oligomerization (Medves et al., 2011). However, further studies looking deeper into the role of these linker regions are missing, hence the knowledge about their function and purpose is still limited.

Interaction partners and functions of the KANK family proteins

KANK1 a novel binding partner of β-catenin and a nucleo-cytoplasmic shuttling protein
Besides the three well characterized domains and the two linker regions, Wang et al. found that KANK1 is a nucleo-cytoplasmic shuttling protein which contains two nuclear location signals (NLS): NLS1 (aa65-68); NLS2 (aa979-992, a bipartite NLS), whereas KANK1-S only contains one NLS due to the missing first 158 amino acids at its N-terminus (Wang et al., 2006). The export of KANK1 (both isoforms) is mediated by nuclear export signals (NES) via the classic chromosome maintenance region 1 (CRM1)/ exportin pathway. KANK1 possesses three NES sites: NES1 (aa43-52); NES2 (aa125-134); NES 3 (aa613-622) whereas KANK1-S only has one NES site. Furthermore, Wang et al. showed via immunoprecipitation that KANK1 and β-catenin can bind to each other; however, they did not specify the exact domains required for this binding. Moreover, they showed that β-catenin translocates together with KANK1 into the nucleus. Thus it seems possible that KANK1 can influence β-catenin-mediated transcription (Wang et al., 2006).

KANK1 binds to several proteins via its coiled coil domains and this binding can be modified by phosphorylation of the coiled coil domains
Coiled coil domains often mediate protein-protein interactions (Wang et al., 2012; Watkins et al., 2015). Thus, it comes to no surprise that over the past two decades several proteins have been identified as binding partners of KANK family proteins by binding to the KANK coiled coil domains, such as: liprin-β1 (van der Vaart et al., 2013); insulin receptor substrate p53 (IRSp53) (Roy et al., 2009); the phosphor-peptide binding protein family 14-3-3 (Kakinuma et al., 2008), or the formin homology protein DAAM1 (Suzuki et al., 2017).

The interaction of KANKs (mainly KANK1) with liprin-β1 is required for their role in the CMSC. Binding to liprin-β1 anchors KANKs and determines their dynamics at the cortex, with KANKs that are lacking the CC1 domain, thus cannot bind to liprin-β1, show much faster exchange than KANKs that are bound to liprins (our unpublished data, see chapter 4).

Kakinuma et al. found that the coiled coild domain of KANK1-S is phosphorylated by Akt kinase. In turn this phosphorylation enhances binding of KANK1-S via its coiled coils to the 14-3-3 protein. Moreover, they reported that KANK1-S inhibits RhoA activation by binding to 14-3-3 and thereby sequestering it from the active 14-3-3 complex, which leads to reduced RhoA activity and ultimately to less stress fiber formation (Kakinuma et al., 2008).

Recently, the same group discovered another interaction partner of KANK1-S, the Disheveled-associated activator of morphogenesis 1 (DAAM1), a formin homology protein which binds to the coiled coil domain of KANK1-S and interacts with RhoA thereby providing another way how KANK1-S can regulate RhoA activity (Suzuki et al., 2017).

Furthermore, Roy et al. found that KANK1-S regulates the activity of another Rho GTPase, Rac1 and thereby mitigates actin remodeling and protrusion formation (Roy et al., 2009). They identified insulin receptor substrate p53 (IRSp53) as a binding partner of KANK1-S, which interacts with the coiled coil domain of KANK1-S. As a result
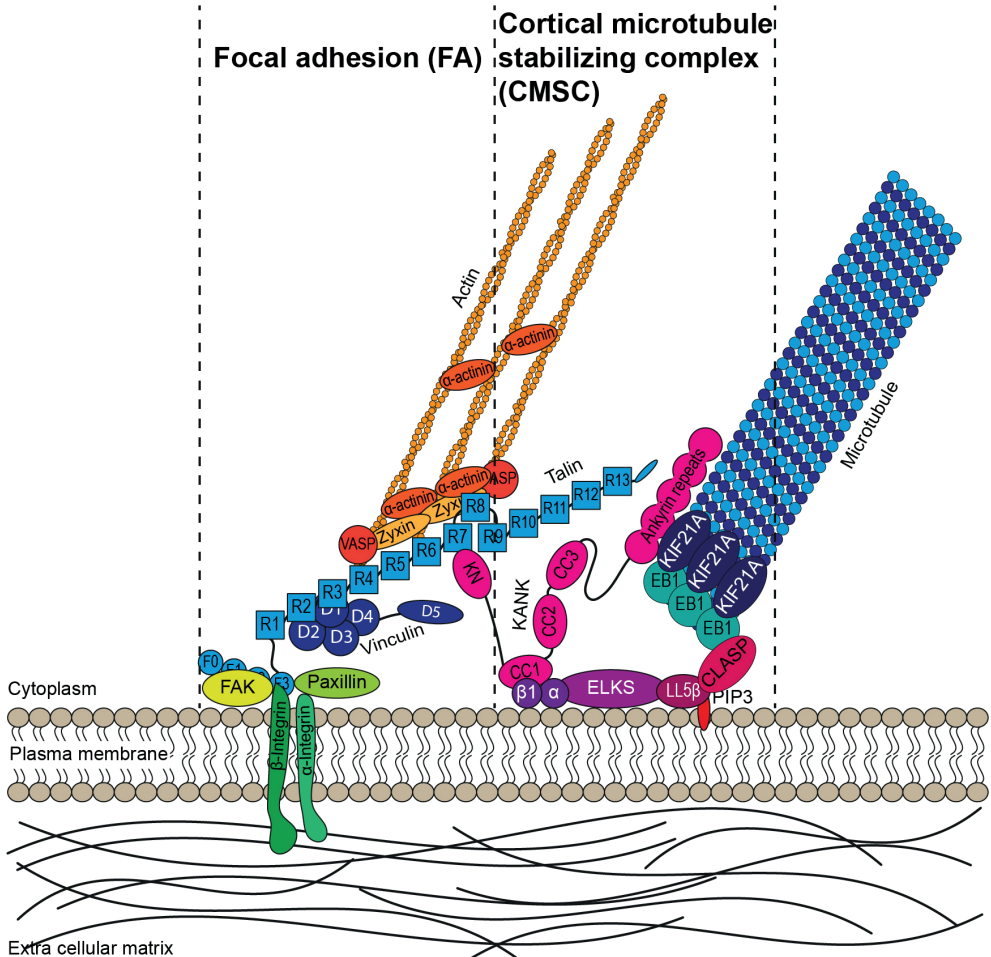
Figure 4. Schematic overview of the CMSC in close proximity to a FA at the cortex
Plus ends of MTs are anchored at the plasma membrane by CLASPs (CLASP1 and CLASP2), ELKS, liprins (α1 and β1, dark violet), and LL5β-containing plaques of the CMSC. CLASP stabilizes MT plus ends. KIF21A inhibits MT growth and thereby prevents overgrowth of MTs at the plasma membrane. KANK family proteins link the CMSC to FAs by directly binding to the FA protein talin and by binding to CMSC components such as liprins. Moreover, KANKs recruit KIF21A to the CMSC.

IRSp53 is unable to bind to active Rac1, and this negatively affects actin remodeling and protrusion formation (Roy et al., 2009).

The interplay between talin and KANKs at FAs
More recently it has been shown that KANK1 binds via its KN domain to the Rod7 (R7) domain of the FA protein talin (Bouchet et al., 2016). Further, it has been demonstrated that by binding to talin KANK1 helps recruiting the CMSC to FAs (Figure 4). The CMSC, a macromolecular complex that contains CLASPs, ELKS, liprins, and LL5β, anchors and stabilizes MT plus-ends at the cortex (Lansbergen et al., 2006; Mimori-Kiyosue et al., 2005; van der Vaart et al., 2013). The kinesin-4 motor protein KIF21A, another component of the CMSC and binding partner of KANK1 and KANK2 inhibits

1

MT polymerization and thus prevents MT overgrowth at the cortex (van der Vaart et al., 2013). Perturbation of the talin-KANK1 interaction leads to the dispersion of the CMSCs at the cortex and to MT overgrowth; yet, it does not significantly affect FA size or disassembly (Bouchet et al., 2016).

Around the same time, another study has demonstrated that KANK2 binds to talin (via its KN motif) (Sun et al., 2016). Moreover, Sun et al. have reported that KANKs play a dual role at FAs: on the one hand, binding of KANKs to talin leads to talin activation and therefore stimulates binding of talin to β-integrins thereby promoting integrin activation. On the other hand, binding of KANKs to talin rod domain R7 also hampers binding of F-actin to the actin binding site (ABS2) of talin therefore weakening the connection between integrins and actomyosin. Ultimately, this leads to reduced force transmission via integrins, which in turn results in adhesion sliding and reduced cell migration speed (Sun et al., 2016). Recently, it has been demonstrated that the interaction between talin rod domain R7 and the KANK1 KN domain (R7/KN complex) is force-regulated (Yu et al., 2019).

Furthermore, a study by Rafiq et al. reported that KANKs (KANK1 and 2) together with GEF-H1, a MT-associated GEF, were required for the MT-mediated regulation of FAs and podosomes and myosin II filaments (Rafiq et al., 2019). They showed that depletion of KANK1 and 2 uncoupled MTs form adhesion complexes which led to the release of GEF-H1 from MTs which has previously only been seen with MT disruption (Chang et al., 2008; Krendel et al., 2002). This in turn resulted in a higher amount of myosin IIA filaments (due to elevated RhoA activity), which led to an increase in FA size (Rafiq et al., 2019).

KANK orthologs in invertebrates

As mentioned previously, there is only a single KANK ortholog in most invertebrates such as flies (*Drosophila*) and nematodes (*C. elegans*). VAB-19 is the KANK ortholog in *C. elegans*. In contrast to the vertebrate KANKs, it contains only four ankyrin repeats at its C-terminus instead of five. Besides, it possesses two conserved domains at the N-terminus named motif A and motif B (these motifs do not resemble the KN nor the coiled coil domains of vertebrate KANKs). Further, it was shown that null mutations in the vab-19 gene are not viable (Ding et al., 2003). VAB-19 plays an important role in the development of the epidermis during *C. elegans* embryonic morphogenesis. Ding et al. have described that through its motifs A and B VAB-19 localizes at the dermis to so-called epidermal attachment complexes. These complexes link the contractile system (actomyosin) of the muscles to the cuticular exoskeleton of the worm (Gieseler et al., 2017). Further, they have described that VAB-19 mutants show perturbed epidermal actin organization in hand with disturbed epidermal elongation and deficient muscle attachment to the dermis. Consequently, this results in paralysis of the embryos. Moreover, Ding et al. have been able to show that expression of human KANK (KANK1-S) in *C. elegans* could partially rescue the phenotype of VAB-19 mutants (Ding et al., 2003).

Later, the same group has demonstrated that VAB-19 binds via its ankyrin repeat domain to the signaling adaptor protein EPS-8 and is thereby likely to recruit it to the epidermal attachment complexes. EPS-8 is required for proper actin organization at the epidermis (Ding et al., 2008). The mammalian EPS-8 interacts with IRSp53, which has been linked

to KANK1 in mammals (Roy et al., 2009), and is important in actin regulation (Disanza et al., 2006).

Besides, VAB-19 is also involved in regulating the formation of basement membrane gaps during uterine-vulval attachment. It has been described that VAB-19 localizes to the sites of basement membrane gap boundaries in vulval cells. There, VAB-19 and the heterodimeric integrin INA-1/PAT-3 limit the expansion of basement membrane gaps (Ihara et al., 2011).

Further, it has also been reported that VAB-19 mutants show perturbed directionality of the UNC-40-mediated axon outgrowth of the hermaphrodite specific motor neuron (HSN) axon (Yang et al., 2014b).

The sole ortholog of the KANK family proteins in *Drosophila*, dKANK, also localizes to attachment sites of muscle to the dermis. Yet, unlike VAB-19 in *C. elegans*, defects in dKANK do not affect muscle function in *Drosophila* larvae; further, complete loss of dKANK does not affect *Drosophila* viability nor fertility (Clohisey et al., 2014). Clohisey et al. have reported that, like human KANK1, dKANK contains nuclear localization signals and nuclear export signals and that it can shuttle between the cytoplasm and the nucleus in a CRM1/exportin-dependent manner. Moreover, they have described that in cultured *Drosophila* cells, dKANK localizes to MT plus ends in an EB1-dependent manner. They also have been able to show that dKANK is a binding partner of EB1. Members of the conserved (microtubule) end binding (EB) family can autonomously recognize growing MT ends. Besides, EBs can bind and consequently recruit a plethora of different binding partners to the growing ends of MTs, such as CLASPs which suppress catastrophes at the MT tip, and consequently affect the dynamics of MT ends (Akhmanova and Steinmetz, 2015). Nonetheless, there have been no reports about a direct interaction between EBs and human KANK family proteins.

KANK family proteins in diseases

KANKs in cancer

As mentioned previously, Sarkar et al. were the first to report on KANK (family proteins) when they studied patients suffering from renal cell carcinoma (RCC). They found that expression of KANK (actually KANK1-S) was reduced in a significant portion of RCC patients. Moreover, Sarkar et al. were able to demonstrate that overexpression of KANK led to reduced cell growth and that tumor growth was perturbed in mice that were injected with KANK-overexpressing HEK cells. Hence, KANK was regarded as a potential tumor suppressor (Sarkar et al., 2002). Since this first report, almost 20 years ago, a potential tumor suppressor role of the KANK family proteins has been suggested in different studies describing various forms of cancer, such as lung cancer (Gu and Zhang, 2018; Kohno et al., 2010), brain glioma (Guo et al., 2014), gastric cancer (Chen et al., 2017), and oral squamous cell carcinoma (Fan et al., 2020),. Some of these studies reported that overexpression of KANK1 resulted in cell cycle arrest in G0/G1 phase (Guo et al., 2014) and stimulated apoptosis via the intrinsic pathway by changing the permeability of the mitochondrial membrane thereby causing cytochrome c to leak out of mitochondria, a process that initiates the apoptosis cascade (Chen et al., 2017; Fan et al., 2020; Gu and Zhang, 2018; Guo et al., 2014).

In another study, Kim et al. showed that the KANK family proteins were substrates

of hypoxia inducible factor 1 A inhibitor (HIF1AN), which hydroxylated specific asparagine residues in the ankyrin repeat domain of KANKs (Kim et al., 2018). HIF1AN functions as an oxygen sensor. Under normoxic conditions (normal levels of oxygen), it would hydroxylate hypoxia inducible factor 1 A (HIF1A), a subunit of the heterodimeric transcription factor HIF-1 (hypoxia inducible factor 1), and by that prevent the activation of HIF-1 (Kaelin and Ratcliffe, 2008). Moreover, Kim et al. found that especially KANK3 was a target of HIF1AN and further, that depletion of KANK3 resulted in increased cell migration and invasion of Hep 3B and 2G cells (both hepatocellular carcinoma cell lines), whereas overexpression of KANK3 reversed these effects. Besides, they found that low levels of KANK3 expression correlated with lower survival rates in hepatocellular carcinoma patients (Kim et al., 2018).

KANKs in other diseases
Besides the reports of the potential role of KANK family proteins as tumor suppressors in cancer, there have been several studies that linked KANKs to other diseases as well. In 2005, Lerer et al. documented a rare case of familial cerebral palsy, a group of permanent movement disorders, in which deletion of KANK1 seemed to be the cause for the disease since a group of 210 healthy control individuals did not show the same deletion (Lerer et al., 2005).

A homozygous missense mutation (Ala670Val) in the ankyrin repeat domain of KANK2 was seen as cause for keratoderma, a hornlike skin condition, and woolly hair in affected individuals of two related families (Ramot et al., 2014). Ramot et al. showed that the missense mutation relieved the previously reported sequestering of steroid receptor coactivators (SRCs) in the cytoplasm (Zhang et al., 2007) by perturbing SRC binding to the KANK2 ankyrin repeat domain. Consequently, SRCs were able to translocate into the nucleus and stimulate the vitamin D receptor which is involved in epidermal differentiation (Ramot et al., 2014).

Recently, KANK family proteins have been suggested to play an evolutionary conserved role in podocyte function (Gee et al., 2015). Podocytes are cells that make up the epithelium of the Bowman's capsule; their orderly function is required for proper ultrafiltration of the blood, whereas podocyte dysfunction is often associated with nephrotic syndrome (Wickelgren, 1999). Gee et al. have been able to demonstrate that KANK family proteins (mainly KANK2), are required for proper podocyte function where they control the activity of RhoA by interacting with Rho GDI. Further, they have seen that depletion of KANK2 leads to increased RhoA activity and that depletion of KANK2 in zebrafish and of dKANK in *Drosophila* perturbed the slit diaphragm filtration structures (Gee et al., 2015).

Concluding remarks
All in all, the KANK family proteins constitute a diverse group of proteins with numerous binding partners and various functions. Despite this diversity it seems that one function has been conserved among KANKs: to serve as a linker at the interface of (cortical) attachment complexes and the cytoskeleton. However, we still know comparatively little about the exact function of the KANKs, the networks through which they operate and about the differences between the four mammalian family members. Thus, further research has to be done to understand the full picture.

1

Scope of the thesis

In this thesis, we characterized the KANK family proteins and their role as mediators of the cross-talk between the microtubule cytoskeleton and integrin-mediated cell-matrix adhesions. We tried to better understand how KANKs are recruited to FAs, how they interact with talin and what other factors contribute to their function and subcellular localization.

In **Chapter 2**, we establish KANK family proteins as novel binding partners of the FA protein talin. Thereby KANKs form the link between FAs and the CMSC. Further, we could show that the talin-KANK interaction is required for proper formation of the CMSC at the cortex and that perturbation of this connection leads to MT overgrowth.

In **Chapter 3**, we describe the interaction between talin and KANK1 in more detail. We found that the interaction between talin rod domain R7 and the KANK1 KN domain is force-regulated and that it can withstand forces in the piconewton range under certain force geometry.

In **Chapter 4**, we focus on the subcellular localization of KANK1 and explain how the clustering of KANKs around FAs is mediated. We were able to demonstrate that this localization is not due to the coiled coil nor the ankyrin repeat domains but due to the linker region L2 of KANK1.

In **Chapter 5**, we describe the differences between KANK1 and KANK2 with a particular focus on their different subcellular localizations and their role in cell migration. KANK1 is predominantly localized at the cell periphery whereas KANK2 is more concentrated in the central region. We were able to show that the localization of KANK2 is mediated by its KN domain and binding to talin. Further, have seen that depletion of both KANK1 and 2 does not affect cell migration of HeLa cells. On the other hand, loss of KANK2 significantly hampered cell migration of SUM159PT breast cancer cells.

In **Chapter 6**, we discuss how KANK family proteins regulate the cross-talk between MTs and FAs. We combine our work on KANKs as linkers between FAs and CMSC (Chapter 2), the force-regulated interaction between talin and KANKs (Chapter 3), the role of KANK1's linker region L2 in localizing KANK1 around FAs (Chapter 4), and the role of KANK family proteins in cell migration (Chapter 5) and put them into broader perspective. Further, we discuss some of the partially contradictory findings on KANK family proteins from us and others. We also present some preliminary data on KANK family proteins in endothelial cells and discuss an involvement of KANKs in ECM reorganization (fibronectin fibrillogenesis) and angiogenesis.

1

References

Akhmanova, A., and M.O. Steinmetz. 2015. Control of microtubule organization and dynamics: two ends in the limelight. Nature Reviews Molecular Cell Biology. 16:711.

Atherton, P., B. Stutchbury, D.Y. Wang, D. Jethwa, R. Tsang, E. Meiler-Rodriguez, P. Wang, N. Bate, R. Zent, I.L. Barsukov, B.T. Goult, D.R. Critchley, and C. Ballestrem. 2015. Vinculin controls talin engagement with the actomyosin machinery. Nat Commun. 6:10038.

Bachir, A.I., J. Zareno, K. Moissoglu, E.F. Plow, E. Gratton, and A.R. Horwitz. 2014. Integrin-associated complexes form hierarchically with variable stoichiometry in nascent adhesions. Curr Biol. 24:1845-1853.

Barczyk, M., S. Carracedo, and D. Gullberg. 2010. Integrins. Cell Tissue Res. 339:269-280.

Bouchet, B.P., R.E. Gough, Y.C. Ammon, D. van de Willige, H. Post, G. Jacquemet, A.M. Altelaar, A.J. Heck, B.T. Goult, and A. Akhmanova. 2016. Talin-KANK1 interaction controls the recruitment of cortical microtubule stabilizing complexes to focal adhesions. Elife. 5.

Brown, C.M., B. Hebert, D.L. Kolin, J. Zareno, L. Whitmore, A.R. Horwitz, and P.W. Wiseman. 2006. Probing the integrin-actin linkage using high-resolution protein velocity mapping. J Cell Sci. 119:5204-5214.

Brown, M.C., and C.E. Turner. 2004. Paxillin: adapting to change. Physiol Rev. 84:1315-1339.

Burridge, K., and M. Chrzanowska-Wodnicka. 1996. Focal adhesions, contractility, and signaling. Annu Rev Cell Dev Biol. 12:463-518.

Burridge, K., and L. Connell. 1983. A new protein of adhesion plaques and ruffling membranes. J Cell Biol. 97:359-367.

Byron, A., J.A. Askari, J.D. Humphries, G. Jacquemet, E.J. Koper, S. Warwood, C.K. Choi, M.J. Stroud, C.S. Chen, D. Knight, and M.J. Humphries. 2015. A proteomic approach reveals integrin activation state-dependent control of microtubule cortical targeting. Nature Communications. 6:6135.

Calderwood, D.A., I.D. Campbell, and D.R. Critchley. 2013. Talins and kindlins: partners in integrin-mediated adhesion. Nat Rev Mol Cell Biol. 14:503-517.

Calderwood, D.A., R. Zent, R. Grant, D.J. Rees, R.O. Hynes, and M.H. Ginsberg. 1999. The Talin head domain binds to integrin beta subunit cytoplasmic tails and regulates integrin activation. J Biol Chem. 274:28071-28074.

Caswell, P.T., S. Vadrevu, and J.C. Norman. 2009. Integrins: masters and slaves of endocytic transport. Nat Rev Mol Cell Biol. 10:843-853.

Chang, Y.C., P. Nalbant, J. Birkenfeld, Z.F. Chang, and G.M. Bokoch. 2008. GEF-H1 couples nocodazole-induced microtubule disassembly to cell contractility via RhoA. Mol Biol Cell. 19:2147-2153.

Changede, R., X. Xu, F. Margadant, and M.P. Sheetz. 2015. Nascent Integrin Adhesions Form on All Matrix Rigidities after Integrin Activation. Dev Cell. 35:614-621.

Chen, T., K. Wang, and X. Tong. 2017. In vivo and in vitro inhibition of human gastric cancer progress by upregulating Kank1 gene. Oncol Rep. 38:1663-1669.

Ciobanasu, C., H. Wang, V. Henriot, C. Mathieu, A. Fente, S. Csillag, C. Vigouroux, B. Faivre, and C. Le Clainche. 2018. Integrin-bound talin head inhibits actin filament barbed-end elongation. J Biol Chem. 293:2586-2596.

Clohisey, S.M., N.S. Dzhindzhev, and H. Ohkura. 2014. Kank Is an EB1 interacting protein that localises to muscle-tendon attachment sites in Drosophila. PLoS One. 9:e106112.

Debrand, E., F.J. Conti, N. Bate, L. Spence, D. Mazzeo, C.A. Pritchard, S.J. Monkley, and D.R. Critchley. 2012. Mice carrying a complete deletion of the talin2 coding sequence are viable and fertile. Biochem Biophys Res Commun. 426:190-195.

del Rio, A., R. Perez-Jimenez, R. Liu, P. Roca-Cusachs, J.M. Fernandez, and M.P. Sheetz. 2009. Stretching single talin rod molecules activates vinculin binding. Science. 323:638-641.

Ding, M., A. Goncharov, Y. Jin, and A.D. Chisholm. 2003. C. elegans ankyrin repeat protein VAB-19 is a component of epidermal attachment structures and is essential for epidermal morphogenesis. Development. 130:5791-5801.

Ding, M., R.S. King, E.C. Berry, Y. Wang, J. Hardin, and A.D. Chisholm. 2008. The cell signaling adaptor protein EPS-8 is essential for C. elegans epidermal elongation and interacts with the ankyrin repeat protein VAB-19. PLoS One. 3:e3346.

Disanza, A., S. Mantoani, M. Hertzog, S. Gerboth, E. Frittoli, A. Steffen, K. Berhoerster, H.J. Kreienkamp, F. Milanesi, P.P. Di Fiore, A. Ciliberto, T.E. Stradal, and G. Scita. 2006. Regulation of cell shape by Cdc42 is mediated by the synergic actin-bundling activity of the Eps8-IRSp53 complex. Nat Cell Biol. 8:1337-1347.

Eden, S., R. Rohatgi, A.V. Podtelejnikov, M. Mann, and M.W. Kirschner. 2002. Mechanism of regulation of WAVE1-induced actin nucleation by Rac1 and Nck. Nature. 418:790-793.

Elliott, P.R., B.T. Goult, P.M. Kopp, N. Bate, J.G. Grossmann, G.C. Roberts, D.R. Critchley, and I.L. Barsukov. 2010. The Structure of the talin head reveals a novel extended conformation of the FERM domain. Structure. 18:1289-1299.

Ezratty, E.J., C. Bertaux, E.E. Marcantonio, and G.G. Gundersen. 2009. Clathrin mediates integrin endocytosis for focal adhesion disassembly in migrating cells. Journal of Cell Biology. 187:733-747.

Ezratty, E.J., M.A. Partridge, and G.G. Gundersen. 2005. Microtubule-induced focal adhesion disassembly is mediated by dynamin and focal adhesion kinase. Nat Cell Biol. 7:581-590.

Fan, H., H. Tian, X. Cheng, Y. Chen, S. Liang, Z. Zhang, Y. Liao, and P. Xu. 2020. Aberrant Kank1 expression regulates YAP to promote apoptosis and inhibit proliferation in OSCC. J Cell Physiol. 235:1850-1865.

Franco, S.J., and A. Huttenlocher. 2005. Regulating cell migration: calpains make the cut. J Cell Sci. 118:3829-3838.

Franco, S.J., M.A. Rodgers, B.J. Perrin, J. Han, D.A. Bennin, D.R. Critchley, and A. Huttenlocher. 2004. Calpain-mediated proteolysis of talin regulates adhesion dynamics. Nat Cell Biol. 6:977-983.

Gee, H.Y., F. Zhang, S. Ashraf, S. Kohl, C.E. Sadowski, V. Vega-Warner, W. Zhou, S. Lovric, H. Fang, M. Nettleton, J.Y. Zhu, J. Hoefele, L.T. Weber, L. Podracka, A. Boor, H. Fehrenbach, J.W. Innis, J. Washburn, S. Levy, R.P. Lifton, E.A. Otto, Z. Han, and F. Hildebrandt. 2015. KANK deficiency leads to podocyte dysfunction and nephrotic syndrome. J Clin Invest. 125:2375-2384.

Geiger, B., and K.M. Yamada. 2011. Molecular architecture and function of matrix adhesions. Cold Spring Harb Perspect Biol. 3.

Gieseler, K., H. Qadota, and G.M. Benian.

2017. Development, structure, and maintenance of C. elegans body wall muscle. WormBook. 2017:1-59.

Gingras, A.R., N. Bate, B.T. Goult, L. Hazelwood, I. Canestrelli, J.G. Grossmann, H. Liu, N.S. Putz, G.C. Roberts, N. Volkmann, D. Hanein, I.L. Barsukov, and D.R. Critchley. 2008. The structure of the C-terminal actin-binding domain of talin. Embo j. 27:458-469.

Gingras, A.R., W.H. Ziegler, A.A. Bobkov, M.G. Joyce, D. Fasci, M. Himmel, S. Rothemund, A. Ritter, J.G. Grossmann, B. Patel, N. Bate, B.T. Goult, J. Emsley, I.L. Barsukov, G.C. Roberts, R.C. Liddington, M.H. Ginsberg, and D.R. Critchley. 2009. Structural determinants of integrin binding to the talin rod. J Biol Chem. 284:8866-8876.

Goksoy, E., Y.Q. Ma, X. Wang, X. Kong, D. Perera, E.F. Plow, and J. Qin. 2008. Structural basis for the autoinhibition of talin in regulating integrin activation. Mol Cell. 31:124-133.

Goult, B.T., N. Bate, N.J. Anthis, K.L. Wegener, A.R. Gingras, B. Patel, I.L. Barsukov, I.D. Campbell, G.C. Roberts, and D.R. Critchley. 2009. The structure of an interdomain complex that regulates talin activity. J Biol Chem. 284:15097-15106.

Goult, B.T., T. Zacharchenko, N. Bate, R. Tsang, F. Hey, A.R. Gingras, P.R. Elliott, G.C. Roberts, C. Ballestrem, D.R. Critchley, and I.L. Barsukov. 2013. RIAM and vinculin binding to talin are mutually exclusive and regulate adhesion assembly and turnover. J Biol Chem. 288:8238-8249.

Gu, Y., and M. Zhang. 2018. Upregulation of the Kank1 gene inhibits human lung cancer progression in vitro and in vivo. Oncol Rep. 40:1243-1250.

Guo, Q., S. Liao, Z. Zhu, Y. Li, F. Li, and

C. Xu. 2018. Structural basis for the recognition of kinesin family member 21A (KIF21A) by the ankyrin domains of KANK1 and KANK2 proteins. Journal of Biological Chemistry. 293:557-566.

Guo, X., W. Fan, X. Bian, and D. Ma. 2014. Upregulation of the Kank1 gene-induced brain glioma apoptosis and blockade of the cell cycle in G0/G1 phase. Int J Oncol. 44:797-804.

Hall, A. 2012. Rho family GTPases. Biochem Soc Trans. 40:1378-1382.

Hemmings, L., D.J. Rees, V. Ohanian, S.J. Bolton, A.P. Gilmore, B. Patel, H. Priddle, J.E. Trevithick, R.O. Hynes, and D.R. Critchley. 1996. Talin contains three actin-binding sites each of which is adjacent to a vinculin-binding site. J Cell Sci. 109 (Pt 11):2715-2726.

Hensley, M.R., Z. Cui, R.F. Chua, S. Simpson, N.L. Shammas, J.Y. Yang, Y.F. Leung, and G. Zhang. 2016. Evolutionary and developmental analysis reveals KANK genes were co-opted for vertebrate vascular development. Sci Rep. 6:27816.

Hodge, R.G., and A.J. Ridley. 2016. Regulating Rho GTPases and their regulators. Nat Rev Mol Cell Biol. 17:496-510.

Horgan, C.P., and M.W. McCaffrey. 2011. Rab GTPases and microtubule motors. Biochem Soc Trans. 39:1202-1206.

Hu, K., L. Ji, K.T. Applegate, G. Danuser, and C.M. Waterman-Storer. 2007. Differential transmission of actin motion within focal adhesions. Science. 315:111-115.

Hynes, R.O. 2002. Integrins: bidirectional, allosteric signaling machines. Cell. 110:673-687.

Ihara, S., E.J. Hagedorn, M.A. Morrissey, Q. Chi, F. Motegi, J.M. Kramer, and D.R. Sherwood.

2011. Basement membrane sliding and targeted adhesion remodels tissue boundaries during uterine-vulval attachment in Caenorhabditis elegans. Nat Cell Biol. 13:641-651.

Kaelin, W.G., Jr., and P.J. Ratcliffe. 2008. Oxygen sensing by metazoans: the central role of the HIF hydroxylase pathway. Mol Cell. 30:393-402.

Kakinuma, N., and R. Kiyama. 2009. A major mutation of KIF21A associated with congenital fibrosis of the extraocular muscles type 1 (CFEOM1) enhances translocation of Kank1 to the membrane. Biochem Biophys Res Commun. 386:639-644.

Kakinuma, N., B.C. Roy, Y. Zhu, Y. Wang, and R. Kiyama. 2008. Kank regulates RhoA-dependent formation of actin stress fibers and cell migration via 14-3-3 in PI3K-Akt signaling. J Cell Biol. 181:537-549.

Kanchanawong, P., G. Shtengel, A.M. Pasapera, E.B. Ramko, M.W. Davidson, H.F. Hess, and C.M. Waterman. 2010. Nanoscale architecture of integrin-based cell adhesions. Nature. 468:580-584.

Kaverina, I., O. Krylyshkina, and J.V. Small. 1999. Microtubule targeting of substrate contacts promotes their relaxation and dissociation. J Cell Biol. 146:1033-1044.

Kaverina, I., K. Rottner, and J.V. Small. 1998. Targeting, capture, and stabilization of microtubules at early focal adhesions. J Cell Biol. 142:181-190.

Kim, I., J. Kang, H.Y. Gee, and J.W. Park. 2018. A novel HIF1AN substrate KANK3 plays a tumor-suppressive role in hepatocellular carcinoma. Cell Biol Int. 42:303-312.

Kimura, K., M. Ito, M. Amano, K. Chihara, Y. Fukata, M. Nakafuku, B. Yamamori, J. Feng, T.

Nakano, K. Okawa, A. Iwamatsu, and K. Kaibuchi. 1996. Regulation of myosin phosphatase by Rho and Rho-associated kinase (Rho-kinase). Science. 273:245-248.

Kohno, T., A. Otsuka, L. Girard, M. Sato, R. Iwakawa, H. Ogiwara, M. Sanchez-Cespedes, J.D. Minna, and J. Yokota. 2010. A catalog of genes homozygously deleted in human lung cancer and the candidacy of PTPRD as a tumor suppressor gene. Genes Chromosomes Cancer. 49:342-352.

Krendel, M., F.T. Zenke, and G.M. Bokoch. 2002. Nucleotide exchange factor GEF-H1 mediates cross-talk between microtubules and the actin cytoskeleton. Nat Cell Biol. 4:294-301.

Krylyshkina, O., K.I. Anderson, I. Kaverina, I. Upmann, D.J. Manstein, J.V. Small, and D.K. Toomre. 2003. Nanometer targeting of microtubules to focal adhesions. J Cell Biol. 161:853-859.

Kumar, A., M. Ouyang, K. Van den Dries, E.J. McGhee, K. Tanaka, M.D. Anderson, A. Groisman, B.T. Goult, K.I. Anderson, and M.A. Schwartz. 2016. Talin tension sensor reveals novel features of focal adhesion force transmission and mechanosensitivity. J Cell Biol. 213:371-383.

Lansbergen, G., I. Grigoriev, Y. Mimori-Kiyosue, T. Ohtsuka, S. Higa, I. Kitajima, J. Demmers, N. Galjart, A.B. Houtsmuller, F. Grosveld, and A. Akhmanova. 2006. CLASPs attach microtubule plus ends to the cell cortex through a complex with LL5beta. Dev Cell. 11:21-32.

Lawson, C., S.T. Lim, S. Uryu, X.L. Chen, D.A. Calderwood, and D.D. Schlaepfer. 2012. FAK promotes recruitment of talin to nascent adhesions to control cell motility. J Cell Biol. 196:223-232.

Lee, H.S., R.M. Bellin, D.L. Walker, B.

Patel, P. Powers, H. Liu, B. Garcia-Alvarez, J.M. de Pereda, R.C. Liddington, N. Volkmann, D. Hanein, D.R. Critchley, and R.M. Robson. 2004. Characterization of an actin-binding site within the talin FERM domain. J Mol Biol. 343:771-784.

Lerer, I., M. Sagi, V. Meiner, T. Cohen, J. Zlotogora, and D. Abeliovich. 2005. Deletion of the ANKRD15 gene at 9p24.3 causes parent-of-origin-dependent inheritance of familial cerebral palsy. Hum Mol Genet. 14:3911-3920.

Li, J., and T.A. Springer. 2017. Integrin extension enables ultrasensitive regulation by cytoskeletal force. Proceedings of the National Academy of Sciences. 114:4685-4690.

Medves, S., L.A. Noel, C.P. Montano-Almendras, R.I. Albu, H. Schoemans, S.N. Constantinescu, and J.B. Demoulin. 2011. Multiple oligomerization domains of KANK1-PDGFRbeta are required for JAK2-independent hematopoietic cell proliferation and signaling via STAT5 and ERK. Haematologica. 96:1406-1414.

Mimori-Kiyosue, Y., I. Grigoriev, G. Lansbergen, H. Sasaki, C. Matsui, F. Severin, N. Galjart, F. Grosveld, I. Vorobjev, S. Tsukita, and A. Akhmanova. 2005. CLASP1 and CLASP2 bind to EB1 and regulate microtubule plus-end dynamics at the cell cortex. J Cell Biol. 168:141-153.

Mitra, S.K., D.A. Hanson, and D.D. Schlaepfer. 2005. Focal adhesion kinase: in command and control of cell motility. Nat Rev Mol Cell Biol. 6:56-68.

Monkley, S.J., C.A. Pritchard, and D.R. Critchley. 2001. Analysis of the mammalian talin2 gene TLN2. Biochem Biophys Res Commun. 286:880-885.

Monkley, S.J., X.H. Zhou, S.J. Kinston, S.M. Giblett, L. Hemmings, H. Priddle, J.E. Brown, C.A. Pritchard, D.R. Critchley, and R. Fässler.

2000. Disruption of the talin gene arrests mouse development at the gastrulation stage. Dev Dyn. 219:560-574.

Otey, C.A., and O. Carpen. 2004. Alpha-actinin revisited: a fresh look at an old player. Cell Motil Cytoskeleton. 58:104-111.

Pan, W., K. Sun, K. Tang, Q. Xiao, C. Ma, C. Yu, and Z. Wei. 2018. Structural insights into ankyrin repeat-mediated recognition of the kinesin motor protein KIF21A by KANK1, a scaffold protein in focal adhesion. J Biol Chem. 293:1944-1956.

Rafiq, N.B.M., Y. Nishimura, S.V. Plotnikov, V. Thiagarajan, Z. Zhang, S. Shi, M. Natarajan, V. Viasnoff, P. Kanchanawong, G.E. Jones, and A.D. Bershadsky. 2019. A mechano-signalling network linking microtubules, myosin IIA filaments and integrin-based adhesions. Nature Materials. 18:638-649.

Raftopoulou, M., and A. Hall. 2004. Cell migration: Rho GTPases lead the way. Dev Biol. 265:23-32.

Ramot, Y., V. Molho-Pessach, T. Meir, R. Alper-Pinus, I. Siam, S. Tams, S. Babay, and A. Zlotogorski. 2014. Mutation in KANK2, encoding a sequestering protein for steroid receptor coactivators, causes keratoderma and woolly hair. J Med Genet. 51:388-394.

Ren, X.D., W.B. Kiosses, and M.A. Schwartz. 1999. Regulation of the small GTP-binding protein Rho by cell adhesion and the cytoskeleton. Embo j. 18:578-585.

Ren, Y., R. Li, Y. Zheng, and H. Busch. 1998. Cloning and characterization of GEF-H1, a microtubule-associated guanine nucleotide exchange factor for Rac and Rho GTPases. J Biol Chem. 273:34954-34960.

Rid, R., N. Schiefermeier, I. Grigoriev, J.V.

Small, and I. Kaverina. 2005. The last but not the least: the origin and significance of trailing adhesions in fibroblastic cells. Cell Motil Cytoskeleton. 61:161-171.

Ridley, A.J., and A. Hall. 1992. The small GTP-binding protein rho regulates the assembly of focal adhesions and actin stress fibers in response to growth factors. Cell. 70:389-399.

Ridley, A.J., H.F. Paterson, C.L. Johnston, D. Diekmann, and A. Hall. 1992. The small GTP-binding protein rac regulates growth factor-induced membrane ruffling. Cell. 70:401-410.

Roy, B.C., N. Kakinuma, and R. Kiyama. 2009. Kank attenuates actin remodeling by preventing interaction between IRSp53 and Rac1. J Cell Biol. 184:253-267.

Saltel, F., E. Mortier, V.P. Hytönen, M.C. Jacquier, P. Zimmermann, V. Vogel, W. Liu, and B. Wehrle-Haller. 2009. New PI(4,5)P2- and membrane proximal integrin-binding motifs in the talin head control beta3-integrin clustering. J Cell Biol. 187:715-731.

Sarkar, S., B.C. Roy, N. Hatano, T. Aoyagi, K. Gohji, and R. Kiyama. 2002. A novel ankyrin repeat-containing gene (Kank) located at 9p24 is a growth suppressor of renal cell carcinoma. J Biol Chem. 277:36585-36591.

Stehbens, S.J., M. Paszek, H. Pemble, A. Ettinger, S. Gierke, and T. Wittmann. 2014. CLASPs link focal-adhesion-associated microtubule capture to localized exocytosis and adhesion site turnover. Nat Cell Biol. 16:561-573.

Sun, Z., M. Costell, and R. Fässler. 2019. Integrin activation by talin, kindlin and mechanical forces. Nat Cell Biol. 21:25-31.

Sun, Z., H.Y. Tseng, S. Tan, F. Senger, L. Kurzawa, D. Dedden, N. Mizuno, A.A. Wasik, M. Thery, A.R. Dunn, and R. Fassler. 2016. Kank2

activates talin, reduces force transduction across integrins and induces central adhesion formation. Nat Cell Biol. 18:941-953.

Suzuki, J.I., B.C. Roy, T. Ogaeri, N. Kakinuma, and R. Kiyama. 2017. Depletion of tumor suppressor Kank1 induces centrosomal amplification via hyperactivation of RhoA. Exp Cell Res. 353:79-87.

Takino, T., Y. Watanabe, M. Matsui, H. Miyamori, T. Kudo, M. Seiki, and H. Sato. 2006. Membrane-type 1 matrix metalloproteinase modulates focal adhesion stability and cell migration. Exp Cell Res. 312:1381-1389.

Thul, P.J., L. Åkesson, M. Wiking, D. Mahdessian, A. Geladaki, H. Ait Blal, T. Alm, A. Asplund, L. Björk, L.M. Breckels, A. Bäckström, F. Danielsson, L. Fagerberg, J. Fall, L. Gatto, C. Gnann, S. Hober, M. Hjelmare, F. Johansson, S. Lee, C. Lindskog, J. Mulder, C.M. Mulvey, P. Nilsson, P. Oksvold, J. Rockberg, R. Schutten, J.M. Schwenk, Å. Sivertsson, E. Sjöstedt, M. Skogs, C. Stadler, D.P. Sullivan, H. Tegel, C. Winsnes, C. Zhang, M. Zwahlen, A. Mardinoglu, F. Pontén, K. von Feilitzen, K.S. Lilley, M. Uhlén, and E. Lundberg. 2017. A subcellular map of the human proteome. Science. 356.

van der Vaart, B., W.E. van Riel, H. Doodhi, J.T. Kevenaar, E.A. Katrukha, L. Gumy, B.P. Bouchet, I. Grigoriev, S.A. Spangler, K.L. Yu, P.S. Wulf, J. Wu, G. Lansbergen, E.Y. van Battum, R.J. Pasterkamp, Y. Mimori-Kiyosue, J. Demmers, N. Olieric, I.V. Maly, C.C. Hoogenraad, and A. Akhmanova. 2013. CFEOM1-associated kinesin KIF21A is a cortical microtubule growth inhibitor. Dev Cell. 27:145-160.

Vicente-Manzanares, M., J. Zareno, L. Whitmore, C.K. Choi, and A.F. Horwitz. 2007. Regulation of protrusion, adhesion dynamics, and polarity by myosins IIA and IIB in migrating cells. J Cell Biol. 176:573-580.

Wang, Y., N. Kakinuma, Y. Zhu, and R. Kiyama. 2006. Nucleo-cytoplasmic shuttling of human Kank protein accompanies intracellular translocation of beta-catenin. J Cell Sci. 119:4002-4010.

Wang, Y., and M.A. McNiven. 2012. Invasive matrix degradation at focal adhesions occurs via protease recruitment by a FAK-p130Cas complex. J Cell Biol. 196:375-385.

Wang, Y., Y. Onishi, N. Kakinuma, B.C. Roy, T. Aoyagi, and R. Kiyama. 2005. Alternative splicing of the human Kank gene produces two types of Kank protein. Biochem Biophys Res Commun. 330:1247-1253.

Wang, Y., X. Zhang, H. Zhang, Y. Lu, H. Huang, X. Dong, J. Chen, J. Dong, X. Yang, H. Hang, and T. Jiang. 2012. Coiled-coil networking shapes cell molecular machinery. Molecular Biology of the Cell. 23:3911-3922.

Wang, Y.L. 2007. Flux at focal adhesions: slippage clutch, mechanical gauge, or signal depot. Sci STKE. 2007:pe10.

Watanabe, N., T. Kato, A. Fujita, T. Ishizaki, and S. Narumiya. 1999. Cooperation between mDia1 and ROCK in Rho-induced actin reorganization. Nat Cell Biol. 1:136-143.

Watanabe, N., P. Madaule, T. Reid, T. Ishizaki, G. Watanabe, A. Kakizuka, Y. Saito, K. Nakao, B.M. Jockusch, and S. Narumiya. 1997. p140mDia, a mammalian homolog of Drosophila diaphanous, is a target protein for Rho small GTPase and is a ligand for profilin. Embo j. 16:3044-3056.

Watkins, A.M., M.G. Wuo, and P.S. Arora. 2015. Protein–Protein Interactions Mediated by Helical Tertiary Structure Motifs. Journal of the American Chemical Society. 137:11622-11630.

Weng, Z., Y. Shang, D. Yao, J. Zhu, and R. Zhang. 2018. Structural analyses of key features in the KANK1.KIF21A complex yield mechanistic insights into the cross-talk between microtubules and the cell cortex. J Biol Chem. 293:215-225.

Wickelgren, I. 1999. First components found for new kidney filter. Science. 286:225-226.

Winograd-Katz, S.E., R. Fässler, B. Geiger, and K.R. Legate. 2014. The integrin adhesome: from genes and proteins to human disease. Nature Reviews Molecular Cell Biology. 15:273-288.

Wolfenson, H., Y.I. Henis, B. Geiger, and A.D. Bershadsky. 2009. The heel and toe of the cell's foot: a multifaceted approach for understanding the structure and dynamics of focal adhesions. Cell Motil Cytoskeleton. 66:1017-1029.

Yang, J., L. Zhu, H. Zhang, J. Hirbawi, K. Fukuda, P. Dwivedi, J. Liu, T. Byzova, E.F. Plow, J. Wu, and J. Qin. 2014a. Conformational activation of talin by RIAM triggers integrin-mediated cell adhesion. Nat Commun. 5:5880.

Yang, Y., W.S. Lee, X. Tang, and W.G. Wadsworth. 2014b. Extracellular matrix regulates UNC-6 (netrin) axon guidance by controlling the direction of intracellular UNC-40 (DCC) outgrowth activity. PLoS One. 9:e97258.

Yao, M., B.T. Goult, H. Chen, P. Cong, M.P. Sheetz, and J. Yan. 2014. Mechanical activation of vinculin binding to talin locks talin in an unfolded conformation. Sci Rep. 4:4610.

Yoshigi, M., L.M. Hoffman, C.C. Jensen, H.J. Yost, and M.C. Beckerle. 2005. Mechanical force mobilizes zyxin from focal adhesions to actin filaments and regulates cytoskeletal reinforcement. J Cell Biol. 171:209-215.

Yu, M., S. Le, Y.C. Ammon, B.T. Goult, A. Akhmanova, and J. Yan. 2019. Force-Dependent Regulation of Talin-KANK1 Complex at Focal Adhesions. Nano Lett. 19:5982-5990.

1

Zaidel-Bar, R., S. Itzkovitz, A. Ma'ayan, R. Iyengar, and B. Geiger. 2007. Functional atlas of the integrin adhesome. Nat Cell Biol. 9:858-867.

Zhang, Y., H. Zhang, J. Liang, W. Yu, and Y. Shang. 2007. SIP, a novel ankyrin repeat containing protein, sequesters steroid receptor coactivators in the cytoplasm. EMBO J. 26:2645-2657.

Zhu, Y., N. Kakinuma, Y. Wang, and R. Kiyama. 2008. Kank proteins: a new family of ankyrin-repeat domain-containing proteins. Biochim Biophys Acta. 1780:128-133.

1

2

Talin-KANK1 interaction controls the recruitment of cortical microtubule stabilizing complexes to focal adhesions

Benjamin P Bouchet[1], Rosemarie E Gough[2], **York-Christoph Ammon**[1], Dieudonnée van de Willige[1], Harm Post[3,4,5,6], Guillaume Jacquemet[7], AF Maarten Altelaar[3,4,5,6], Albert JR Heck[3,4,5,6], Benjamin T Goult[2]*, Anna Akhmanova[1]*

1 Cell Biology, Department of Biology, Faculty of Science, Utrecht University, Utrecht, The Netherlands
2 School of Biosciences, University of Kent, Canterbury, United Kingdom
3 Biomolecular Mass Spectrometry and Proteomics, Utrecht University, Utrecht, The Netherlands
4 Bijvoet Center for Biomolecular Research, Utrecht University, Utrecht, The Netherlands
5 Utrecht Institute for Pharmaceutical Sciences, Utrecht University, Utrecht, The Netherlands
6 The Netherlands Proteomics Centre, Utrecht University, Utrecht, The Netherlands;
7 Turku Centre for Biotechnology, University of Turku, Turku, Finland

* Corresponding authors

Abstract

The cross-talk between dynamic microtubules and integrin-based adhesions to the extracellular matrix plays a crucial role in cell polarity and migration. Microtubules regulate the turnover of adhesion sites, and, in turn, focal adhesions promote the cortical microtubule capture and stabilization in their vicinity, but the underlying mechanism is unknown. Here, we show that cortical microtubule stabilization sites containing CLASPs, KIF21A, LL5β and liprins are recruited to focal adhesions by the adaptor protein KANK1, which directly interacts with the major adhesion component, talin. Structural studies showed that the conserved KN domain in KANK1 binds to the talin rod domain R7. Perturbation of this interaction, including a single point mutation in talin, which disrupts KANK1 binding but not the talin function in adhesion, abrogates the association of microtubule-stabilizing complexes with focal adhesions. We propose that the talin-KANK1 interaction links the two macromolecular assemblies that control cortical attachment of actin fibers and microtubules.

Introduction

Cell adhesions to the extracellular matrix support epithelial integrity and cell migration, and also provide signaling hubs that coordinate cell proliferation and survival (Hynes, 1992). Integrin-based adhesions (focal adhesions, FAs) are large macromolecular assemblies, in which the cytoplasmic tails of integrins are connected to the actin cytoskeleton. One of the major components of FAs is talin, a ~2500 amino acid dimeric protein, which plays a key role in adhesion formation by activating integrins (Anthis et al., 2009), coupling them to cytoskeletal actin (Atherton et al., 2015), regulating adhesion dynamics and recruiting different structural and signaling molecules (Calderwood et al., 2013; Gardel et al., 2010; Wehrle-Haller, 2012).

While the major cytoskeletal element associated with FAs is actin, microtubules also play an important role in adhesion by regulating the FA turnover (Akhmanova et al., 2009; Byron et al., 2015; Kaverina et al., 1999, 1998; Krylyshkina et al., 2003; Small and Kaverina, 2003; Stehbens and Wittmann, 2012; Yue et al., 2014). The recent proteomics work showed that microtubule-FA cross-talk strongly depends on the activation state of the integrins (Byron et al., 2015). Microtubules can affect adhesions by serving as tracks for delivery of exocytotic carriers (Stehbens et al., 2014), by controlling endocytosis required for adhesion disassembly (Ezratty et al., 2005; Theisen et al., 2012) and by regulating the local activity of signaling molecules such as Rho GTPases (for review, see [Kaverina and Straube, 2011; Stehbens and Wittmann, 2012]).

In contrast to actin, which is directly coupled to FAs, microtubules interact with the plasma membrane sites that surround FAs. A number of proteins have been implicated in microtubule attachment and stabilization in the vicinity of FAs. Among them are the microtubule plus end tracking proteins (+TIPs) CLASP1/2 and the spectraplakin MACF1/ACF7, which are targeted to microtubule tips by EB1, and a homologue of EB1, EB2, which binds to mitogen-activated protein kinase kinase kinase kinase 4 (MAP4K4) (Drabek et al., 2006; Honnappa et al., 2009; Kodama et al., 2003; Mimori-Kiyosue et al., 2005). The interaction of CLASPs with the cell cortex depends on the phosphatidylinositol 3, 4, 5-trisphosphate (PIP3)-interacting protein LL5β, to which CLASPs bind directly, and is partly regulated by PI-3 kinase activity (Lansbergen et al., 2006). Other components of the same cortical assembly are the scaffolding proteins liprin-a1 and b1, a coiled-coil adaptor ELKS/ERC1, and the kinesin-4 KIF21A (Lansbergen et al., 2006; van der Vaart et al., 2013). Both liprins and ELKS are best known for their role in organizing presynaptic secretory sites (Hida and Ohtsuka, 2010; Spangler and Hoogenraad, 2007); in agreement with this function, ELKS is required for efficient constitutive exocytosis in HeLa cells (Grigoriev et al., 2007, 2011). LL5β, liprins and ELKS form micrometer-sized cortical patch-like structures, which will be termed here cortical microtubule stabilization complexes, or CMSCs. The CMSCs are strongly enriched at the leading cell edges, where they localize in close proximity of FAs but do not overlap with them ([Lansbergen et al., 2006; van der Vaart et al., 2013], reviewed in [Astro and de Curtis, 2015]). They represent a subclass of the previously defined plasma membrane-associated platforms (PMAPs) (Astro and de Curtis, 2015), which have overlapping components such as liprins, but may not be necessarily involved in microtubule regulation, as is the case for liprin-ELKS complexes in neurons, where they are part of cytomatrix at the

active zone (Gundelfinger and Fejtova, 2012).

Several lines of evidence support the importance of the CMSC-FA cross-talk. In migrating keratinocytes, LL5β and CLASPs accumulate around FAs and promote their disassembly by targeting the exocytosis of matrix metalloproteases to FA vicinity (Stehbens et al., 2014). Furthermore, liprin-a1, LL5α/β and ELKS localize to protrusions of human breast cancer cells and are required for efficient cell migration and FA turnover (Astro et al., 2014). In polarized epithelial cells, LL5β and CLASPs are found in the proximity of the basal membrane, and this localization is controlled by the integrin activation state (Hotta et al., 2010). CLASP and LL5-mediated anchoring of MTs to the basal cortex also plays a role during chicken embryonic development, where it prevents the epithelial-mesenchymal transition of epiblast cells (Nakaya et al., 2013). LL5β, CLASPs and ELKS were also shown to concentrate at podosomes, actin-rich structures, which can remodel the extracellular matrix (Proszynski and Sanes, 2013). Interestingly, LL5β-containing podosome-like structures are also formed at neuromuscular junctions (Kishi et al., 2005; Proszynski et al., 2009; Proszynski and Sanes, 2013), and the complexes of LL5β and CLASPs were shown to capture microtubule plus ends and promote delivery of acetylcholine receptors (Basu et al., 2015, 2014; Schmidt et al., 2012).

While the roles of CMSCs in migrating cells and in tissues are becoming increasingly clear, the mechanism underlying their specific targeting to integrin adhesion sites remains elusive. Recently, we found that liprin-β1 interacts with KANK1 (van der Vaart et al., 2013), one of the four members of the KANK family of proteins, which were proposed to act as tumor suppressors and regulators of cell polarity and migration through Rho GTPase signaling (Gee et al., 2015; Kakinuma et al., 2008, 2009; Li et al., 2011; Roy et al., 2009). KANK1 recruits the kinesin-4 KIF21A to CMSCs, which inhibits microtubule polymerization and prevents microtubule overgrowth at the cell edge (Kakinuma and Kiyama, 2009; van der Vaart et al., 2013). Furthermore, KANK1 participates in clustering of the other CMSC components (van der Vaart et al., 2013).

Here, we found that KANK1 is required for the association of the CMSCs with FAs. The association of KANK1 with FAs depends on the KN domain, a conserved 30 amino acid polypeptide sequence present in the N-termini of all KANK proteins. Biochemical and structural analysis showed that the KN domain interacts with the R7 region of the talin rod. Perturbation of this interaction both from the KANK1 and the talin1 side prevented the accumulation of CMSC complexes around focal adhesions and affected microtubule organization around FAs. We propose that KANK1 molecules, recruited by talin to the outer rims of FA, serve as 'seeds' for organizing other CMSC components in the FA vicinity through multivalent interactions between these components. This leads to co-organization of two distinct cortical assemblies, FAs and CMSCs, responsible for the attachment of actin and microtubules, respectively, and ensures effective cross-talk between the two types of cytoskeletal elements.

Results

Identification of talin1 as a KANK1 binding partner

Our previous work showed that the endogenous KANK1 colocalizes with LL5β, liprins

and KIF21A in cortical patches that are closely apposed to, but do not overlap with FAs (van der Vaart et al., 2013). We confirmed these results both in HeLa cells and the HaCaT immortal keratinocyte cell line, in which CMSC components CLASPs and LL5β were previously shown to strongly cluster around FAs and regulate their turnover during cell migration (Stehbens et al., 2014) (Figure 1—figure supplement 1A,B). Inhibition of myosin-II with blebbistatin, which reduces tension on the actin fibers and affects the activation state of FA molecules, such as integrins and talin (Parsons et al., 2010), caused not only FA disassembly but also a strong reduction in clustering of CMSC components at the cell periphery (Figure 1—figure supplement 2A,B), as described previously (Stehbens et al., 2014). To investigate this effect in more detail, we partially inhibited contractility using a Rho-associated protein kinase 1 (ROCK1) inhibitor, Y-27632 (Oakes et al., 2012). In these conditions, the number of FAs was not affected although their size was reduced (Figure 1—figure supplement 2C–E). This treatment was sufficient to diminish CMSC clustering at the cell edge (Figure 1—figure supplement 2C,F). Interestingly, at the same time we observed a very significant increase in the overlap of KANK1 with FA adhesion markers (Figure 1—figure supplement 2C,G). Live imaging of KANK1 together with the FA marker paxillin showed a gradual redistribution of KANK1 into the areas occupied by FAs upon ROCK1 inhibitor-induced attenuation of contractility (Figure 1—figure supplement 2H, Video 1). These data indicate that the organization of CMSCs at the cell cortex might be controlled by interactions with tension-sensitive components of FAs.

To identify the domains of KANK1 required for cortical localization, we performed deletion mapping. KANK1 comprises an N-terminal KANK family-specific domain of unknown function, the KN domain (residues 30–68) (Kakinuma et al., 2009), a coiled coil region, the N-terminal part of which interacts with liprin-b1, and a C-terminal ankyrin repeat domain, which binds to KIF21A (van der Vaart et al., 2013), while the rest of the protein is predicted to be unstructured (Figure 1A). Surprisingly, the KN domain alone strongly and specifically accumulated within FAs (Figure 1B). A similar localization was also seen with a somewhat larger N-terminal fragment of KANK1, Nter, as well as the Nter-CC1 deletion mutant, which contained the first, liprin-b1-binding coiled coil region of KANK1 (Figure 1A,B). However, an even larger N-terminal part of KANK1, encompassing the whole coiled coil domain (Nter-CC) showed a pronounced enrichment at the FA rim (Figure 1A,B). The KANK1 deletion mutant missing only the C-terminal ankyrin repeat domain (ΔANKR) was completely excluded from FAs but accumulated in their immediate vicinity, similar to the full-length KANK1 (Figure 1A,B). A tight ring-like localization at the outer rim of FAs was also observed with a KANK1 mutant, which completely missed the coiled coil region but contained the ankyrin repeat domain (ΔCC), while the mutant which missed just the KN domain showed no accumulation around FAs (Figure 1A,B). To test whether the exclusion of larger KANK1 fragments from the FA core was simply due to the protein size, we fused GFP-tagged KN domain to the bacterial protein β-D-galactosidase (LacZ), but found that this fusion accumulated inside and not around FAs (Figure 1—figure supplement 3). Since GFP-KN-LacZ and GFP-KANK1-ΔANKRD have a similar size (1336 and 1400 amino acids, respectively), but one accumulates inside FAs, while the other is excluded to their periphery, this result suggests that features other than the mere protein size determine the specific localization
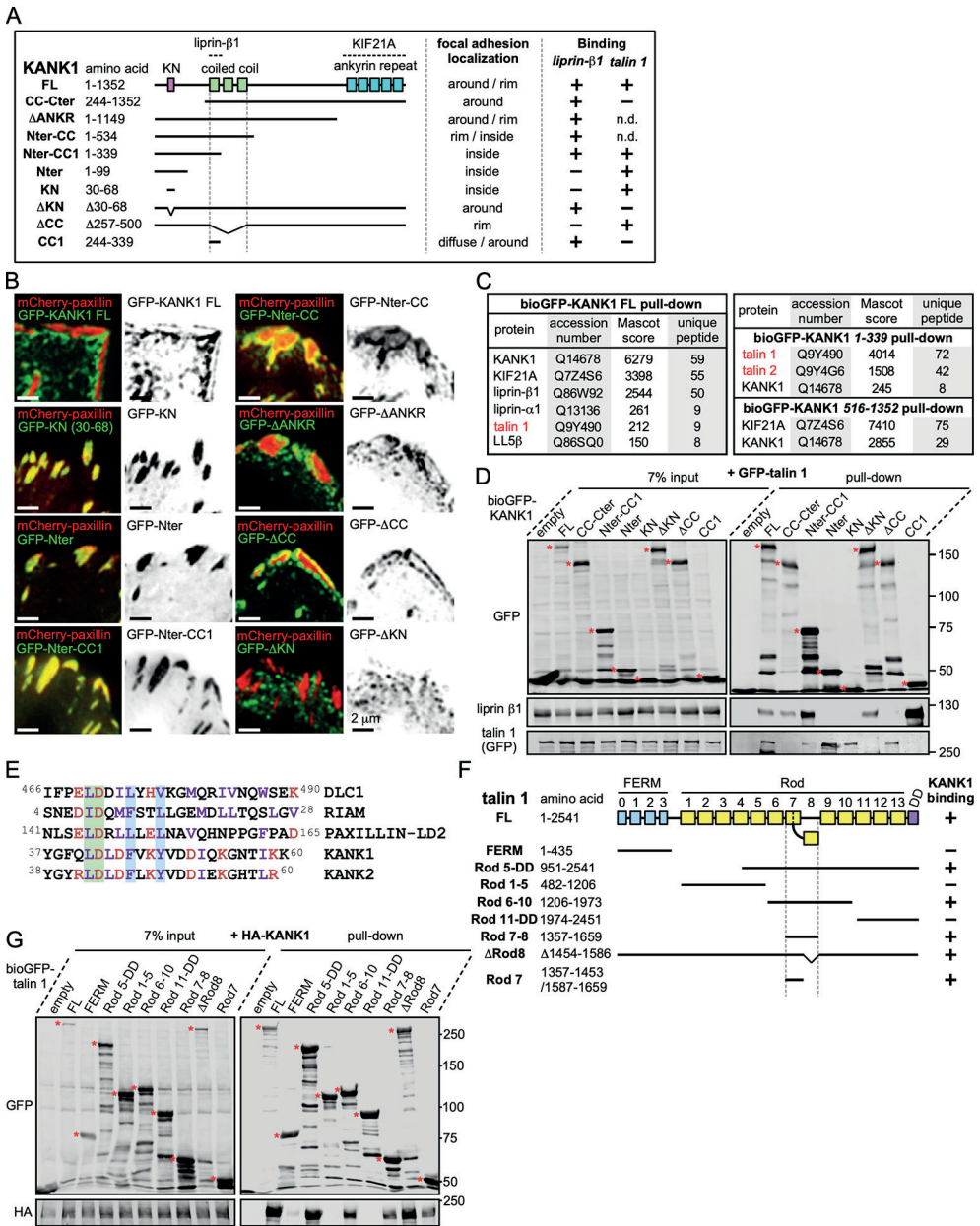
Figure 1. The KN motif of KANK1 interacts with the R7 domain of talin1

(**A**) Schematic representation of KANK1 and the deletion mutants used in this study, and the summary of their interactions and localization. N.d., not determined in this study. (**B**) TIRFM images of live HeLa cells transiently expressing the indicated GFP-tagged KANK1 deletion mutants together with the focal adhesion marker mCherry-paxillin. In these experiments, endogenous KANK1 and KANK2 were also expressed. (**C**) Identification of the binding partners of Bio-GFP-tagged KANK1 and its indicated deletion Figure 1 continued on next page mutants by using streptavidin pull down assays from HEK293T cells combined with mass spectrometry. (**D**) Streptavidin pull down assays with the BioGFP-tagged KANK1 or the indicated KANK1 mutants, co-expressed with GFP-talin1 in HEK293T cells, analyzed by Western blotting with the indicated antibodies. (**E**) Sequence alignment of KANK1 and KANK2 with the known

talin-binding sites of DLC1, RIAM and Paxillin. The LD-motif and the interacting hydrophobic residues are highlighted green and blue respectively. (**F**) Schematic representation of talin1 and the deletion mutants used in this study, and their interaction with KANK1. (**G**) Streptavidin pull down assays with the BioGFP-tagged talin1 or the indicated talin1 mutants, co-expressed with HA-KANK1 in HEK293T cells, analyzed by Western blotting with the indicated antibodies.

of KANK1 to the FA rim. We conclude that the KN domain of KANK1 has an affinity for FAs, but the presence of additional KANK1 sequences prevents the accumulation of the protein inside FAs and instead leads to the accumulation of KANK1 at the FA periphery. To identify the potential FA-associated partners of KANK1, we co-expressed either full-length KANK1 or its N-terminal and C-terminal fragments fused to GFP and a biotinylation (Bio) tag together with biotin ligase BirA in HEK293T cells and performed streptavidin pull down assays combined with mass spectrometry. In addition to the already known binding partners of KANK1, such as KIF21A, liprins and LL5β, we identified talin1 among the strongest hits (Figure 1C). Talin2 was also detected in a pull down with the KANK1 N-terminus though not with the full-length protein (Figure 1C). The interaction between KANK1 and talin1 was confirmed by Western blotting, and subsequent deletion mapping showed that the talin1-binding region of KANK1 encompasses the KN domain (Figure 1A,D), while liprin-β1 binds to the N-terminal part of the coiled coil domain, as shown previously (van der Vaart et al., 2013).

Sequence analysis of the KN domain showed that it is predicted to form a helix and contains a completely conserved leucine aspartic acid-motif (LD-motif) (Alam et al., 2014; Zacharchenko et al., 2016). The LD-motifs in RIAM (Goult et al., 2013), DLC1 and Paxillin (Zacharchenko et al., 2016) have recently been identified as talin-binding sites that all interact with talin via a helix addition mechanism. Alignment of the KN domain of KANK with the LD-motif of DLC1, RIAM and Paxillin (Zacharchenko et al., 2016) revealed that the hydrophobic residues that mediate interaction with talin are present in the KN domain (Figure 1E).

Using deletion analysis, we mapped the KANK1-binding site of talin1 to the central region of the talin rod, comprising the R7-R8 domains (Figure 1F). This R7-R8 region of talin is unique (Gingras et al., 2010), as the 4-helix bundle R8 is inserted into a loop of the 5-helix bundle R7, and thus protrudes from the linear chain of 5-helix bundles of the talin rod (Figures 1F, 2A). This R8 domain serves as a binding hub for numerous proteins including vinculin, synemin and actin (Calderwood et al., 2013). R8 also contains a prototypic recognition site for LD-motif proteins, including DLC1 (Figure 2B), Paxillin and RIAM (Zacharchenko et al., 2016). Based on the presence of the LD-binding site, we anticipated that KANK1 would also interact with R8. However, deletion mapping revealed that KANK1 in fact binds to the talin1 rod domain R7 (Figure 1F,G), suggesting that KANK1 interacts with a novel binding site on talin1.

Structural characterization and mutational analysis of the KANK1-talin1 complex
To explore the interaction between talin1 and KANK1 in more detail, we used NMR chemical shift mapping using 15N-labeled talin1 R7-R8 (residues 1357–1653) and a synthetic KANK1 peptide of the KN domain, KANK1(30–60). The addition of the KANK1(30–60) peptide resulted in large spectral changes (Figure 2C), most of which were in the slow exchange regime on the NMR timescale indicative of a tight interaction.
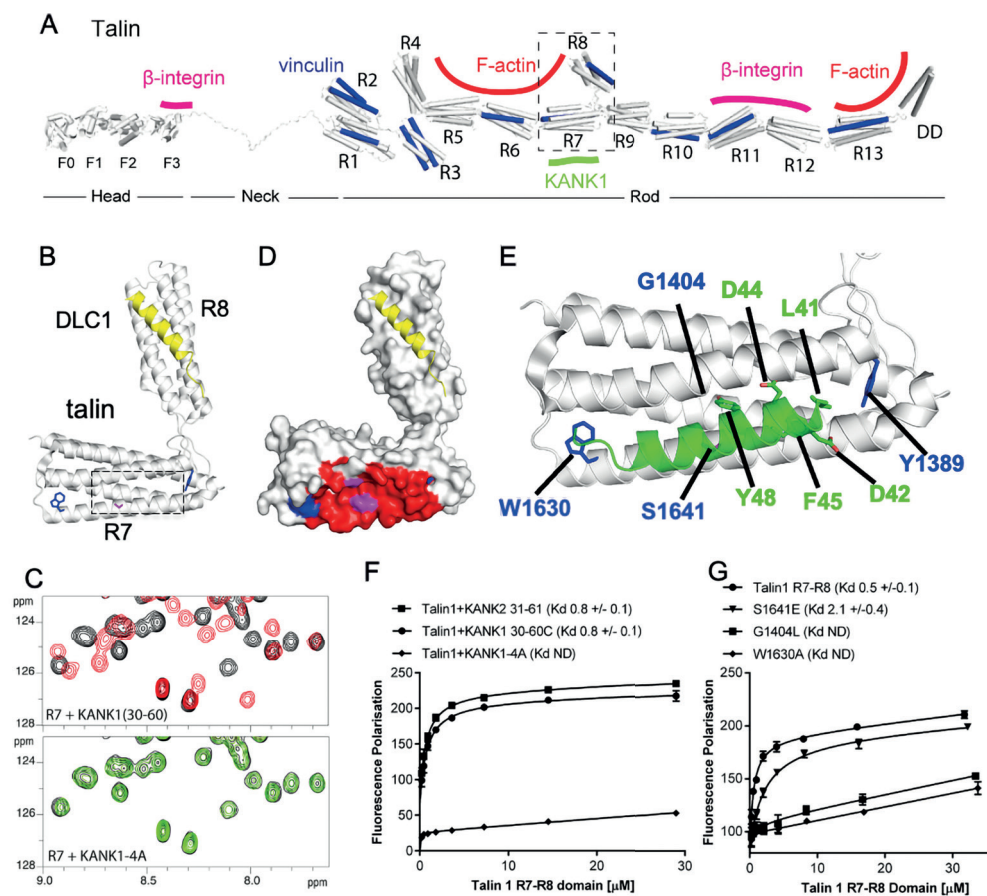
2

Figure 2. Biochemical and structural characterization of the Talin-KANK interaction
(**A**) Schematic representation of Talin1, with F-actin, β-integrin and vinculin binding sites highlighted. The KANK1 binding site on R7 is also shown. (**B**) The structure of the complex between talin1 R7-R8 (white) and the LD-motif of DLC1 (yellow) bound on the R8 subdomain (PDB ID. 5FZT, [Zacharchenko et al., 2016]). Residues W1630 and Y1389 (blue) and S1641 (magenta) are highlighted. (**C–D**) The KANK KN domain binds to a novel site on talin R7. 1H,15N HSQC spectra of 150 mM 15N-labelled talin1 R7 (residues 1357–1659 D1454–1586) in the absence (black) or presence of KANK1(30–68)C peptide (red) (top panel) or KANK1-4A (green) (bottom panel) at a ratio of 1:3. (**D**) Mapping of the KANK1 binding site on R7 as detected by NMR using weighted chemical shift differences (red) – mapped onto the R7-R8 structure in (B). Residues W1630 and Y1389 (blue) and G1404 and S1641 (magenta) are highlighted. (**E**) Structural model of the talin1:KANK1 interface. Ribbon representation of the KANK1 binding site, comprised of the hydrophobic groove between helices 29 and 36 of R7. Two bulky conserved residues, W1630 and Y1389 (blue) hold these two helices apart forming the binding interface. A small glycine side chain (G1404) creates a pocket between the helices. S1641 (magenta) has been shown previously to be a phosphorylation site (Ratnikov et al., 2005). The KN peptide (green) docked onto the KANK binding surface. (**F–G**) Biochemical characterization of the talin:KANK interaction. (F) Binding of BODIPY-labeled KANK1(30–60) C, KANK2(31–61)C and KANK1-4A peptides to Talin1 R7-R8 (1357–1659) was measured using a Fluorescence Polarization assay. (G) Binding of BODIPY-labeled KANK1(30–60)C to wild type R7-R8, R7-R8 S1641E, R7-R8 G1404L and R7-R8 W1630A. Dissociation constants ± SE (mM) for the interactions are indicated in the legend. All measurements were performed in triplicate. ND, not determined.

In agreement with the pull down data, the signals that shifted in slow exchange upon the addition of KANK1(30–60) mapped largely onto the R7 domain with only small progressive shift changes evident on R8. To validate R7 as the major KANK1-binding site on talin, we repeated the NMR experiments using the individual domains, R8 (residues 1461–1580) and R7 (residues 1359–1659 D1454–1586). Addition of KANK1(30–60) induced small chemical shift changes on the R8 domain indicative of a weak interaction (most likely due to the interaction of LD with the LD-recognition box on R8). However, the addition of a 0.5 molar ratio of KANK1(30–60) to R7 induced large spectral changes with many of the peaks displaying two locations, corresponding to the free peak position and the bound peak position. This is indicative of slow-exchange and confirms a high affinity interaction between R7 and KANK1. The KN peptide is the first identified ligand for the R7 domain.

NMR chemical shifts also provide information on the residues involved in the interaction, as the peaks in the 15N-HSQC spectrum pertain to individual residues in the protein. To map these chemical shift changes onto the structure of R7-R8, it was first necessary to complete the backbone chemical shift assignments of the R7 domain. This was achieved using conventional triple resonance experiments as described previously (Banno et al., 2012), using 13C,15N labeled R7. The chemical shift changes mapped predominantly onto one face of R7, comprised of helices 2 and 5 of the 5-helix bundle (talin rod helices 29 and 36), as shown in Figure 2D–E.

Our recent elucidation of the interaction between the LD-motif of DLC1 and talin R8 has generated insight into how LD-motifs are recognized by helical bundles (PDB ID. 5FZT, [Zacharchenko et al., 2016]). In the DLC1:talin R8 complex the DLC1 peptide adopts a helical conformation that packs against two helices on the side of the helical bundle. It is becoming increasingly clear that other LD-motif proteins bind to talin through a similar interaction mode (Zacharchenko et al., 2016). The surface of α2 and α5 on R7 forms a hydrophobic groove that the KANK1 helix docks into. A striking feature of this KANK1 binding surface is that the two helices are held apart by the conserved aromatic residues, W1630 at the end of α5 and Y1389 at the end of α2 (Figure 2B,E). W1630 and Y1389 thus essentially serve as molecular rulers, separating helices α2 and α5 by ~8A° (compared with ~5–6A° for the other bundles in R7-R8). The spacing between the two helices is enhanced further as the residues on the inner helical faces, S1400, G1404, S1411 on α2 and S1637 and S1641 on α5, have small side chains which have the effect of creating two conserved pockets midway along the hydrophobic groove of the KANK1-binding site (Figure 2E).

The talin-binding site on KANK1 is unusual as it contains a double LD-motif, LDLD. The structure of R7 revealed a potential LD-recognition box with the positive charges, K1401 and R1652 positioned on either side to engage either one, or both, of the aspartic residues. Using the docking pro- gram HADDOCK (van Zundert et al., 2016), we sought to generate a structural model of the KANK1/R7 complex, using the chemical shift mapping on R7 and a model of KANK1(30–60) as a helix (created by threading the KANK1 sequence onto the DLC1 LD-motif helix). This analysis indi- cated that the KANK-LD helix can indeed pack against the sides of α2 and α5 (Figure 2E). Interestingly, all of the models, irrespective of which way the KANK1 helix ran along the surface, positioned the bulky aromatic residue, Y48 in KANK1, in the hydrophobic

pocket created by G1404. This raised the possibility that mutation of G1404 to a bulky hydrophobic residue might block KANK1 binding by preventing Y48 engagement. We also noticed that S1641, one of the small residues that create the pocket, has been shown to be phosphorylated in vivo (Ratnikov et al., 2005) and might have a regulatory function in the KANK1-talin1 interaction.

To test these hypotheses, we generated a series of point mutants in talin R7 and also in the KANK1 KN-domain, designed to disrupt the talinR7/KANK1 interaction. On the KANK1 side, we mutated the LDLD motif to AAAA, (the KANK1-4A mutant), while on the talin1 side, we generated a series of R7 mutants. These included G1404L, in which a bulky hydrophobic residue was introduced instead of glycine to occlude the hydrophobic pocket in R7, S1641E, a phosphomimetic mutant aimed to test the role of talin phosphorylation in regulating KANK1 binding, and W1630A, a substitution that would remove one of the molecular rulers holding α2 and α5 helices apart at a fixed distance. These mutants were introduced into talin1 R7-R8 and the structural integrity of the mutated proteins confirmed using NMR (Figure 2—figure supplement 1). The relative binding affinities were measured using an *in vitro* fluorescence polarization assay. In this assay, the KANK1(30–60) peptide is fluorescently labeled with BODIPY and titrated with an increasing concentration of talin R7-R8, and the binding between the two polypeptides results in an increase in the fluorescence polarization signal (Figure 2F). The KANK1-4A mutant abolished binding to talin (Figure 2C,F). The S1641E mutant had only a small effect on binding (Figure 2G), suggesting that either talin1 phosphorylation does not play a major role in modulating the interaction with KANK1 or that the S-E mutation is not a good phosphomimetic, possibly because phosphorylation might also affect helix formation integrity, an effect not mimicked by a single aspartate residue. However, strikingly, both the W1630A and the G1404L mutants abolished binding of KANK1 to talin R7 (Figure 2G), confirming the validity of our model. Finally, we also tested whether the KN-R7 interaction is conserved in talin2 and KANK2, and found that this was indeed the case (Figure 2—figure supplement 2). We conclude that the conserved KN domain of KANKs is a talin-binding site.

Talin1-KANK1 interaction controls cortical organization of CMSC components

Next, we set out to test the importance of the identified interactions in a cellular context by using the KANK1-4A and the talin G1404L mutants. We chose the G1404L talin mutant over W1630A for our cellular studies, because removing the bulky tryptophan from the hydrophobic core of the R7 might have the off target effect of perturbing the mechanical stability of R7, and our recent studies showed that the mechanostability of R7 is important for protecting R8 from force-induced talin extension (Yao et al., 2016). As could be expected based on the binding experiments with purified protein fragments, the 4A mutation reduced the interaction of the full-length KANK1 with talin1 in a pull-down assay (Figure 3A). An even stronger reduction was observed when KANK-ΔCC or the KN alone were tested (Figure 3A). Furthermore, the introduction of the G1404L mutation abrogated the interaction of full-length talin1 or its R7 fragment with full-length KANK1 (Figure 3B).

To investigate the localization of KANK1-4A, we used HeLa cells depleted of endogenous KANK1 and KANK2, the two KANK isoforms present in these cells based
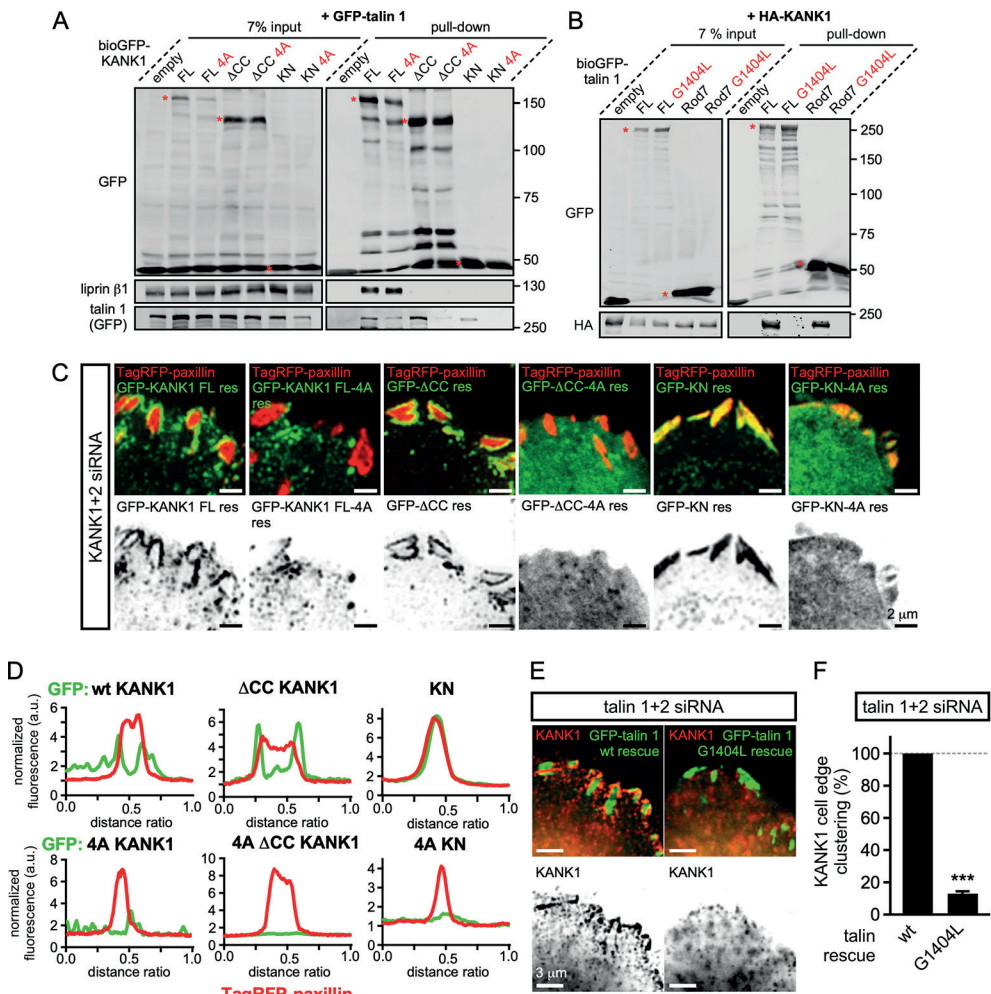
Figure 3. KANK1-talin interaction is required for recruiting KANK1 to FAs

(**A**) Streptavidin pull-down assays with the BioGFP-tagged KANK1 or the indicated KANK1 mutants, co-expressed with GFP-talin1 in HEK293T cells, analyzed by Western blotting with the indicated antibodies. (**B**) Streptavidin pull down assays with the BioGFP-tagged talin1 or the indicated talin1 mutants, co-expressed with HA-KANK1 in HEK293T cells, analyzed by Western blotting with the indicated antibodies. (**C**) TIRFM images of live HeLa cells depleted of KANK1 and KANK2 and co-expressing the indicated siRNA- resistant GFP-KANK1 fusions and TagRFP-paxillin. (**D**) Fluorescence profile of GFP-tagged mutants and TagRFP-paxillin based on line scan measurement across the FA area in TIRFM images as in panel (C). (**E**) Widefield fluorescence images of HeLa cells depleted of endogenous talin1 and talin2, rescued by the expression of the wild type GFP-tagged mouse talin1 or its G1404L mutant and labeled for endogenous KANK1 by immunofluorescence staining. (**F**) Quantification of peripheral clustering of KANK1 in cells treated and analyzed as in (E) (n=12, 6 cells per condition). Error bar, SEM; ***p<0.001, Mann-Whitney U test.

on our proteomics studies (van der Vaart et al., 2013) (Figure 3—figure supplement 1A), in order to exclude the potential oligomerization of the mutant KANK1 with the endogenous proteins. Rescue experiments were performed using GFP-KANK1, resistant for the used siRNAs due to several silent mutations (van der Vaart et al., 2013), or its 4A mutant. We also included in this analysis a KANK1 mutant lacking the liprin-β1-

binding coiled coil domain (the ΔCC deletion mutant, Figure 1A), and the 4A-version of the KANK1-ΔCC deletion mutant. Total Internal Reflection Fluorescence Microscopy (TIRFM)-based live imaging showed that, consistent with our previous results, the GFP-tagged wild type KANK1 strongly accumulated in cortical patches that were tightly clustered around FAs (Figure 3C,D). The KANK1-ΔCC mutant, which lacked the liprin-β1-binding site but contained an intact KN motif, showed highly specific ring-like accumulations at the rims of FAs (Figure 3C,D). In contrast, KANK1- 4A was not clustered anymore around FAs but was dispersed over the cell cortex (Figure 3C,D). The KANK1-ΔCC-4A mutant, lacking both the liprin-β1 and the talin-binding sites, and the KN-4A mutant were completely diffuse (Figure 3C,D).

To test the impact of the talin1-G1404L mutant, we depleted both talin1 and talin2, which are co- expressed in HeLa cells (Figure 3—figure supplement 1B), and rescued them by introducing mouse GFP-talin1, which was resistant to used siRNAs. The depletion of the two talin proteins resulted in a dramatic loss of FAs and cell detachment from coverslips (data not shown), in agreement with the well-established essential role of talin1 in FA formation (Calderwood et al., 2013; del Rio et al., 2009; Yan et al., 2015; Yao et al., 2014). Therefore, in this experiment only cells expressing GFP- talin1 displayed normal attachment and spreading (Figure 3—figure supplement 1C). The GFP- talin1-G1404L mutant could fully support cell attachment and spreading, although the cell area was slightly increased compared to cells rescued with the wild type GFP-talin1 (Figure 3—figure supple- ment 1C–E). The number and size of focal adhesions were not significantly different between the cells rescued with the wild type talin1 or its G1404L mutant (Figure 3—figure supplement 1F,G), indicating that the mutant is functional in supporting FA formation. Strikingly, while in cells expressing the wild-type talin1, KANK1 was prominently clustered around FAs, it was dispersed over the plasma membrane in cells expressing talin1-G1404L (Figure 3E,F, Figure 1—figure supplement 1). We conclude that perturbing the KANK1-talin interaction, including the use of a single point mutation in the ~2500 amino acid long talin1 protein, which does not interfere with the talin function in FA formation, abrogates KANK1 association with FAs.

We next tested whether mislocalization of KANK1 due to the perturbation of KANK1-talin1 binding affected other CMSC components. The localization of GFP-KANK1 and its mutants relative to FAs labeled with endogenous markers was very similar to that described above based on live imaging experiments (Figure 4A). Co-depletion of KANK1 and KANK2 abolished clustering of CMSC components, such as LL5β and KIF21A at the cell edge (Figure 4B,C). Wild type GFP-KANK1 could rescue cortical clustering of these proteins in KANK1 and KANK2-depleted cells (Figure 4B,C). How- ever, this was not the case for the KANK1-4A mutant, the KANK1-ΔCC mutant or the KANK1 version bearing both mutations (Figure 4B,C). Importantly, the dispersed puncta of the KANK1-4A mutant still colocalized with LL5β, as the binding to liprin-β1 was intact in this mutant (Figure 3A, Figure 4B,C), while the FA-associated rings of KANK1-ΔCC, the mutant deficient in liprin-β1 binding, showed a mutually exclusive localization with LL5β (Figure 4B). In contrast, KIF21A, which binds to the ankyrin repeat domain of KANK1, could still colocalize with KANK1-ΔCC at FA rims (Figure 4B). The overall accumulation of KIF21A at the cell periphery was, however, reduced,
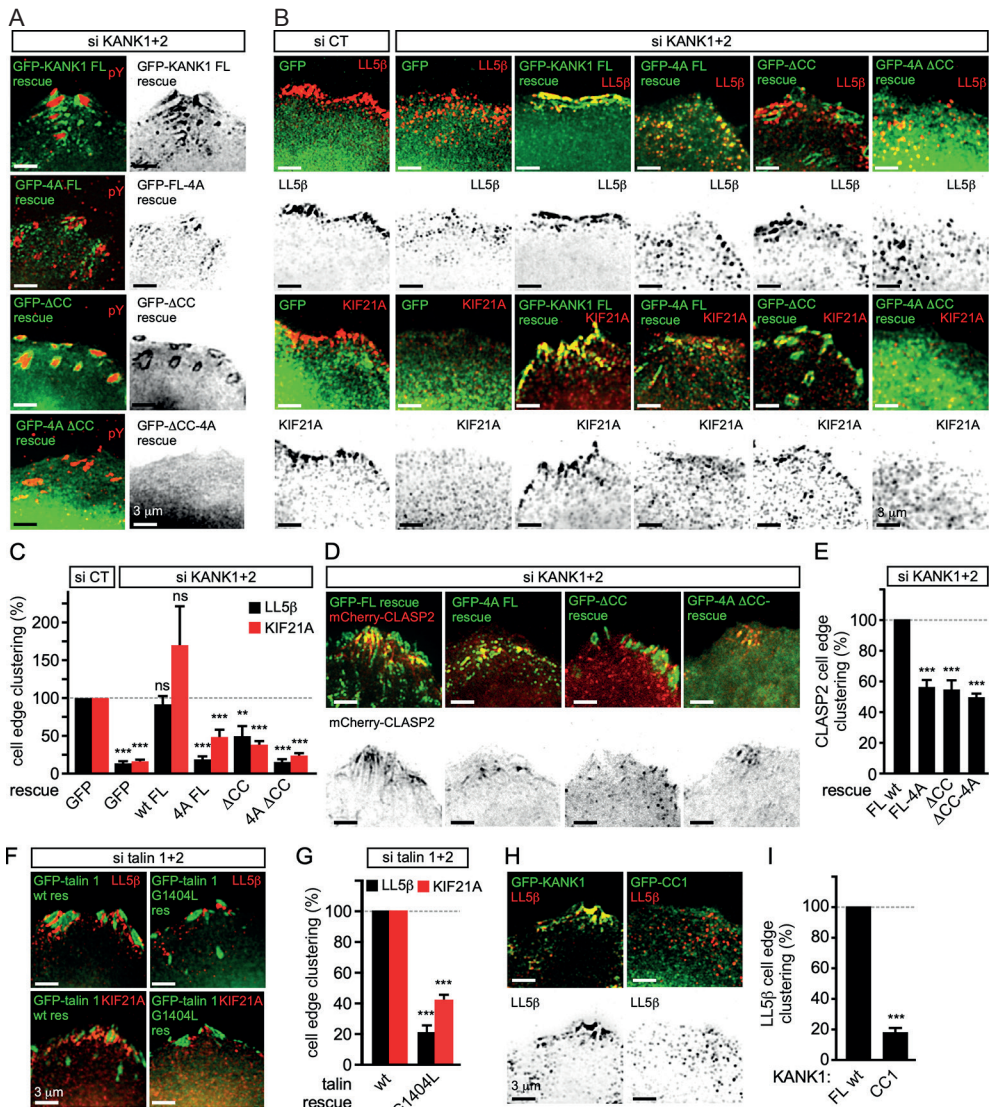
Figure 4. KANK1-talin interaction is required for recruiting CMSCs to FAs.
(**A**) Widefield fluorescence images of HeLa cells depleted of KANK1 and KANK2 and expressing the indicated siRNA-resistant GFP-KANK1 fusions (rescue), stained for the FA marker phospho-tyrosine (pY). (**B**) Widefield fluorescence images of HeLa cells transfected with the control siRNA or siRNAs against KANK1 and KANK2, expressing GFP alone or the indicated siRNA-resistant GFP-KANK1 fusions and stained for LL5β or KIF21A. (**C**) Quantification of peripheral clustering of LL5β and KIF21A in cells treated as in panel (B) (n=12, 5–6 cells per condition). (**D**) TIRFM images of live HeLa cells depleted of KANK1 and KANK2 and co-expressing the indicated siRNA-resistant GFP-KANK1 fusions and mCherry-CLASP2. (**E**) Quantification of peripheral clustering of mCherry-CLASP2 in cells treated as in panel (D) (n=20, 8 cells per condition). (**F**) Widefield fluorescence images of HeLa cells transfected with the indicated GFP-KANK1 fusions and stained for endogenous LL5β. (**G**) Quantification of peripheral clustering of LL5β in cells treated as in panel (F) (n=12, 6 cells per condition). (**H**) Widefield fluorescence images of HeLa cells transfected with GFP-tagged KANK1 or its CC1 mutant and stained for LL5β. (**I**) Quantification of peripheral clustering of LL5β cells treated as in panel (H) (n=12, 6 cells per condition). Error bars, SEM; ns, non-significant; **p<0.005; ***p<0.001, Mann-Whitney U test.

in line with the strongly reduced KANK1 peripheral clusters observed with the KANK1-ΔCC mutant. The diffuse localization of the KANK1-4A-ΔCC mutant led to the strongly dispersed distribution of the CMSC markers (Figure 4B,C). Furthermore, only the full-length wild type KANK1, but neither the 4A nor ΔCC mutant could support efficient accumulation of CLASP2 at the peripheral cell cortex in KANK1 and KANK2-depleted cells (Figure 4D,E), in line with the fact that cortical recruitment of CLASPs depends on LL5β (Lansbergen et al., 2006).

Next, we investigated whether disrupting the KANK1-talin1 interaction from the talin1 side would affect also CMSC localization and found that this was indeed the case: both LL5β and KIF21A were clustered around FAs in talin1 and talin2-depleted cells rescued with the wild type GFP-talin1, but not in the cells expressing the GFP-talin1-G1404L mutant, deficient in KANK1 binding (Figure 4F,G).

Our data showed that KANK1-ΔCC could not support proper clustering of CMSC components at the cell edge in spite of its tight accumulation at the FA rims. These data indicate that in addition to binding to talin1, the localization of CMSC clusters depends on the KANK1-liprin-β1 connection. This notion is supported by the observation that the overexpressed coiled coil region of KANK1 (CC1), which can compete for liprin-β1 binding but cannot interact with talin1, acted as a very potent dominant negative, which suppressed accumulation of LL5β at the cell periphery (Figure 4H,I). We conclude that the core CMSC protein LL5β as well as the microtubule-binding CMSC components KIF21A and CLASP2 depend on the KANK1 interaction with both talin1 and liprin-β1 for their efficient clustering in the vicinity of focal adhesions at the cell periphery.

Disruption of KANK1-talin1 binding perturbs microtubule plus end organization at the cell periphery

We next investigated the impact of the disruption of KANK1-talin1 interaction on microtubule organization. Due to their stereotypic round shape, HeLa cells represent a particularly convenient model for studying the impact of CMSCs on the distribution and dynamics of microtubule plus ends (Lansbergen et al., 2006; Mimori-Kiyosue et al., 2005; van der Vaart et al., 2013). In this cell line, microtubules grow rapidly in the central parts of the cell, while at the cell margin, where CMSCs cluster in the vicinity of peripheral FAs, microtubule plus ends are tethered to the cortex and display persistent but slow growth due to the combined action of several types of microtubule regulators, including CLASPs, spectraplakins and KIF21A (Drabek et al., 2006; Mimori-Kiyosue et al., 2005; van der Vaart et al., 2013). This type of regulation prevents microtubule overgrowth at the cell edge and results in an orderly arrangement of microtubule plus ends perpendicular to the cell margin (van der Vaart et al., 2013) (Figure 5A). In cells with perturbed CMSCs, microtubule plus ends at the cell periphery become disorganized: the velocity of their growth at the cell margin increases, and their orientation becomes parallel instead of being perpendicular to the cell edge (van der Vaart et al., 2013) (Figure 5A).

Using live cell imaging of the microtubule plus end marker EB3-mRFP in KANK1/2 depleted cells rescued with the wild-type GFP-KANK1, we could indeed show that microtubule plus end growth velocity was almost 2.5 times slower at the cell margin compared to the central part of the cell, and the majority of microtubules at the cell
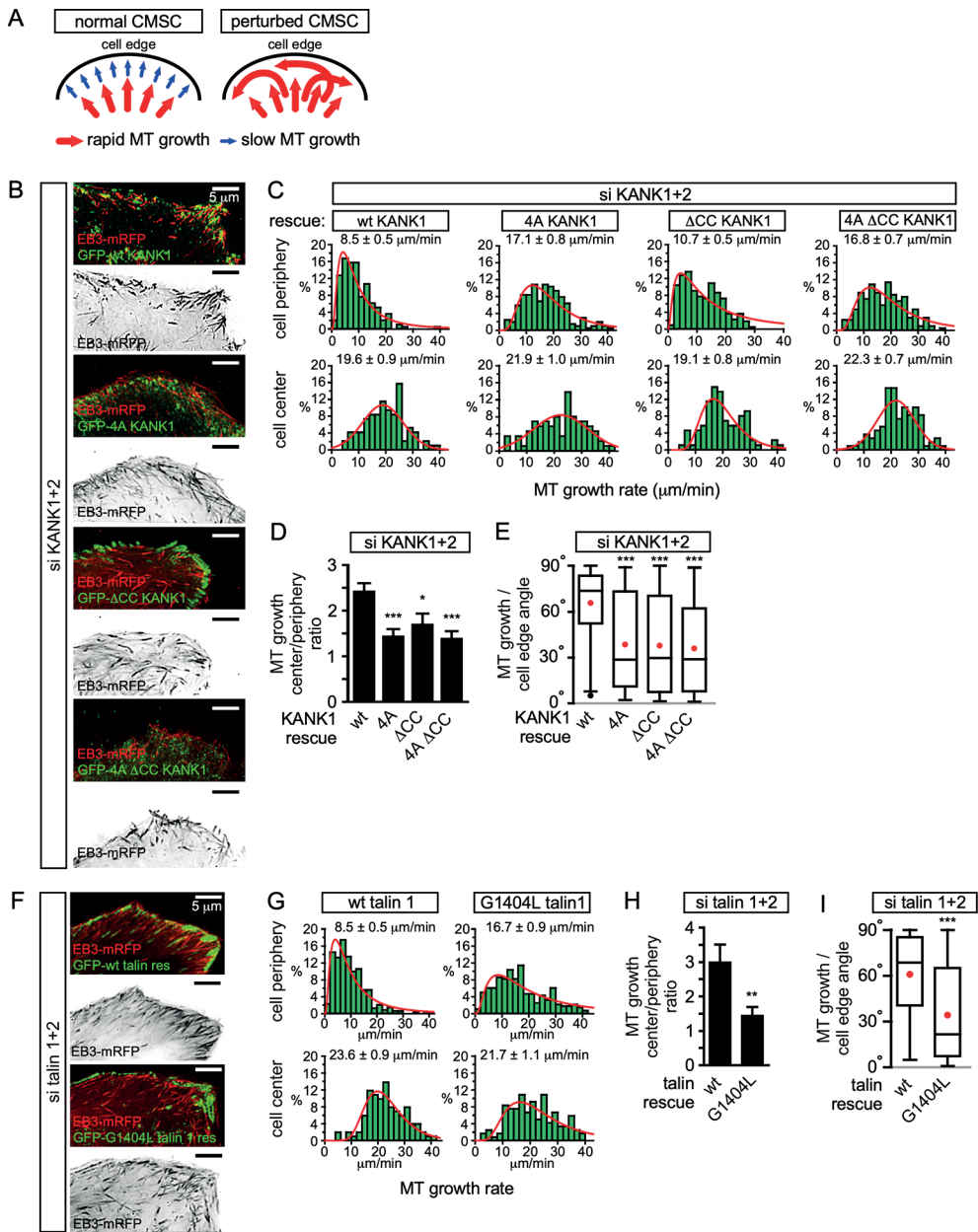
Figure 5. The role of talin-KANK1 interaction in regulating microtubule plus end dynamics around FAs

(**A**) Schematic representation of the pattern of microtubule growth in control HeLa cells and in cells with perturbed CMSCs, based on (van der Vaart et al., 2013). (**B**) TIRFM images of live HeLa cells depleted of KANK1 and KANK2 and co-expressing the indicated siRNA-resistant GFP-KANK1 fusions and EB3-mRFP. Images are maximum intensity projection of 241 images from time lapse recording of both fluorescence channels. (**C**) Distributions of microtubule growth rates at the 3 mm broad cell area adjacent to the cell edge, and in the central area of the ventral cortex for the cells treated as described in (B) (n=87–153, 7–8 cells). (**D**) Ratio of microtubule growth rate in the cell center and at the cell edge for the cells treated as described in B (n=7–8 cells). (**E**) Angles of microtubule growth relative to the cell

margin for the cells treated as described in B. Box plots indicate the 25th percentile (bottom boundary), median (middle line), mean (red dots), 75th percentile (top boundary), nearest observations within 1.5 times the interquartile range (whiskers) and outliers (black dots) (n=93–114, 7– 8 cells). (**F**) TIRFM images of live HeLa cells depleted of talin1 and talin 2 and co-expressing the indicated GFP-talin1 fusions and EB3-mRFP. Images are maximum intensity projection of 241 images from time lapse recordings of both fluorescence channels. (**G**) Distributions of microtubule growth rates at the 3 mm broad cell area adjacent to the cell edge, and in the central area of the ventral cortex for the cells treated as described in F (n=88–154, 7 cells). (**H**) The ratio of microtubule growth rate in the cell center and at the cell edge for the cells treated as described in panel (F) (n=7 cells). (I) Angles of microtubule growth relative to the cell margin for the cells treated as described in F. Box plots as in (E) (n=155–166, 10 cells). In all plots: error bars, SEM; ns, non-significant; **p<0.01; **p<0.005; ***p<0.001, Mann-Whitney U test.

margin grew at a 60–80˚angle to the cell edge (Figure 5B–E). In the KANK1/2 depleted cells expressing KANK1 mutants, the velocity of microtubule growth in central cell regions was not affected, but the growth rate at the cell periphery increased, and microtubules were growing at oblique angles to the cell margin (Figure 5B–E). The increase of the microtubule growth rate observed with the GFP-KANK1-ΔCC mutant was less strong than with the two 4A mutants (Figure 5B–E). This can be explained by the fact that GFP-KANK1-ΔCC was strongly clustered at FA rims (Figure 3C, Figure 5B), and, through its ankyrin repeat domain, could still recruit some KIF21A, a potent microtubule polymerization inhibitor (van der Vaart et al., 2013).

The results with rescue of talin1 and talin2 co-depletion with GFP-talin1 or its G1404L mutant fully supported the conclusions obtained with the KANK1-4A mutant: while in GFP-talin1-expressing cells microtubule growth at the cell edge was three fold slower than in the cell center, only a 1.5 fold difference was observed in GFP-talin1-G1404L expressing cells, and the proportion of microtubules growing parallel rather than perpendicular to the cell edge greatly increased (Figure 5F–I). We conclude that a single point mutation in talin1, which does not interfere with FA formation, is sufficient to perturb CMSC clustering and, as a consequence, induce microtubule disorganization in the vicinity of peripheral FAs.

Discussion

In this study, we have shown that the conserved KN motif of KANK1 represents an LD-type ligand of talin, which allows this adaptor protein to accumulate in the vicinity of integrin-based adhesions. This function is likely to be conserved in the animal kingdom, as the KANK orthologue in *C. elegans*, Vab-19, in conjunction with integrins, plays important roles in a dynamic cell-extracellular matrix adhesion developmental process (Ihara et al., 2011). The exact impact of KANK1-talin binding likely depends on the specific system, as the loss of KANK proteins was shown to reduce motility of HeLa cells and podocytes (Gee et al., 2015; Li et al., 2011), but promote insulin-dependent cell migration in HEK293 cells (Kakinuma et al., 2008).

An important question is how KANK-talin1 binding mediates the localization of KANK1 to the rim but not the core of FAs. One possibility, suggested by our deletion analysis of KANK1, is that while the KN peptide alone can penetrate into FAs, larger KN-containing protein fragments are sterically excluded from the dense actin-containing core of the FA. However, our experiment with the KN-LacZ fusion did not support this simple

idea, indicating that the underlying mechanism is likely to be more complex and might involve specific disordered or ordered domains and additional partners of KANK1, or other regulatory mechanisms. Interestingly, we found that reducing contractility with a ROCK1 inhibitor caused an increase in overlap of KANK1 with FA markers, suggesting that the interaction between KANK1 and talin might be mechanosensitive. An exciting possibility is that full length KANK1 can efficiently interact only with talin molecules at the periphery of focal adhesions because they are not fully incorporated into the focal adhesion structure and are thus less stretched. The KANK1 binding site on talin R7 overlaps with the high affinity actin binding site in talin (which spans R4-R8) (Atherton et al., 2015) and it is possible that different conformational populations of talin exist within adhesions and link to different cytoskeletal components.

Another important question is how KANK1 binding to the rim of focal adhesions can promote CMSC accumulation around these structures, a spatial arrangement in which most of the CMSC mol- ecules cannot be in a direct contact with FAs. Previous work on CMSC complexes showed that they are formed through an intricate network of interactions. The 'core' components of these complexes, which can be recruited to the plasma membrane independently of each other, are LL5β (and in some cells, its homologue LL5α), liprins and KANKs (of which KANK1 seems to predominate in HeLa cells) (Astro and de Curtis, 2015; Hotta et al., 2010; Lansbergen et al., 2006; van der Vaart et al., 2013) (Figure 6A). The clustering of CMSC components is mutually dependent and relies on homo- and heterodimerization of liprins α1 and β1, the association between KANK1 and liprin-β1, the scaffolding protein ELKS, which binds to both LL5β and liprin-α1, and possibly additional interactions (Astro and de Curtis, 2015; Lansbergen et al., 2006; van der Vaart et al., 2013), while the microtubule-binding proteins, such as CLASPs and KIF21A, seem to associate as a second 'layer' with the membrane-bound CMSC-assemblies (Figure 6A). The CMSC 'patches' can remain relatively stable for tens of minutes, while their individual components are dynamic and exchange with different, characteristic turnover rates (van der Vaart et al., 2013).

The dynamic assemblies of CMSC components, which are spatially separate from other plasma membrane domains and which rely on multivalent protein-protein interactions, are reminiscent of cytoplasmic and nucleoplasmic membrane-unbounded organelles such as P granules and stress granules, the assembly of which has been proposed to be driven by phase transitions (Astro and de Curtis, 2015; Brangwynne, 2013; Hyman and Simons, 2012). The formation of such structures, which can be compared to liquid droplets, can be triggered by local concentration of CMSC components. It is tempting to speculate that by concentrating KANK1 at the FA rims, talin1 helps to 'nucleate' CMSC assembly, which can then propagate to form large structures surrounding FAs (Figure 6B). Additional membrane-bound cues, such as the presence of PIP3, to which LL5β can bind (Paranavitane et al., 2003), can further promote CMSC coalescence by increasing concentration of CMSC players in specific areas of the plasma membrane. This model helps to explain why the CMSC accumulation at the cell periphery is reduced but not abolished when PI3 kinase is inhibited (Lansbergen et al., 2006), and why the clustering of all CMSC components is mutually dependent. Most importantly, this model accounts for the mysterious ability of the two large and spatially distinct macromolecular assemblies, FAs and CMSCs, to form in close proximity of each other.
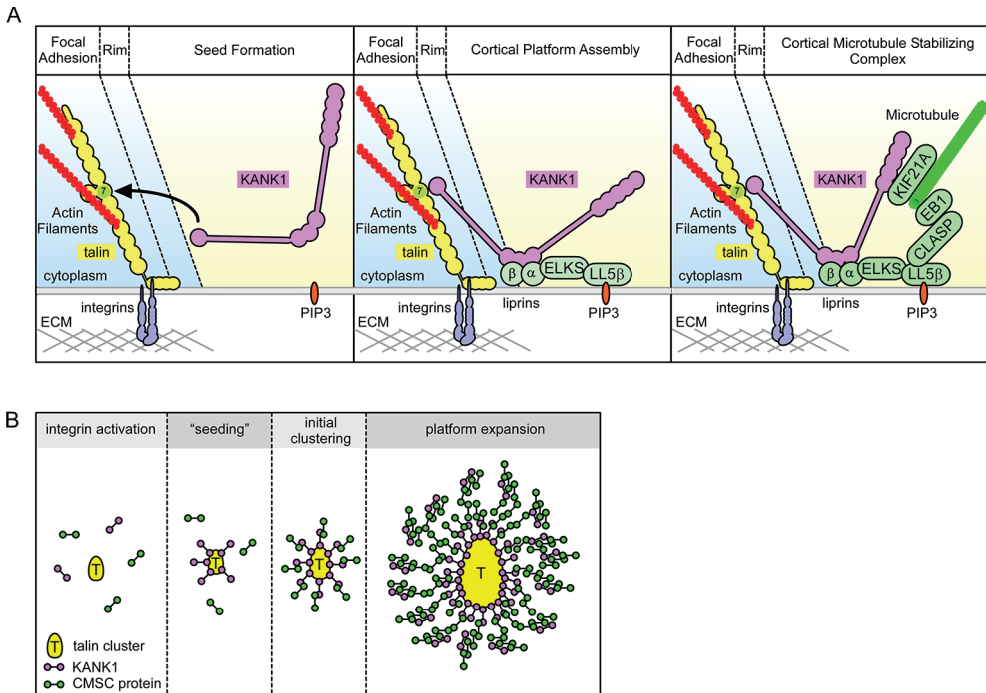
Figure 6. Model of talin-directed assembly of cortical microtubule stabilizing complex
(**A**) Three-step CMSC clustering around focal adhesion: 1) KANK1 binds talin rod domain R7 via the KN motif, 2) KANK1 initiates a cortical platform assembly by binding liprin-β1 via its CC1 domain, 3) completion of CMSC assembly by further clustering of liprins, ELKS, LL5β, CLASP and KIF21A around FA. (**B**) KANK1 binding to nascent talin clusters acts as a 'seed' for macromolecular complex assembly and organization around a FA.

To conclude, our study revealed that a mechanosensitive integrin-associated adaptor talin not only participates in organizing the actin cytoskeleton but also directly triggers formation of a cortical microtubule-stabilizing macromolecular assembly, which surrounds adhesion sites and controls their formation and dynamics by regulating microtubule-dependent signaling and trafficking.

Experimental procedures

Cell culture and transfection

HeLa Kyoto cell line was described previously (Lansbergen et al., 2006; Mimori-Kiyosue et al., 2005). HEK293T cells were purchased from ATCC; culture and transfection of DNA and siRNA into these cell lines was performed as previously described (van der Vaart et al., 2013). HaCaT cells were purchased at Cell Line Service (Eppelheim, Germany) and cultured according to manufacturer's instructions. The cell lines were routinely checked for mycoplasma contamination using LT07-518 Mycoalert assay (Lonza, Switzerland). The identity of the cell lines was monitored by immunofluorescence-staining-based analysis with multiple markers. Blebbistatin was purchased from Enzo Life Sciences and used at 50 mM. Serum starvation in HeLa cells was done for 48 hr and focal adhesion assembly was stimulated by incubation with fetal calf serum-containing medium with or without blebbistatin for 2 hr. ROCK1 inhibitor Y-27632 was purchased at Sigma-Aldrich and used at 1 or 10 mM. Double stable HeLa cell line expressing GFP-KANK1 and TagRFP-paxillin was made by viral infection. We used a pLVIN-TagRFP-paxillin-based lentivirus and a pQC-GFP-KANK1-based retrovirus packaged in HEK293T cells using respectively Lenti-X HTX packaging and pCL-Ampho vectors. Antibiotic selection was applied to cells 48 hr after infection using 500 mg/ml G418 (Geneticin, Life Technologies) and 1 mg/ml puromycin (InvivoGen).

DNA constructs and siRNAs

BioGFP-tagged KANK1 mutants were constructed using PCR and pBioGFP-C1 vector as previously described (van der Vaart et al., 2013). Rescue constructs for BioGFP-tagged KANK1 were either based on the version previously described (van der Vaart et al., 2013) or a version obtained by PCR-based mutagenesis of the sequence AGTCAGCGTCTGCGAA to GGTGAGTGTGTGTGAG. mCherry-tagged paxillin construct was made by replacing GFP from pQC-GPXN (Bouchet et al., 2011) by mCherry (pmCherry-C1, Clontech). TagRFP-tagged paxillin construct was made by PCR-based amplification and cloning in pTagRFP-T-C1 (kind gift from Y. Mimori-Kiyosue, Riken Institute, Japan). HA-tagged KANK1 construct was generated by cloning KANK1 coding sequence into pMT2- SM-HA (gift of C. Hoogenraad, Utrecht University, The Netherlands). pLVX-IRES-Neo (pLVIN) vectors was constructed by cloning the IRES-neomycin resistance cassette from the pQCXIN plasmid (Clontech) into the pLVX-IRES-Puro plasmid (Clontech). The lentiviral Lenti-X HTX Packaging vector mix was purchased from Clontech. The retroviral packaging vector pCL-Ampho was kindly provided by E. Bindels, Erasmus MC, The Netherlands. The retroviral pQC-GFP-KANK1 vector was constructed by cloning GFP-KANK1 in pQCXIN and the lentiviral pLVIN-TagRFP-paxillin vector was constructed by cloning TagRFP-paxillin in pLVIN. BirA coding vector was described before (van der Vaart et al., 2013). GFP-tagged mouse talin 1 construct was a kind gift from Dr. A Huttenlocher (Addgene plasmid # 26724) (Franco et al., 2004). GFP-tagged KN-LacZ fusion was made using PCR-based amplification of KN and LacZ (kind gift, C. Hoogenraad, Utrecht University, The Netherlands), pBioGFP-C1 vector and Gibson Assembly mix (New England Biolabs). Site directed mutagenesis of KANK1 and talin1 constructs was realized by overlapping PCR-based

strategy and validated by sequencing. mCherry-tagged CLASP2 construct was a gift from A. Aher (Utrecht University, The Netherlands). Single siRNAs were ordered from Sigma-Aldrich or Ambion, used at 5–15 nM, validated by Western blot analysis and/ or immunofluorescence, and target sequences were the following: human KANK1 #1, CAGAGAAGGACATGCGGAT; human KANK1#2, GAAGTCAGCGTCTGCGAAA, human KANK2#1, ATGTCAACGTGCAAGATGA; human KANK2 #2, TCGAGAATCTCAGCACATA; human talin 1 #1, TCTGTACTGAGTAATAGCCAT; human talin 1 #2, TGAATGTCCTGTCAACTGCTG; human talin 2 #1, TTTCGTTTTCATCTACTCCTT; human talin 2 #2, TTCGTGTTTGGATTCGTCGAC. The combination of siRNAs talin1 #2 and talin2#1 was the most efficient and was used for the experiments shown in the paper.

Pull down assays and mass spectrometry

Streptavidin-based pull down assays of biotinylated proteins expressed using pBioGFP-C1 constructs transfected in HEK293T cells was performed and analyzed as previously described (van der Vaart et al., 2013). For mass spectrometry sample preparation, streptavidin beads resulting from pull-downs assays were ran on a 12% Bis-Tris 1D SDS-PAGE gel (Biorad) for 1 cm and stained with colloidal coomassie dye G-250 (Gel Code Blue Stain Reagent, Thermo Scientific). The lane was cut and treated with 6.5 mM dithiothreitol (DTT) for 1 hr at 60 ℃ for reduction and 54 mM iodoacetamide for 30 min for alkylation. The proteins were digested overnight with trypsin (Promega) at 37℃. The peptides were extracted with 100% acetonitrile (ACN) and dried in a vacuum concentrator. For RP- nanoLC-MS/MS, samples were resuspended in 10% formic acid (FA) / 5% DMSO and was analyzed using a Proxeon Easy-nLC100 (Thermo Scientific) connected to an Orbitrap Q-Exactive mass spectrometer. Samples were first trapped (Dr Maisch Reprosil C18, 3 mm, 2 cm × 100 mm) before being separated on an analytical column (Agilent Zorbax 1.8 mm SB-C18, 40 cm × 50 mm), using a gradient of 180 min at a column flow of 150 nl min-1. Trapping was performed at 8 mL/min for 10 min in sol- vent A (0.1 M acetic acid in water) and the gradient was as follows 15- 40% solvent B (0.1 M acetic acid in acetonitrile) in 151 min, 40–100% in 3 min, 100% solvent B for 2 min, and 100% solvent A for 13 min. Nanospray was performed at 1.7 kV using a fused silica capillary that was pulled in-house and coated with gold (o.d. 360 mm; i.d. 20 mm; tip i.d. 10 mm). The mass spectrometers were used in a data-dependent mode, which automatically switched between MS and MS/MS. Full scan MS spec- tra from m/z 350 – 1500 were acquired at a resolution of 35.000 at m/z 400 after the accumulation to a target value of 3E6. Up to 20 most intense precursor ions were selected for fragmentation. HCD fragmentation was performed at normalized collision energy of 25% after the accumulation to a target value of 5E4. MS2 was acquired at a resolution of 17,500 and dynamic exclusion was enabled. For data analysis, raw files were processed using Proteome Discoverer 1.4 (version 1.4.1.14, Thermo Scientific, Bremen, Germany). Database search was performed using the swiss-prot human database (version 29th of January 2015) and Mascot (version 2.5.1, Matrix Science, UK) as the search engine. Carbamidomethylation of cysteines was set as a fixed modification and oxidation of methionine was set as a variable modification. Trypsin was specified as enzyme and up to two miss cleavages were allowed. Data filtering was performed using a percolator

(Ka ̈ll et al., 2007), resulting in 1% false discovery rate (FDR). Additional filter was ion score >20.

Antibodies and immunofluorescence cell staining
Antibodies against HA and GFP tags, and liprin β1 used for Western blot analysis were previously described (van der Vaart et al., 2013). Rabbit antibodies against KANK1 (HPA005539) and KANK2 (HPA015643) were purchased at Sigma-Aldrich. Western blot analysis of KANK1 was performed using rabbit polyclonal KANK1 antibody (A301-882A) purchased at Bethyl Laboratories. Talin immunofluorescence staining was performed using mouse monoclonal 8d4 antibody (Sigma-Aldrich). Western blot analysis of talin 1 and 2 expression was performed using respectively the isotype specific mouse monoclonal 97H6 (Sigma-Aldrich) and 68E7 (Abcam) antibodies. Ku80 (7/u80) antibody was purchased from BD Biosciences. Immunofluorescence staining of KANK1, LL5β, liprin-β1, KIF21A and CLASP2 in HeLa and HaCaT cells was performed using the antibodies and procedures previously described (Lansbergen et al., 2006; van der Vaart et al., 2013). F-actin was stained using Alexa Fluor 594-conjugated phalloidin (Life Technologies). Phospho-tyrosine mouse antibody (PT-66) was purchased from Sigma-Aldrich and rabbit FAK phospho-tyrosine 397 was purchased from Biosource.

Microscopy and analysis
Fixed samples and corresponding immunofluorescence images were acquired using widefield fluorescence illumination on a Nikon Eclipse 80i or Ni upright microscope equipped with a CoolSNAP HQ2 CCD camera (Photometrics) or a DS-Qi2 camera (Nikon) an Intensilight C-HGFI precentered fiber illuminator (Nikon), ET-DAPI, ET-EGFP and ET-mCherry filters (Chroma), Nikon NIS Br software, Plan Apo VC 100x NA 1.4 oil, Plan Apo Lambda 100X oil NA 1.45 and Plan Apo VC 60x NA 1.4 oil (Nikon) objectives. TIRFM-based live cell imaging was performed using the setup described before (van der Vaart et al., 2013) or a similar Nikon Ti microscope-based Ilas2 system (Roper Scientific, Evry, FRANCE) equipped with dual laser illuminator for azimuthal spinning TIRF (or Hilo) illumination, 150 mW 488 nm laser and 100 mW 561 nm laser, 49,002 and 49,008 Chroma filter sets, EMCCD Evolve mono FW DELTA 512x512 camera (Roper Scientific) with the intermediate lens 2.5X (Nikon C mount adapter 2.5X), CCD camera CoolSNAP MYO M-USB-14-AC (Roper Scientific) and controlled with MetaMorph 7.8.8 software (Molecular Devices). Simultaneous imaging of green TIRFM imaging was performed as described before (van der Vaart et al., 2013) or using the Optosplit III image splitter device (Andor) on the Ilas2 system.

For presentation, images were adjusted for brightness and processed by Gaussian blur and Unsharp mask filter using ImageJ 1.47v (NIH). Fluorescence profiles are values measured by line scan analysis in ImageJ, normalized by background average fluorescence, expressed as a factor of the baseline value obtained for individual channel and plotted as a function of maximum length factor of the selection line (distance ratio). Protein clustering at the cell edge is the ratio of the total fluorescence in the first 5 μm from the cell edge to the next 5 μm measured by line scan analysis in ImageJ after thresholding for cell outline marking and out-of-cell region value assigned to zero. The results were plotted as percentage of control condition average value. FA counting

and area measurement was performed using Analyze Particles under ImageJ on focal adhesion binary mask obtained after Gaussian blur/threshold-based cell outline marking and background subtraction (rolling ball radius, 10 pixels). KANK1/talin colocalization was analyzed using Pearson R value provided by Colocalization Analysis plugin under FiJi-ImageJ and a 3 μm diameter circular ROI centered on talin clusters detected by immunofluorescent staining.

nEB3-mRFP dynamics was recorded by 0.5 s interval time lapse TIRF imaging. Microtubule growth was measured using kymographs obtained from EB3-mRFP time lapse image series, plotted and presented as previously described (van der Vaart et al., 2013). Ratio of microtubule growth in cell center to periphery was obtained as values for individual cells. Microtubule growth trajectory angle to the cell edge was manually measured in ImageJ using tracks obtained by maximum intensity pro- jection of EB3-mRFP image series.

Expression of recombinant talin polypeptides

The cDNAs encoding murine talin1 residues 1357–1653 (R7-R8), 1357–1653 D1454–1586 (R7) and 1461–1580 (R8) were synthesized by PCR using a mouse talin1 cDNA as template and cloned into the expression vector pet151-TOPO (Invitrogen) (Gingras et al., 2010). Talin mutants were synthe- sized by GeneArt. Talin polypeptides were expressed in *E. coli* BL21(DE3) cultured either in LB for unlabeled protein, or in M9 minimal medium for the preparation of isotopically labeled samples for NMR. Recombinant His-tagged talin polypeptides were purified by nickel-affinity chromatography following standard procedures. The His-tag was removed by cleavage with AcTEV protease (Invitro- gen), and the proteins were further purified by anion-exchange. Protein concentrations were deter- mined using their respective extinction coefficient at 280 nm.

Fluorescence polarization assays

KANK peptides with a C-terminal cysteine residue were synthesized by Biomatik (USA):

```
KANK1(30—60)C     PYFVETPYGFQLDLDFVKYVDDIQKGNTIKKC
KANK1(30—68)C     PYFVETPYGFQLDLDFVKYVDDIQKGNTIKKLNIQKRRKC
KANK1—4A          PYFVETPYGFQAAAAFVKYVDDIQKGNTIKKLNIQKRRKC
KANK2(31—61)C     PYSVETPYGYRLDLDFLKYVDDIEKGHTLRRC
```

Fluorescence Polarization was carried out on KANK peptides with a carboxy terminal cysteine.

Peptide stock solutions were made in PBS (137 mM NaCl, 27 mM KCl, 100 mM Na2HPO4, 18 mM KH2PO4), 100 mg/ml TCEP and 0.05% Triton X-100, and coupled via the carboxy terminal cysteine to the Thiol reactive BIODIPY TMR dye (Invitrogen). Uncoupled dye was removed by gel filtration using a PD-10 column (GE Healthcare). The labeled peptide was concentrated to a final concentra- tion of 1 mM using a centricon with 3K molecular weight cut off (Millipore).

The Fluorescence Polarization assay was carried out on a black 96well plate (Nunc). Titrations were performed in triplicate using a fixed 0.5 μM concentration of peptide and an increasing concentration of Talin R7-R8 protein within a final volume of 100

μl of assay buffer (PBS). Fluorescence Polarization measurements were recorded on a BMGLabTech CLARIOstar plate reader at room tem- perature and analyzed using GraphPad Prism (version 6.07). Kd values were calculated with a nonlinear curve fitting using a one site total and non-specific binding model.

NMR spectroscopy

NMR experiments for the resonance assignment of talin1 R7, residues 1357–1653 D1454–1586 were carried out with 1 mM protein in 20 mM sodium phosphate, pH 6.5, 50 mM NaCl, 2 mM dithiothreitol, 10% (v/v) 2H2O. NMR spectra were obtained at 298 K using a Bruker AVANCE III spectrometer equipped with CryoProbe. Proton chemical shifts were referenced to external 2,2-dimethyl-2-sila-pentane-5-sulfonic acid, and 15N and 13C chemical shifts were referenced indirectly using recommended gyromagnetic ratios (Wishart et al., 1995). The spectra were processed using Topspin and analyzed using CCPN Analysis (Skinner et al., 2015). Three-dimensional HNCO, HN(CA)CO, HNCA, HN(CO)CA, HNCACB, and CBCA(CO)NH experiments were used for the sequential assignment of the backbone NH, N, CO, CA, and CB resonances.

The backbone resonance assignments of mouse talin1 R7 (1357–1653 D1454–1586) have been deposited in the BioMagResBank with the accession number 19139.

2

Author contributions

BPB, BTG, Conception and design, Acquisition of data, Analysis and interpretation of data, Drafting or revising the article; REG, Y-CA, DvdW, HP, Acquisition of data, Analysis and interpretation of data, Drafting or revising the article; GJ, Conception and design, Drafting or revising the article, Contributed unpublished essential data or reagents; AFMA, Analysis and interpretation of data, Drafting or revising the article; AJRH, AA, Conception and design, Analysis and interpretation of data, Drafting or revising the article

Acknowledgements

Competing interests

AA: Reviewing editor, eLife. The other authors declare that no competing interests exist.

References

Akhmanova A, Stehbens SJ, Yap AS. 2009. Touch, grasp, deliver and control: functional cross-talk between microtubules and cell adhesions. Traffic 10:268–274. doi: 10.1111/j.1600-0854.2008.00869.x

Alam T, Alazmi M, Gao X, Arold ST. 2014. How to find a leucine in a haystack? Structure, ligand recognition and regulation of leucine-aspartic acid (LD) motifs. Biochemical Journal 460:317–329. doi: 10.1042/BJ20140298

Anthis NJ, Wegener KL, Ye F, Kim C, Goult BT, Lowe ED, Vakonakis I, Bate N, Critchley DR, Ginsberg MH, Campbell ID. 2009. The structure of an integrin/talin complex reveals the basis of inside-out signal transduction. The EMBO Journal 28:3623–3632. doi: 10.1038/emboj.2009.287

Astro V, Chiaretti S, Magistrati E, Fivaz M, de Curtis I. 2014. Liprin-a1, ERC1 and LL5 define polarized and dynamic structures that are implicated in cell migration. Journal of Cell Science 127:3862–3876. doi: 10.1242/jcs.155663

Astro V, de Curtis I. 2015. Plasma membrane-associated platforms: dynamic scaffolds that organize membrane-associated events. Science Signaling 8:re1. doi: 10.1126/scisignal.aaa3312

Atherton P, Stutchbury B, Wang D-Y, Jethwa D, Tsang R, Meiler-Rodriguez E, Wang P, Bate N, Zent R, Barsukov IL, Goult BT, Critchley DR, Ballestrem C. 2015. Vinculin controls talin engagement with the actomyosin machinery. Nature Communications 6:10038. doi: 10.1038/ncomms10038

Banno A, Goult BT, Lee H, Bate N, Critchley DR, Ginsberg MH. 2012. Subcellular localization of talin is regulated by inter-domain interactions. Journal of Biological Chemistry 287:13799–13812. doi: 10.1074/jbc.M112.341214

Basu S, Sladecek S, Martinez de la Pen˜ a y Valenzuela I, Akaaboune M, Smal I, Martin K, Galjart N, Brenner HR. 2015. CLASP2-dependent microtubule capture at the neuromuscular junction membrane requires LL5b and actin for focal delivery of acetylcholine receptor vesicles. Molecular Biology of the Cell 26:938–951. doi: 10.1091/mbc.E14-06-1158

Basu S, Sladecek S, Pemble H, Wittmann T, Slotman JA, van Cappellen W, Brenner HR, Galjart N. 2014. Acetylcholine receptor (AChR) clustering is regulated both by glycogen synthase kinase 3b (GSK3b)-dependent phosphorylation and the level of CLIP-associated protein 2 (CLASP2) mediating the capture of microtubule plus-ends. Journal of Biological Chemistry 289:30857–30867. doi: 10.1074/jbc.M114.589457

Bouchet BP, Fauvet F, Grelier G, Galmarini CM, Puisieux A. 2011. p21(Cip1) regulates cell-substrate adhesion and interphase microtubule dynamics in untransformed human mammary epithelial cells. European Journal of Cell Biology 90:631–641. doi: 10.1016/j.ejcb.2011.03.002

Brangwynne CP. 2013. Phase transitions and size scaling of membrane-less organelles. Journal of Cell Biology 203:875–881. doi: 10.1083/jcb.201308087

Byron A, Askari JA, Humphries JD, Jacquemet G, Koper EJ, Warwood S, Choi CK, Stroud MJ, Chen CS, Knight D, Humphries MJ. 2015. A proteomic approach reveals integrin activation state-dependent control of microtubule cortical targeting. Nature Communications 6:6135. doi: 10.1038/ncomms7135

Calderwood DA, Campbell ID, Critchley DR. 2013. Talins and kindlins: partners in integrin-mediated adhesion. Nature Reviews Molecular Cell Biology 14:503–517. doi: 10.1038/nrm3624

del Rio A, Perez-Jimenez R, Liu R, Roca-

2

Cusachs P, Fernandez JM, Sheetz MP. 2009. Stretching single talin rod molecules activates vinculin binding. Science 323:638–641. doi: 10.1126/science.1162912

Drabek K, van Ham M, Stepanova T, Draegestein K, van Horssen R, Sayas CL, Akhmanova A, Ten Hagen T, Smits R, Fodde R, Grosveld F, Galjart N. 2006. Role of CLASP2 in microtubule stabilization and the regulation of persistent motility. Current Biology 16:2259–2264. doi: 10.1016/j.cub.2006.09.065

Ezratty EJ, Partridge MA, Gundersen GG. 2005. Microtubule-induced focal adhesion disassembly is mediated by dynamin and focal adhesion kinase. Nature Cell Biology 7:581–590. doi: 10.1038/ncb1262

Franco SJ, Rodgers MA, Perrin BJ, Han J, Bennin DA, Critchley DR, Huttenlocher A. 2004. Calpain-mediated proteolysis of talin regulates adhesion dynamics. Nature Cell Biology 6:977–983. doi: 10.1038/ncb1175

Gardel ML, Schneider IC, Aratyn-Schaus Y, Waterman CM. 2010. Mechanical integration of actin and adhesion dynamics in cell migration. Annual Review of Cell and Developmental Biology 26:315–333. doi: 10.1146/annurev.cellbio.011209.122036

Gee HY, Zhang F, Ashraf S, Kohl S, Sadowski CE, Vega-Warner V, Zhou W, Lovric S, Fang H, Nettleton M, Zhu Jun-yi, Hoefele J, Weber LT, Podracka L, Boor A, Fehrenbach H, Innis JW, Washburn J, Levy S, Lifton RP, et al. 2015. KANK deficiency leads to podocyte dysfunction and nephrotic syndrome. Journal of Clinical Investigation 125:2375–2384. doi: 10.1172/JCI79504

Gingras AR, Bate N, Goult BT, Patel B, Kopp PM, Emsley J, Barsukov IL, Roberts GC, Critchley DR. 2010. Central region of talin has a unique fold that binds vinculin and actin. Journal of Biological Chemistry 285:29577–29587. doi: 10.1074/jbc.M109.095455

Goult BT, Zacharchenko T, Bate N, Tsang R, Hey F, Gingras AR, Elliott PR, Roberts GC, Ballestrem C, Critchley DR, Barsukov IL. 2013. RIAM and vinculin binding to talin are mutually exclusive and regulate adhesion assembly and turnover. Journal of Biological Chemistry 288:8238–8249. doi: 10.1074/jbc.M112.438119

Grigoriev I, Splinter D, Keijzer N, Wulf PS, Demmers J, Ohtsuka T, Modesti M, Maly IV, Grosveld F, Hoogenraad CC, Akhmanova A. 2007. Rab6 regulates transport and targeting of exocytotic carriers. Developmental Cell 13:305–314. doi: 10.1016/j.devcel.2007.06.010

Grigoriev I, Yu KL, Martinez-Sanchez E, Serra-Marques A, Smal I, Meijering E, Demmers J, Peränen J, Pasterkamp RJ, van der Sluijs P, Hoogenraad CC, Akhmanova A. 2011. Rab6, Rab8, and MICAL3 cooperate in controlling docking and fusion of exocytotic carriers. Current Biology 21:967–974. doi: 10.1016/j.cub.2011.04.030

Gundelfinger ED, Fejtova A. 2012. Molecular organization and plasticity of the cytomatrix at the active zone. Current Opinion in Neurobiology 22:423–430. doi: 10.1016/j.conb.2011.10.005

Hida Y, Ohtsuka T. 2010. CAST and ELKS proteins: structural and functional determinants of the presynaptic active zone. Journal of Biochemistry 148:131–137. doi: 10.1093/jb/mvq065

Honnappa S, Gouveia SM, Weisbrich A, Damberger FF, Bhavesh NS, Jawhari H, Grigoriev I, van Rijssel FJ, Buey RM, Lawera A, Jelesarov I, Winkler FK, Wüthrich K, Akhmanova A, Steinmetz MO. 2009. An EB1-binding motif acts as a microtubule tip localization signal. Cell 138:366–376. doi: 10.1016/j.cell.2009.04.065

Hotta A, Kawakatsu T, Nakatani T, Sato T, Matsui C, Sukezane T, Akagi T, Hamaji T, Grigoriev I, Akhmanova A, Takai Y, Mimori-Kiyosue Y. 2010. Laminin-based cell adhesion anchors microtubule plus ends to the epithelial cell basal cortex through LL5a/b. Journal of Cell Biology 189:901–917. doi: 10.1083/jcb.200910095

Hyman AA, Simons K. 2012. Cell biology. Beyond oil and water–phase transitions in cells. Science 337:1047–1049. doi: 10.1126/science.1223728

Hynes RO. 1992. Integrins: versatility, modulation, and signaling in cell adhesion. Cell 69:11–25. doi: 10.1016/0092-8674(92)90115-S

Ihara S, Hagedorn EJ, Morrissey MA, Chi Q, Motegi F, Kramer JM, Sherwood DR. 2011. Basement membrane sliding and targeted adhesion remodels tissue boundaries during uterine-vulval attachment in Caenorhabditis elegans. Nature Cell Biology 13:641–651. doi: 10.1038/ncb2233

Kakinuma N, Kiyama R. 2009. A major mutation of KIF21A associated with congenital fibrosis of the extraocular muscles type 1 (CFEOM1) enhances translocation of Kank1 to the membrane. Biochemical and Biophysical Research Communications 386:639–644. doi: 10.1016/j.bbrc.2009.06.109

Kakinuma N, Roy BC, Zhu Y, Wang Y, Kiyama R. 2008. Kank regulates RhoA-dependent formation of actin stress fibers and cell migration via 14-3-3 in PI3K-Akt signaling. The Journal of Cell Biology 181:537–549. doi: 10.1083/jcb.200707022

Kakinuma N, Zhu Y, Wang Y, Roy BC, Kiyama R. 2009. Kank proteins: structure, functions and diseases. Cellular and Molecular Life Sciences 66:2651–2659. doi: 10.1007/s00018-009-0038-y

Käll L, Canterbury JD, Weston J, Noble WS, MacCoss MJ. 2007. Semi-supervised learning for peptide identification from shotgun proteomics datasets. Nature Methods 4:923–925. doi: 10.1038/nmeth1113

Kaverina I, Krylyshkina O, Small JV. 1999. Microtubule targeting of substrate contacts promotes their relaxation and dissociation. The Journal of Cell Biology 146:1033–1044. doi: 10.1083/jcb.146.5.1033

Kaverina I, Rottner K, Small JV. 1998. Targeting, capture, and stabilization of microtubules at early focal adhesions. The Journal of Cell Biology 142:181–190. doi: 10.1083/jcb.142.1.181

Kaverina I, Straube A. 2011. Regulation of cell migration by dynamic microtubules. Seminars in Cell & Developmental Biology 22:968–974. doi: 10.1016/j.semcdb.2011.09.017

Kishi M, Kummer TT, Eglen SJ, Sanes JR. 2005. LL5beta: a regulator of postsynaptic differentiation identified in a screen for synaptically enriched transcripts at the neuromuscular junction. The Journal of Cell Biology 169:355–366. doi: 10.1083/jcb.200411012

Kodama A, Karakesisoglou I, Wong E, Vaezi A, Fuchs E. 2003. ACF7: an essential integrator of microtubule dynamics. Cell 115:343–354. doi: 10.1016/S0092-8674(03)00813-4

Krylyshkina O, Anderson KI, Kaverina I, Upmann I, Manstein DJ, Small JV, Toomre DK. 2003. Nanometer targeting of microtubules to focal adhesions. The Journal of Cell Biology 161:853–859. doi: 10.1083/jcb.200301102

Lansbergen G, Grigoriev I, Mimori-Kiyosue Y, Ohtsuka T, Higa S, Kitajima I, Demmers J, Galjart N, Houtsmuller AB, Grosveld F, Akhmanova A. 2006. CLASPs attach microtubule plus ends to the cell cortex through a complex with LL5beta. Developmental Cell 11:21–32. doi:

2

2

10.1016/j.devcel.2006.05.012

Li C-C, Kuo J-C, Waterman CM, Kiyama R, Moss J, Vaughan M. 2011. Effects of brefeldin A-inhibited guanine nucleotide-exchange (BIG) 1 and KANK1 proteins on cell polarity and directed migration during wound healing. PNAS 108:19228–19233. doi: 10.1073/pnas.1117011108

Mimori-Kiyosue Y, Grigoriev I, Lansbergen G, Sasaki H, Matsui C, Severin F, Galjart N, Grosveld F, Vorobjev I, Tsukita S, Akhmanova A. 2005. CLASP1 and CLASP2 bind to EB1 and regulate microtubule plus-end dynamics at the cell cortex. The Journal of Cell Biology 168:141–153. doi: 10.1083/jcb.200405094

Nakaya Y, Sukowati EW, Sheng G. 2013. Epiblast integrity requires CLASP and Dystroglycan-mediated microtubule anchoring to the basal cortex. The Journal of Cell Biology 202:637–651. doi: 10.1083/jcb.201302075

Oakes PW, Beckham Y, Stricker J, Gardel ML. 2012. Tension is required but not sufficient for focal adhesion maturation without a stress fiber template. The Journal of Cell Biology 196:363–374. doi: 10.1083/jcb. 201107042

Paranavitane V, Coadwell WJ, Eguinoa A, Hawkins PT, Stephens L. 2003. LL5beta is a phosphatidylinositol (3,4,5)-trisphosphate sensor that can bind the cytoskeletal adaptor, gamma-filamin. Journal of Biological Chemistry 278:1328–1335. doi: 10.1074/jbc.M208352200

Parsons JT, Horwitz AR, Schwartz MA. 2010. Cell adhesion: integrating cytoskeletal dynamics and cellular tension. Nature Reviews Molecular Cell Biology 11:633–643. doi: 10.1038/nrm2957

Proszynski TJ, Gingras J, Valdez G, Krzewski K, Sanes JR. 2009. Podosomes are present in a postsynaptic apparatus and participate in its maturation. PNAS 106:18373–18378. doi: 10.1073/pnas.0910391106

Proszynski TJ, Sanes JR. 2013. Amotl2 interacts with LL5 , localizes to podosomes and regulates postsynaptic differentiation in muscle. Journal of Cell Science 126:2225–2235. doi: 10.1242/jcs.121327

Ratnikov B, Ptak C, Han J, Shabanowitz J, Hunt DF, Ginsberg MH. 2005. Talin phosphorylation sites mapped by mass spectrometry. Journal of Cell Science 118:4921–4923. doi: 10.1242/jcs.02682

Roy BC, Kakinuma N, Kiyama R. 2009. Kank attenuates actin remodeling by preventing interaction between IRSp53 and Rac1. The Journal of Cell Biology 184:253–267. doi: 10.1083/jcb.200805147

Schmidt N, Basu S, Sladecek S, Gatti S, van Haren J, Treves S, Pielage J, Galjart N, Brenner HR. 2012. Agrin regulates CLASP2-mediated capture of microtubules at the neuromuscular junction synaptic membrane. The Journal of Cell Biology 198:421–437. doi: 10.1083/jcb.201111130

Skinner SP, Goult BT, Fogh RH, Boucher W, Stevens TJ, Laue ED, Vuister GW. 2015. Structure calculation, refinement and validation using CcpNmr Analysis. Acta Crystallographica Section D Biological Crystallography 71:154–161. doi: 10.1107/S1399004714026662

Small JV, Kaverina I. 2003. Microtubules meet substrate adhesions to arrange cell polarity. Current Opinion in Cell Biology 15:40–47. doi: 10.1016/S0955-0674(02)00008-X

Spangler SA, Hoogenraad CC. 2007. Liprin-alpha proteins: scaffold molecules for synapse maturation. Biochemical Society Transactions 35:1278–1282. doi: 10.1042/BST0351278

Stehbens S, Wittmann T. 2012. Targeting and transport: how microtubules control focal adhesion dynamics. The Journal of Cell Biology

198:481–489. doi: 10.1083/jcb.201206050

Stehbens SJ, Paszek M, Pemble H, Ettinger A, Gierke S, Wittmann T. 2014. CLASPs link focal-adhesion-associated microtubule capture to localized exocytosis and adhesion site turnover. Nature Cell Biology 16:561–573. doi: 10.1038/ncb2975

Theisen U, Straube E, Straube A. 2012. Directional persistence of migrating cells requires Kif1C-mediated stabilization of trailing adhesions. Developmental Cell 23:1153–1166. doi: 10.1016/j.devcel.2012.11.005

van der Vaart B, van Riel WE, Doodhi H, Kevenaar JT, Katrukha EA, Gumy L, Bouchet BP, Grigoriev I, Spangler SA, Yu KL, Wulf PS, Wu J, Lansbergen G, van Battum EY, Pasterkamp RJ, Mimori-Kiyosue Y, Demmers J, Olieric N, Maly IV, Hoogenraad CC, et al. 2013. CFEOM1-associated kinesin KIF21A is a cortical microtubule growth inhibitor. Developmental Cell 27:145–160. doi: 10.1016/j.devcel.2013.09.010

van Zundert GC, Rodrigues JP, Trellet M, Schmitz C, Kastritis PL, Karaca E, Melquiond AS, van Dijk M, de Vries SJ, Bonvin AM. 2016. The HADDOCK2.2 web server: user-friendly integrative modeling of biomolecular complexes. Journal of Molecular Biology 428:720–725. doi: 10.1016/j.jmb.2015.09.014

Wehrle-Haller B. 2012. Assembly and disassembly of cell matrix adhesions. Current Opinion in Cell Biology 24: 569–581. doi: 10.1016/j.ceb.2012.06.010

Wishart DS, Bigam CG, Yao J, Abildgaard F, Dyson HJ, Oldfield E, Markley JL, Sykes BD. 1995. 1H, 13C and 15N chemical shift referencing in biomolecular NMR. Journal of Biomolecular NMR 6:135–140. doi: 10.1007/BF00211777

Yan J, Yao M, Goult BT, Sheetz MP. 2015. Talin dependent mechanosensitivity of cell focal adhesions. Cellular and Molecular Bioengineering 8:151–159. doi: 10.1007/s12195-014-0364-5

Yao M, Goult BT, Chen H, Cong P, Sheetz MP, Yan J. 2014. Mechanical activation of vinculin binding to talin locks talin in an unfolded conformation. Scientific Reports 4:4610. doi: 10.1038/srep04610

Yao M, Goult BT, Klapholz B, Hu X, Toseland CP, Guo Y, Cong P, Sheetz MP, Yan J. 2016. The mechanical response of talin. Nature Communications 7:11966. doi: 10.1038/ncomms11966

Yue J, Xie M, Gou X, Lee P, Schneider MD, Wu X. 2014. Microtubules regulate focal adhesion dynamics through MAP4K4. Developmental Cell 31:572–585. doi: 10.1016/j.devcel.2014.10.025

Zacharchenko T, Qian X, Goult BT, Jethwa D, Almeida TB, Ballestrem C, Critchley DR, Lowy DR, Barsukov IL. 2016. LD motif recognition by talin: structure of the talin-DLC1 complex. Structure 24:1130–1141. doi: 10.1016/j.str.2016.04.016

2

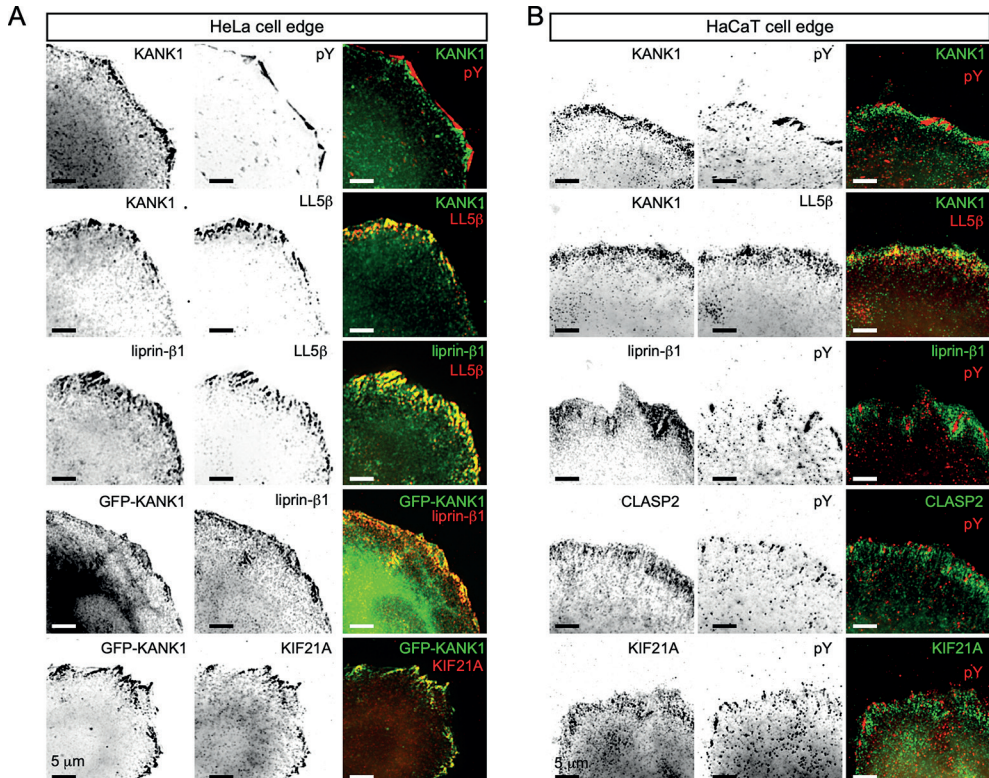# Supplementary figures

Figure 1—figure supplement 1. KANK1 colocalizes with CMSC components around FAs
(**A**) Widefield fluorescence images of HeLa cells stained for endogenous proteins as indicated. In the two bottom panels, cells were transfected with GFP-KANK1. pY, phospho-tyrosine, a FA marker. (**B**) Widefield fluorescence images of HaCaT cells stained for endogenous proteins as indicated.
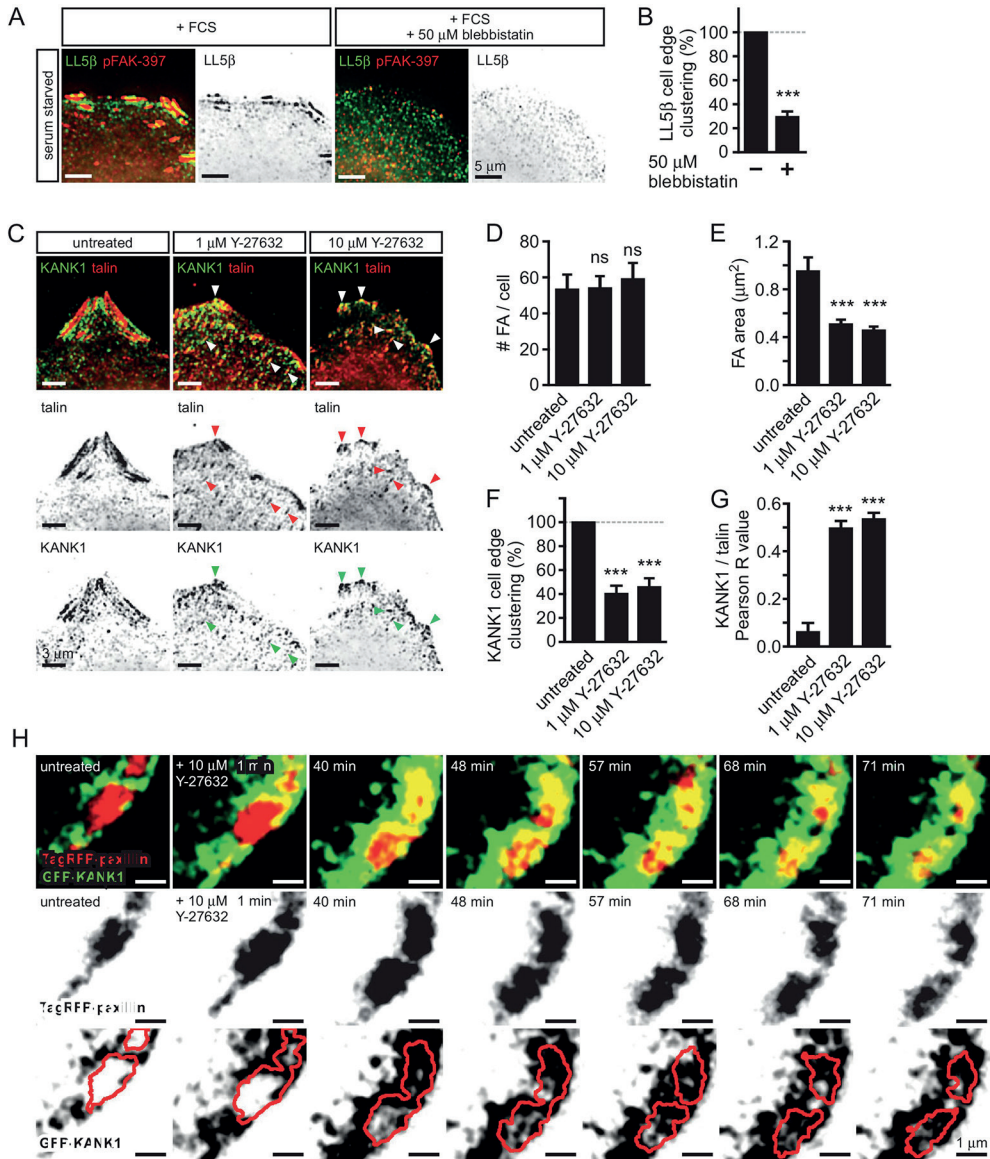
Figure 1—figure supplement 2. Role of myosin II activity in KANK1 localization to FA
(**A**) Widefield fluorescence images of serum-starved HeLa cells stimulated with fetal calf serum with or without blebbistatin and stained as indicated. (**B**) Quantification of peripheral clustering of LL5b in cells treated as in panel (A) (n=25–30, 6 cells per condition). (**C**) Widefield fluorescence images of HeLa treated for 45 min with the ROCK1 inhibitor Y-27632 at indicated concentrations and stained as indicated. (**D–E**) Average FA number (D) and individual area (E) in cells treated as in (C) (373–642 FAs/condition averaged per cell; n=7). (**F**) Quantification of peripheral clustering of KANK1 in cells treated as in panel (C) (n=12, 5 cells per condition). (**G**) Quantification of KANK1 and talin colocalization. Pearson R value, n=30 in 10–12 cells per conditions. (**H**) Dual fluorescence time-lapse images acquired using TIRFM in HeLa cells stably expressing TagRFP-paxillin and GFP-KANK1 and treated as indicated. Red line, FA rim obtained by using a threshold- based mask. In all plots: error bar, SEM; ns, non-significant, ***p<0.001, Mann- Whitney U test.
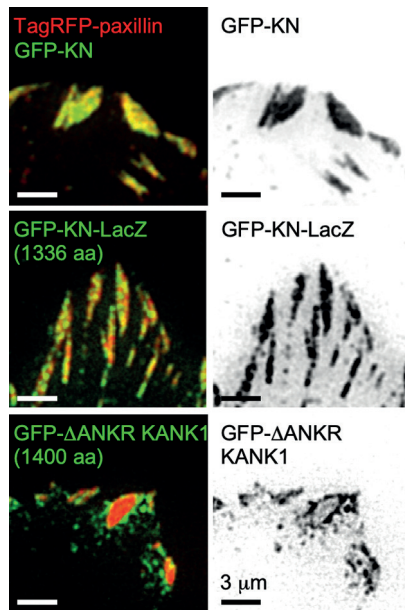
Figure 1—figure supplement 3. FA localization of KN-bearing proteins
GFP-KN-LacZ fusion localizes to the inner part of FAs. TIRFM images of live HeLa cells transfected with TagRFP-paxillin and GFP-tagged KN peptide, ΔANKR KANK1 mutant or KN-LacZ.

2
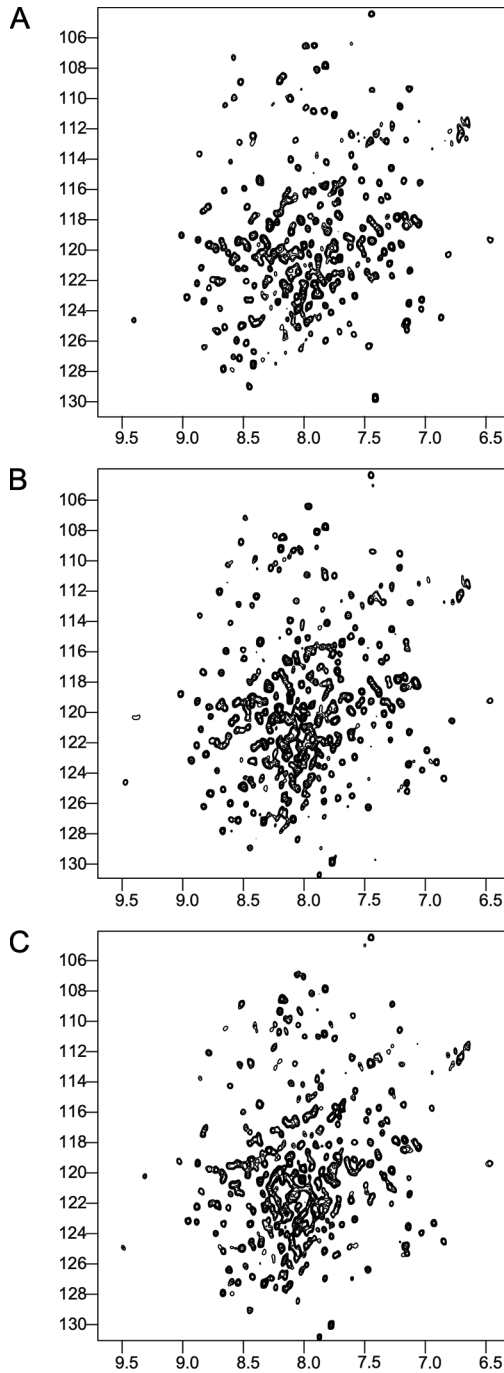
Figure 2—figure supplement 1. NMR validation of the Talin1 R7-R8 mutants
1H,15N HSQC spectra of; (**A**) Talin1 R7-R8 domain, (**B**) G1404L Talin1 R7-R8 mutant, and (**C**) W1630A Talin1 R7-R8 Mutant. The mutant spectra show good peak distribution with uniform intensity similar to the wildtype suggesting that they are correctly folded.

2
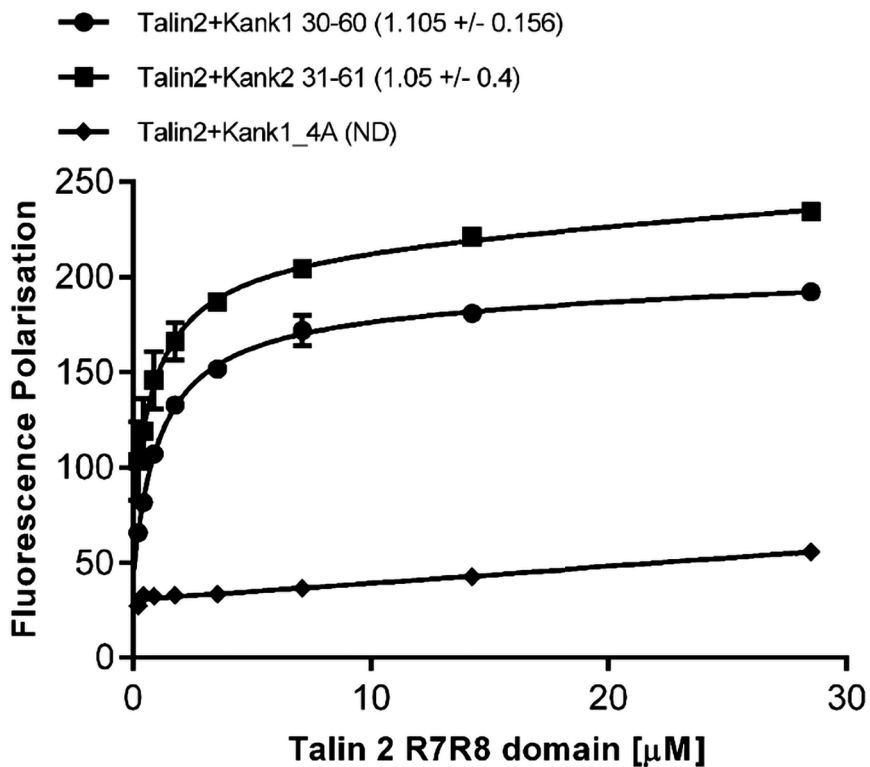
Figure 2—figure supplement 2. Biochemical characterization of the Talin2:KANK interaction
Binding of BODIPY-labeled KANK1(30–60)C, KANK2(31–61)C and KANK1-4A peptides to Talin2 R7-R8 measured using a Fluorescence Polarization assay. Dissociation constants ± SE (mM) for the interactions are indicated in the legend. ND, not determined.
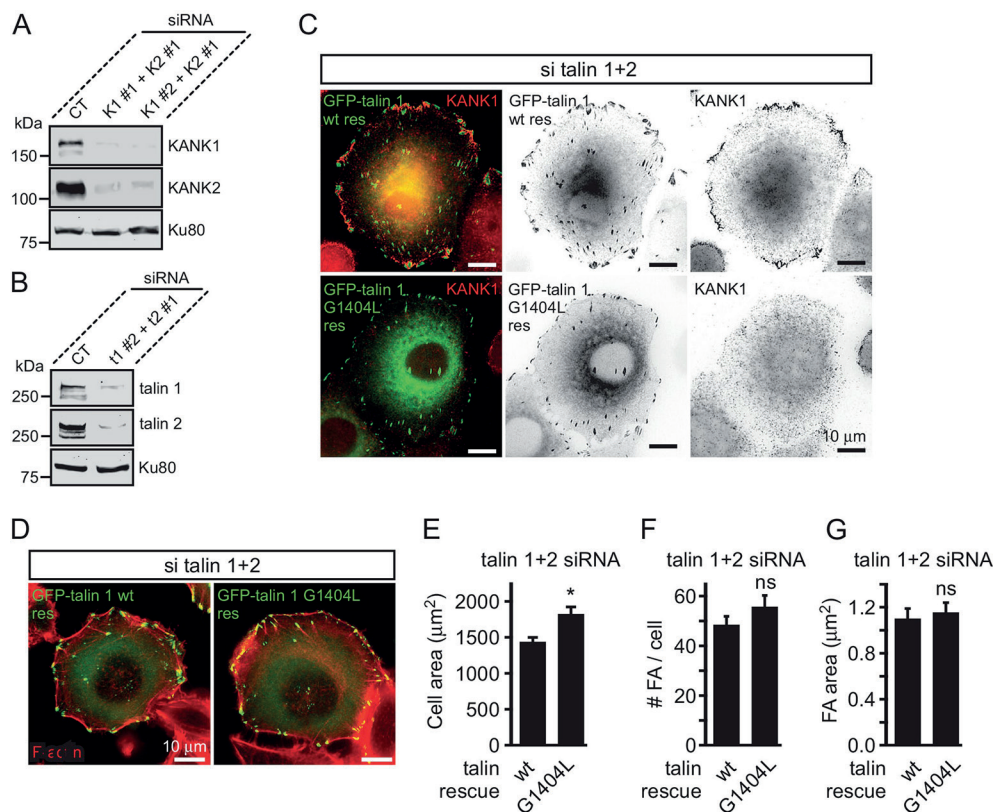
Figure 3—figure supplement 1. Validation of KANK1/2 and talin1/2 knockdown and effect of disrupted KANK/talin 1 binding in cell spreading and FA formation in HeLa cells
(**A–B**) Western blot analysis of KANK1/KANK2 (A), and talin1/talin2 (B) co-depletion by independent siRNAs (KANK1#1, K1 #1, KANK1#2, K1 #2 and KANK2#1, K2 #1; talin1 #2, t1 #2 and talin2#1, t2 #1) compared to control siRNA (CT). Ku80, loading control. (**C**) HeLa cells co-depleted of talin1 and talin2 were transfected with the indicated talin1 fusions and stained for the endogenous KANK1. (**D**) Fluorescent F-actin staining in cells treated as in (C). (**E–G**) Cell area (E), FA count (F) and FA area (G) in cells treated as in (C) (n=12 cells, 577–664 FAs analyzed). In all plots: error bar, SEM; ns, non-significant, *p<0.05, Mann- Whitney U test.

3

Force-dependent regulation of Talin-KANK1 complex at focal adhesions

Miao Yu[1#], Shimin Le[2#], **York-Christoph Ammon**[3#], Benjamin T Goult[4], Anna Akhmanova[3*], and Jie Yan[1,2,5*]

1 Mechanobiology Institute, National University of Singapore, Singapore
2 Department of Physics, National University of Singapore, Singapore
3 Cell Biology, Department of Biology, Faculty of Science, Utrecht University, Utrecht, The Netherlands
4 School of Biosciences, University of Kent, Canterbury, United Kingdom
5 Centre for Bioimaging Sciences, National University of Singapore, Singapore

* Corresponding authors

# These authors contributed equally

Abstract

KANK proteins mediate cross-talk between dynamic microtubules and integrin-based adhesions to the extracellular matrix. KANKs interact with the integrin/actin-binding protein talin and with several components of microtubule-stabilizing cortical complexes. Due to actomyosin contractility, the talin-KANK complex is likely under mechanical force, and its mechanical stability is expected to be a critical determinant of KANK recruitment to focal adhesions. Here, we quantified the lifetime of the complex of the talin rod domain R7 and the KN domain of KANK1 under shear-force geometry and found that it can withstand forces for seconds to minutes over a physiological force range up to 10 pN. Complex stability measurements combined with cell biological experiments suggest that shear-force stretching promotes KANK1 localization to the periphery of focal adhesions. These results indicate that the talin-KANK1 complex is mechanically strong, enabling it to support the cross-talk between microtubule and actin cytoskeleton at focal adhesions.

3

Introduction

Integrin-based adhesions (focal adhesions, FAs) are large macromolecular assemblies, which are crucial for cell migration, growth, and proliferation, as well as tissue formation and maintenance, because they transmit mechanical force and regulatory signals between cells and the extracellular matrix (ECM).[1,2] The molecular architecture of FAs is built up by a set of proteins including talin, paxillin, vinculin, and filamentous actin.[3] FAs are dynamic assemblies of these proteins that assemble on the cytoplasmic face of the integrin, and their life cycle is regulated by the coordinated actions of both actomyosin and the microtubule (MT) cytoskeleton.[4] MTs interact with FAs through a network of scaffolding proteins, among which the evolutionarily conserved KANK family proteins play a crucial role.[5]

The KANK family of proteins (KANK1−KANK4) are characterized by their unique structure, with the family specific KN motif at the N-terminus, followed by coiled-coil domains and ankyrin-repeats (Ank domain) in the C-terminal region[6] (see Figure 1a, left panel). The KN motif consists of 22−23 residues and is highly conserved across the KANK family.[7] KANK proteins interact with the cortical MT stabilization complexes (CMSCs) by binding to liprin-β1 through their coiled-coil domain. Moreover, KANK1 recruits KIF21A to CMSCs through the Ank domain.[8,9] By interacting with talin through the KN domain, KANK1 and KANK2 recruit to the peripheral zone of FA ("FA belt") the scaffolding protein liprin-β1, which tethers additional CMSC components and connect the MT targeting machinery to integrins.[7,10] Through these interactions, KANK proteins mediate a cross-talk between actin cytoskeleton and microtubule cytoskeleton networks at FAs.[5,7,10,11]

Talin is a mechanosensitive protein that links the integrin- mediated cell-matrix contacts to the actin cytoskeleton. Talin comprises an N-terminal FERM domain that binds to the cytoplasmic tails of integrins and a C-terminal rod domain containing 13 α-helical bundles (R1−R13) terminating with a single α-helix that mediates talin dimerization.[12] It also contains three actin binding sites located at the C-terminal end (ABS3),[13] four consecutive α-helical bundles in the rod (R4-R8, ABS2),[12,14,15] and an additional binding site located at the N-terminus (ABS1).[16] Both talin isoforms, talin1 and talin2, were shown to interact with KANK1 and KANK2 through the KN-domain, which is an α-helix containing a leucine-aspartic acid (LD) motif.[17] The KN-domain interacts with the talin R7 domain via the "helix-addition" binding mode, whereby the KANK KN-domain packs against the side of the 5-helix R7 bundle (see Figure 1a, right panel).[7,10,18] KANK1/2 binding to talin R7 can interfere with the actin binding to ABS2.[10]

The talin-R7/KANK-KN (R7/KN) complex is likely subject to mechanical force due to actomyosin contractility that generates a pulling force on talin.[15,19] The F-actin binding through ABS3 subjects all the domains in the talin rod to mechanical stretching.[20] As talin is tethered to the integrin at the plasma membrane, the mechanical deformation of talin under tensile force is expected to increase the distance between R7 and the membrane, which, in turn, would result in mechanical stretching of the region of KANK1/2 between the cortex-associated coiled coil domain and the talin R7- associated KN domain (Figure 1a).

The crucial role of KANK1/2−talin interaction in KANK's functions implies that the

3

R7/KN complex should be able to withstand physiological levels of forces. It has been shown that the forces in talin-mediated force transmission pathways are typically on the order of a few piconewtons (pN).[21–24] The lifetime of talin in FAs was estimated using fluorescence recovery after photobleaching (FRAP) assay in the order of a few tens of seconds.[25,26] Based on this information, we hypothesized that the R7/KN complex can withstand forces of a few piconewtons over a time scale on the order of seconds to minutes.

In cells, the force applied to the R7/KN complex is through the C-termini of R7 and KN (Figure 1a). Depending on the distance between the talin−FERM associated with integrin at the membrane and the KANK-coiled coil domain associated with the CMSC complex on membrane, and the angle of the talin rod relative to the two, the force on talin R7 and that on KANK-KN can have an angle in the range of $90° ≤ θ ≤ 180°$ (Figure 1a). The two extremes correspond to shear-force geometry ($θ = 180°$) and unzip-force geometry ($θ = 90°$), which are known to correspond to the strongest and weakest mechanical stabilities of a molecular complex, respec- tively.[27–29] We reasoned that the more mechanically stable R7/KN complex under shear force predominates the talin− KANK linkage. In this work, we used magnetic tweezers[30,31] to investigate the mechanical stability of R7/KN complex under the shear-force geometry (see Figure 1a, right (top panel) and Figure 1b). Furthermore, we performed cell biological experiments to test whether shear-force stretching geometry can promote KANK1 localization to the periphery of FAs. Our results suggest that the talin−KANK1 complex is mechanically strong, enabling it to support the cross-talk between microtubule and actin cytoskeleton at FAs, and shear-force stretching can promote KANK1 localization to the FA belt.

Results

R7/KN Complex Can Resist Piconewton-Range Shear Force

Measuring biomolecular interactions under mechanical force with magnetic tweezers is complicated by the presence of two molecules. One strategy to study such interactions is to tether the superparamagnetic bead on one molecule (e.g., the KN domain), which would bind to the other molecule (e.g., talin R7) tethered to the surface. In this scenario, force exerted on the bead is transmitted to the interaction interface. However, after a single force extension cycle, the tether would be lost due to dissociation of the complex. A meaningful experiment would thus require stretching of many independent tethers, which makes it difficult to perform experiments with high throughput.

To enable precise direct quantification of molecular complexes under the shear-force geometry (Figure 1a, right (top panel)), we performed the experiments using a novel single-molecule detector. The detector was comprised of an R7 domain of talin1 and a KN domain of KANK1, connected by a long flexible linker (222 a.a.), mainly derived from the FH1 domain of Diaph1, which we have characterized previously[32] (see Figure 1b). We also included two well-characterized titin I27 domains in the detector, which serve as a molecular spacer between the target R7/KN complex and the surface (Figure 1b). An avi-tag is inserted near the C-terminus of the R7 domain, and a spy-tag is attached at the C-terminus of the second I27 domain (Figure 1b). In addition, each domain is
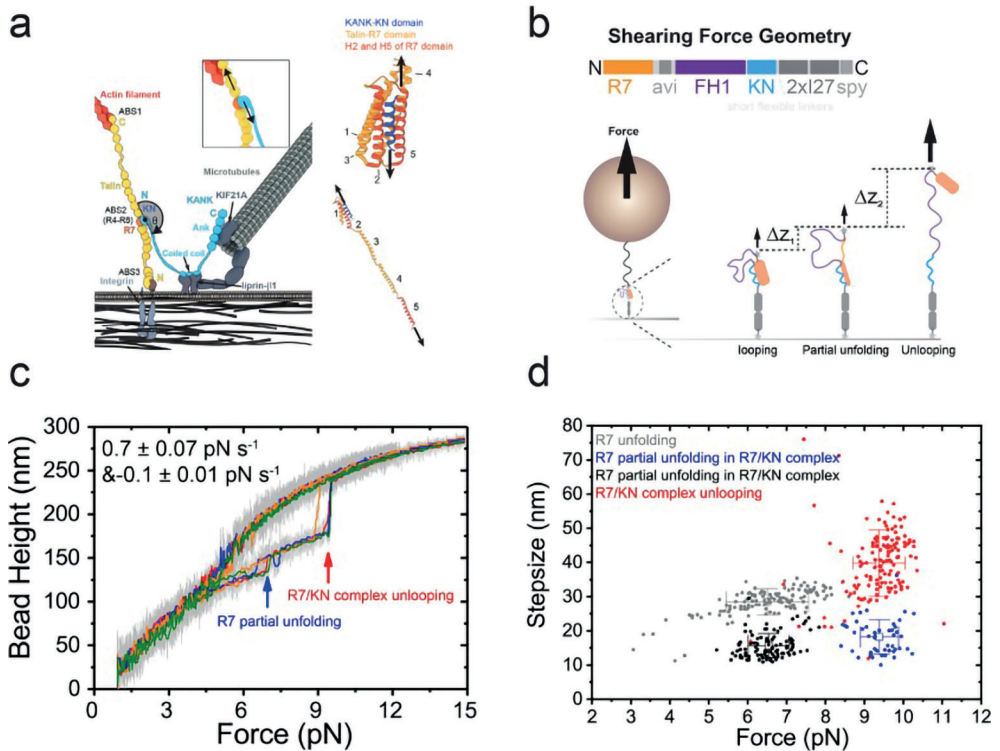
Figure 1. Mechanical stability of the R7/KN complex.
(**a**) Illustration of the talin and KANK interaction at FAs. Left panel: the FA core of integrin coupled to the actin cytoskeleton via talin. KANK (blue) mediates the linkage between talin and the CMSC (indicated liprin-β1, a component of CMSC), which binds to MTs. Inset: the geometry of the forces acting on the talin-R7:KANK-KN interaction. Right panel: structural model of the R7/KN complex under shear-force geometry at low force (top) and high force (bottom). (**b**). Top panel: single-molecule detector construct of R7/KN complex (N-to-C terminus): R7 domain, avi-tag, FH1 linker, KANK1-KN domain, two I27 domains, and spy-tag. Bottom panel: Force is applied through the C-termini of KANK1-KN and Talin1-R7. The R7/KN complex formed at low forces can be unlooped at increased force, R7/KN complex partially unfolding can occur before unlooping. The difference in bead height between the paired-looped state, and partially unfolded state is indicated by Δz_1, and that between partially unfolded state and the unpaired-unlooped state is indicated by Δz_2. (**c**) Four representative color-indicated force-extension curves of the single-molecule detector at force loading rates of 0.70 ± 0.07 pN s^{-1} (force increase) and -0.1 ± 0.01 pN s^{-1} (force decrease). The large extension jumps (red arrow) at ~9 pN corresponds to unlooping of the R7/KN complex; The smaller extension jumps (blue arrow) at 6-7 pN corresponds to partial unfolding of the R7 domain in the R7/KN complex. (d) The force-step size graph of the two extension jumps of R7/KN complex during force increase (~0.7 pN s^{-1}), which reveals three distinct groups indicated by red, blue and black colors. The red data points represent R7/KN complex unlooping, with force of 9.4 ± 0.1 pN (mean ± s.e.) and step size of 39.8 ± 0.8 nm. The black and blue data points represent the partial unfolding of talin1-R7 domain in the R7/KN complex with force of 6.5 ± 0.1 pN and step size of 15.6 ± 0.4 nm (black) and of 9.4 ± 0.1 pN and of 18.2 ± 0.7 nm (blue), respectively. Data obtained for single R7 domain unfolding during force increase (grey data points, ~0.5 pN s^{-1}) are provided for comparison, with force of 6.5 ± 0.1 pN and step size of 28.5 ± 0.3 nm. Over 100 data points were obtained from at least five independent tethers for R7 partial unfolding, R7/KN complex unlooping, and single R7 domain unfolding. The error bars in the graph indicate the mean value and standard deviation of the data in each group.

surrounded by short flexible linkers of several residues to ensure the flexibility of the detector. The detector was tethered between a coverslip and a 572-bp DNA handle linked 2.8-µm-diameter superparamagnetic bead (the DNA handle serves as a molecular spacer

between the complex and the bead), and was stretched by forces applied using magnetic tweezers that were made in-house.[30,31,33] In this design, after the R7/KN complex dissociates, the tether promotes complex reformation after force is released. Thus, one tether can be reused multiple times, which increases the throughput of the experiments. The detector has two conformational states: a looped state, where R7 and KN form a complex, and an unlooped state, where the R7 and KN are separated. Because of the long flexible linker, when subjected to force, the two states have significant differences in extension. The height of the bead in the longer unlooped state is higher than that in the shorter looped state, and this difference can be detected by the setup in real time at a nanometer spatial resolution for the bead height.[30]

Using this experimental setup, we obtained the force-dependent time traces of the bead height change. Figure 1c shows representative force-bead height curves during four consecutive cycles of force-increase (loading rate of 0.7 ± 0.07 pN s^{-1}) and force-decrease (loading rate of -0.1 ± 0.01 pN s^{-1}) scans (indicated by different colors) of a single tether. Two stepwise extension increases were observed during the force-increase scan: one at ~6.5 pN, with a step size of ~15 nm (blue arrow), and the other at ~9.5 pN, with a step size of ~40 nm (red arrow). Since the KN domain is an unstructured peptide and R7 is not under force if the R7/KN complex is disengaged (Figure 1b), it is unlikely to have unlooping in the first step and unfolding in the second step. Therefore, we can assign the first stepwise extension increase to be partial unfolding of the R7/KN complex and the second step can be assigned to be complete rupture of the complex, which results in unlooping of the detector. The complex could also be ruptured in a one-step process with a larger step size (see Figure S1 in the Supporting Information), which can be explained by concurrent partial unfolding and unlooping, or direct unlooping without partial unfolding of the complex.

Figure 1d shows the force-step size graph of the transition events obtained. The data suggest that the partial unfolding in the two-step process could occur at two distinct mechanical stability groups (black and blue), indicated by the well- separated unfolding forces at 6.5 ± 0.5 pN (mean ± standard deviation) and at 9.4 ± 0.5 pN, respectively. For comparison, unfolding of R7 alone occurs at forces of ~6.5 ± 1.1 pN with a step size of 28.5 ± 3.9 nm (Figure 1d, gray). The presence of two mechanically stable groups of partial unfolding of talin R7 in the R7/KN complex likely indicates the presence of two transition pathways with different force-dependent kinetics. Despite the different transition forces, the two groups of partial unfolding have very similar transition step sizes of 15.6 ± 3.6 nm and 18.2 ± 5.0 nm. Such step sizes are much shorter than the extension change expected from dissociation of the R7/KN complex, which is consistent with the explanation that they correspond to partial unfolding of the R7/KN complex. Fitting the partial-unfolding force distributions for the black and blue groups with Bell's model[34,35] reveals large transition distances of 6−8 nm associated with partial unfolding of the R7/KN complex (see Figures S2 and S3 in the Supporting Information), suggesting large conformational changes of the R7/KN complex preceding the partial unfolding transitions.

The red group, which is characterized with a large step size of 39.8 ± 9.7 nm and a transition force of 9.4 ± 0.7 pN, represents the complete rupture of the R7/KN complex. Data in this group include the second stepwise extension increases in the two-step process

and the stepwise extension increases in the single-step process. Direct unlooping without partial unfolding is expected to be associated with a step size of ~55 nm at ~10 pN, because of the presence of the long flexible linker and based on worm-like-chain (WLC) model estimation (see Supplementary Text S2 in the Supporting Information).[32,36,37] In contrast, if partial unfolding precedes the final rupturing of the complex, the extension of the linker is pre-extended (Figure 1b). As a result, the step size associated with the final rupturing of the complex can be significantly less. This explains why the step sizes of the unlooping spread over a range from 15 nm to 55 nm (Figure 1d, red). Similar to the partial unfolding transition, a large transition distance of ~8 nm was estimated for the unlooping transition based on Bell's model fitting, suggesting a large conformational change of the R7/KN complex preceding the final rupture of the complex (see Figure S2 in the Supporting Information).

R7/KN Complex Exhibits Catch-to-Slip Bond Switching Behavior
In order to quantify the mechanical stability of the R7/KN complex, we measured the lifetime of the R7/KN complex at different forces using a force-jump-cycle procedure by holding the R7/KN complex at different forces and recording the dwell time until the unlooping transition occurred. Briefly, in each force-jump cycle, the molecule was first held at a low force of ~2 pN for ~10 s (blue data in Figure 2a) to allow the formation of the R7/KN complex, and then jumped to ~4 pN for 1 s to check whether the R7/KN complex was formed or not, since there is a distinct bead height difference between the paired and unpaired states of the molecule at ~4 pN (magenta data in Figure 2a). The force then jumped to the target force (e.g., ~7.2 pN, red data in Figure 2a) and kept at that force for sufficiently long time until the complete rupture of the R7/KN complex was observed. Figure 2a shows a representing time trace of the bead height recorded at ~7.2 pN (four further time traces are shown in Figure S4 in the Supporting Information), where the looped state of the detector lasted for ~25 s until unlooping (indicated by the red arrow) after the force jumped to ~7.2 pN. During the ~25 s before the unlooping transition, reversible stepwise bead height changes of step sizes of ~15 nm (indicated by blue arrows) resulted from partial unfolding/refolding of the R7/ KN complex.
Figure 2b shows the resulting force-dependent lifetime of the R7/KN complex (gray data points). At each force, 50−200 data points were obtained from at least five independent tethers. The data can be fitted with exponentially decaying function (see Figure S5), which determines the time constant (i.e., the average lifetime) at different forces (red circles). The data reveal that the R7/KN complex can last for seconds to minutes over a force range up to 10 pN, with the maximum lifetime occurring at ~6 pN. The nonmonotonic force- dependence of the mechanical lifetime of the R7/KN complex indicates a switch from a catch-bond behavior (lifetime increases as force increases) to a slip-bond behavior (lifetime decreases as force increases) at forces of ~6 pN. The possible causes of this catch-to-slip switch behavior are discussed in the Discussion section.

Membrane Tethering Promotes Force-Dependent KN Localization to FA Periphery
The mechanical stability of the R7/KN complex is expected to have a strong dependence on the pulling geometry. We reasoned that KANK proteins may enrich at locations of FAs where the mechanical stability of the talin−KANK association is maximized. To test
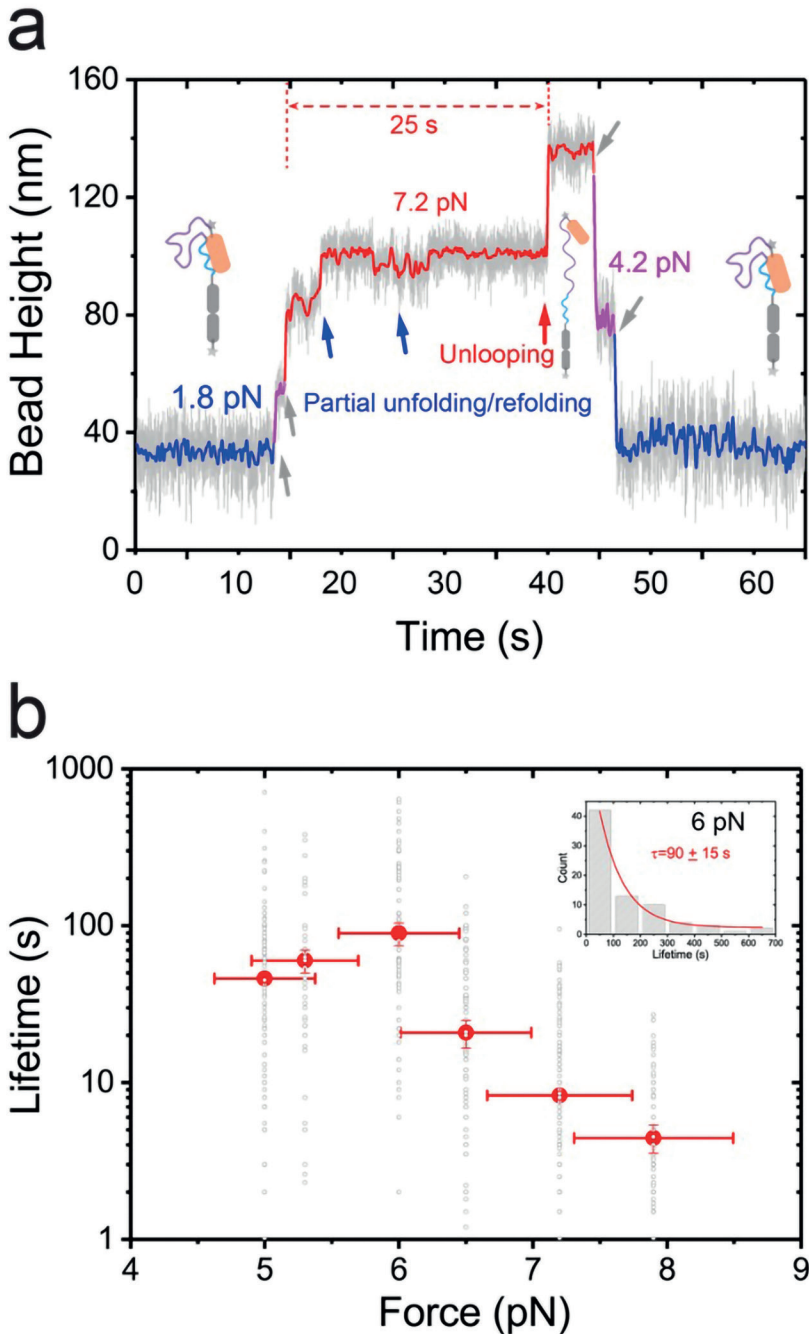
Figure 2. Mechanical lifetime of the R7/KN complex.
(a) Representative time trace of extension change during force-jumping assay to quantify the mechanical lifetime of the R7/KN complex at various forces. In such an assay, after jumping from 1.8 pN to a higher force, the average lifetime of the complex at the higher force is measured in multiple cycles. In this example, the lifetime (~25 s, indicated by dashed red arrow) of the complex at 7.2 pN in one force jump

is shown. Blue arrows indicate stepwise extension changes associated with partial unfolding/refolding prior to unlooping. The red arrow indicates stepwise extension change associated with unlooping. The grey arrows indicate force change-induced bead height changes during force jumps. The insets show the sketches of the detector in the looped state at ~1.8 pN and the unlooped state at ~7.2 pN. Additional examples of time trace extension change during force-jumping assay are shown in Supplementary Figure S4. (b) Force-dependent lifetime of the R7/KN complex. The hollow grey circles represent each individual lifetime measured. The red solid circles represent the characteristic lifetime obtained from exponential decay fitting of the raw data at each force. Inset shows a representative exponential fitting for data obtained at 6 pN, the exponential decay fitting of the lifetime distributions at all forces are shown in Supplementary Figure S5. The lateral-error bar indicates 10% force calibration error of the magnetic tweezers system. The vertical-error bar indicates s.e. of the mean value of the lifetime. 50-200 data points were obtained from at least five independent tethers at each force.

whether shear-force geometry leading to stronger mechanical stability could be a potential mechanism contributing to the peripheral localization of KANK proteins at FAs,[7,10] we examined whether the KN domain, which, by itself, localizes throughout the FA,[7,10] would display a different localization if tethered to the plasma membrane imposing a pulling geometry on the interaction with talin. To achieve this, we fused a membrane anchoring CAAX-motif of Ras GTPase to the C-terminus of the KN domain (Figure 3a). To exclude the potential effects of endogenous KANKs on the localization of KANK fragments, we used HeLa cells that were knocked out for KANK2 and depleted of KANK1, the two predominant KANK isoforms in these cells[8] (see Figures S6a and S6b in the Supporting Information). Interestingly, the KN domain, either alone or with the adjacent "L1" linker region C-terminal of the KN domain (Figure 3a), localized throughout the FA, whereas the CAAX-fused version of KN-L1 was enriched at the periphery of FAs in a pattern that was reminiscent of the localization of the full-length KANK1 (see Figures 3b−d, as well as Figure S7 in the Supporting Information) in low expressing cells. In contrast, the L1-CAAX fusion without the KN domain was distributed evenly at the plasma membrane and showed no enrichment at FAs (see Figures 3c and 3d). The observed differences in the localization of KN-L1 and KN-L1-CAAX were unlikely to be due to the effects of these constructs on the FAs, as these constructs had no significant impact on the FA number and the size (see Figure S6c). FRAP-based analysis of the turnover of different KN constructs showed that their localization reflected the part of the FA where they are preferentially recruited (throughout FA for KN or KN-L1, peripherally for KN-L1-CAAX) rather than some complex redistribution of the construct within FA after the binding (Figures 3e and 3f). These results are consistent with the hypothesis that plasma membrane tethering, which is expected to lead to a shear-force geometry of the talin−KANK1 interaction, can promote KANK1 enrichment at the FA periphery, possibly because the mechanical stability of KANK/ talin association is maximized at these sites. To investigate whether the peripheral distribution of KN-L1- CAAX is dependent on the pulling forces exerted on FAs, we attenuated these forces using the ROCK1 inhibitor Y27632, which induces gradual FA disassembly (see Figures S8a−S8d in the Supporting Information). Although the KN and KN-L1 fragments strongly colocalized with the FA marker paxillin at all time points, the KN-L1+CAAX fusion was located at the FA periphery but moved into the core of FA after the ROCK inhibitor treatment (Figure S8a). This was reflected by an increase in the correlation coefficient between the two signals (Figure S8b) and was also observed in live cells (Figure S8e). These data were similar to those obtained for full-length KANK1 in ROCK inhibitor-treated cells (Figure
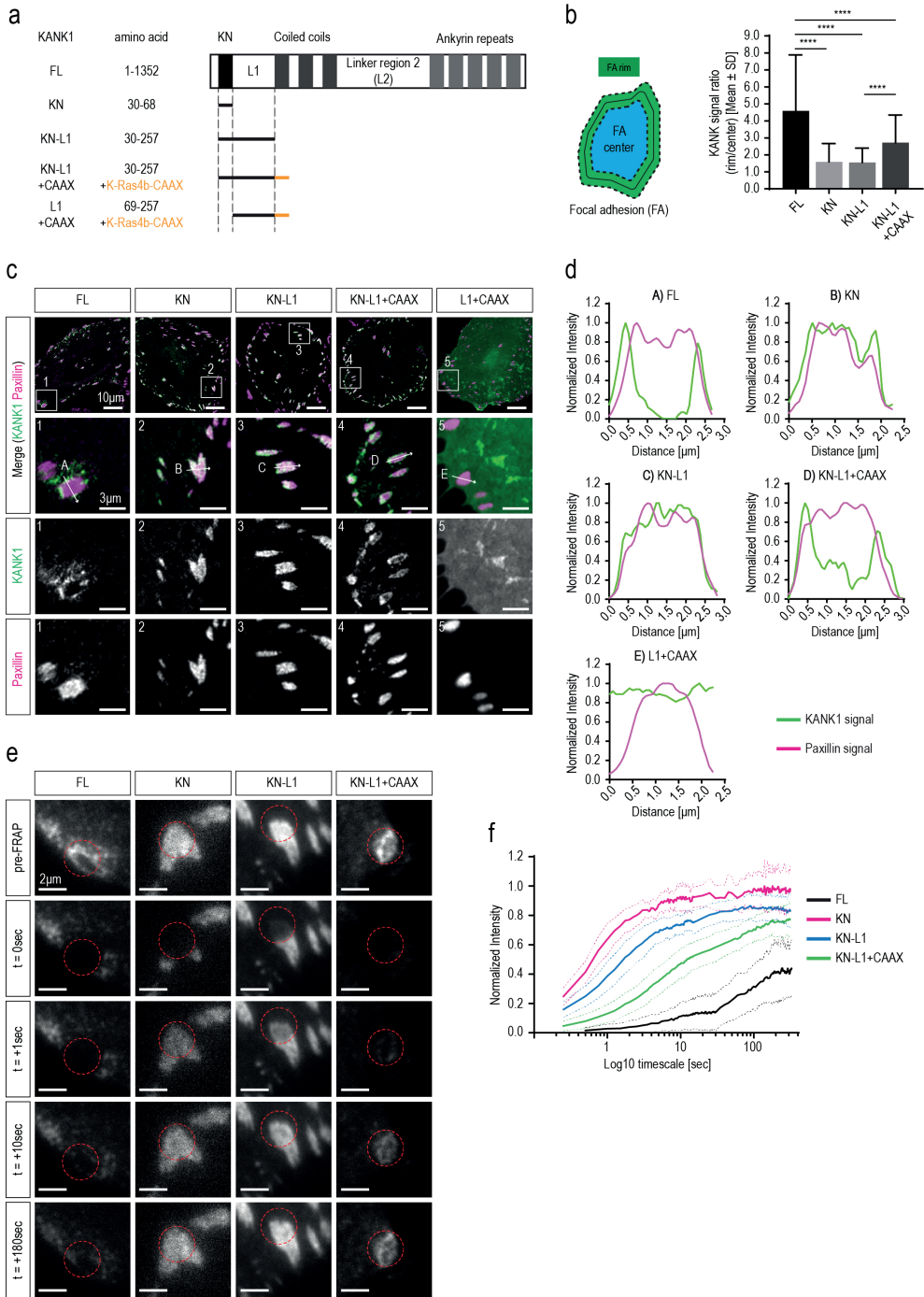
3

Figure 3. Localization of KANK1 and its KN-containing fragments at FAs.
(**a**) Schematic representation of full-length KANK1 and the different KANK1 fragments. CAAX, contains the membrane anchoring motif from K-Ras4b. (**b**) Quantification of KANK1 clustering at FAs. The left panel illustrates how the clustering of the different KANK1 constructs was analyzed: A ratio of the

KANK1 signal at the FA rim, which extends 0.2 μm beyond the FA outline and 0.2 μm into the FA to the KANK1 signal at the FA central part, was measured. The right panel shows the bar plot with the ratios expressed as mean ± SD. For each condition, 143 – 225 FAs were analyzed in at least two independent experiments (FL n=145 [2 experiments]; KN n=171 [3 experiments]; KN-L1 n=143 [2 experiments], KN-L1+CAAX n=225 [2 experiments]). For statistical analysis a one-way ANOVA test was performed using GraphPad Prism software (****, p < 0.0001). (**c,d**) Localization of the indicated KANK1 constructs in HeLa cells. HeLa cells knockout for KANK2 and depleted of KANK1 using siRNA transfection were transiently transfected with GFP-tagged and siRNA-resistant KANK1 constructs (green). Cells were fixed and stained for the endogenous FA protein paxillin (magenta). Full-length KANK1 localizes exclusively to the FA rim (enlargement 1 line scan in Fig. 3c,d-A) and is absent from the central area of FAs (see line scan Fig. 3d-A). The KANK1-KN and the KANK1-KN-L1 constructs overlap with FAs and show high abundance in the central area of FAs (enlargement 2 and 3 and line scans in Fig. 3c,d-B and C). The addition of the membrane anchoring CAAX motif to the KANK1-KN-L1 construct (KANK1-KN-L1+CAAX) leads to the enrichment in FA rim area (enlargement 4 and line scan in Fig. 3c,d-D). The membrane anchoring CAAX motif without the talin binding KN domain (KANK1-L1+CAAX) shows even distribution at the plasma membrane and no enrichment at FAs (enlargement 5 and line scan in Fig 3d-E). The arrows (A-E) represent the direction of the line scans shown in Fig. 3d. Three more line scans were performed for each of the 5 original line scans, results are shown in Figure S7. (**e**) Single frames of FRAP experiments in HeLa cells prepared as described above. A pre-FRAP image, the first frame after photobleaching (t = 0 sec) and the indicated time points after FRAP of a 2.3-μm-diameter circle region in the KANK1 patch are shown. (**f**) Quantification of fluorescence recovery. The graph shows mean curves (bold lines) ± SD (light dotted lines) over time. For each condition, in total 18 – 40 KANK1 patches were analyzed in two independent experiments (FL n=26; KN n=18; KN-L1 n=31; KN-L1+CAAX n=40).

S8a−S8f), although full-length KANK1 never showed such a complete overlap with FA markers as the different KN fusions, because it also partly colocalized with the liprin-containing cortical sites (Figures S8a−S8f). Our data support the idea that forces exerted on talin play an important role in the localization of plasma membrane-tethered KN domain to the periphery of FAs.

Discussion

Using a novel single-molecule detector to study protein− protein interactions with magnetic tweezers, we have quantified the mechanical stability of the talin−KANK complex. We find that, under shear-force geometry, this complex can withstand forces of several piconewtons for seconds to minutes. This force range lies within the physiological force level in the talin-mediated force-trans- mission pathway measured using a single-molecule force sensor.[15,21,23,38,39] The survival time scale over this force range is similar to the talin lifetime in FAs in living cells (tens of seconds), based on talin turnover rate measurements.[25,26,40] Therefore, the R7/KN complex is able to support a mechanically stable connection between talin and KANK1.

Because of the highly conserved sequences of KN motifs among all four KANK family proteins, similar mechanical stability can be expected for the complexes formed between R7 and KN from different KANK proteins. Together, these results suggest that the R7-KN interaction is capable of mediating a robust cross-talk between the actomyosin network and MTs at FAs. The functional implications of this cross-talk deserve further exploration. For example, a recent paper reported that depletion of either KANK1 or KANK2 or overexpression of the KN domain led to FA enlargement,[11] whereas we and others have observed no strong effects of KANK loss or KN expression on FA size or disassembly.[7,10] Whether this reflects the distinct cell types used or other experimental

differences requires further investigation.

An important finding is that the R7/KN complex has a maximum lifetime at forces of ~6 pN, indicating a catch-bond kinetics at forces below 6 pN. The catch-bond kinetics refers to an anti-intuitive phenomenon where the molecular lifetime increases as the force applied to the interacting molecules increases, which is often observed at a physiological level of forces[41–43] under shear-force geometry.[27,28,44] At forces above 6 pN, the R7/KN complex follows a slip-bond kinetics, which refers to quicker molecular dissociation at increased forces. Together, the R7/KN complex exhibits catch-to-slip switching behavior, which has an apparent advantage to define an optimal force range for stable talin/KANK connection.

As suggested in previous theoretical studies, such catch-to- slip switch behavior can be explained by multidimension models such as single-state multipathway models where the transitions starting from the same native state can follow different pathways, and multistate models where the transitions can start from different force-dependent competitive "native" states, each following a single pathway leading to unfolding/rupturing,[45–49] or by differential entropic elastic extension fluctuation of the molecule in the native and the transition states at low forces (typically a few piconewtons), where the entropic elastic extension fluctuation cannot be ignored.[27,28,50] Since the unlooping transition of the R7/KN detector could occur in two steps or one step at forces on the level of a few piconewtons, all these mechanisms are eligible candidates for the observed catch-to-slip switch behavior in our experiments.

Interestingly, we observed that the R7/KN complex can undergo partial unfolding before complete dissociation. Since KN is a single peptide in the R7/KN complex, the intrinsically disordered FH1 cannot contribute to unfolding signals,[32] and the two I27 domains have an ultraslow unfolding rate at forces below 20 pN (<0.001/s per domain),[27] this partial unfolding should occur via the unraveling of a few α-helices in R7. The R7 domain contains five α-helices (H1−H5) and, based on the step size (~15 nm) of the partial unfolding and the corresponding unfolding force, we estimated that, under these conditions, approximately three α-helices should be unraveled from R7 and released under force. A previous molecular docking study suggested that the KN peptide mainly interacts with helices H2 and H5 in R7 (Figure 1a).[7] Since the force is applied to the C-termini of KN and H5 of R7, according to the structure predicted based on molecular docking, one must assume that H5 needs to dissociate from KN. The step size of 15 nm observed for the partial unfolding suggests that H4 and H3 are likely also unraveled from R7. Based on this model, in the partially unfolded R7/KN complex, the KN peptide could remain bound to the H1/H2 coiled coil through the predicted interaction with H2 and potential interacting sites on the exposed H1 (Figure 1a, right (bottom panel)).

The mechanical stability of the R7/KN complex is expected to have a strong dependence on the pulling geometry. In this work, we quantified the mechanical stability of the R7/KN under the shear-force geometry, which provides the highest mechanical stability. We reason that this pulling geometry may play the most important role in mediating the stable connection between actomyosin network and CMSCs, since the R7/KN complexes formed under a less-stable pulling geometry may dissociate quickly. One could imagine that KANK proteins are likely enriched at locations under optimal pulling geometry (shear-force geometry) and optimal force range (~6 pN).

Interestingly, KANK proteins are enriched at the periphery of FAs.[7,10] It remains unclear whether this localization can be explained by the mechanical stability of the talin−KANK complex, or whether it requires interactions between KANKs, talin, and other proteins. It is thought that competition between the KN domain and actin is a factor that contributes to the exclusion of KANKs from the FA cores.[5,7] However, this mechanism is not sufficient to explain the peripheral enrichment of KANK at FAs, because the KN domain alone binds to talin throughout a focal adhesion (see, e.g., Figure 3). Experiments in cells have revealed that KANK1-KN-L1-CAAX preferentially localized to the periphery of FAs in low- expressing cells, while KANK1-KN and KANK1-KN-L1 without the CAAX motif were distributed more evenly throughout FAs, and the KANK1-L1-CAAX without the KN domain resulted in complete loss of the FA localization. Since the KANK1-KN-L1-CAAX construct lacks the domains interacting with any known KANK1 partners except talin, these results are consistent with the idea that the KN domain directs the FA localization of KANK and that the membrane tethering creates a shear-force geometry, which promotes KANK enrichment at FA periphery by increasing the mechanical stability of the talin−KANK linkage. Further support for the importance of forces exerted on the talin−KANK linkage for KANK localization is provided by the experiments on ROCK inhibition, which show that both full-length KANK1 and the membrane-tethered KN domain redistribute into the FA core when actomyosin contractility is attenuated. It will be interesting to measure the forces in talin molecules at different locations in FAs, which may provide additional insights into whether the optimal mechanical stability is a mechanism underlying the distribution of KANK proteins at FAs.

The single-molecule detector approach described in this study provides a highly effective way to directly quantify the mechanical stability of binary molecular complexes formed by two proteins or between two domains within one protein. In the future, applications of this approach will allow quantification of the mechanical stability of several crucial connections involved in various mechanotransduction pathways at different types of cell−ECM and cell−cell adhesions.

Experimental procedures

Single-Protein Manipulation and Analysis.
All *in vitro* single-protein stretching experiments were performed using a vertical magnetic tweezers setup.[30,31] The channel is combined with a disturbance-free, rapid solution-exchange method[51] to avoid flow-drag during sample preparation. Experiments were performed in solution containing 1X PBS, 1% BSA, 2 mM DTT, and 10 mM sodium L-ascorbate at 21 ± 1 °C. In typical magnetic tweezers experiments, the height of the superparamagnetic bead from the bottom coverslip surface is recorded. The bead-height change is the extension change of the molecule when the force applied to the bead remains constant. When the force applied to the bead changes, the bead-height change is a combined effect of the forcedependent elastic extension change of the molecule and bead-rotation due to force-change-induced torque rebalance.[33,52] Therefore, a concurrent stepwise bead-height change is usually observed during force jump (which takes ≤ 0.25 s in our setup). On the other hand, during the linear force-increase/force-decrease scans with a loading rate of ~0.5−1 pN s^{-1} used in our study, the stepwise bead-height change is the same as the stepwise extension change of the molecule. This is because the force change over the time window of the stepwise transition (≤ 0.01 s, the temporal resolution of our setup) is negligible (≤ 0.01 pN). More details of plasmid constructs, protein expression, and data analysis can be found in Supplementary Text S1 and S2 in the Supporting Information.

Cell culture and transfection
HeLa cells knocked out for KANK2 were cultured in a DMEM medium with 10% (v/v) fetal calf serum and with 1% (v/v) penicillin/streptomycin. The cell line was routinely checked for mycoplasma contamination using Mycoalert assay (LT07−318, Lonza), following the supplier's instructions. Transfection of DNA and siRNA into these cells was performed as previously described in the work reported by van der Vaart et al.[8] siRNAs were transfected using HiPerFect (Qiagen) at a concentration of 20 nM and cells were analyzed 72 h after transfection. DNA constructs were transfected using FuGene6 (Promega). More details of antibodies and immunofluorescence staining, DNA constructs and siRNAs, transfection procedures, generation of HeLa KANK2 knockout cell line, fluorescence microscopy and analysis, and fluorescence recovery after photobleaching and data analysis can be found in Supplementary Text S3−S9 in the Supporting Information.

Data availability
The authors declare that all data supporting the findings of this study are available within the article and its Supplementary Information or from the corresponding author upon reasonable request.

Author Contributions

J.Y. M.Y. and S.L. designed the study. M.Y., S.L. performed the single-molecule stretching experiments and analyzed the data; Y.A. and A.A. designed and performed the cell imaging experiments and data analysis. J.Y., M.Y., S.L., Y.A., B.G. and A.A. interpreted the data. J.Y. M.Y. and S.L. wrote the paper. J.Y. and A.A. supervised the study.

Acknowledgements

3

1. Arnaout, M. A.; Goodman, S. L.; Xiong, J. P. Curr. Opin. Cell Biol. 2007, 19 (5), 495−507.

2. Elosegui-Artola, A.; Oria, R.; Chen, Y.; Kosmalska, A.; Perez- Gonzalez, C.; Castro, N.; Zhu, C.; Trepat, X.; Roca-Cusachs, P. Nat. Cell Biol. 2016, 18 (5), 540−8.

3. Kanchanawong, P.; Shtengel, G.; Pasapera, A. M.; Ramko, E. B.; Davidson, M. W.; Hess, H. F.; Waterman, C. M. Nature 2010, 468 (7323), 580−4.

4. Fletcher, D. A.; Mullins, R. D. Nature 2010, 463 (7280), 485− 92.

5. Chen, N. P.; Sun, Z.; Fassler, R. Curr. Opin. Cell Biol. 2018, 54, 130−136.

6. Kakinuma, N.; Zhu, Y.; Wang, Y.; Roy, B. C.; Kiyama, R. Cell. Mol. Life Sci. 2009, 66 (16), 2651−9.

7. Bouchet, B. P.; Gough, R. E.; Ammon, Y. C.; van de Willige, D.; Post, H.; Jacquemet, G.; Altelaar, A. M.; Heck, A. J.; Goult, B. T.; Akhmanova, A. eLife 2016, 5. DOI: 10.7554/eLife.18124.

8. van der Vaart, B.; van Riel, W. E.; Doodhi, H.; Kevenaar, J. T.; Katrukha, E. A.; Gumy, L.; Bouchet, B. P.; Grigoriev, I.; Spangler, S. A.; Yu, K. L.; Wulf, P. S.; Wu, J.; Lansbergen, G.; van Battum, E. Y.; Pasterkamp, R. J.; Mimori-Kiyosue, Y.; Demmers, J.; Olieric, N.; Maly, I. V.; Hoogenraad, C. C.; Akhmanova, A. Dev. Cell 2013, 27 (2), 145−160.

9. Guo, Q.; Liao, S.; Zhu, Z.; Li, Y.; Li, F.; Xu, C. J. Biol. Chem. 2018, 293 (2), 557−566.

10. Sun, Z.; Tseng, H. Y.; Tan, S.; Senger, F.; Kurzawa, L.; Dedden, D.; Mizuno, N.; Wasik, A. A.; Thery, M.; Dunn, A. R.; Fassler, R. Nat. Cell Biol. 2016, 18 (9), 941−53.

11. Rafiq, N. B. M.; Nishimura, Y.; Plotnikov, S. V.; Thiagarajan, V.; Zhang, Z.; Shi, S.; Natarajan, M.; Viasnoff, V.; Kanchanawong, P.; Jones, G. E.; Bershadsky, A. D. Nat. Mater. 2019, 18 (6), 638−649.

12. Goult, B. T.; Zacharchenko, T.; Bate, N.; Tsang, R.; Hey, F.; Gingras, A. R.; Elliott, P. R.; Roberts, G. C.; Ballestrem, C.; Critchley, D. R.; Barsukov, I. L. J. Biol. Chem. 2013, 288 (12), 8238−49.

13. Gingras, A. R.; Bate, N.; Goult, B. T.; Hazelwood, L.; Canestrelli, I.; Grossmann, J. G.; Liu, H.; Putz, N. S.; Roberts, G. C.; Volkmann, N.; Hanein, D.; Barsukov, I. L.; Critchley, D. R. EMBO J. 2008, 27 (2), 458−69.

14. Atherton, P.; Stutchbury, B.; Wang, D. Y.; Jethwa, D.; Tsang, R.; Meiler-Rodriguez, E.; Wang, P.; Bate, N.; Zent, R.; Barsukov, I. L.; Goult, B. T.; Critchley, D. R.; Ballestrem, C. Nat. Commun. 2015, 6, 10038.

15. Kumar, A.; Ouyang, M.; Van den Dries, K.; McGhee, E. J.; Tanaka, K.; Anderson, M. D.; Groisman, A.; Goult, B. T.; Anderson, K. I.; Schwartz, M. A. J. Cell Biol. 2016, 213 (3), 371−83.

16. Hemmings, L.; Rees, D. J.; Ohanian, V.; Bolton, S. J.; Gilmore, A. P.; Patel, B.; Priddle, H.; Trevithick, J. E.; Hynes, R. O.; Critchley, D. R. J. Cell Sci. 1996, 109 (Pt 11), 2715−2726.

17. Alam, T.; Alazmi, M.; Gao, X.; Arold, S. T. Biochem. J. 2014, 460 (3), 317−29.

18. Goult, B. T.; Yan, J.; Schwartz, M. A. J. Cell Biol. 2018, 217, 3776−3784.

19. (19) Margadant, F.; Chew, L. L.; Hu, X.; Yu,

H.; Bate, N.; Zhang, X.; Sheetz, M. PLoS Biol. 2011, 9 (12), No. e1001223.

20. Yan, J.; Yao, M.; Goult, B. T.; Sheetz, M. P. Cell. Mol. Bioeng. 2015, 8 (1), 151−159.

21. Grashoff, C.; Hoffman, B. D.; Brenner, M. D.; Zhou, R.; Parsons, M.; Yang, M. T.; McLean, M. A.; Sligar, S. G.; Chen, C. S.; Ha, T.; Schwartz, M. A. Nature 2010, 466 (7303), 263−6.

22. Austen, K.; Ringer, P.; Mehlich, A.; Chrostek-Grashoff, A.; Kluger, C.; Klingner, C.; Sabass, B.; Zent, R.; Rief, M.; Grashoff, C. Nat. Cell Biol. 2015, 17 (12), 1597−606.

23. Ringer, P.; Weissl, A.; Cost, A. L.; Freikamp, A.; Sabass, B.; Mehlich, A.; Tramier, M.; Rief, M.; Grashoff, C. Nat. Methods 2017, 14 (11), 1090−1096.

24. Yao, M.; Goult, B. T.; Klapholz, B.; Hu, X.; Toseland, C. P.; Guo, Y.; Cong, P.; Sheetz, M. P.; Yan, J. Nat. Commun. 2016, 7, 11966.

25. Himmel, M.; Ritter, A.; Rothemund, S.; Pauling, B. V.; Rottner, K.; Gingras, A. R.; Ziegler, W. H. J. Biol. Chem. 2009, 284 (20), 13832−13842.

26. Hakonardottir, G. K.; Lopez-Ceballos, P.; Herrera-Reyes, A. D.; Das, R.; Coombs, D.; Tanentzapf, G. Mol. Biol. Cell 2015, 26 (22), 4149−4162.

27. Yuan, G.; Le, S.; Yao, M.; Qian, H.; Zhou, X.; Yan, J.; Chen, H. Angew. Chem., Int. Ed. 2017, 56 (20), 5490−5493.

28. Guo, S.; Tang, Q.; Yao, M.; You, H.; Le, S.; Chen, H.; Yan, J. Chem. Sci. 2018, 9 (27), 5871−5882.

29. Wang, X.; Ha, T. Science 2013, 340 (6135), 991−4.

30. Chen, H.; Fu, H.; Zhu, X.; Cong, P.; Nakamura, F.; Yan, J. Biophys. J. 2011, 100 (2), 517−23.

31. Le, S.; Liu, R.; Lim, C. T.; Yan, J. Methods 2016, 94, 13−8.

32. Yu, M.; Le, S.; Efremov, A. K.; Zeng, X.; Bershadsky, A.; Yan, J. Nano Lett. 2018, 18 (8), 5239−5247.

33. Zhao, X.; Zeng, X.; Lu, C.; Yan, J. Nanotechnology 2017, 28 (41), 414002.

34. Bell, G. I. Science 1978, 200 (4342), 618−27.

35. Le, S.; Yu, M.; Hovan, L.; Zhao, Z.; Ervasti, J.; Yan, J. ACS Nano 2018, 12 (12), 12140−12148.

36. Marko, J. F.; Siggia, E. D. Macromolecules 1995, 28 (26), 8759−8770.

37. Bustamante, C.; Marko, J. F.; Siggia, E. D.; Smith, S. Science 1994, 265 (5178), 1599−600.

38. Morimatsu, M.; Mekhdjian, A. H.; Adhikari, A. S.; Dunn, A. R. Nano Lett. 2013, 13 (9), 3985−9.

39. Roca-Cusachs, P.; Conte, V.; Trepat, X. Nat. Cell Biol. 2017, 19 (7), 742−751.

40. Hernandez-Varas, P.; Berge, U.; Lock, J. G.; Stromblad, S. Nat. Commun. 2015, 6, 7524.

41. Huang, D. L.; Bax, N. A.; Buckley, C. D.; Weis, W. I.; Dunn, A. R. Science 2017, 357 (6352), 703−706.

42. Sarangapani, K. K.; Qian, J.; Chen, W.; Zarnitsyna, V. I.; Mehta, P.; Yago, T.; McEver, R. P.; Zhu, C. J. Biol. Chem. 2011, 286 (37), 32749−61.

3

43. Sokurenko, E. V.; Vogel, V.; Thomas, W. E. Cell Host Microbe 2008, 4 (4), 314−23.

44. Marshall, B. T.; Long, M.; Piper, J. W.; Yago, T.; McEver, R. P.; Zhu, C. Nature 2003, 423 (6936), 190−3.

45. Evans, E.; Leung, A.; Heinrich, V.; Zhu, C. Proc. Natl. Acad. Sci. U. S. A. 2004, 101 (31), 11281−6.

46. Barsegov, V.; Thirumalai, D. Proc. Natl. Acad. Sci. U. S. A. 2005, 102 (6), 1835−9.

47. Pierse, C. A.; Dudko, O. K. Phys. Rev. Lett. 2017, 118 (8), 088101.

48. Pereverzev, Y. V.; Prezhdo, O. V.; Forero, M.; Sokurenko, E. V.; Thomas, W. E. Biophys. J. 2005, 89 (3), 1446−54.

49. Bartolo, D.; Derenyi, I.; Ajdari, A. Phys. Rev. E: Stat. Phys., Plasmas, Fluids, Relat. Interdiscip. Top. 2002, 65 (5), 051910.

50. Guo, S.; Efremov, A. K.; Yan, J. Commun. Chem. 2019, 2 (1), 30.

51. Le, S.; Yao, M.; Chen, J.; Efremov, A. K.; Azimi, S.; Yan, J. Nucleic Acids Res. 2015, 43 (17), No. e113.

52. Fu, H.; Le, S.; Chen, H.; Muniyappa, K.; Yan, J. Nucleic Acids Res. 2013, 41 (2), 924−32.

Supplementary Figures
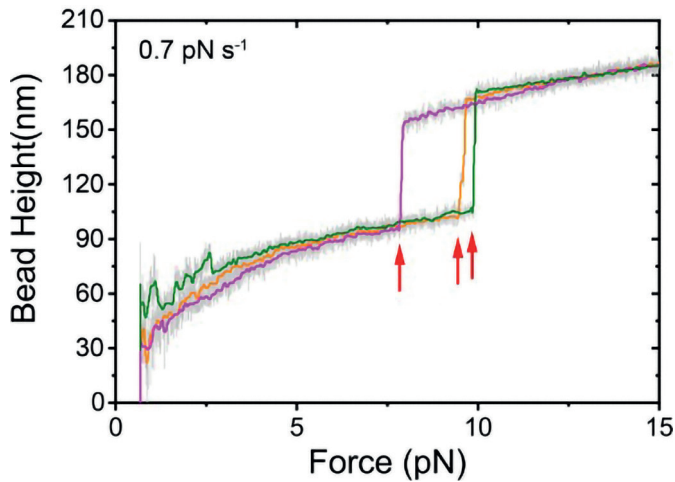
Supplementary Figure S1.
Three representative single-step unlooping (red arrows) of the R7/KN complex during force-increase scan with a loading rate of ~0.7 pN s^{-1}. Here we note that, the increase/decrease steps of the green line at forces <2 pN were caused by environmental noise during the experiments.
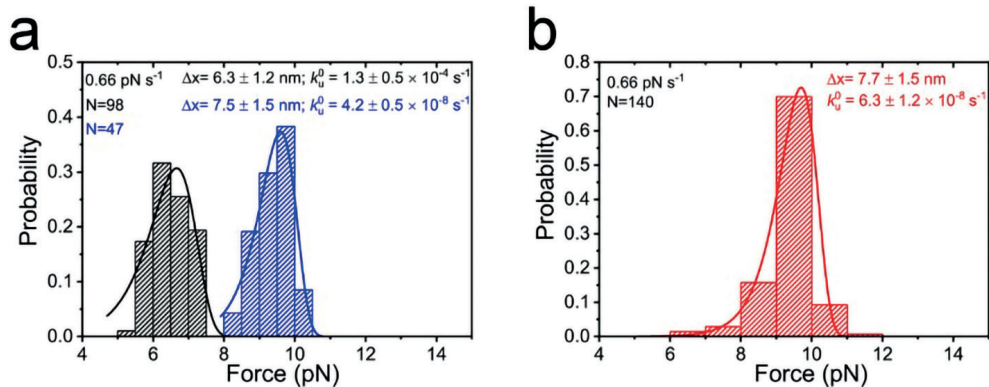
Supplementary Figure S2. The partial unfolding and unlooping force distribution of the R7/KN complex
(**a**). Normalized histograms of R7/KN complex partial unfolding forces. The black and blue groups in the panel correspond to the two groups indicated in Fig.1d. The black and blue curves are the Bell's model fitting of partial unfolding force distributions for the black and blue groups, respectively. (**b**). Normalized histograms of R7/KN complex unlooping (complete rupture) forces. The red line is the Bell's model fitting of unlooping force distribution. The resulting fitting parameters (transition distance Δx and extrapolated zero-force unfolding/unlooping rate k_u^0) are indicated in the figure panels correspondingly.
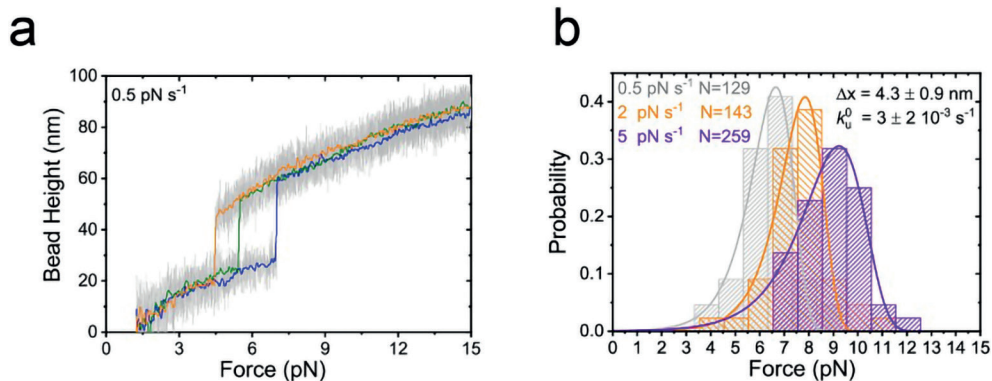
Supplementary Figure S3. Force response of talin R7 domain
(**a**) Typical force-bead height curves of the R7 domain at a force loading rate of 0.5 pN s^{-1}. Three representative consecutive force-scans are shown, indicated by different colors. (**b**) Normalized histograms of R7 unfolding force distributions at three different force loading rates (0.5 pN s^{-1}, 2 pN s^{-1} and 5 pN s^{-1}), indicated by different colors. Colored lines indicate the Bell's model fitting of the unfolding force distributions. The resulting fitting parameters (transition distance Δx and extrapolated zero-force unfolding rate k$_u$^{0}) are indicated in the figure panels correspondingly.
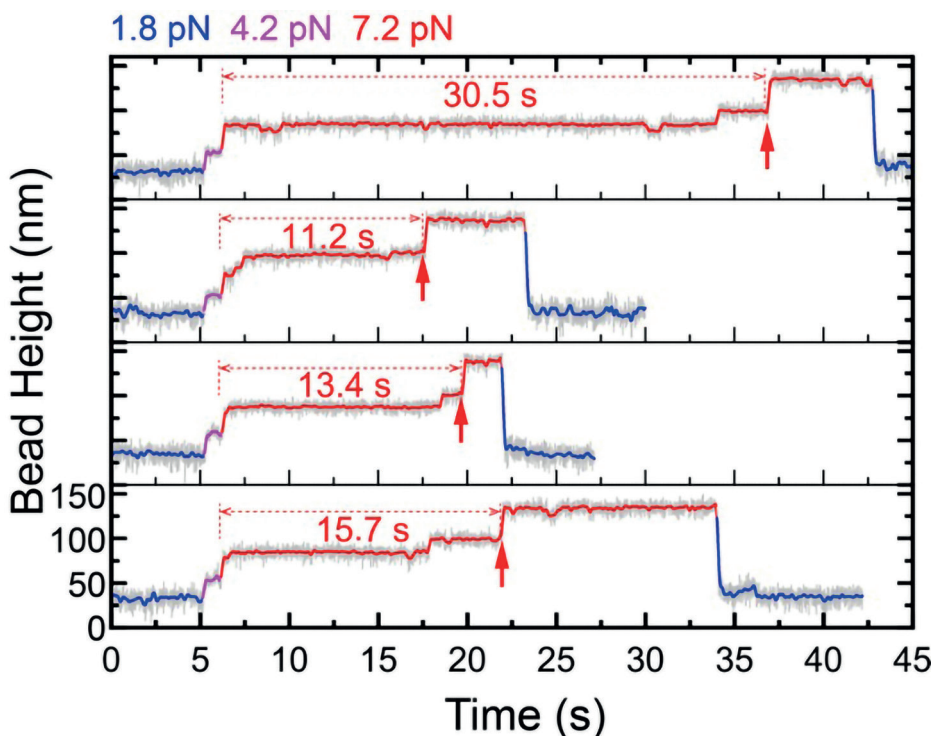
Supplementary Figure S4. Representative time-bead height traces of the R7/KN complex at 7.2 pN
Four representative time-bead height traces of complete rupture of R7/KN complex at ~ 7.2 pN. The complete rupture transition of the complex is indicated by red up arrow in each trace. The lifetime of the

complex in each trace is indicated by the red dashed arrow.
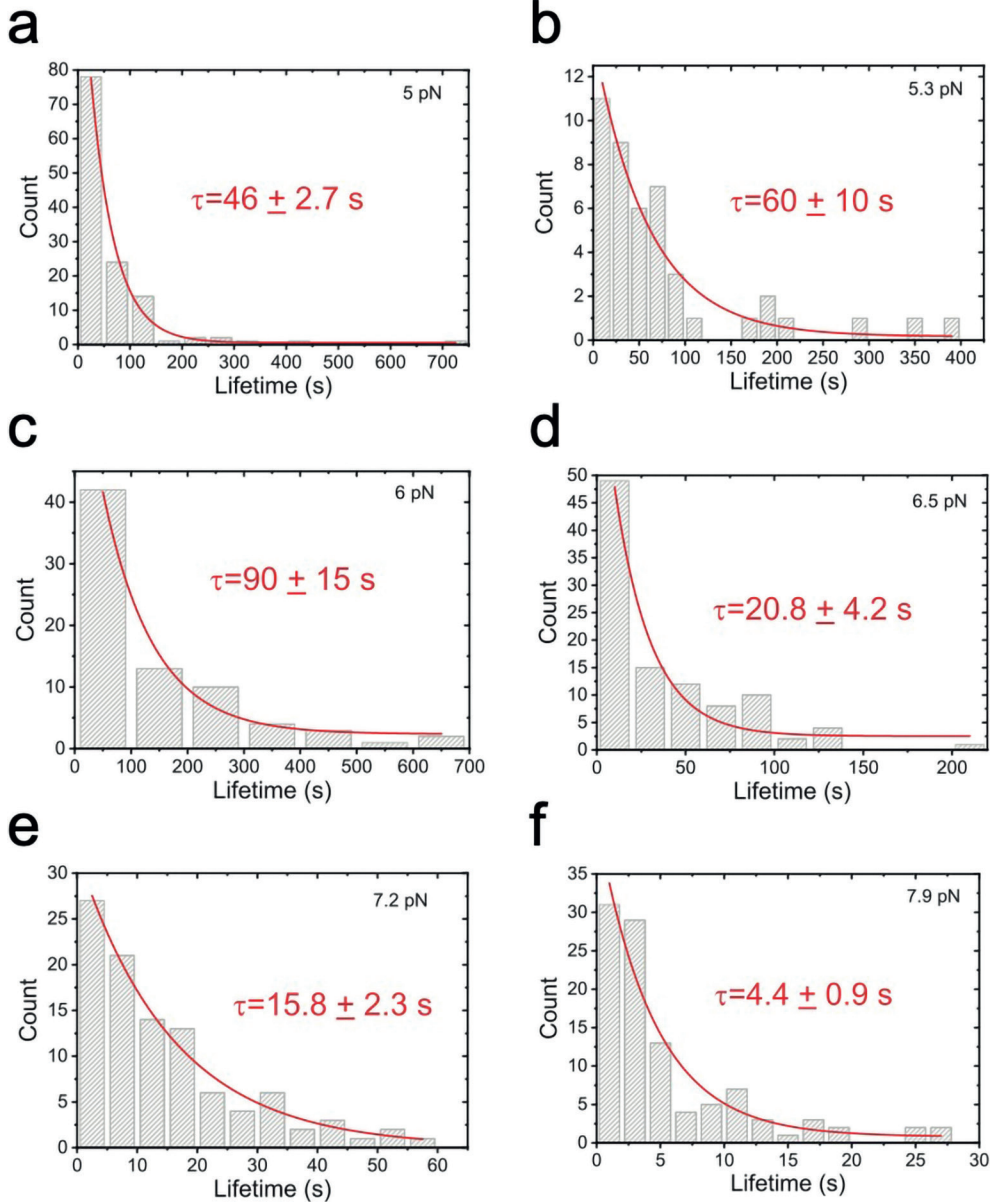
Supplementary Figure S5. The force-dependent lifetime distributions of R7/KN complex
R7/KN complex lifetime distribution and the corresponding exponential decay fitting (red lines) at different forces (panels **a-f**) in the range of 5-8 pN. The resulting time constant, τ of the lifetime and the corresponding fitting error at each force are indicated in the corresponding panel.

a

150 kDa

KANK2 → ← Nonspecific band

100 kDa

Loading control (Ku80) →

75 kDa

HeLa control   HeLa-K2-KO

250 kDa

KANK1 →

150 kDa

Loading control (Ku80) →

75 kDa

HeLa-K2-KO non transfected   HeLa-K2-KO +siLuciferase   HeLa-K2-KO +siKANK1

b

KANK1 | Talin | Talin KANK1 | KANK2 | Talin | Talin KANK2

HeLa control

HeLa-K2-KO

HeLa-K2-KO + siLuc

HeLa-K2-KO + siK1

10µm

c

A) Focal adhesion (FA) size

FA size [µm²] (Mean ± SD)

FL (siLuc), FL (siK1), KN (siLuc), KN (siK1), KN-L1 (siLuc), KN-L1 (siK1), KN-L1+CAAX (siLuc), KN-L1+CAAX (siK1), L1+CAAX (siLuc), L1+CAAX (siK1)

B) Focal adhesions (FAs) per cell

FAs per cell (Mean ± SD)

FL (siLuc), FL (siK1), KN (siLuc), KN (siK1), KN-L1 (siLuc), KN-L1 (siK1), KN-L1+CAAX (siLuc), KN-L1+CAAX (siK1), L1+CAAX (siLuc), L1+CAAX (siK1)

3

Supplementary Figure S6. FA size and number in cells transfected with different KANK1 constructs
(**a**) Western blot analysis of KANK2 knockout cells (right panel) and the knockdown efficiency of KANK1 (left panel) in HeLa cells knockout for KANK2. The nonspecific protein band running slightly above the band corresponding to endogenous KANK2 (~ 120 kDa) is indicated by an arrow. Ku80 was used as a loading control. (**b**) Localization of endogenous KANK1 and KANK2 in control HeLa cells (HeLa control), HeLa cells that are knockout for KANK2 (HeLa-K2-KO) and that are either depleted (+siK1) or not depleted (+siLuc) of KANK1. Cells were fixed and stained for endogenous KANK1 or KANK2 (green) and the endogenous FA protein talin (magenta). In control HeLa cells, both endogenous KANK1 and KANK2 localize to the FA rim. (**c**) Analysis of FA size (left) and number (right) in HeLa cells knockout for KANK2 that are either depleted (siK1) or not depleted (siLuc) of endogenous KANK1 and that were transfected with the five KANK1 constructs that we use in our experiments (FL, KN, KN-L1, L1+CAAX and KN-L1+CAAX). For each condition, 14 – 24 cells and 414 – 899 FAs were analyzed in two independent experiments (FL (siLuc) n=899 FAs [23 cells]; FL (siK1) n=766 FAs [21 cells]; KN (siLuc) n=804 FAs [24 cells]; KN (siK1) n=796 FAs [20 cells]; KN-L1 (siLuc) n=880 FAs [21 cells]; KN-L1 (siK1) n=838 FAs [21 cells]; L1+CAAX (siLuc) n=529 FAs [18 cells]; L1+CAAX (siK1) n=414 FAs [14 cells]; KN-L1+CAAX (siLuc) n=639 FAs [17 cells]; KN-L1+CAAX (siK1) n=698 FAs [19 cells]).

3
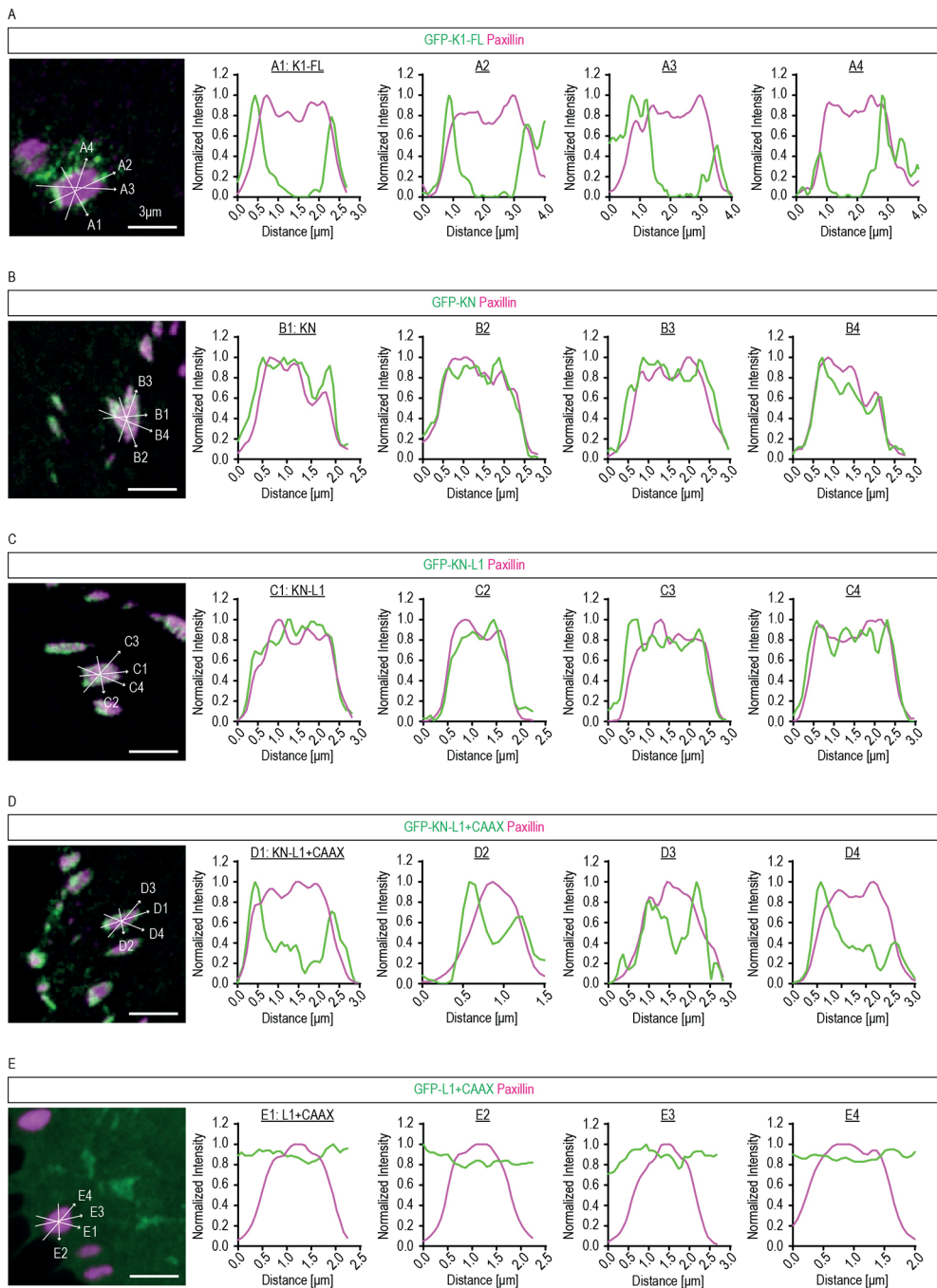
Supplementary Figure S7. Localization of KANK1 and its KN-containing fragments at FAs with three additional line scans.

Three more line scans performed for each of the 5 original line scans (corresponding to Figure 3c,d). The lines were drawn through the center of the adhesion trying to cover an array of different angles for the line

scan. The labeled arrows (e.g. a1-a4) correspond to the plot profiles with the same label on the left. (**a**) Full-length KANK1 localizes exclusively to the FA rim and is absent from the central area of FAs. (**b,c**) The KANK1-KN and the KANK1-KN-L1 constructs overlap with FAs and show high abundance in the central area of FAs. (**d**) The addition of the membrane anchoring CAAX motif to the KANK1-KN-L1 construct (KANK1- KN-L1+CAAX) leads to the enrichment in FA rim area. (**e**) The membrane anchoring CAAX motif without the talin binding KN domain (KANK1-L1+CAAX) shows even distribution at the plasma membrane and no enrichment at FAs.

3
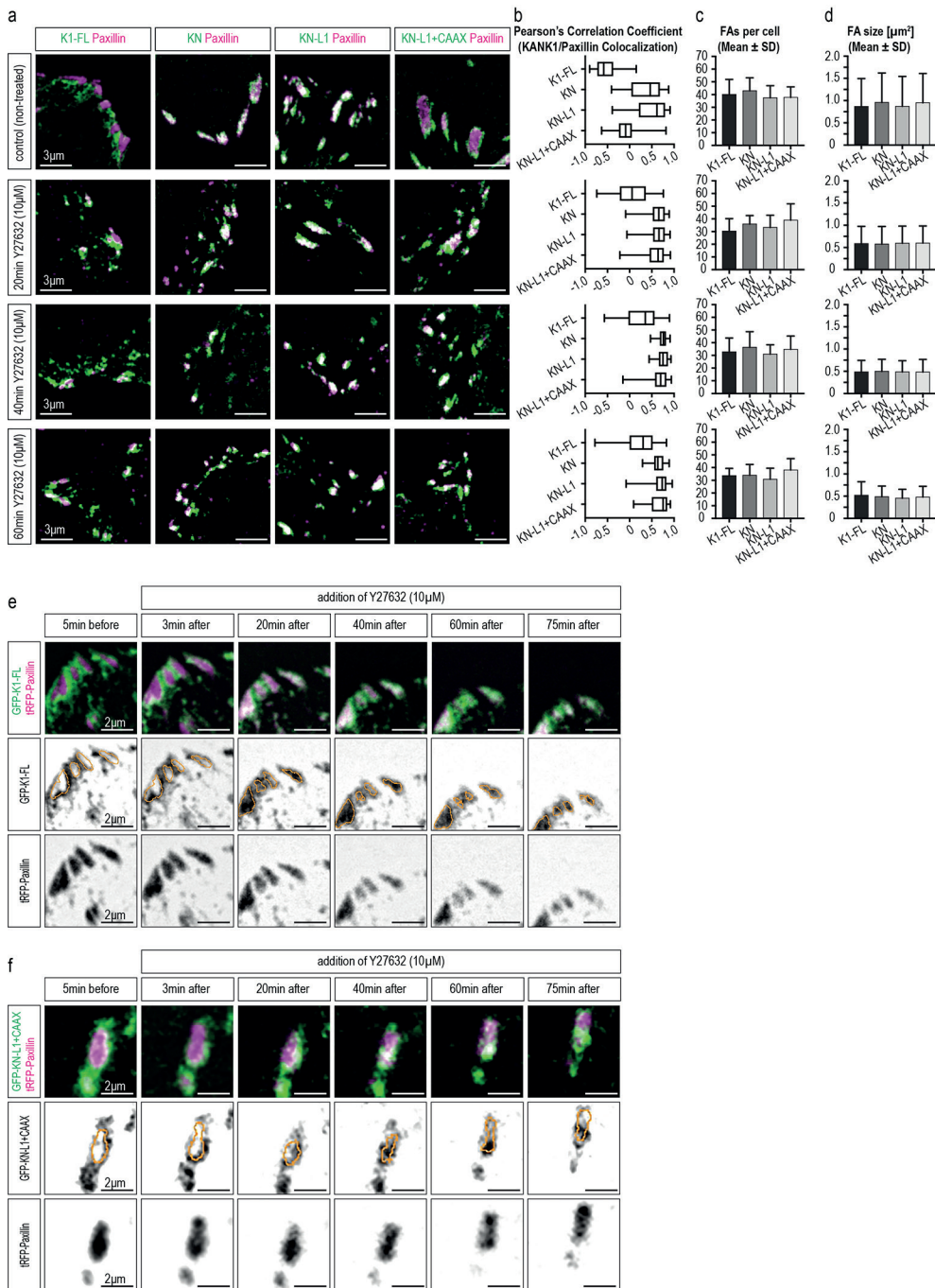
Supplementary Figure S8. Effect of ROCK1 inhibition on the localization of KANK at the focal adhesion rim.

(**a**) Localization of KANK1 and its KN-containing constructs in HeLa cells after treatment with the Rho-associated coiled coil-containing protein kinase 1 (ROCK1) inhibitor Y27632. HeLa cells knockout for KANK2 were depleted of endogenous KANK1 and afterwards transiently transfected with the different GFP-labeled and siRNA-resistant KANK1 constructs (green). Before fixation, the medium was exchanged

for medium containing 10 µM of the ROCK inhibitor Y27632 and the cells were incubated for 20, 40, or 60 minutes respectively (the untreated control cells received normal medium without Y27632). After the incubation, the cells were fixed with PFA and stained for the endogenous focal adhesion protein paxillin (magenta). In the untreated cells, full-length KANK1 and the KANK1-KN-L1+CAAX localize outside around FAs or tightly at the FA rim respectively, whereas the KANK1-KN and KANK1-KN-L1 show high abundance in the central area of FAs (see also Fig. 3c and 3d). Already after 20 minutes of treatment with the ROCK inhibitor, full-length KANK1 begins to partially overlap with the focal adhesion protein paxillin. Moreover, the KANK1- KN-L1+CAAX construct shows strong overlap with the central area of focal adhesions similar to the two other KN-containing constructs (KANK1-KN and KANK1-KN-L1) in the untreated control cells. (**b**) Quantification of the colocalization of KANK and paxillin in cells treated with the ROCK1 inhibitor Y27632 as in (a). Pearson's correlation coefficient, n = 50 in 10 cells per condition. Results are presented as Box-Whisker-Plots, whiskers ranging from minimum to maximum. (**c&d**) Average focal adhesion number (c) and average size (area) of individual focal adhesions (d) in cells treated with the ROCK1 inhibitor Y27632 as in (a). (304 - 430 FAs/condition in 10 cells per condition (FL (untreated) n=401 FAs; KN (untreated) n=430 FAs; KN-L1 (untreated) n=375 FAs; KN-L1+CAAX (untreated) n=378 FAs; FL (20min Y27632) n=304 FAs; KN (20min Y27632) n=339 FAs; KN-L1 (20min Y27632) n=347 FAs; KN-L1+CAAX (20min Y27632) n=391 FAs; FL (40min Y27632) n=328 FAs; KN (40min Y27632) n=364 FAs; KN-L1 (40min Y27632) n=310 FAs; KN-L1+CAAX (40min Y27632) n=348 FAs; FL (60min Y27632) n=336 FAs; KN (60min Y27632) n=317 FAs; KN-L1 (60min Y27632) n=308 FAs; KN-L1+CAAX (60min Y27632) n=381 FAs)). (**e&f**) Single frames of dual fluorescence time-lapse images acquired by TIRF microscopy. HeLa cells knockout for KANK2 were depleted of endogenous KANK1 and afterwards transiently transfected with GFP-tagged si-RNA-resistant full-length KANK1 (e) or KANK1-KN-L1+CAAX (f) (both green) and TagRFP-paxillin (magenta). The cells were treated on-stage with the ROCK1 inhibitor Y27632 (10 µM). Orange line, FA outline obtained by using a threshold-based mask to indicate how over time KANK overlaps with the FA area.

3

Supplemental experimental procedures

Supplementary Text S1. DNA constructs and protein expression
The DNA fragments encoding talin1-R7 (residues 1354-1453 and 1587-1658 of TLN1_MOUSE) and KANK1-KN (residues 30-68 of KANK1_HUMAN) were amplified by PCR using the template plasmids.[1] The DNA fragments encoding avi-tag (GLNDIFEAQKIEWHE) and FH1 domain (residues 582-764 of DIAP1_HUMAN) were synthesized by GeneArt. The DNA fragments where then assembled into the pET151 vector by HiFi DNA Assembly (NEBuilder®). The plasmid was co-transformed with a BirA plasmid and expressed in Escherichia coli BL21 (DE3) cultured in LB-media with D-Biotin (Sigma Aldrich), and affinity purified through 6His-tag.

Supplementary Text S2. Theoretical models of force responses of the folded/ unfolded protein domain/complex
The force-extension curves of a looped R7/KN complex and the folded R7 domain is determined by the rigid rotation fluctuation of a characteristic rigid body with a length $b \sim 4.5$ nm, which is the distance between the two forceattaching points (i.e., the N- to C- terminal distance in our experiment), estimated from the PDB files of the R7/ KN complex or folded R7 domain,[1] respectively. These force-extension curves can be described by the freelyjointedchain polymer model with a single segment:

$$x^{\text{FJC}}(f) = b\left(\coth\left(\frac{fb}{k_BT}\right) - \frac{k_BT}{fb}\right)$$

The unlooped R7-KN detector or the unfolded state of a R7 domain can be a flexible peptide chain, and this force-extension curve can be described by the worm-like chain (WLC) polymer model[2] through the Marko–Siggia formula with a bending persistence length of $A \sim 0.8$ nm:

$$\frac{fA}{k_BT} = \frac{1}{4\left(1 - \frac{x^{\text{WLC}}(f)}{l}\right)^2} - \frac{1}{4} + \frac{x^{\text{WLC}}(f)}{l}$$

where $l = n * l_0$ is the contour length of the unlooped linker or the unfolded domain, n is the number of residues of the linker or the domain, $l_0 = 0.38$ nm is the contour length of per residue. Hence the looping/unlooping or the unfolding/refolding step size is the extension differences before and after unlooping or unfolding at the transition force, i.e.,

$$\Delta x(f) = x^{\text{WLC}}(f) - x^{\text{FJC}}(f)$$

Supplementary Text S3. Antibodies and Immunofluorescence staining
Cells seeded on 12 mm glass coverslips for immunofluorescence staining were allowed to attach at least overnight. The following day, the cells were either fixed with 4 % PFA in PBS for 15 minutes at room temperature (staining for paxillin) or with ice-cold methanol for 7 minutes at -20 ºC (staining for KANK1+2 and talin). After 1x washing with PBS, the cells were permeabilized for 4 minutes at room temperature (RT) using permeabilization buffer (0.2 % TritonX- 100 (Sigma) in PBS). Thereafter, the cells were blocked in blocking buffer (0.05 % Tween-20 (Sigma) and 2 % BSA (Carl Roth) in PBS) for 1 hour at RT. After blocking, the cells were incubated with primary antibodies diluted in blocking buffer for 1 hour at RT. After incubation, the cells were washed 5 times for

2 minutes with wash buffer (0.05 % Tween-20 in PBS); followed by 1 hour incubation with the fluorescently labeled secondary antibodies diluted in blocking buffer. The cells were washed 5 times for 2 minutes with wash buffer and afterwards, dehydrated using first 70 % and then 100 % ethanol. Finally, the cells/coverslips were mounted on glass slides using Vectashield mounting medium (H-1000, Vector laboratories). Commercially available antibodies against KANK1 (Atlas antibodies, HPA005539), KANK2 (Atlas antibodies, HPA015643), paxillin (BD Biosciences, 610620), and talin (clone 8d4, Sigma, SAB4200694) were used. Alexa-488 and Alexa-594 conjugated goat antibodies against rabbit and mouse IgG were purchased from Invitrogen.

For the localization of KANK1 and its KN-containing fragments at FAs as well as for the experiments using the ROCK1 inhibitor Y27632, we used GFP- labeled KANK1 constructs and stained for the endogenous FA protein paxillin using the primary antibody described above and the Alexa-594 conjugated goat antibody against mouse IgG.

For the characterization of the HeLa cells knockout for KANK2 and the knockdown efficiency of KANK1, we used antibodies against KANK1 and KANK2 (both rabbit and described above) as well as antibodies against the FA proteins talin and paxillin (both mouse and described above). As the secondary antibodies we used the Alexa-488 conjugated goat antibody against rabbit and the Alexa-594 conjugated goat antibody against mouse.

Supplementary Text S4. DNA constructs and siRNAs

KANK1 siRNAs and the BioGFP-tagged KANK1 full-length and KANK1-KN constructs were described previously[1]. The BioGFP-tagged KANK1-KN-L1, KANK1-L1+CAAX and KANK1-KN-L1+CAAX fusion constructs were made using PCR-based amplification of KN, the linker region 1 (and CAAX), pBioGFP-C1 vector and Gibson Assembly mix (New England Biolabs) as previously described.[1]

Cell culture. HeLa cells were cultured in DMEM medium with 10 % fetal calf serum and with 1 % penicillin/streptomycin. The cell lines were routinely checked for mycoplasma contamination using the Mycoalert assay (LT-07-318, Lonza) following the supplier's instructions. For all cell imaging experiments in this study, we used HeLa cells knockout for KANK2 (see Generation of KANK2 knockout cell line for more details).

siRNA and DNA transfections. Transfection of DNA and siRNA into HeLa (KANK2 knockout) cells was performed as previously described.[3] In brief, for siRNA transfections, cells were trypsinized and ~100,000 cells per well were seeded in 6-well cell culture plates and transfected using 20 nM of siRNA per well using HiPerFect transfection reagent (Qiagen) by adding the siRNA/HiPerFect mixture to the cell suspension (siKANK1: CAGAGAAGGACAUGCGGAU). The cells were allowed to attach overnight. The following day, the cells were trypsinized and seeded on 12 mm glass coverslips (10,000 - 15,000 cells per well for immunofluorescence staining) or on 4-well chambered coverglasses (40,000 cells per well for live-cell experiments). Again, the cells were allowed to attach overnight. The following day, the medium was refreshed and the cells were transfected with DNA (0.5 µg DNA/well) using FuGene6 (Promega) transfection reagent. The cells were incubated with the DNA/FuGene6 mixture overnight. The following day, ~72 hours after the siRNA transfection and ~24 hours after the DNA transfection, the cells were either fixed for immunofluorescence staining or used for live-

cell experiments. For the DNA transfection with the CRISPR/Cas9 vector, HeLa cells were seeded in 6-well cell culture plates (100,000 cells per well) and allowed to attach overnight. The following day, they were transfected using FuGene6 transfection reagent (2 μg DNA/well).

Generation of HeLa KANK2-knockout cell line. To generate a KANK2 knockout cell line we followed the protocol for CRISPR/Cas9 mediated knockout as described by Ran et al.[4] In brief, guide RNA for human KANK2 was designed using the online CRISPR design tool provided by the Broad Institute (http://crispr.mit.edu) and cloned into the pSpCas0(BB)-2A-Puro (PX459) expression vector (GACCCCCTATGGCTACCGCC). HeLa cells were transfected with the vectors using FuGene6 transfection reagent. The following day, the cells were washed with PBS and subsequently cultured in the selection medium (DMEM medium with 10 % fetal calf serum, 1 % penicillin/streptomycin, supplemented with 2 μg/mL puromycin) for at least 48 hours; the selection medium was refreshed every 24 hours. After selection, the cells were cultured in normal medium (DMEM medium with 10 % fetal calf serum and 1 % penicillin/streptomycin) and allowed to recover for 2 – 3 days. Afterwards, a first check of the knockout efficiency was done by immunofluorescence staining followed by isolation of individual clones, which were further characterized by immunofluorescence staining and Western blotting.

Western blot analysis of KANK1 and KANK2 and antibodies. To obtain whole cell lysates for Western blot analysis, cells were lysed in a non-ionic detergent- based buffer (50 mM Tris-HCL, 150 mM NaCl, 1 mM EDTA, protease inhibitor cocktail (Roche), 1 % Triton-X100) for 10 minutes on ice. Afterwards, the suspension was centrifuged at 13,200 rpm at 4 °C for 15 minutes. The protein concentration of the supernatant was measured using the colorimetric bicinchoninic acid (BCA) assay, using a BCA kit (#23225 ThermoFisher) following the supplier's instructions. The following SDS-PAGE and Western blot analysis were performed according to standard procedures. The same commercially available antibodies against KANK1 and 2 were used as for immunofluorescence staining (see Antibodies and Immunofluorescence staining); furthermore, an antibody against Ku80 (BD Biosciences, 611360) was used. For the detection, near infrared (NIR) fluorescence technology was used (Li-Cor Biosciences, Odyssey system), using infrared dye conjugated goat antibodies against mouse and rabbit (Li-Cor Biosciences).

Supplementary Text S5. Fluorescence microscopy and analysis

Live-cell fluorescence TIRF imaging of cells expressing GFP-labeled KANK1 constructs and Fluorescence Recovery After Photobleaching (FRAP) experiments, as well as live-cell dual fluorescence time-lapse TIRF imaging of cells co-expressing GFP-labeled KANK1 constructs and TagRFP-paxillin were performed on an inverted research microscope Nikon Eclipse Ti-E (Nikon) with the perfect focus system (Nikon), equipped with Nikon Apo TIRF 100x N.A. 1.49 oil objective (Nikon) and iLas2 system (Dual Laser illuminator for azimuthal spinning TIRF (or Hilo) illumination and Simultaneous Targeted Laser Action) from Roper Scientific (Evry, FRANCE). The system was also equipped with ASI motorized stage MS-2000-XY (ASI), CoolSNAP MYO CCD camera (Photometrics) and controlled by the MetaMorph 7.8 software (Molecular Devices). For imaging of green fluorescence and FRAP experiments a Stradus 488 nm

(150 mW) (Vortran) laser was used as light source and the filter set ET-GFP (49002) (Chroma) was used. For dual fluorescence time-lapse TIRF imaging of green and red fluorescence a Stradus 488 nm (150 mW) (Vortran) laser and an OBIS 561-100LS (561 nm, 100mW) (Coherent) laser were used as light sources respectively, and the filter set ET-GFPmCherry (59022) (Chroma) was used. To keep the cells at 37 °C, a stage top incubator model INUBG2E-ZILCS (Tokai Hit) was used. Images were acquired at 15.4 pixels/μm with exposure time 100 milliseconds at various frames per second (for FRAP, see the text below). Cells were plated on 4-well chambered coverglass (LabTek, 155383) and maintained at 37 °C and 5 % CO2.

Images of fixed cells were collected with a Nikon Eclipse Ni upright wide field fluorescence microscope and a Nikon DS-Qi2 CMOS camera (Nikon), using Plan Apo Lambda 100x N.A. 1.45 oil objective (Nikon) and Nikon NIS (Br) software (Nikon). Nikon Intensilight C-HGFI was used as a light source. For imaging of green and red fluorescence the filter sets ET-GFP (49002) ET- mCherry (49008) (both Chroma) were used respectively.

For presentation and analysis, images were subtracted for background (rolling ball radius 10 pixels) and adjusted for brightness and contrast using ImageJ 1.50b (NIH).

KANK1 localization at FAs was quantified as the ratio of the integrated density of the KANK1 signal in the FA rim area (0.2 μm beyond the FA outline and 0.2 μm inside of the FA) to the FA central area (FA area without the outmost 0.2 μm). FA outlines were obtained by thresholding and using Analyze Particles under ImageJ (only FAs with the size of at least 1.0 μm^2 were analyzed). For statistical analysis, a one-way ANOVA was performed using Prism 7 software (GraphPad).

For analysis of FA size and number, the FA outlines were obtained as described above and the area was measured by using Analyze Particles in ImageJ (only FAs bigger than 0.25 μm^2 were included in the analysis).

Fluorescence profiles of GFP-labeled KANK1 and paxillin were obtained by line scan analysis in ImageJ normalized by the maximum fluorescence intensity of the corresponding channel.

Supplementary Text S6. FRAP experiments and analysis

FRAP experiments were performed using the TIRF microscope setup described above. FRAP measurements were performed by bleaching 2.3-μm-diameter circle in GFP-KANK1 patches at FAs followed by 15 seconds imaging with a frame interval of 0.25 seconds per frame and 5 minutes imaging with a frame interval of 5 seconds (for KANK1-KN, KN-L1 and KN-L1+CAAX). For the slower recovering KANK1-FL, after photobleaching followed 30 seconds imaging with a frame interval of 0.5 seconds and 5 minutes imaging with a frame interval of 5 seconds. Per cell, 4 - 5 KANK1 patches were bleached simultaneously. Mean fluorescence intensities were measured from a 2.3-μm-diameter circle region within the original photobleached region. The mean intensity of this region was double corrected for background fluorescence and photobleaching as previously described.[5]

Supplementary Text S7. ROCK1 inhibition and immunofluorescence stainings

HeLa cells knockout for KANK2 were depleted of endogenous KANK1 via siRNA-

mediated knockdown, they were plated on 12 mm glass coverslips (15,000 cells per coverslip) and transiently transfected with GFP-tagged siRNAresistant KANK constructs as described above. On the day of the immunofluorescence staining, 72 hours after the siRNA transfection, the medium was exchange and the cells were incubated in medium supplemented with 10 μM ROCK1 inhibitor Y27632 (Sigma, 688000) for 20, 40, or 60 minutes respectively. The untreated control cells received normal medium and were fixed together with the treated cells after 60 minutes. After the incubation the cells were fixed and stained for endogenous paxillin as described above.

Supplementary text S8. KANK and paxillin colocalization analysis after ROCK1 inhibition

For presentation and analysis, images were processed as described above. Due to the diminishing effect of the ROCK1 inhibitor on focal adhesion size, it was not possible to analyze the clustering/colocalization of KANK at the focal adhesions as described above. As an alternative, to analyze the colocalization of KANK and paxillin, we used the Pearson correlation coefficient provided by the Colocalization Analysis plugin under Fiji-ImageJ and a 1-μm-diameter circular ROI (region of interest) centered on paxillin clusters detected by immunofluorescence staining as described previously.[1]

Supplementary text S9. Dual fluorescence time-lapse TIRF microscopy of HeLa cells treated with the ROCK1 inhibitor Y27632

The dual fluorescence time-lapse experiments of HeLa cells treated with Y27632 were performed with the same TIRF microscopy setup as described above. In brief, HeLa cells knockout for KANK2 were depleted of endogenous KANK1 and afterwards plated on 4-well chambered coverglass (LabTek, 155383). The following day, the cells were transfected with GFP-tagged and siRNA-resistant KANK constructs and TagRFP-paxillin which was described previously1. On the day of the experiment, the cells received fresh medium and were placed on the microscope one hour before the start of the actual experiment to acclimate to the new condition. The cells were imaged at a frame rate of 1 – 2 minutes per frame. 5 – 10 minutes after the start of the experiment, medium supplemented with the ROCK1 inhibitor Y27632 was added on stage to the cells (to reach a final concentration of 10 μM).

Supplementary references

1. Bouchet, B. P. et al. Talin-KANK1 interaction controls the recruitment of cortical microtubule stabilizing complexes to focal adhesions. Elife 5, doi:10.7554/eLife.18124 (2016).

2. Marko, J. F. & Siggia, E. D. Stretching DNA. Macromolecules 28, 8759-8770, doi:10.1021/ma00130a008 (1995).

3. van der Vaart, B. et al. CFEOM1-associated kinesin KIF21A is a cortical microtubule growth inhibitor. Dev Cell 27, 145-160, doi:10.1016/j.devcel.2013.09.010 (2013).

4. Ran, F. A. et al. Genome engineering using the CRISPR-Cas9 system. Nat Protoc 8, 2281-2308, doi:10.1038/nprot.2013.143 (2013).

5. Phair, R. D. et al. Global nature of dynamic protein-chromatin interactions in vivo: three-dimensional genome scanning and dynamic interaction networks of chromatin proteins. Mol Cell Biol 24, 6393-6402, doi:10.1128/MCB.24.14.6393-6402.2004 (2004).

3

4

Analysis of the role of KANK1 self-association in its localization to the FA rim

York-Christoph Ammon[1], Miquel Muñoz Ordoño[1], Aidan Estelle[2], Rejina B Khan[3], Abhimanyu Singh[3], Benjamin T Goult[3], Elisar Barbar[2], Anna Akhmanova[1*]

1 Cell Biology, Neurobiology and Biophysics, Department of Biology, Faculty of Science, Utrecht University, Utrecht, The Netherlands

2 Department of Biochemistry and Biophysics, Oregon State University, Corvallis, OR. USA

3 School of Biosciences, University of Kent, Canterbury, United Kingdom

* Corresponding author

Abstract

Microtubules and their regulatory effect on integrin-mediated cell-matrix adhesions play an essential role in cell polarity and motility. The plus ends of microtubules are anchored and stabilized by the cortical microtubule stabilizing complex (CMSC) at the cell cortex close to cell-matrix adhesions. KANK1 can bind to the major adhesion protein talin as well as to several components of the CMSC and thereby directly link the two multi-protein complexes to each other. However, the exact mechanism confining the CMSC and especially KANK1 to the focal adhesion rim is unknown. Here, we show that the previously poorly characterized linker region L2 of KANK1 is able to prevent the protein from penetrating into adhesions. Moreover, biochemical assays indicate that KANK1 is able to self-associate. These results suggest that self-association of KANK1 could lead to the formation of protein clusters and that clustering would prevent it from interacting with talin within the inner part of focal adhesions. This in turn would lead to spatial separation of CMSC and talin at the cell cortex.

4

Introduction

Cell-matrix adhesions are essential for multicellular organisms as they mediate the connection of the cells to the extracellular matrix (ECM). In this way, they contribute to tissue integrity as they keep the cells in place (Parsons et al., 2010). On the other hand, cell-matrix adhesions are also important for cell motility since they can transduce mechanical forces to the ECM and vice versa and thereby promote the translocation of the cell body (Vicente-Manzanares and Horwitz, 2011). Usually cell-matrix adhesions are formed by heterodimeric α/β-integrin transmembrane receptors (integrins). Integrins span through the plasma membrane (PM) and bind to ECM proteins, such as fibronectin or collagen (Bachir et al., 2014; Winograd-Katz et al., 2014). Cell-matrix adhesions develop from small nascent adhesion complexes into mature focal adhesions (FAs) in a force-dependent (actomyosin-dependent) manner (Vicente-Manzanares et al., 2007; Wolfenson et al., 2009). FAs are highly organized dense macromolecular assemblies (Geiger and Yamada, 2011; Kanchanawong et al., 2010; Winograd-Katz et al., 2014). The FA adaptor protein talin connects the integrins to the actomyosin cables and thereby functions as a "molecular clutch" (Case and Waterman, 2015; Klapholz and Brown, 2017). It has been shown that microtubules (MTs) play a critical role in the life cycle of FAs since they regulate their dynamics (Seetharaman and Etienne-Manneville, 2019) and also function as tracks for the transport of signaling molecules and FA components (Stehbens and Wittmann, 2012). The plus ends of MTs are attached and stabilized in the vicinity of FAs by cortical MT stabilizing complexes (CMSC), which contain CLASPs (CLASP1 and 2), ELKS, liprins (α1 and β1) and LL5β (Lansbergen et al., 2006; Mimori-Kiyosue et al., 2005; van der Vaart et al., 2013). It has been shown that the kidney ankyrin repeat domain-containing protein1 (KANK1) can bind to talin and thereby connect the CMSC to FAs. Moreover, it has been demonstrated that the talin-KANK1 interaction is required for the correct assembly of the CMSC (Bouchet et al., 2016). In mammals, there exist four KANK homologs (KANK1 – 4). All four human KANK proteins show similar structure with three domains. At their N-terminus, they possess the KANK N-terminal (KN) domain. It is connected via a linker region L1 to the coiled coil (CC) domains. In total, there are four conserved CC domains (CC1 – 4) in KANK proteins of which the number and composition vary among the different family members. It has been shown that the CC1 domain binds to liprins which in turn anchors KANKs to cortex (van der Vaart et al., 2013). Via a long linker region L2, the CC domains are connected to the highly conserved C-terminal ankyrin repeat (Ankr) domain (Kakinuma et al., 2009; Zhu et al., 2008).

In the present study, we further characterize KANK family proteins and gain deeper insights into the factors that determine their subcellular localization at FAs. We show that the poorly characterized linker region L2 of KANK1 is able to prevent the KN domain from penetrating into FAs. We find that the L2 region mediates binding to a novel KANK1 interaction partner: the hub protein dynein light chain LC8. Moreover, in an initial pulldown assay, we observe that the L2 region can bind full length KANK1 and thus is likely to promote KANK1 self-association/clustering. This in turn could keep the KN domain out of FAs, suggesting that KANK1 oligomerization might be an important factor in its self-association.
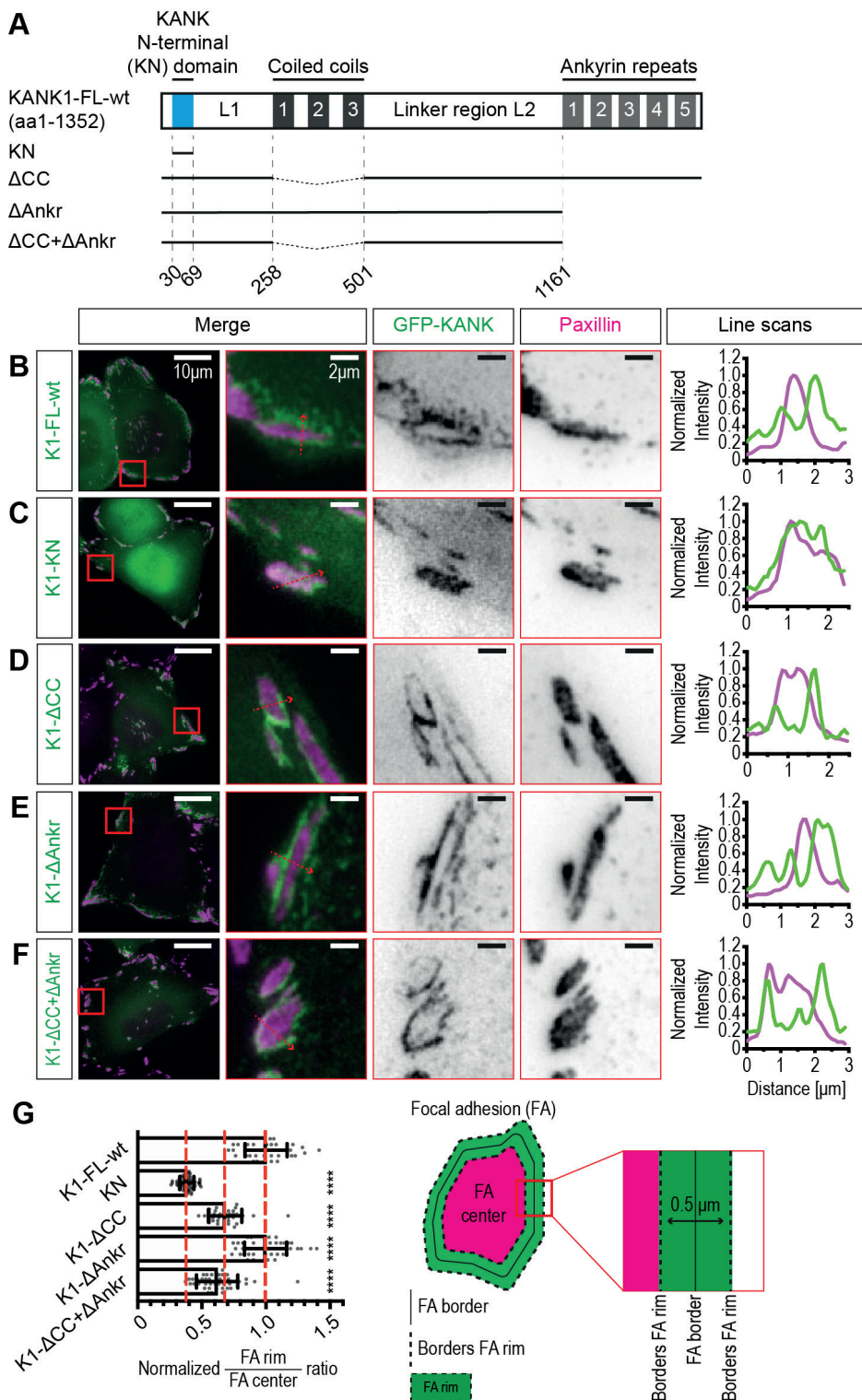
Results

KANK1 fragments show three distinct localization patterns at FAs

From previous studies it is known that full-length KANK1 and KANK2 can both interact with the FA protein talin at the cell cortex and that both encircle FAs and form distinct cortical patches distributed around FAs. Yet, the KN domain alone, which mediates binding to talin, strongly overlaps with the FA signal (Bouchet et al., 2016; Sun et al., 2016). Besides, in a more recent study, it was shown by us that the interaction between talin and KANK1 is likely subjected to mechanical forces when KANK1 is anchored to the PM. Moreover, we could demonstrate that this likely promoted sequestration of KANK1 at the FA rim (Yu et al., 2019). Nonetheless, to gain more insight how the localization of KANK1 at FAs is regulated and which other factors besides mechanical forces might contribute to this process, we generated several truncated KANK1 constructs (see Figure 1A). These GFP-tagged constructs were expressed in HeLa cells, in which endogenous KANK1 and 2, the two KANK proteins present in HeLa cells, were knocked out by CRISPR/Cas9-mediated technology (Supplementary Figure S1). Subsequently, the cells were fixed and stained for the endogenous FA protein paxillin. Thereafter, we analyzed the localization of the KANK1 constructs around FAs by comparing the KANK1 signal at the FA rim to the KANK1 signal at the FA center (Figure 1G). Full-length KANK1 (K1-FL-wt) localized to FA rim and formed patches around FAs but was absent from their central parts (Figure 1B), whereas the KN domain alone strongly overlapped with FAs (Figure 1C). When all three coiled coil domains were removed (K1-ΔCC), the patchy accumulation outside FAs was abrogated and the construct was strongly enriched at the FA rim (Figure 1D). The removal of the Ankr domain (K1-ΔAnkr) had no significant effect on the localization compared to K1-FL-wt (Figure 1E). When both the CC and Ankr domains were deleted simultaneously (KANK1-ΔCC+ΔAnkr), the construct again showed strong enrichment at the FA rim (Figure 1F), similar to the KANK1-ΔCC construct. This was unexpected as we had hypothesized that either the CC or the Ankr domain would be required to keep KANK1 out of FAs by mediating interactions with other proteins, thereby attaching KANK1 to the PM so that the talin-KANK1 complex would be subjected to mechanical forces which would promote KANK1 recruitment to the FA rim. Nonetheless, it seemed that the CC and Ankr domain were not essential for keeping KANK1 out of FA center. On the other hand, the CC domain was responsible for

Figure 1. KANK1 constructs show three distinct localization patterns at FAs

(**A**) Schematic overview of the KANK1 constructs lacking different domains. (**B-F**) Subcellular localization of the GFP-tagged constructs (green) from (A) in HeLa KANK1-& KANK2-KO cells. Cells were fixed and stained for the endogenous FA protein paxillin (magenta) ~24 hours after DNA transfection. The right panel shows the plotted fluorescence intensities of the GFP-KANK (green) and paxillin (magenta) along the line indicated by the dashed red arrow in the inset. The fluorescence intensities were normalized to the maximum intensity of the corresponding channel. (**G**) Quantification of the localization of KANK1 around FAs. The right panel shows how the FA rim, which is in total 0.5 μm wide, was defined. It extends 0.25 μm beyond the FA border and reaches 0.25 μm into the FA. Fluorescence intensity of the KANK1 signal at the FA rim has been divided by the fluorescence intensity of the KANK1 signal at the FA center. Both signal intensities have first been divided by the corresponding area. Subsequently the FA rim/FA center ratios were normalized to the average FA rim/FA center ratio of full-length KANK1 (see Methods for details). The values are shown as mean ± SD; **** $p < 0.0001$ (Ordinary One-Way ANOVA (Dunnett's Multiple Comparison Test)) (34 – 60 cells have been analyzed per condition in 2 – 3 independent experiments).

A KANK N-terminal (KN) domain; Coiled coils; Ankyrin repeats

KANK1-FL-wt (aa1-1352): L1, 1 2 3, Linker region L2, 1 2 3 4 5

KN
ΔCC
ΔAnkr
ΔCC+ΔAnkr

30 69 258 501 1161

B K1-FL-wt — Merge (10μm, 2μm) | GFP-KANK | Paxillin | Line scans

C K1-KN

D K1-ΔCC

E K1-ΔAnkr

F K1-ΔCC+ΔAnkr

Line scans: Normalized Intensity vs Distance [μm]

G Normalized FA rim / FA center ratio

K1-FL-wt, KN, K1-ΔCC, K1-ΔAnkr, K1-ΔCC+ΔAnkr — ****

Focal adhesion (FA): FA center, FA border, Borders FA rim, FA rim, 0.5 μm

4

107

the patchy cortical localization around FAs since all constructs lacking the CC domain showed strong accumulation at the FA rim. It was shown that the CC1 domain mediated binding to liprins (van der Vaart et al., 2013). Indeed, KANK1 construct lacking only the CC1 domain (KANK1-ΔCC1) was strongly enriched at the FA rim just like the KANK1-ΔCC construct, which is missing all three single CC domains. On the other hand, a KANK1 construct missing two other CC domains (KANK1-ΔCC2+3) showed broad cortical accumulation around FAs comparable to K1-FL-wt (Supplementary Figure S2).

Taken together, the localization of different KANK1 constructs at FAs can be categorized into three distinct groups. The first group is represented by the constructs that localize to FA rim and cortical patches in the vicinity of FAs, like full-length KANK1 and K1-ΔAnkr. It appears that the CC1 domain, and thus likely the interaction with liprins that is mediated by CC1, is responsible for this broad distribution around FAs. The second group includes the constructs that miss the CC1 domain and cannot bind to liprins and are tightly clustered at the FA rim. The third group are the constructs that completely overlap with FAs, like the KN domain.

Interestingly, the KANK1-ΔCC+ΔAnkr construct which only consists of the KN domain and the two linker regions L1 and L2 did not accumulate inside FAs but was clustered tightly at the FA rim like the KANK1-ΔCC. Thus, it seems likely that the linker regions are contributing to sequestering KANK1 at the FA rim.

The linker region L2 of KANK1 prevents the KN domain from penetrating into the central part of FAs

From our experiments it seemed likely that the linker regions L1 and L2 of KANK1 could be responsible for keeping KANK1 at the FA rim. However, in a previous study we have shown that the smaller linker region L1 fused to the KN domain (KN-L1 construct) was insufficient to recruit the KN domain to the FA rim (Yu et al., 2019) (see also Supplementary Figure S2). Thus, the localization of the KANK1-ΔCC+ΔAnkr construct to the FA rim was probably due to the long linker region L2. Therefore, we generated a fusion construct by attaching the L2 region of KANK1 directly to the KN domain of KANK1 (KN+L2). Besides, to test the effect of the L2 region from another KANK homolog, we also made a chimeric construct fusing KANK1 KN domain to the linker region L2 of KANK2 which is considerably shorter than the L2 region of KANK1 (353 compared to 659 amino acids; Figure 2A). When the KN+L2 construct was expressed in HeLa K1+K2-KO cells, it tightly accumulated at the FA rim (Figure 2B). In contrast, the linker region L2 of KANK2 was not able to recruit the KN domain to the FA rim, as the KN+K2-L2 construct overlapped with the FA signal (Figure 2C). A sequence alignment of the two L2 linker regions of KANK1 and KANK2 showed that the C-terminal parts of the L2 regions shared homology (~40% similarity), whereas, the N-terminal parts were specific for each of the two proteins. Thus, we generated two additional fusion constructs splitting the linker region L2 of KANK1 into an N-terminal and C-terminal part and attaching them to the KN domain (KN+501-916 and KN+918-1160 respectively). When these constructs were expressed in HeLa K1+K2-KO cells, the KANK1-specific N-terminal part of the L2 region was sufficient to sequester the KN domain at the FA rim (Figure 2D). On the other hand, the C-terminal part of the L2 region that shares homology with the L2 region of KANK2 could not keep the KN

domain out of FAs (Figure 2E). Fusing the KANK2 L2 region to the KN+501-916 construct (KN+501-916+K2-L2) did not have any additional effects on the enrichment at the FA rim (Figure 2F).

We also tested whether the KN domain could make a difference. Therefore, we made two more constructs fusing the KANK2 KN domain directly to the L2 regions of KANK1 or KANK2 respectively (K2-KN+K1-L2 and K2-KN+K2-L2). We found the KN of the two KANKs were similar in these assays: K2-KN+K1-L2 construct was enriched at the FA rim whereas the K2-KN+K2-L2 construct overlapped with FAs (Supplementary Figure S2).These data suggest that the KANK1 linker region L2, and, more specifically, the N-terminal part of that region (501-916), can recruit the KN domain to the FA rim. Moreover, this property appears to be KANK1-specific as the linker region L2 of KANK2, which shares homology with the C-terminal part of KANK1 L2 region, cannot prevent the KN domain from entering the central part of FAs.

The different KANK constructs show three discrete types of dynamics corresponding to the three distinct localizations at FAs

To better understand the different localizations of KANK deletion mutants at FAs, we analyzed their dynamics (Figure 3A) using fluorescence recovery after photobleaching (FRAP). Different GFP-tagged KANK constructs were expressed in KANK1-& KANK2-depleted HeLa cells, KANK patches at FAs were photobleached and we measured the fluorescence recovery over time. Full-length KANK1 showed slow recovery after photobleaching and a large immobile fraction (~60%) (Figure 3B-C). In contrast, the KN domain alone showed a rapid and almost complete recovery after photobleaching within a few seconds with hardly any immobile fraction (~10%). This implied that the interactions of the KN domain alone at FAs are very short-lived (Figure 3B-C). The K1-ΔCC construct showed moderate recovery and a smaller immobile fraction (30-40%) compared to K1-FL-wt (Figure 3B-C). The difference between full length KANK1 and K1-ΔCC was due to the CC1 domain which mediates liprin binding: the recovery of K1-ΔCC1 was similar to that of K1-ΔCC, whereas the recovery of K1-ΔCC2+3 was similar to that of intact KANK1 (Supplementary Figure S3).

The KN+L2 construct showed similar dynamics at FAs as the K1-ΔCC: Its recovery rate and immobile fraction were comparable (Figure 3B & D). Yet, when the KANK1 linker region L2 was substituted with that of KANK2 (KN+K2-L2 construct), the construct showed much faster recovery than the KN+L2 construct and a much smaller immobile fraction that was comparable to that of the KN domain alone (Figure 3B & E).

These data suggest that the dynamics of KANK1/KANK2 constructs correlates with their localization at FAs: the constructs accumulating at the FA rim and surrounding patches, such as full length KANK1, tightly associate with the cell cortex, which is likely at least partly due to their interaction with liprins, while the KN domain exchanges rapidly within FAs. The addition of the L2 linker region, which is sufficient for KN sequestration to the FA rim, slows down its exchange and increases its immobile fraction.

Dynein light chain LC8 can bind to the linker region L2 of KANK1 but it is not responsible for its localization to FA rim

How does the KANK1 linker region L2 sequester the KN domain at the FA rim? One
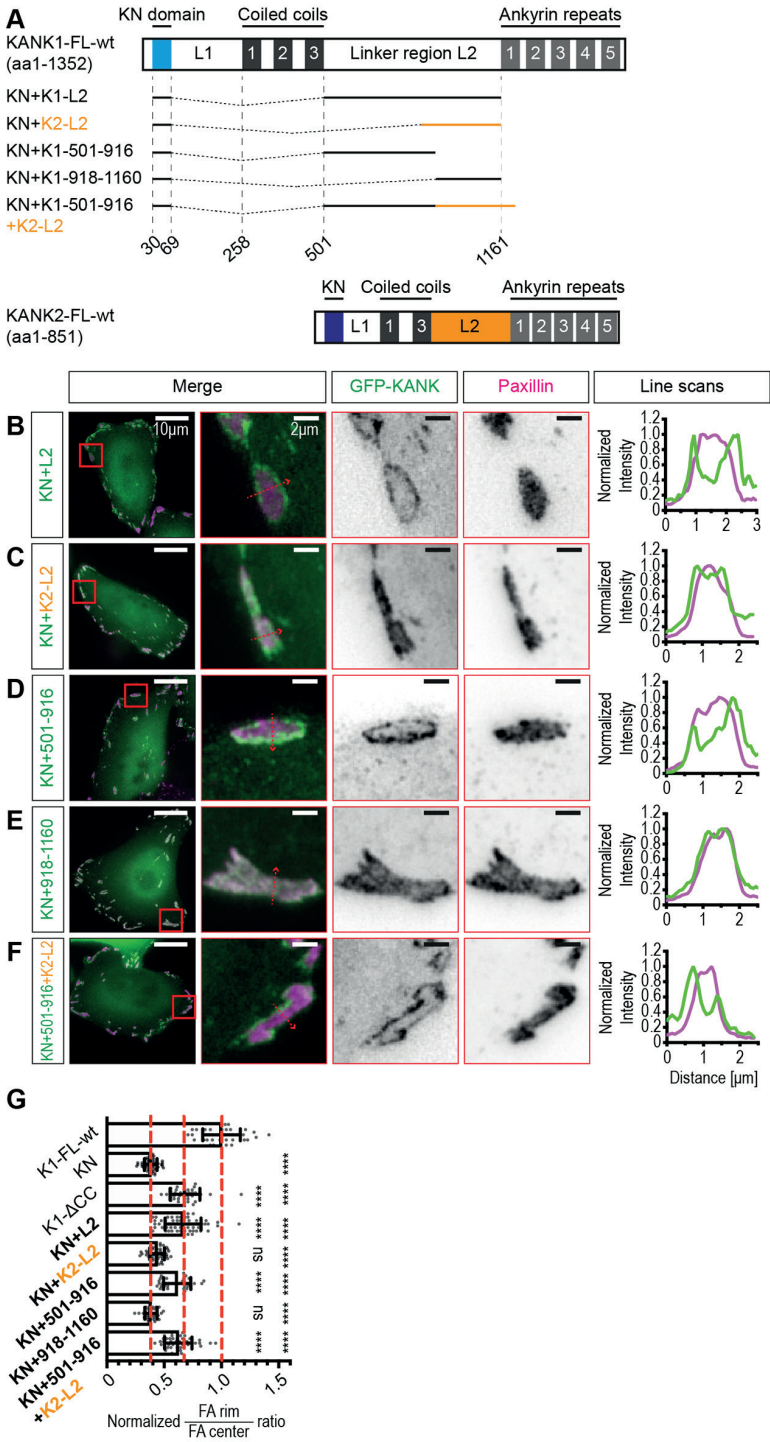
4

Figure 2. The KANK1 linker region L2 sequesters the KN domain to FA rim
(**A**) Schematic overview of the different KN domain fusion constructs. (**B-F**) Subcellular localization of the GFP-tagged constructs (green) from (A) in HeLa K1+K2-KO cells. Around 24 hours after DNA

possible explanation is that the L2 region might function as a binding site for a hitherto unknown partner of KANK1, which in turn would promote the enrichment of KANK1 at the FA rim. One potentially interesting candidate is the dynein light chain LC8 (hereafter simply LC8) which was also present in the pulldown mass spectrometry analysis of full-length KANK1 (Bouchet, unpublished data; Supplementary Figure S4). LC8 is a small protein of around 8 kDa, which was initially described as a subunit of the dynein motor complex (Rapali et al., 2011). Later, it was found that the function of LC8 goes beyond being part of the dynein motor complex. It has been shown that LC8, which forms dimers, functions as a dynamic hub that can promote dimerization of its binding partners (Barbar, 2008). LC8 interacts with a 8-amino acid recognition motif, which is composed of a central 3-amino acid anchor (usually threonine (T), glutamine (Q), threonine (T)) which is flanked by 2 – 3 amino acids, within an intrinsically disordered region (IDR) of its binding partner (Liang et al., 1999). Thereby, LC8 shows great flexibility in recognizing different 8-amino acid recognition motifs (Clark et al., 2016). Recently, Jespersen et al. have introduced a new prediction algorithm (LC8Pred) to screen for possible LC8 recognition motifs and thereby identify potential new LC8 binding partners (Jespersen et al., 2019). LC8Pred algorithm predicted several possible recognition motifs within KANK1. Furthermore, it was shown that LC8 forms cortical patch-like structures in close proximity to FAs (Jespersen et al., 2019). Thus, LC8 seemed to be a promising candidate as new interaction partner of KANK1.

When staining for the endogenous FA protein paxillin and endogenous KANK1 or KANK2 in HeLa cells stably expressing endogenous levels of a C-terminally tagged LC8-GFP fusion generated by BAC TransgeneOmics (Poser et al., 2008), the LC8 signal strongly overlapped with KANK1 patches around FAs (Figure 4A). On the other hand, LC8 showed little co-localization with KANK2 patches (Figure 4A). Removal of endogenous KANK1 from these HeLa cells, via siRNA-mediated knockdown, led to the loss of LC8 around FAs, whereas the removal of endogenous KANK2 did not affect the localization of LC8 (Figure 4A).

The LC8Pred algorithm predicted a total of 67 possible LC8 recognition motifs throughout KANK1(Supplementary Table 1), with 36 motifs located in the L2 region (Figure 2B). To narrow down the number of potential LC8 binding sites, several truncated KANK1 constructs were generated (Figure 4B). The bioGFP-tagged constructs were used in streptavidin-based pulldown assays, using a C-terminally tagged LC8-mCherry fusion as prey protein. The constructs that contained the linker region L2 were able to pull down LC8, whereas the KN domain (1 motif) and the ankyrin repeats (15 motifs) did not bind LC8, very likely because they are folded, whereas the LC8Pred algorithm does not account for the secondary structure of analyzed sequences. Interestingly, it seemed that the coiled coil domains (10 predicted motifs) were also able to bind to LC8, yet,
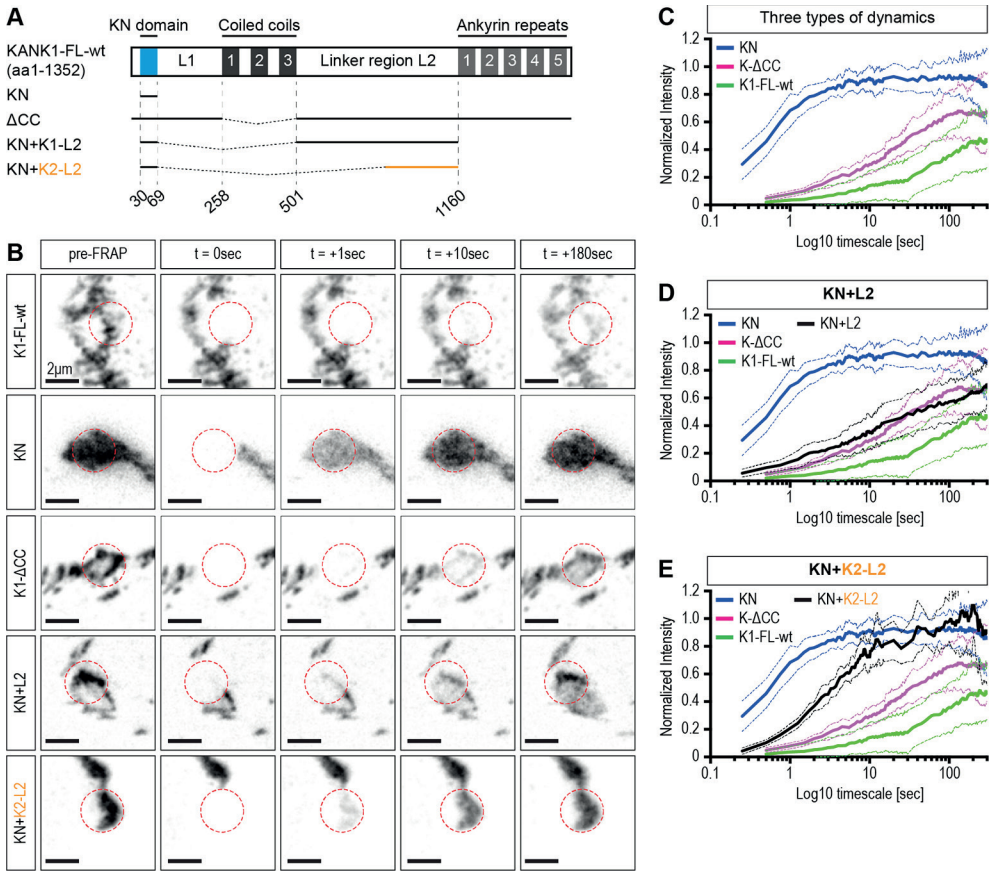
Figure 3. Analysis of the dynamics of different KANK1 deletion mutants using FRAP
(**A**) Schematic overview of the different KANK1/KANK2 constructs used in FRAP experiments. (**B**) Single frames of FRAP experiments with HeLa K1+K2-KO cells overexpressing the different GFP-labeled KANK1 constructs from (A). The stills show a baseline (pre-FRAP), the first frame after photobleaching (t = 0 sec) and the indicated time points after FRAP of a 2.5 µm-diameter circle region in the KANK1 patch. (**D-E**) Quantification of fluorescence recovery. The graph shows mean curves (bold lines) ± SD (light dotted lines) over time. For each condition, in total 16 – 31 KANK patches were analyzed in two independent experiments.

much less effectively than the L2 region (Figure 4C). Co-expressing these bioGFP-tagged KANK1 constructs with LC8-mCherry in HeLa KANK1+2-KO cells confirmed the findings of the pulldown assays (Supplementary Figure S4). As the binding of LC8 via the CC domain seemed very weak, we decided to focus on the linker region L2. To further narrow down the binding region within L2, we generated several truncations of the L2 region, which were fused to the KN domain (Figure 4D). The streptavidin-based pulldown assay revealed that LC8 binds to the N-terminal 300 amino acid fragment of the linker region L2 (amino acids 501-800), which contained 19 possible LC8 binding motifs (Figure 4E).

Next, we wanted to test what happens to KANK1 localization at FAs when the binding to LC8 was abolished. Therefore, we mutated all 19 possible LC8 binding motifs within

Figure 4. Dynein light chain LC8 is a binding partner of KANK1 that associates with KANK1 linker region L2

(A) HeLa cells stably expressing LC8-GFP (green) were transfected with siRNAs against Luciferase (control, siLuciferase), KANK1 (siKANK1) or KANK2 (siKANK2)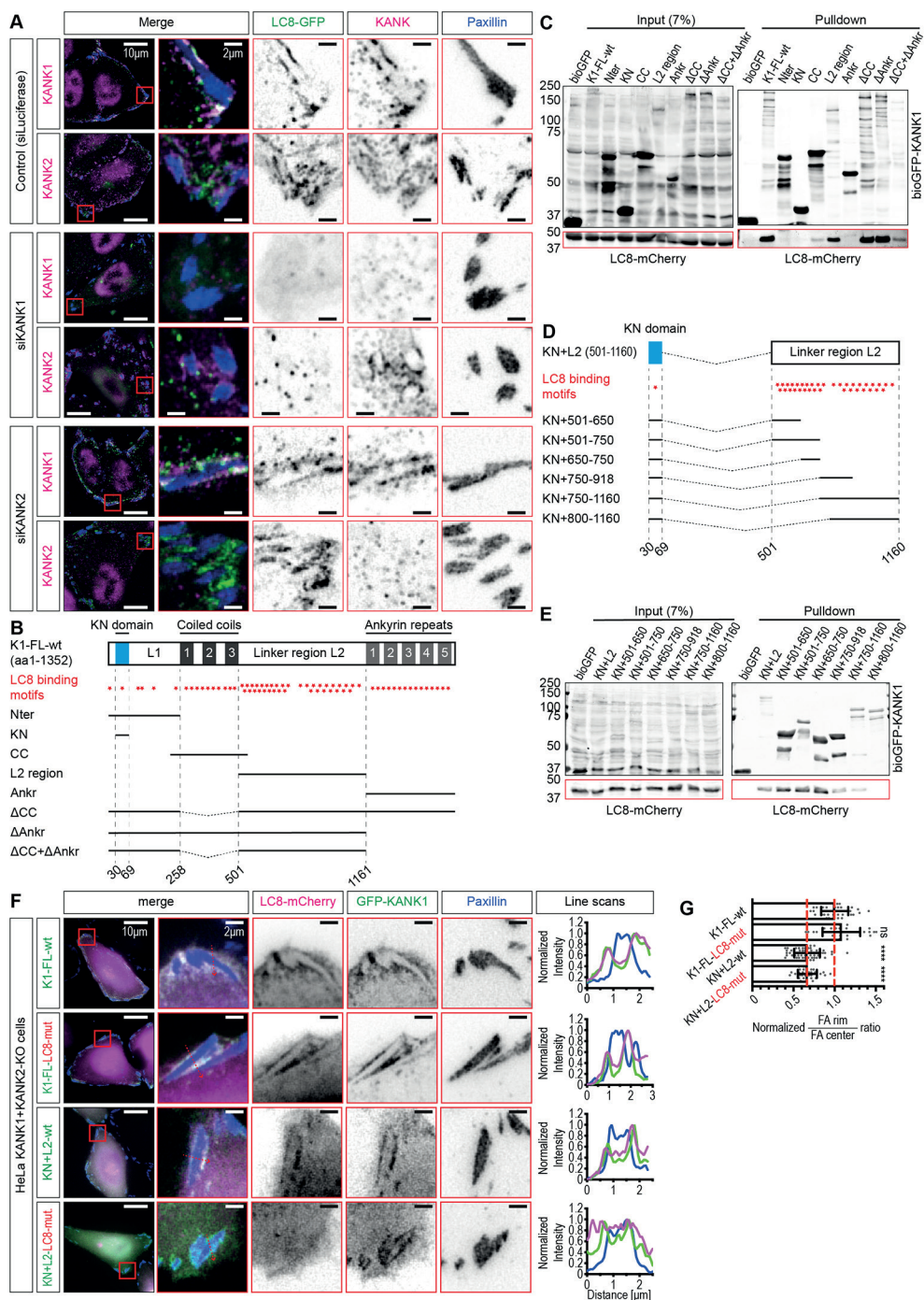. Cells were fixed and stained for endogenous KANK1, KANK2 (magenta) and the FA protein paxillin (blue) ~48 – 72 hours after siRNA transfection. (B)

Schematic overview of the different KANK1 fragments to narrow down the binding sites for LC8. (**C**) Pull-down using bioGFP-tagged constructs from (B) and using LC8-mCherry as prey protein (LC8 is shown in the red box below the bioGFP-KANK1 constructs). (**D**) Schematic overview of different truncated version of KN+L2 to further map the LC8 binding site in the linker region L2. Potential LC8 recognition motifs and their localization are indicated as red asterisks. (**E**) Pulldown using bioGFP-tagged constructs from (D) and LC8-mCherry as prey protein (LC8 is shown in the red box below the bioGFP-KANK constructs). (**F**) Subcellular localization of KANK1 constructs of which the LC8 recognition motifs within the linker region L2 have been mutated. HeLa K1+K2-KO cells were co-transfected with the GFP-tagged KANK1 (green) constructs and LC8-mCherry (magenta). Around 24 hours after DNA transfection, the cells were fixed and stained for endogenous paxillin (blue). The right panel shows the plotted fluorescence intensities of the GFP-KANK (green), LC8-mCherry (magenta) and paxillin (blue) along the line indicated by the dashed red arrow in the inset. The fluorescence intensities were normalized to the maximum intensity of the corresponding channel. (**G**) Quantification of the localization of the different KANK1 constructs around FAs, performed as in Figure 1G. The FA rim/FA center ratios were normalized to the average FA rim/FA center ratio of full-length KANK1. The values are shown as mean ± SD, ns not significant, **** $p < 0.0001$ (Ordinary One-Way ANOVA (Dunnett's Multiple Comparison Test)) (31 – 59 cells have been analyzed per condition in 2 – 3 independent experiments).

the L2 region (501-800). The triplet anchor motifs were substituted for triple alanine. Thereafter, we substituted the corresponding region within the linker L2 with this mutated fragment in full-length KANK1 (K1-FL-LC8-mutant) and in the KN+L2 construct (KN+L2-LC8-mutant). When performing pulldown assays with these new constructs, we observed that the K1-FL-LC8-mutant construct could still associate with LC8, and this was likely due to LC8-binding sites in the CC domain. However, the KN+L2-LC8-mutant construct could not bind to LC8 anymore (Supplementary Figure S4). When we co-expressed these constructs together with LC8-mCherry in HeLa KANK1+2-KO cells, we saw that the K1-FL-LC8-mutant construct clustered around FAs, comparable to K1-FL-wt. Moreover, the construct co-localized with LC8 around FAs, which was likely due to the CC domain. On the other hand, the KN+L2-LC8-mutant construct was not able to bind to LC8. Consequently, there was no LC8 present at the cortex around FAs. Yet, despite not being able to bind to LC8 anymore, the KN+L2-LC8-mutant construct did not overlap with FAs but was enriched at the FA rim like the KN+L2 construct (Figure 4F-G).

We conclude that the linker region L2 of KANK1 mediates binding to a hitherto unknown interaction partner of KANK1, the dynamic hub protein LC8. Yet, we saw that this interaction is not required to sequester KANK1 at the FA rim. On the contrary, it appears that KANK1 is crucial to recruit LC8 to the cell cortex to the vicinity of FAs. The function of this KANK1-LC8 interaction needs to be studied further.

KANK1 linker region L2 participates in oligomerization of KANK1

Even though previous experiments have shown that the recruitment of the KN domain to the FA rim by the linker region L2 was LC8-independent, they led us to our next steps. It is known that LC8 usually interacts with a recognition motif within an intrinsically disordered region (IDR) of its partner (Liang et al., 1999). Moreover, IDRs have been shown to participate in phase separation of many proteins, such as the RNA binding protein Fused in Sarcoma (FUS) (Qamar et al., 2018) or the DDX3 RNA helicase LAF-1 in *C. elegans*. Therefore, we were interested whether an IDR of another protein fused to the KANK1 KN domain could sequester the KN domain at the FA rim. To test this, we generated a new construct by fusing the KANK1 KN domain to the IDR of SLAIN2. To

account for the size difference between a single SLAIN2 IDR (369 aa) and the KANK1 L2 region (659 aa) we used a tandem repeat of the SLAIN2 IDR (KN+2xSLN2-IDR) (Figure 5A). SLAIN2 is a so-called MT plus end-tracking protein (+TIP) which associates with CLASPs and which is required for persistent MT growth (van der Vaart et al., 2011); it does not bind to FAs. The GFP-tagged KN+2xSNL2-IDR construct was expressed in HeLa K1+K2-KO cells. After fixation, the cells were stained for endogenous paxillin to analyze the localization of the new construct at FAs. The tandem repeat of the SLAIN2 IDR was indeed capable of sequestering the KN domain at the FA rim (Figure 5 B&E). Thus, this result suggested that phase separation could contribute to preventing the KN domain from entering the FA core.

Consequently, we wanted to know whether KANK1 linker region L2 is an IDR prone to phase separation. To test this, we wanted to see whether the KANK1 L2 region forms condensates when highly overexpressed in cells. Therefore, the GFP-tagged single L2 regions of KANK1 and KANK2 as well as the KN+L2 and the KN+K2-L2 constructs were cloned into high expression vector pTT5 and overexpressed in HeLa K1+K2-KO cells. As control we overexpressed the KN+2XSLN2-IDR constructs (cloned into a pTT5 vector) in HeLa K1+K2-KO cells as it is known that SLAIN2 can form condensates upon overexpression (van der Vaart et al., 2011). The KN+2xSLN2-IDR construct formed condensates that were dispersed throughout the whole cell. Overexpression of the KANK1 linker region L2 alone led to the formation of small condensate-like structures in some cells. Yet, in most cells, L2 was strongly accumulated in big clusters/aggregates in the perinuclear region (Figure 5C). For the KN+L2 construct condensate-like structures could be observed as well. However, like the KANK1 L2 region alone, it also showed strong accumulation in big clusters/aggregates in the perinuclear region (Figure 5C). Interestingly, the KANK2 L2 region alone as well as the KN+K2-L2 construct also formed big clusters around the nucleus, and these clusters were even bigger than the KANK1 L2 clusters (Figure 5C). Based on these results, the formation of condensates/ clusters after overexpression did not seem to be KANK1-specific as the KANK2 linker region L2 also formed clusters.

Nonetheless, we took this line of research one step further. It has been shown that IDRs can self-associate via cation-π interactions between aromatic amino acids, such as tyrosine, and basic residues, such as arginine, and thereby they can promote phase separation. Moreover, it has been demonstrated that by perturbing the cation-π interactions between IDRs one can abolish phase separation (Wang et al., 2018). To assess whether KANK1 L2 region mediates sequestration of the KN domain at the FA rim via cation-π interactions with other IDRs, we had all 23 arginine (R) residues within the L2 region mutated to glycine (G). Subsequently, the L2 regions of full-length KANK1 and the KN+L2 construct were substituted with the mutated linker region L2 (K1-FL-R-G-mutant and KN+L2-R-G-mutant respectively) (Figure 5A). The GFP-tagged constructs (in EGFP-C1 vectors not high expressing pTT5 vectors) were expressed in HeLa K1+K2-KO cells to analyze their localization at FAs. However, mutating the L2 regions of two constructs did not cause them to localize into the FA core. The K1-FL-R-G-mutant construct showed patchy localization around FAs comparable to K1-FL-wt. The KN+L2-R-G-mutant was enriched at the FA rim like the KN+L2 construct (Figure 5D-E). Thus, these experiments showed that it is unlikely that KANK1 L2 region promotes the sequestration of the KN
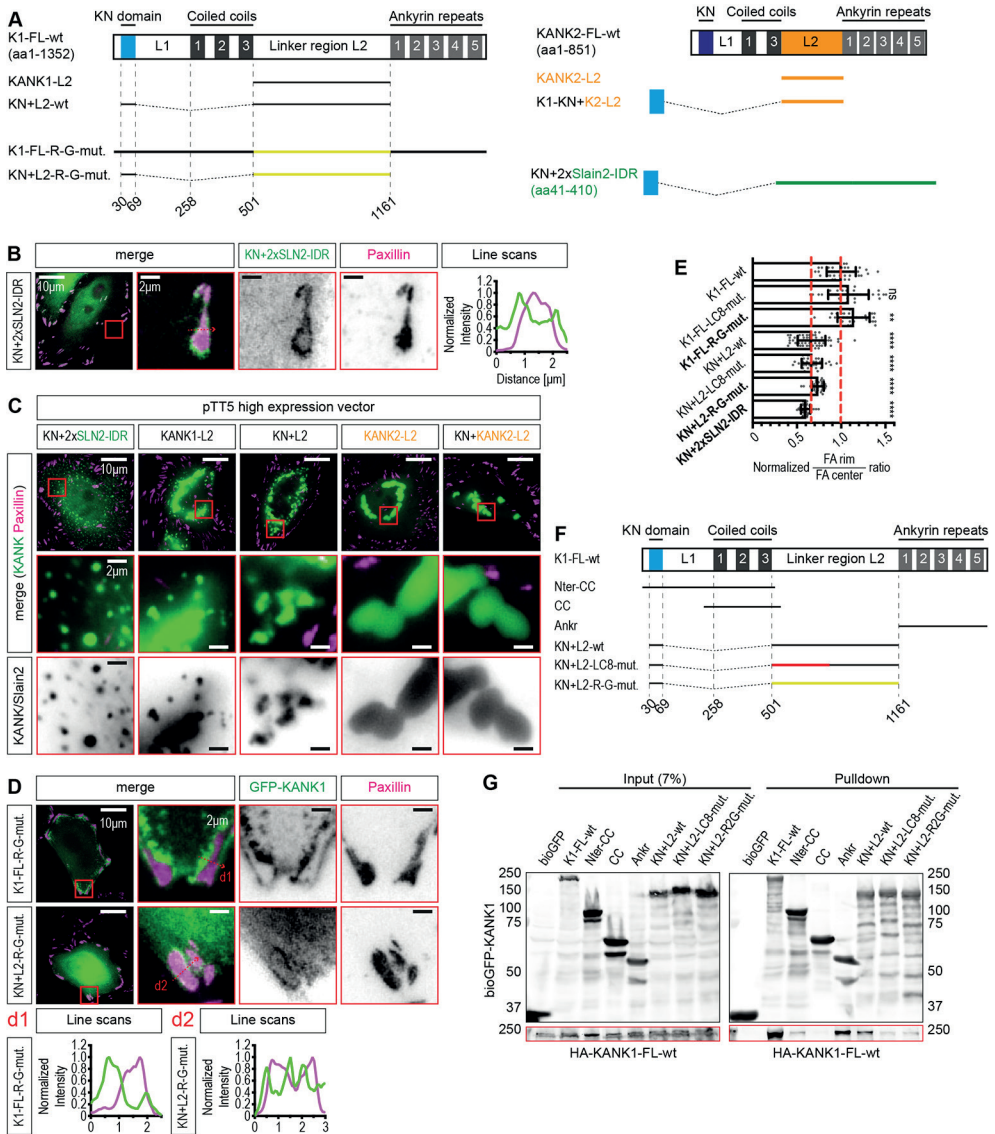
Figure 5. Analysis of KANK1 self-association

(**A**) Schematic overview of different KANK1 constructs including KN fusion constructs that were fused to a tandem repeat of the IDR of SLAIN2. (**B**) Subcellular localization of GFP-tagged KN+2xSLN2-IDR construct (green) in HeLa K1+K2-KO cells that were fixed and stained for paxillin (magenta). The right panel shows the plotted fluorescence intensities of the GFP-KANK (green), LC8-mCherry (magenta) and paxillin (blue) along the line indicated by the dashed red arrow in the inset. The fluorescence intensities were normalized to the maximum intensity of the corresponding channel. (**C - D**) Overexpression of different GFP-tagged KANK fusion constructs in HeLa K1+K2-KO cells that were fixed and stained for paxillin (magenta) to analyze formation of biomolecular condensates. (**E**) Quantification of the localization of KN+2x-SLN2-IDR, K1-FL-R-G-mutant and KN+L2-R-G-mutant at FAs performed as in Figure 1G (the three new constructs are indicated in bold). The other constructs are shown for comparison. The FA rim/FA center ratios were normalized to the average FA rim/FA center ratio of full-length KANK1. The values are shown as mean ± SD; ns not significant, ** $p < 0.01$, **** $p < 0.0001$ (Ordinary One-Way ANOVA (Dunnett's Multiple Comparison Test)) (29 – 59 cells have been analyzed per condition in 2 – 3 independent experiments).

(**F**) Schematic overview of different KANK1 constructs used to analyze the ability of the KANK1 L2 region to oligomerize. (**G**) Pulldown using bioGFP-tagged constructs from (F) and using HA-tagged full-length KANK1 as prey protein (HA-K1-FL-wt is shown in the red boxes below the bioGFP-KANK1 constructs).

domain at the FA rim via cation-π interactions with other proteins.

Yet, we wanted to assess the ability of different KANK1 constructs, including the KN+L2 constructs with mutated L2 regions, to self-associate. Therefore, we performed an initial streptavidin-based pulldown experiment with the bioGFP-tagged KANK1 constructs (Figure 5F) and analyzed their binding to HA-tagged full-length KANK1. Interestingly, all of the tested constructs, except for the three coiled coil domains alone (CC construct) and the negative bioGFP control, were able to bind to HA-K1-FL-wt (Figure 5G). Thus, it seems likely that several domain/regions of KANK1 could contribute to KANK1 self-association/oligomerization including the L2 region. Despite the mutations in the L2 region, the two KN+L2 mutant constructs could still bind to HA-KANK1-FL. These data suggest that sequestration of KN domain at FA rim via KANK1 L2 region could be mediated via self-association which seems to be independent of LC8 and cation-π interactions. Nonetheless, more thorough research is necessary to confirm these results and to gain more insight into how KANK1 proteins exactly mediate self-association/oligomerization.

Discussion

In this study we have tried to gain further insight into the localization of KANK1 to FA rim and the role of the different KANK1 domains in this process. We found that based on the localization at FAs, KANK1 deletion mutants can be categorized into three distinct groups. The first group includes the constructs that localize to FA rim and patches around FAs, like full-length KANK1. The second group of constructs, like KANK1-ΔCC, localize exclusively to the FA rim. The third group, such as the KN domain alone, completely overlaps with FAs. The CC domain, more precisely the CC1 domain which mediates binding to liprins, is responsible for the patchy localization around FAs. Yet, it seems that neither the CC nor the Ankr domains are essential to exclude KANK1 (or the KN domain) from the FA center and to recruit it to the FA rim as a KANK1-ΔCC+ΔAnkr construct still localizes exclusively to the FA rim. This property is mediated by the linker region L2 of KANK1. Furthermore, it seems that the potential to exclude the KN domain from the FA center lies within the N-terminal portion of the L2 region (amino acids 501-916), which is specific for KANK1. When fused to KANK1 KN domain, the shorter L2 region of KANK2, which shares homology (~40% similarity) with the C-terminal part of the KANK1 L2 region, is not able to prevent the KN domain from penetrating into FAs. Remarkably, full-length KANK2 does not overlap with peripheral FAs but shows localization to the FA rim and patches around FAs (Supplementary Figure S2). The L2 region of KANK1 is one of the factors, but not the only factor that promotes the enrichment of KN domain at the FA rim.

Interestingly, we found that the dynamic behavior of the KANK1/KANK2 constructs correlated with these three distinct localization patterns. Full-length-KANK1-like constructs show slow recovery after photobleaching and a large immobile fraction (~60%). KANK1-ΔCC-like constructs recover faster and have a smaller immobile fraction than
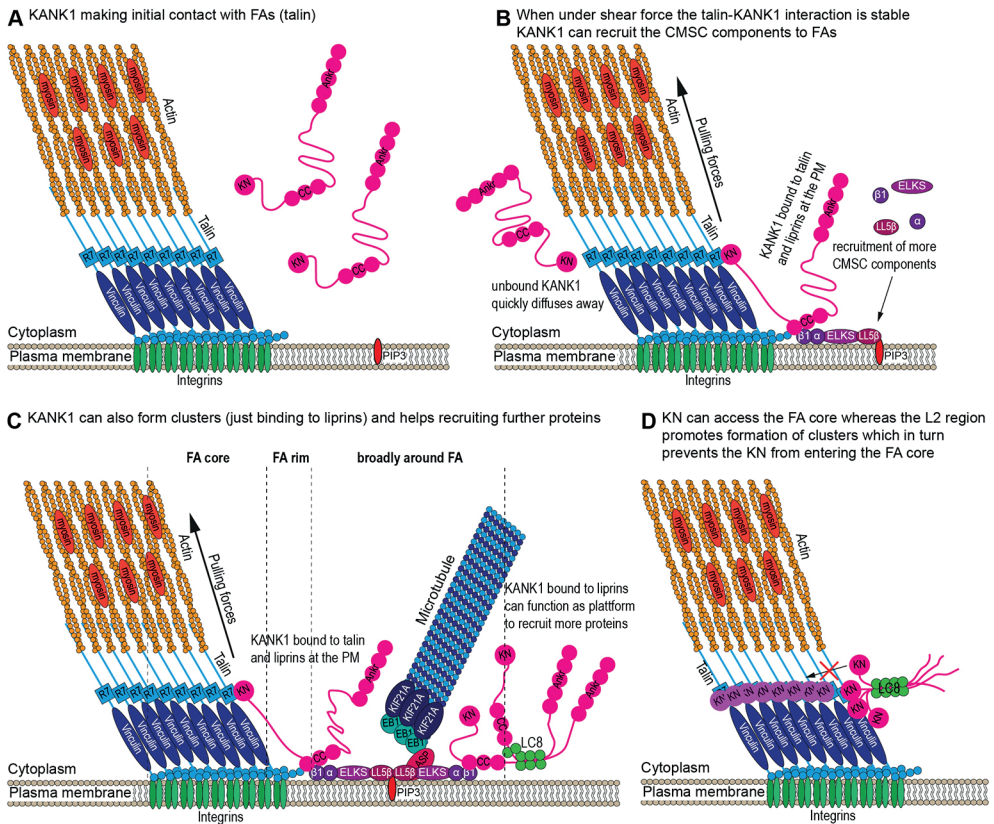
Figure 6. Model of different KANK1 subpopulations at FAs

(**A**) KANK1 proteins can interact with talin at FAs. (**B - C**) KANK1 proteins that are bound to both talin and liprins are likely subjected to mechanical forces which have a certain stabilizing effect on the talin-KANK1 interaction. Consequently, these KANK1 proteins can dwell at FAs longer. Thereby, they can promote the recruitment and assembly of the CMSC. Moreover, some KANK1 proteins that are located more broadly around FAs where they interact with other CMSC proteins such as liprins without interacting with talin may not be subjected to mechanical forces. These 2nd layer KANK1 proteins likely function as a scaffold to re-cruit further proteins to the cell cortex. (**D**) Model explaining how the KANK1 linker region L2 could prevent the KN domain from penetrating into the FA center. Due to its small size and the absence of long-lasting interactions, the KN domain alone (purple) can easily access the tightly packed FA core and bind to talin proteins located at the FA center. On the other hand, when the KN domain is fused to the linker region L2 (magenta), it is possible that the L2 region promotes the association and clustering with other L2 regions of other KANK1 proteins. Consequently, the KANK1 proteins or their KN+L2 deletion mutants form clus-ters which in turn could be too bulky (steric hinderance) and thereby sequester the KN domain at the FA rim. It is possible that the hub protein LC8 (green circles) helps to stabilize the KN+L2 self-association.

full-length KANK1-like constructs (30-40%). Finally, the KN-like constructs recover very rapidly and display only a very small immobile fraction (~10%). The liprin-binding CC1 domain is responsible for the difference between the full-length KANK1-like and the KANK1-ΔCC-like constructs. Interestingly, the KN fusion constructs containing linker regions of KANK1 and KANK2 showed dynamics that correlated with their localization. The KN+L2 construct with KANK1 linker, which is enriched at the FA rim, showed similar recovery and immobile fraction after photobleaching as KANK1-ΔCC. In contrast, the behavior of the KN+K2-L2 construct, which completely overlaps

with FAs, was more similar to the behavior of the KN domain alone: It recovered more rapidly than KANK1-ΔCC or KN+L2 and its immobile fraction was comparable to that of the KN domain alone. The sequestration of KANK1 deletion mutants at the FA rim thus appears to be associated with their tighter binding to FAs, association with other cortical proteins or with each other.

Our initial hypothesis was that the L2 region might function as a binding site for a previously unknown interaction partner of KANK1, which in turn mediates the exclusion of the KN domain from the FA center. Indeed, we found a new interaction partner of KANK1, the hub protein LC8 and showed that it interacts with the L2 region. Yet, the recruitment of the KN domain to the FA rim was LC8-independent as the KN+L2-LC8-mutant construct, which cannot bind LC8 anymore, was still enriched at the FA rim. Actually, it appeared that the cortical localization of LC8 was KANK1-dependent. However, the function of this KANK1-LC8 interaction remains unclear. We cannot exclude that other proteins bind to the L2 region of KANK1, but our mass spectrometry-based analysis (Bouchet, unpublished data) yielded no obvious candidates.

Next, we considered whether KANK1 sequestration at FA rim represents a case of liquid-liquid phase separation. Over the past decade, the concept of phase separation has emerged as the explanation for different processes of membrane-less compartmentalization within cells (Banani et al., 2017; Sear, 2007; Stradner et al., 2004). Thereby, multivalent proteins undergo self-assembly to locally increase their concentration, which in turn leads to the formation of biomolecular condensates (Banani et al., 2017; Wheeler and Hyman, 2018). Besides, it has been shown that many scaffold proteins, which bind and thereby concentrate their interaction partners, contain IDRs or are completely disordered proteins (Posey et al., 2018). In support of this idea, a tandem-repeat of the IDR of the +TIP SLAIN2 was able to keep the KN domain out of FAs as the KN+2xSLN2-IDR construct also clustered tightly at the rim of FAs. Nonetheless, from our experiments and sequence analyses of the L2 region we could not obtain a clear proof that phase separation is the driving force behind the L2-mediated sequestering of the KN domain at the FA rim. An interesting experiment would be to treat cells with 1,6-hexanediol which rapidly dissolves biomolecular condensates (Itakura et al., 2018; Shin and Brangwynne, 2017) and to see how this treatment affects the localization of the KN+L2 construct at the FA rim.

In order to contribute to phase separation, L2 would need to self-associate one way or another. Sequence analyses of the KANK1 linker region L2 predicted a potential coiled coil domain between amino acids 819-883, thus within the N-terminal part of L2 which keeps the KN out of FAs. This predicted coiled coil was mentioned in a previous study describing a fusion gene of *KANK1* and *platelet-derived growth factor receptor β* (*PDGFRβ*). It was shown that KANK1 mediated oligomerization of the *KANK1:PDGFRβ* gene product via the N-terminal region of the linker region L2 which is N-terminal of the predicted CC domain. Yet, from these experiments it did not seem that the predicted CC was involved in KANK1 oligomerization (Medves et al., 2011). One of the goals of our ongoing research to analyze the role of the predicted CC domain in KANK1 self-association and KN separation at the FA rim.

To test the oligomerization potential of different KANK1 constructs, we performed pulldown assays by determining their ability to bind full-length KANK1. Our preliminary

assays revealed that among other domains of KANK1, such as the ankyrin repeats, the L2 region is likely able to bind to full-length KANK1 even when highly mutated. However, further research needs to be done to confirm these findings. An extended series of pulldown assays would be required. Thereby, one could first use smaller fragments of KANK1, for example those employed to map the LC8 bindings sites. Moreover, it would be important to use different fragments of KANK1, such as the L2 region alone, as prey to get a better understanding of intramolecular interactions within KANK1. Another interesting experiment would be to co-express the linker region L2 together with K1-FL-wt or the KN+L2 construct in HeLa K1+K2-KO cells to see whether the L2 can be recruited to FAs by other KANK1, as by itself, the L2 region alone is diffusely distributed throughout the cytoplasm (Supplementary Figure S4).

The new insights about the role of the linker region L2 in the subcellular localization of KANK1 do not contradict our previous findings showing that mechanical forces contribute to the subcellular localization of KANK1 at FAs (Yu et al., 2019). We assume that it is possible that the localization of KANK1 at FA is regulated/affected by different factors. One could think of a model in which several subpopulations of KANK1 proteins exist at FAs (Figure 6A-C). There could be KANK1 proteins that are bound to both talin and liprins, and such molecules could be expected to be subjected to mechanical forces (Figure 6B). As it was shown by us previously, mechanical forces can strengthen the talin-KANK1 interaction to a certain degree (Yu et al., 2019). Consequently, one could imagine that these force-regulated KANK1 proteins dwell longer at FAs and can thereby form the basis for the recruitment of the other components of the CMSC to FAs and finally to the assembly of the CMSC (Figure 6C). Moreover, there could be KANK1 proteins that are only bound to liprins around FAs in a "second layer", where they function as a scaffold to recruit even more (CMSC) proteins to FAs (Figure 6C). Besides, there could be KANK1 proteins that are neither bound to talin nor liprins but bound to other KANK1 proteins at the cortex (Figure 6C). One could imagine that the dynamic hub protein LC8 might contribute to this process as it is known that LC8 promotes dimerization of its interaction partners and stabilizes them (Barbar, 2008).

With regard to the question how the KN domain is prevented from entering the FA center by the linker region L2 one could imagine a model in which L2 leads to the formation of bulky clusters that are excluded from densely packed FA areas where talin is attached to actin cables and other adaptors (Burridge, 2017; Kanchanawong et al., 2010; Wolfenson et al., 2009). Thus, one could imagine that the small KN domain alone could easily access the core of the highly organized FAs and thereby completely overlap with the FA (Figure 6D). On the other hand, when fused to the linker region L2, the L2 region could promote self-association of the KN+L2 constructs which in turn could result in clusters that are too bulky to penetrate into the FA core. Consequently, the KN+L2 construct is enriched at the FA rim. In a previous study, we tried to address this issue and fused the KN domain to β-galactosidase from *E. coli* (KN+lacZ construct). We chose β-galactosidase from *E. coli* since we wanted to prevent any interferences due to possible interactions with other proteins. Yet, this absence of interactions with other proteins could have been the reason why the KN+lacZ construct was able to penetrate into FAs like the KN domain alone (Bouchet et al., 2016).

Last but not least, the role of talin in regulation of the KANK1 localization at FAs

would also be interesting to analyze more thoroughly. Talin is the major adaptor protein of FAs (Klapholz and Brown, 2017). It binds with its N-terminal talin head domain (THD) to the cytosolic tails of β-integrins whereas the talin rod binds to actomyosin (Case and Waterman, 2015). The talin rod consists of 13 rod domains (R1 – R13) and a dimerization domain (DD) (Goult et al., 2013). Besides, two of the three actin binding sites (ABS) are located within the talin rod: ABS2 within rod domains R4 – R8 and ABS3 within R13 and DD (Atherton et al., 2015; Gingras et al., 2008; Hemmings et al., 1996). It would be interesting to gain more insights into whether there are differences in the activation/conformational state of talin molecules at the FA rim compared to the FA core and how these could affect interaction with KANK1. It has been shown that tensile forces exerted on FAs are usually highest at the FA center (Plotnikov et al., 2012). More recently, it has been shown that FA regions under high tension correlate with highly organized parallel aligned actin bundles (Kumar et al., 2018). Thus, one could imagine that the FA core is densely packed with proteins that are recruited to talin under high tension, such as vinculin (Atherton et al., 2015; Goult et al., 2013), and thereby the FA core becomes less accessible for bulky protein clusters. This would fit with our proposed model from above. Nonetheless, it would also be important to learn more about the talin-actin interaction and how it might affect binding to KANK as the ABS2 ranges from R4 to R8 and thereby it includes the R7 domain to which the KN domain binds (Bouchet et al., 2016; Sun et al., 2016). Moreover, studies are now indicating that not ABS3 at the very C-terminus of talin but the more central ABS2 could be the major tension-bearing ABS in talin (Atherton et al., 2015; Kumar et al., 2016). Therefore, one could think that KANK and actin might compete for binding to talin. This notion is supported by a study about KANK2 in mouse fibroblasts where KANK2 seems to weaken the talin-actomyosin linkage (Sun et al., 2016). Thus, one could imagine that talin molecules at the FA rim might be predominantly connected to actin via the ABS3 whereas at the FA core they could be mainly connected to actin via ABS2. Thereby, talin-KANK interactions at the FA rim would be competing less with actin for talin binding.

Taken together, in our study we have shown that the previously poorly characterized linker region L2 of KANK1 is capable of excluding the KN domain from the FA center. Moreover, we have seen that KANK1 proteins can self-associate and that the L2 region participates in the KANK1 oligomerization. However, the exact mechanism how KANK1 oligomerizes remains to be determined and will be subject of future research.

4

Experimental Procedures

Cell culture and DNA/siRNA transfections

HeLa (Kyoto) cells stably expressing LC8-GFP were a kind gift from I. Poser and A. Hyman (Max Planck Institute of Molecular Cell Biology and Genetics, Dresden, Germany) (Poser et al., 2008). The HeLa (Kyoto) KANK1+KANK2-KO cell line was generated by CRISPR/Cas9-mediated knockout as described below. The HeLa cell lines were cultured in DMEM medium. HEK293T cells were cultured in DMEM:F10 medium (1:1, v/v). All media were supplemented with 10 % (v/v) fetal calf serum and with Penicillin/Streptomycin (100 units/mL penicillin and 100 μg/mL streptomycin). All cells were grown at 37 °C in humidified incubators at 5% CO_2 atmosphere. The cells were routinely checked for mycoplasma contamination using the Mycoalert assay (Lonza, LT07-518).

Transfection of DNA and siRNA into HeLa cells and of DNA into HEK293T cells was performed as previously described (van der Vaart et al., 2013). In brief, HeLa cells were transfected with siRNAs using HiPerFect (Qiagen). The siRNA-transfected cells were analyzed 48 – 72 hours after transfection. HeLa cells were transfected with DNA constructs using FuGene6 (Promega). The cells were analyzed 24 hours after DNA transfection. HEK293T cells were transfected with DNA using polyethyleneimine (PEI). The cells were harvested for pulldown assays around 24 hours after transfection.

DNA constructs and siRNAs

The BioGFP-tagged KANK1 and KANK2 fusion constructs were made using PCR-based amplification of different KANK1 or KANK2 fragments. These fragments were cloned into pBioGFP-C1 vector using Gibson Assembly mix (New England Biolabs) as described previously (Bouchet et al., 2016). The KANK1 linker region L2 fragments carrying mutations of the LC8 recognition motifs (L2-LC8-mutant) or in which the arginine residues have been substituted with glycine residues (L2-R-G-mutant) were synthesized by Integrated DNA Technologies (IDT, USA). Subsequently these fragments were cloned into the corresponding KANK constructs. For analysis of condensate formation, the corresponding KANK constructs were cloned into the high expression vector pTT5-GFP-C1. The LC8-mCherry fusion construct was made by PCR-based amplification of LC8 and cloning it into the pmCherry-N1 vector.

The same siRNAs against KANK1 and KANK2 were used as described previously (Bouchet et al., 2016) to deplete HeLa LC8-GFP cells of KANK1 and KANK2: control siRNA (siLuciferase) GTGCGTTGCTAGTACCAAC; siKANK1 CAGAGAAGGACATGCGGAT; siKANK2 ATGTCAACGTGCAAGATGA.

Generation of HeLa KANK1+KANK2-KO cell line

The HeLa KANK1+KANK2-KO cell line was generated by using the previously described HeLa KANK2-KO cell line (Yu et al., 2019) and following the protocol for CRISPR/Cas9 mediated knockout as described in the literature (Ran et al., 2013). In brief, guide RNA against human KANK1 was designed using the online CRISPR design tool provided by the Broad Institute (http://crispr.mit.edu) and cloned into the pSpCas0(BB)-2A-Puro (PX459) expression vector (KANK1-guideRNA: GTTTAGTCATCTCCCGGTCA).

HeLa KANK2-KO cells were transfected with the vector using FuGene6 transfection reagent. The following day, the cells were washed with PBS and subsequently cultured in the selection medium (DMEM medium with 10 % fetal calf serum, 1 % penicillin/ streptomycin, supplemented with 2 µg/mL puromycin) for at least 48 hours; the selection medium was refreshed every 24 hours. After selection, the cells were cultured in normal medium (DMEM medium with 10 % fetal calf serum and 1 % penicillin/streptomycin) and allowed to recover for 2 – 3 days. Afterwards, a first check of the knockout efficiency was done by immunofluorescence staining followed by isolation of individual clones, which were further characterized by immunofluorescence staining and Western blotting.

Western blot analysis of HeLa KANK1+KANK2-KO cells

To obtain whole cell lysates for Western blot analysis, cells were lysed in a non-ionic detergent-based buffer (50 mM Tris-HCL, 150 mM NaCl, 1 mM EDTA, protease inhibitor cocktail (Roche), 1 % Triton-X100) for 10 minutes on ice. Afterwards, the suspension was centrifuged at 13,200 rpm at 4 °C for 15 minutes. The protein concentration of the supernatant was measured using the colorimetric bicinchoninic acid (BCA) assay, using a BCA kit (ThermoFisher, #23225) following the supplier's instructions. The following SDS-PAGE and Western blot analysis were performed according to standard procedures. The same commercially available antibodies against KANK1 and 2 were used as for immunofluorescence staining (*see Antibodies and Immunofluorescence staining*); furthermore, an antibody against Ku80 (BD Biosciences, 611360) was used. For the detection, near infrared (NIR) fluorescence technology was used (Li-Cor Biosciences, Odyssey system), using infrared dye conjugated goat antibodies against mouse and rabbit (Li-Cor Biosciences).

Streptavidin-based pulldown assays

Streptavidin-based pulldown assays of biotinylated KANK constructs expressed using BioGFP-tagged-KANK constructs in HEK293T cells were performed as previously described (van der Vaart et al., 2013). In brief, HEK293T cells were seeded in 10 cm plastic culture dishes to ~80 % confluence, the cells were allowed to attach overnight. The following day, the cells were transfected with the BioGFP-tagged KANK constructs together with biotin-ligase BirA (5µg DNA per construct) using PEI. In parallel, 1 – 2 10 cm plastic culture dishes were transfected with the prey protein only (LC8-mCherry, or HA-KANK1-FL, 10µg DNA) using PEI. The DNA/PEI suspensions were added to the cells dropwise. Thereafter, the cells were incubated for 24 hours at 37 °C in 5 % CO2 atmosphere in humidified incubators. After incubation, the cells were harvested on ice using ice-cold PBS and a spatula to scrape them from the dishes. The harvested cells were pelleted and subsequently lysed using a non-ionic detergent-based lysis buffer (50 mM HEPES pH 7.4, 150 mM NaCl, 1 mM EDTA, protease inhibitor cocktail (Roche), 1 % Triton-X100) for 10 minutes on ice. Afterwards, the suspension was centrifuged at 13,200 rpm at 4 °C for 15 minutes. In the meantime, the magnetic streptavidin beads (ThermoFisher, 11206D) were blocked in lysis buffer supplemented with 5% chicken egg white (Sigma) for 30 minutes at RT. Thereafter, the lysate of the prey protein was equally distributed among the biotinylated GFP-tagged KANK constructs. Thereafter, the lysate mixes were incubated with the streptavidin beads for 2 hours at 4 °C, except

for 7 % of each lysate mix which was kept as "input" control. DTT-containing SDS-PAGE protein sample buffer was added to the input control. After incubation of the lysates with the streptavidin beads, the beads were washed 5 times using the lysis buffer and a magnetic "DynaMag" rack (ThermoFisher, 12321D). Thereafter, DTT-containing SDS-PAGE protein sample buffer was added to the beads.

The following SDS-PAGE and Western blot analysis were performed according to standard procedures. Commercially available antibodies against GFP (Abcam, ab6556), mCherry (clone 1C51, Abcam, ab125096) and HA (clone 16B12, BioLegend/Covance, MMS-101P) were used. For the detection, near infrared fluorescence technology was used (Li-Cor Biosciences, Odyssey system), using infrared dye conjugated goat antibodies against mouse and rabbit (Li-Cor Biosciences).

FRAP experiments using GFP-KANK constructs in HeLa KANK1+KANK2-KO cells

HeLa KANK1+KANK2-KO cells were seeded in 4-well chambered cover glasses (LabTek, 155383) (20,000 – 30,000 cells/well) and allowed to attach overnight. The following day, the medium was refreshed, and the cells were transfected with DNA (0.5 µg DNA/well) using FuGene6 (Promega) transfection reagent. The cells were incubated with the DNA/FuGene6 mixture overnight. The following day (~24 hours after the DNA transfection), the cells were used for live-cell imaging FRAP experiments.

KANK rescue experiments using HeLa KANK1+KANK2-KO cells

HeLa KANK1+KANK2-KO cells were seeded on 12 mm glass coverslips (10,000 – 15,000 cells per coverslip) and allowed to attach overnight. The following day, the medium was refreshed, and the cells were transfected with DNA (0.5 µg DNA/well) using FuGene6 (Promega) transfection reagent. The cells were incubated with the DNA/FuGene6 mixture overnight. The following day (~24 hours after the DNA transfection), the cells were fixed for immunofluorescence staining.

siRNA-mediated knockdown of KANK1 and KANK2 in HeLa LC8-GFP cells

HeLa LC8-GFP cells were seeded were seeded in 6-well culture plates and transfected using 20nM per siRNA per well using HiPerFect (Qiagen) and adding the siRNA/transfection reagent mix to the cell suspension. The cells were allowed to attach and to incubate in the siRNA/transfection reagent-containing medium overnight. The following day, the cells were washed 2-times with PBS and incubated for another 24 hours. The following day (~48 hours after siRNA transfection), the cells were trypsinized and seeded on 12mm glass coverslips (10,000 – 15, 000 cells per coverslip) and allowed to attach overnight. The following day (~72 hours after siRNA transfection), the cells were washed with PBS and fixed for immunofluorescence staining.

Antibodies and Immunofluorescence staining

Cell fixation and staining were performed as previously described (van der Vaart et al., 2013). In brief, the cells were either fixed with 4 % PFA in PBS for 15 minutes at room temperature (staining GFP-KANK constructs, LC8-GFP/mCherry and paxillin) or with ice-cold methanol for 7 minutes at -20 ºC (staining of endogenous KANK1,

KANK2 and talin). After one-time washing with PBS, the cells were permeabilized for 4 minutes at room temperature (RT) using permeabilization buffer (0.2 % TritonX-100 (Sigma) in PBS). Thereafter, the cells were blocked in blocking buffer (0.05 % Tween-20 (Sigma) and 2 % BSA (Carl Roth) in PBS) for 1 hour at RT. After blocking, the cells were incubated with primary antibodies diluted in blocking buffer for 1 hour at RT. After incubation, the cells were washed 5 times for 2 minutes with wash buffer (0.05 % Tween-20 in PBS); followed by 1 hour incubation with the fluorescently labeled secondary antibodies diluted in blocking buffer. The cells were washed 5 times for 2 minutes with wash buffer and afterwards, dehydrated using first 70 % and then 100 % ethanol. Finally, the coverslips were mounted on glass slides using Vectashield mounting medium (Vector laboratories, H-1000).

Commercially available antibodies against KANK1 (Atlas antibodies, HPA005539), KANK2 (Atlas antibodies, HPA015643), talin (clone 8d4, Sigma, SAB4200694); and paxillin (clone 165, BD Biosciences, 610620) were used. Alexa-405, Alexa-488 and Alexa-594 conjugated goat antibodies against rabbit and mouse IgG were purchased from Invitrogen.

Microscopy and image analysis

Live-cell fluorescence TIRF imaging of cells expressing GFP-labeled KANK1 constructs and Fluorescence Recovery After Photobleaching (FRAP) experiments were performed on an inverted research microscope Nikon Eclipse Ti-E (Nikon) with the perfect focus system (Nikon), equipped with Nikon Apo TIRF 100x N.A. 1.49 oil objective (Nikon) and iLas2 system (Dual Laser illuminator for azimuthal spinning TIRF (or Hilo) illumination and Simultaneous Targeted Laser Action) from Roper Scientific (Evry, FRANCE). The system was also equipped with ASI motorized stage MS-2000-XY (ASI), CoolSNAP MYO CCD camera (Photometrics) and controlled by the MetaMorph 7.8 software (Molecular Devices). For imaging of green fluorescence and FRAP experiments a Stradus 488 nm (150 mW) (Vortran) laser was used as light source and the filter set ET-GFP (49002) (Chroma) was used. To keep the cells at 37 °C, a stage top incubator model INUBG2E-ZILCS (Tokai Hit) was used. Images were acquired at 15.4 pixels/μm with exposure time 100 milliseconds at various frames per second (for FRAP, see the text below). Cells were maintained at 37 °C and 5 % CO2.

Images of fixed cells were collected with a Nikon Eclipse Ni upright wide field fluorescence microscope and a Nikon DS-Qi2 CMOS camera (Nikon), using Plan Apo Lambda 100x N.A. 1.45 oil objective (Nikon) and Nikon NIS (Br) software (Nikon). Nikon Intensilight C-HGFI was used as a light source. For imaging of blue, green and red fluorescence the filter sets ET-BFP2 (49021), ET-GFP (49002), and ET-mCherry (49008) (all Chroma) were used respectively.

For presentation, images were adjusted for brightness and contrast using ImageJ 1.50b (NIH).

For analysis of KANK localization at FAs, the outlines of FAs were obtained first. Background subtraction (rolling ball radius, 20 pixels) was applied to the FA channel. Subsequently, the image was thresholded (Default setting) and the FA outlines were acquired using the Analyze particles function in ImageJ (only FA particles bigger than 1 μm2 were included). Thereafter, background subtraction (rolling ball radius, 20 pixels)

was applied to the GFP-KANK channel. The previously obtained FA outlines were first expanded by 0.25 µm. Then, the integrated density and area of the expanded FA outlines in the GFP-KANK1 channel were measured. Thereafter, the expanded FA outlines were shrunk by 0.5 µm and the integrated density and area of the shrunk FA outlines in the GFP-KANK channel were measured again. The intensity at the FA rim was calculated by subtraction of the second measurement (FA center) from the first measurement (outer). Both intensities were divided by the area of the corresponding region. Finally, the FA rim/FA center ratio was normalized to the average FA rim/FA center ratio of K1-FL-wt.

$$\frac{\text{FA rim}}{\text{FA center}} \text{ ratio} = \frac{\frac{(\text{Outer Intensity} - \text{FA center intensity})}{(\text{Outer area} - \text{FA center area})}}{\frac{\text{FA center intensity}}{\text{FA center area}}}$$

$$\text{Normalized } \frac{\text{FA rim}}{\text{FA center}} \text{ ratio} = \frac{\frac{\text{FA rim}}{\text{FA center}} \text{ ratio}}{\text{average } \frac{\text{FA rim}}{\text{FA center}} \text{ ratio } (K1-FL-wt)}$$

Statistical analyses were performed using Prism 7 (GraphPad).

For FRAP experiments, the TIRF setup described above was used. FRAP measurements were performed by bleaching a 2.5-µm-diameter circle in GFP-KANK patches at FAs followed by 15 seconds imaging with a frame interval of 0.25 seconds per frame and 5 minutes imaging with a frame interval of 5 seconds (for KN, KN+L2, KN+K2-L2). For the slower recovering KANK constructs (K1-FL-wt, K1-ΔCC, K1-ΔCC1, K1-ΔCC2+3), after photobleaching followed 30 seconds imaging with a frame interval of 0.5 seconds and 5 minutes imaging with a frame interval of 5 seconds. Per cell, 3 – 5 KANK1 patches were photobleached simultaneously. Mean fluorescence intensities were measured from a 2.5 µm-diameter circular region within the original photobleached region. The mean intensity of this region was double corrected for background fluorescence and photobleaching as previously described (Phair et al., 2004).

For line scans of GFP-labeled KANK constructs, LC8-mCherry and paxillin fluorescence profiles were obtained by line scan analysis in ImageJ. The fluorescence profiles were normalized by the maximum fluorescence intensity of the corresponding channel.

References

Atherton, P., B. Stutchbury, D.Y. Wang, D. Jethwa, R. Tsang, E. Meiler-Rodriguez, P. Wang, N. Bate, R. Zent, I.L. Barsukov, B.T. Goult, D.R. Critchley, and C. Ballestrem. 2015. Vinculin controls talin engagement with the actomyosin machinery. Nat Commun. 6:10038.

Bachir, A.I., J. Zareno, K. Moissoglu, E.F. Plow, E. Gratton, and A.R. Horwitz. 2014. Integrin-associated complexes form hierarchically with variable stoichiometry in nascent adhesions. Curr Biol. 24:1845-1853.

Banani, S.F., H.O. Lee, A.A. Hyman, and M.K. Rosen. 2017. Biomolecular condensates: organizers of cellular biochemistry. Nature Reviews Molecular Cell Biology. 18:285-298.

Barbar, E. 2008. Dynein light chain LC8 is a dimerization hub essential in diverse protein networks. Biochemistry. 47:503-508.

Bouchet, B.P., R.E. Gough, Y.C. Ammon, D. van de Willige, H. Post, G. Jacquemet, A.M. Altelaar, A.J. Heck, B.T. Goult, and A. Akhmanova. 2016. Talin-KANK1 interaction controls the recruitment of cortical microtubule stabilizing complexes to focal adhesions. Elife. 5.

Burridge, K. 2017. Focal adhesions: a personal perspective on a half century of progress. Febs j. 284:3355-3361.

Case, L.B., and C.M. Waterman. 2015. Integration of actin dynamics and cell adhesion by a three-dimensional, mechanosensitive molecular clutch. Nature Cell Biology. 17:955.

Clark, S., A. Nyarko, F. Löhr, P.A. Karplus, and E. Barbar. 2016. The Anchored Flexibility Model in LC8 Motif Recognition: Insights from the Chica Complex. Biochemistry. 55:199-209.

Geiger, B., and K.M. Yamada. 2011. Molecular architecture and function of matrix adhesions. Cold Spring Harb Perspect Biol. 3.

Gingras, A.R., N. Bate, B.T. Goult, L. Hazelwood, I. Canestrelli, J.G. Grossmann, H. Liu, N.S. Putz, G.C. Roberts, N. Volkmann, D. Hanein, I.L. Barsukov, and D.R. Critchley. 2008. The structure of the C-terminal actin-binding domain of talin. Embo j. 27:458-469.

Goult, B.T., T. Zacharchenko, N. Bate, R. Tsang, F. Hey, A.R. Gingras, P.R. Elliott, G.C. Roberts, C. Ballestrem, D.R. Critchley, and I.L. Barsukov. 2013. RIAM and vinculin binding to talin are mutually exclusive and regulate adhesion assembly and turnover. J Biol Chem. 288:8238-8249.

Hemmings, L., D.J. Rees, V. Ohanian, S.J. Bolton, A.P. Gilmore, B. Patel, H. Priddle, J.E. Trevithick, R.O. Hynes, and D.R. Critchley. 1996. Talin contains three actin-binding sites each of which is adjacent to a vinculin-binding site. J Cell Sci. 109 (Pt 11):2715-2726.

Itakura, A.K., R.A. Futia, and D.F. Jarosz. 2018. It Pays To Be in Phase. Biochemistry. 57:2520-2529.

Jespersen, N., A. Estelle, N. Waugh, N.E. Davey, C. Blikstad, Y.-C. Ammon, A. Akhmanova, Y. Ivarsson, D.A. Hendrix, and E. Barbar. 2019. Systematic identification of recognition motifs for the hub protein LC8. Life Science Alliance. 2:e201900366.

Kakinuma, N., Y. Zhu, Y. Wang, B.C. Roy, and R. Kiyama. 2009. Kank proteins: structure, functions and diseases. Cell Mol Life Sci. 66:2651-2659.

Kanchanawong, P., G. Shtengel, A.M. Pasapera, E.B. Ramko, M.W. Davidson, H.F. Hess, and C.M. Waterman. 2010. Nanoscale architecture of integrin-based cell adhesions. Nature. 468:580-584.

Klapholz, B., and N.H. Brown. 2017. Talin - the master of integrin adhesions. J Cell Sci. 130:2435-2446.

Kumar, A., K.L. Anderson, M.F. Swift, D. Hanein, N. Volkmann, and M.A. Schwartz. 2018. Local Tension on Talin in Focal Adhesions Correlates with F-Actin Alignment at the Nanometer Scale. Biophys J. 115:1569-1579.

Kumar, A., M. Ouyang, K. Van den Dries, E.J. McGhee, K. Tanaka, M.D. Anderson, A. Groisman, B.T. Goult, K.I. Anderson, and M.A. Schwartz. 2016. Talin tension sensor reveals novel features of focal adhesion force transmission and mechanosensitivity. J Cell Biol. 213:371-383.

Lansbergen, G., I. Grigoriev, Y. Mimori-Kiyosue, T. Ohtsuka, S. Higa, I. Kitajima, J. Demmers, N. Galjart, A.B. Houtsmuller, F.

4

Grosveld, and A. Akhmanova. 2006. CLASPs attach microtubule plus ends to the cell cortex through a complex with LL5beta. Dev Cell. 11:21-32.

Liang, J., S.R. Jaffrey, W. Guo, S.H. Snyder, and J. Clardy. 1999. Structure of the PIN/LC8 dimer with a bound peptide. Nat Struct Biol. 6:735-740.

Medves, S., L.A. Noel, C.P. Montano-Almendras, R.I. Albu, H. Schoemans, S.N. Constantinescu, and J.B. Demoulin. 2011. Multiple oligomerization domains of KANK1-PDGFRbeta are required for JAK2-independent hematopoietic cell proliferation and signaling via STAT5 and ERK. Haematologica. 96:1406-1414.

Mimori-Kiyosue, Y., I. Grigoriev, G. Lansbergen, H. Sasaki, C. Matsui, F. Severin, N. Galjart, F. Grosveld, I. Vorobjev, S. Tsukita, and A. Akhmanova. 2005. CLASP1 and CLASP2 bind to EB1 and regulate microtubule plus-end dynamics at the cell cortex. J Cell Biol. 168:141-153.

Parsons, J.T., A.R. Horwitz, and M.A. Schwartz. 2010. Cell adhesion: integrating cytoskeletal dynamics and cellular tension. Nat Rev Mol Cell Biol. 11:633-643.

Phair, R.D., P. Scaffidi, C. Elbi, J. Vecerova, A. Dey, K. Ozato, D.T. Brown, G. Hager, M. Bustin, and T. Misteli. 2004. Global nature of dynamic protein-chromatin interactions in vivo: three-dimensional genome scanning and dynamic interaction networks of chromatin proteins. Mol Cell Biol. 24:6393-6402.

Plotnikov, S.V., A.M. Pasapera, B. Sabass, and C.M. Waterman. 2012. Force fluctuations within focal adhesions mediate ECM-rigidity sensing to guide directed cell migration. Cell. 151:1513-1527.

Poser, I., M. Sarov, J.R. Hutchins, J.K. Hériché, Y. Toyoda, A. Pozniakovsky, D. Weigl, A. Nitzsche, B. Hegemann, A.W. Bird, L. Pelletier, R. Kittler, S. Hua, R. Naumann, M. Augsburg, M.M. Sykora, H. Hofemeister, Y. Zhang, K. Nasmyth, K.P. White, S. Dietzel, K. Mechtler, R. Durbin, A.F. Stewart, J.M. Peters, F. Buchholz, and A.A. Hyman. 2008. BAC TransgeneOmics: a high-throughput method for exploration of protein function in mammals. Nat Methods. 5:409-415.

Posey, A.E., A.S. Holehouse, and R.V. Pappu. 2018. Phase Separation of Intrinsically Disordered Proteins. Methods Enzymol. 611:1-30.

Qamar, S., G. Wang, S.J. Randle, F.S. Ruggeri, J.A. Varela, J.Q. Lin, E.C. Phillips, A. Miyashita, D. Williams, F. Ströhl, W. Meadows, R. Ferry, V.J. Dardov, G.G. Tartaglia, L.A. Farrer, G.S. Kaminski Schierle, C.F. Kaminski, C.E. Holt, P.E. Fraser, G. Schmitt-Ulms, D. Klenerman, T. Knowles, M. Vendruscolo, and P. St George-Hyslop. 2018. FUS Phase Separation Is Modulated by a Molecular Chaperone and Methylation of Arginine Cation-π Interactions. Cell. 173:720-734.e715.

Ran, F.A., P.D. Hsu, J. Wright, V. Agarwala, D.A. Scott, and F. Zhang. 2013. Genome engineering using the CRISPR-Cas9 system. Nat Protoc. 8:2281-2308.

Rapali, P., Á. Szenes, L. Radnai, A. Bakos, G. Pál, and L. Nyitray. 2011. DYNLL/LC8: a light chain subunit of the dynein motor complex and beyond. Febs j. 278:2980-2996.

Sear, R.P. 2007. Dishevelled: a protein that functions in living cells by phase separating. Soft Matter. 3:680-684.

Seetharaman, S., and S. Etienne-Manneville. 2019. Microtubules at focal adhesions - a double-edged sword. J Cell Sci. 132.

Shin, Y., and C.P. Brangwynne. 2017. Liquid phase condensation in cell physiology and disease. Science. 357.

Stehbens, S., and T. Wittmann. 2012. Targeting and transport: How microtubules control focal adhesion dynamics. Journal of Cell Biology. 198:481-489.

Stradner, A., H. Sedgwick, F. Cardinaux, W.C.K. Poon, S.U. Egelhaaf, and P. Schurtenberger. 2004. Equilibrium cluster formation in concentrated protein solutions and colloids. Nature. 432:492-495.

Sun, Z., H.Y. Tseng, S. Tan, F. Senger, L. Kurzawa, D. Dedden, N. Mizuno, A.A. Wasik, M. Thery, A.R. Dunn, and R. Fassler. 2016. Kank2 activates talin, reduces force transduction across integrins and induces central adhesion formation. Nat Cell Biol. 18:941-953.

van der Vaart, B., C. Manatschal, I. Grigoriev,

4

V. Olieric, S.M. Gouveia, S. Bjelic, J. Demmers, I. Vorobjev, C.C. Hoogenraad, M.O. Steinmetz, and A. Akhmanova. 2011. SLAIN2 links microtubule plus end-tracking proteins and controls microtubule growth in interphase. J Cell Biol. 193:1083-1099.

van der Vaart, B., W.E. van Riel, H. Doodhi, J.T. Kevenaar, E.A. Katrukha, L. Gumy, B.P. Bouchet, I. Grigoriev, S.A. Spangler, K.L. Yu, P.S. Wulf, J. Wu, G. Lansbergen, E.Y. van Battum, R.J. Pasterkamp, Y. Mimori-Kiyosue, J. Demmers, N. Olieric, I.V. Maly, C.C. Hoogenraad, and A. Akhmanova. 2013. CFEOM1-associated kinesin KIF21A is a cortical microtubule growth inhibitor. Dev Cell. 27:145-160.

Vicente-Manzanares, M., and A.R. Horwitz. 2011. Cell migration: an overview. Methods Mol Biol. 769:1-24.

Vicente-Manzanares, M., J. Zareno, L. Whitmore, C.K. Choi, and A.F. Horwitz. 2007. Regulation of protrusion, adhesion dynamics, and polarity by myosins IIA and IIB in migrating cells. J Cell Biol. 176:573-580.

Wang, J., J.M. Choi, A.S. Holehouse, H.O. Lee, X. Zhang, M. Jahnel, S. Maharana, R. Lemaitre, A. Pozniakovsky, D. Drechsel, I. Poser, R.V. Pappu, S. Alberti, and A.A. Hyman. 2018. A Molecular Grammar Governing the Driving Forces for Phase Separation of Prion-like RNA Binding Proteins. Cell. 174:688-699.e616.

Wheeler, R.J., and A.A. Hyman. 2018. Controlling compartmentalization by non-membrane-bound organelles. Philos Trans R Soc Lond B Biol Sci. 373.

Winograd-Katz, S.E., R. Fässler, B. Geiger, and K.R. Legate. 2014. The integrin adhesome: from genes and proteins to human disease. Nature Reviews Molecular Cell Biology. 15:273-288.

Wolfenson, H., Y.I. Henis, B. Geiger, and A.D. Bershadsky. 2009. The heel and toe of the cell's foot: a multifaceted approach for understanding the structure and dynamics of focal adhesions. Cell Motil Cytoskeleton. 66:1017-1029.

Yu, M., S. Le, Y.C. Ammon, B.T. Goult, A. Akhmanova, and J. Yan. 2019. Force-Dependent Regulation of Talin-KANK1 Complex at Focal Adhesions. Nano Lett. 19:5982-5990.

Zhu, Y., N. Kakinuma, Y. Wang, and R.

Kiyama. 2008. Kank proteins: a new family of ankyrin-repeat domain-containing proteins. Biochim Biophys Acta. 1780:128-133.

4

Supplementary Material
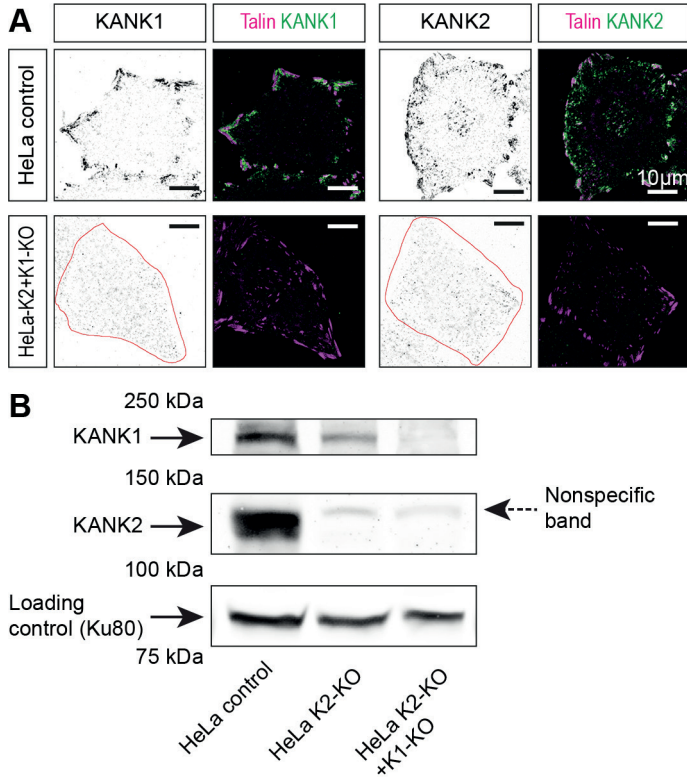
Supplementary Figure S1. Characterization of HeLa cells knockout for endogenous KANK1 and KANK2

(**A**) Control HeLa cells and HeLa cells knockout for KANK1 and KANK2 were stained for endogenous KANK1, KANK2 (green) together with talin (magenta). No KANK1 or KANK2 structures can be found in the HeLa K1+K2-KO cells. (**B**) Western blot analysis of HeLa K1+K2-KO cells. The nonspecific protein band running slightly above the band corresponding to endogenous KANK2 (~ 120 kDa) is indicated by a dashed arrow. The bands for KANK1 and KANK2 are indicated by arrows. Ku80 was used as a loading control.
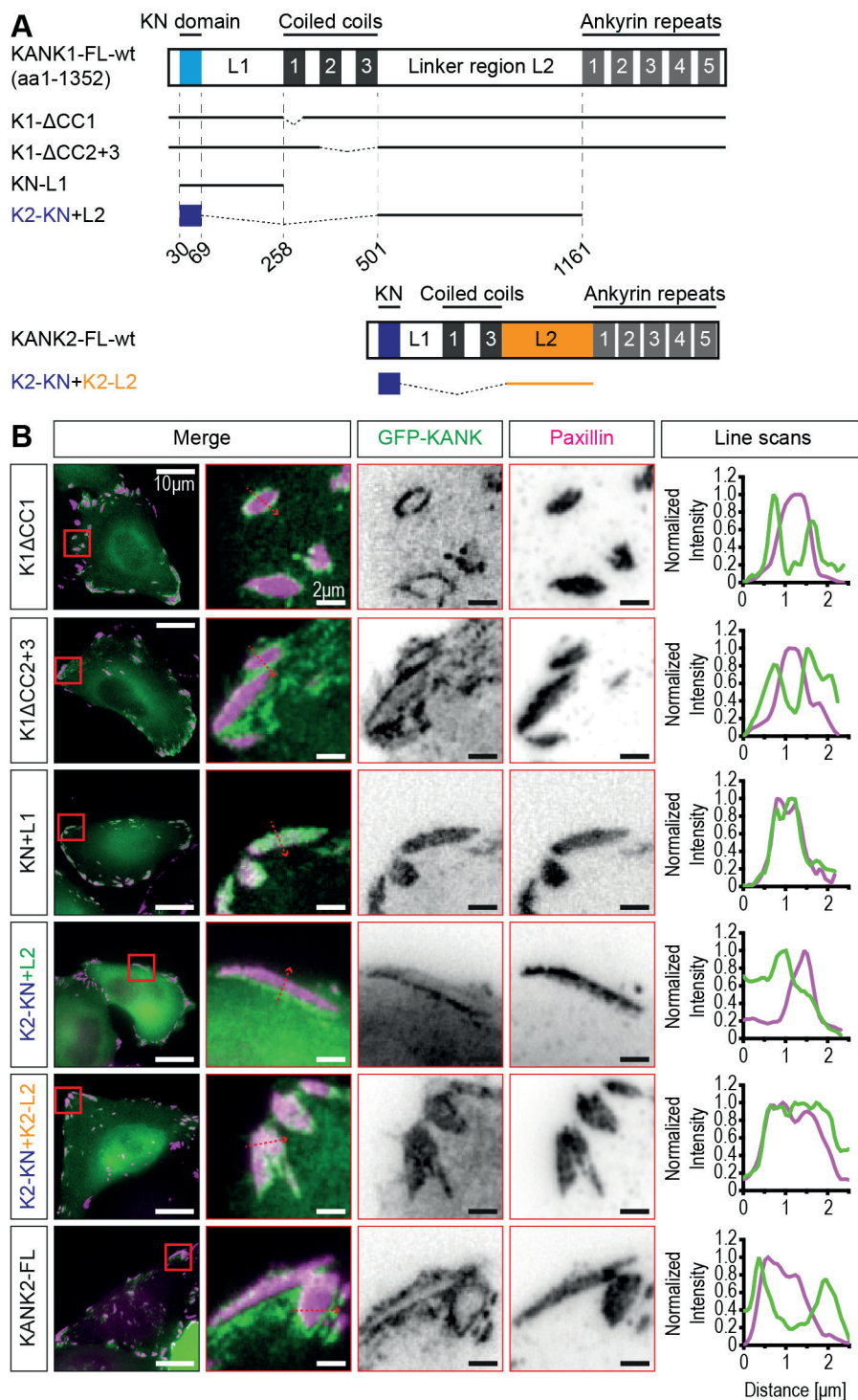
Supplementary Figure S2, related to Figure 1 and 2. Localization of different KANK constructs at FAs

(**A**) Schematic overview of different KANK1 and KANK2 constructs. (**B**) GFP-tagged KANK constructs (green) from (A) were overexpressed in HeLa K1+K2-KO cells. The cells were fixed and stained for endogenous paxillin (magenta). The KANK1-ΔCC1 is enriched at the FA rim whereas the KANK1-ΔCC2+3 localizes more broadly around FAs. The short linker region L1 cannot prevent the KN domain from accumulating in the central part of FAs. Full-length KANK2 localizes to the FA rim as well as to patches around FAs. The right panel shows the plotted fluorescence intensities of the GFP-KANK (green) and paxillin (magenta) along the line indicated by the dashed red arrow in the inset. The fluorescence intensities were normalized to the maximum intensity of the corresponding channel.
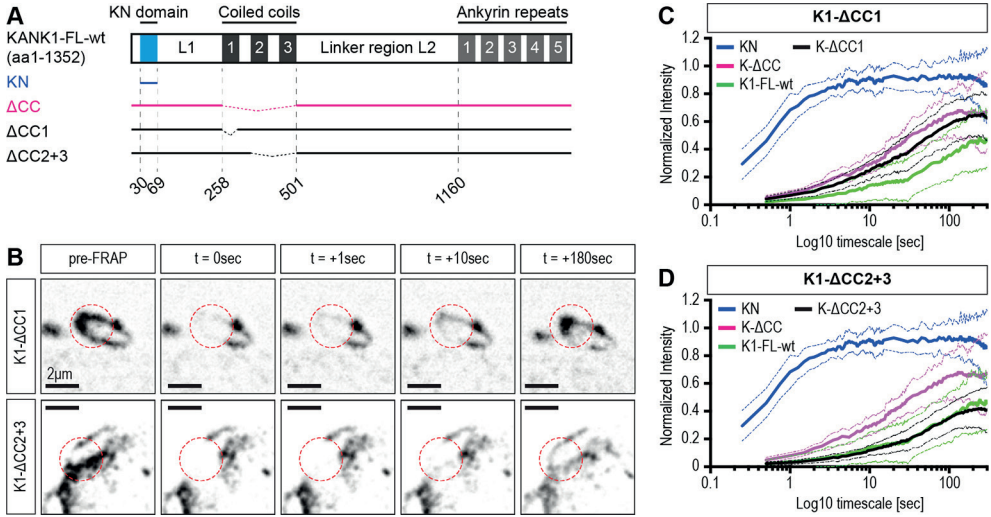
Supplementary Figure S3, related to Figure 3. Analysis of the dynamics of different KANK1 deletion mutants using FRAP

(**A**) Schematic overview of the different KANK1 constructs used in FRAP experiments. (**B**) Single frames of FRAP experiments with HeLa K1+K2-KO cells expressing the different GFP-labeled KANK1 constructs from (A). The stills show a baseline (pre-FRAP), the first frame after photobleaching (t = 0 sec) and the indicated time points after FRAP of a 2.5-μm-diameter circle region in the KANK1 patch. (**C-D**) Quantification of fluorescence recovery. The graph shows mean curves (bold lines) ± SD (light dotted lines) over time. For each condition, in total 24 – 28 KANK patches were analyzed in two independent experiments.
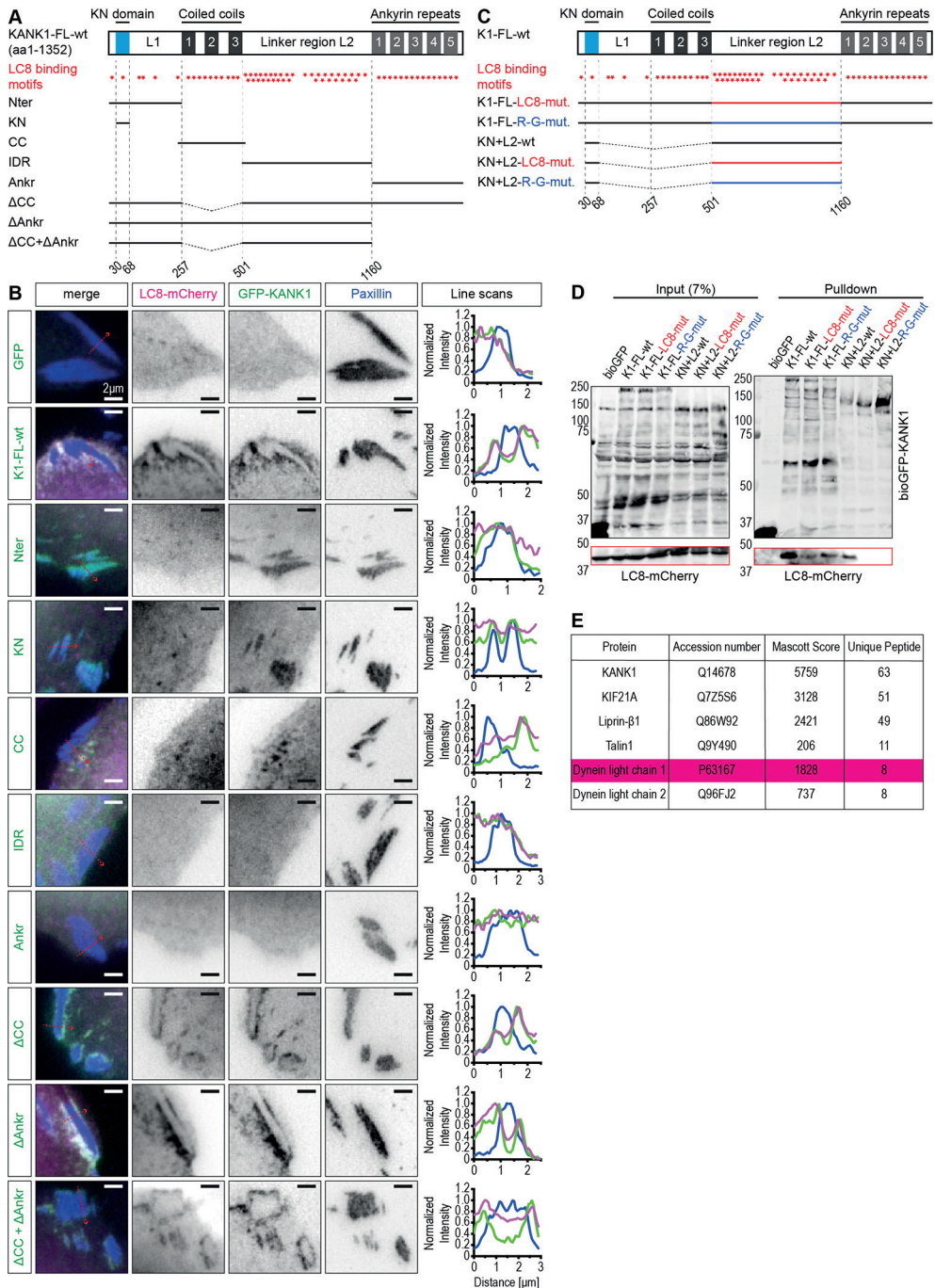
Supplementary Figure S4, related to Figure 4. Characterization of the interaction between KANK1 and LC8

(**A**) Schematic overview of the different KANK1 fragments used to identify the binding region of LC8. (**B**) The GFP-tagged KANK1 fragments (green) from (A) were co-expressed with LC8-mCherry (magenta) in HeLa K1+K2-KO cells. The cells were fixed and stained for the endogenous paxillin (blue). The right panel shows the plotted fluorescence intensities of the GFP-KANK (green), LC8-mCherry (magenta) and

133

paxillin (blue) along the line indicated by the dashed red arrow in the inset. The fluorescence intensities were normalized to the maximum intensity of the corresponding channel. (**C**) Schematic overview of the different KANK1 constructs carrying mutated linker region L2 used in the pulldown assay. (**D**) Pulldown using bioGFP-tagged constructs from (C) and using LC8-mCherry as prey protein (LC8 is shown in the red box below the bioGFP-KANK1 constructs). The full-length KANK1 constructs with the mutation in the L2 region can still bind to LC8 whereas the corresponding KN+L2 constructs cannot bind to LC8 anymore. (**E**) Identification of the binding partners of bioGFP-tagged full-length KANK1 by using streptavidin pull down assays from HEK293T cells combined with mass spectrometry. The dynamic hub protein dynein light chain LC8 is indicated in magenta.

4

Motif	Amino Acid Score	Volume and Polarity Score	Anchor position	Domain/Re
KQTSTQTV	4.40512020847	3.81781411385	710	L2
KDIAVLLY	-4.27251437923	2.99714089756	1319	Ankr
ASRGVNTE	14.1163162559	2.56244688388	651	L2
KCGGLQSG	-3.89925393974	1.89403932799	913	L2
VDKATMAQ	6.06371597875	1.2883301759	506	L2
AAVGTLVE	5.88192439883	1.09794067001	430	CC
NDPKALTS	-9.18768184629	0.757971709289	1106	L2
AMLGVMTE	4.37552830403	0.567299121236	448	CC
SPLSSQTS	1.89828504053	0.335619907221	921	L2
RIQKLLAE	-15.1516989697	0.319858683199	834	L2
LRYVINLA	-22.3071031163	-9.15023701789	1156	L2
LKTNLNLK	-26.2124514995	-8.49550109297	621	L2
MLSACNLL	-23.4704563211	-7.14247333534	1094	L2
TLSPVNLT	-23.3603010088	-7.11536882242	954	L2
GYTPIMLA	-21.7542493136	-6.93377108619	1201	Ankr
DGSTALSI	-25.9850082565	-6.55668856918	1305	Ankr
TLSSINSV	-17.4425035214	-6.02771766544	874	L2
NFAKAQSP	-8.49364355494	-5.87775902612	1330	Ankr
TIKRLNIQ	-15.5414075389	-5.68285442138	62	KN
DADVCNVD	-16.9285014605	-5.45752990196	1188	Ankr
EIVKLLLA	-25.3396190515	-5.41020434233	1286	Ankr
TIPVLQVK	-29.5695615082	-5.38052119239	288	CC
QMGSLNSQ	-13.0379953663	-5.13846522519	863	L2
SLSSSNSD	-8.93528990214	-4.6040682999	96	L1
GVGQININ	-14.5638336792	-4.51870112053	765	L2
QRAASQIN	-0.777013237736	-4.47245574952	313	CC
GVGTLLSG	-25.7743957962	-4.40482476106	742	L2
AASQINVC	1.46756240813	-4.15324186163	315	CC
CGADVNIQ	-4.73644669574	-4.02143801302	1261	Ankr
EIVKLLLD	-19.715548254	-4.0188659333	1181	Ankr
IMLAALAA	-18.8753271785	-3.99630449256	1205	Ankr
MRFCLNTL	-16.192411308	-3.96157841422	1116	L2
TLLKTNLN	-18.4125258311	-3.86984649027	619	L2
VEAVVQTR	0.391053420821	-3.86666488972	521	L2
YRLEVQLR	-8.80241566945	-3.75355981742	475	CC
LIARSQVT	-6.07138159546	-3.65102204893	112	L1
GCGDVNAK	-20.8378814042	-3.58321607772	1227	Ankr
EQQTLLAE	-20.2856561679	-3.54465160986	841	L2
GQTALMLA	-22.3225984213	-3.35226590794	1239	Ankr
AGNASQLE	-6.13002174328	-3.17544490575	331	CC
LKQELQAA	-13.058025824	-3.09142215207	493	CC
SVTEAMLG	-10.1877780757	-2.9771814272	444	CC
VNDLTLLK	-21.0034724027	-2.68326497939	615	L2
IGVGTLLS	-7.6974097162	-2.37644799928	741	L2
VHQFTNTE	5.80068039995	-2.3612700651	685	L2
CTNTCLST	-6.53240348527	-2.24475827679	700	L2
GSLNSQLI	-7.46999930589	-2.13748140489	865	L2
SAIPAMVG	-10.8789215629	-2.11793812752	1135	L2
IVKLLLAQ	-22.0559106941	-2.10198307554	1287	Ankr
GSTALMCA	-7.2304286617	-2.00998908067	1272	Ankr
NAKASQAG	1.48829833076	-1.91388217977	1232	Ankr
MVKGLLAC	-16.6710406321	-1.85101438484	1254	Ankr
IESCTNTC	5.44430698384	-1.78457802135	697	L2
QLISTLSS	-3.93459246236	-1.75775822277	870	L2
AEQQTLLA	-4.64752933972	-1.74526372771	840	L2
TSTESLSS	-2.33553518337	-1.59631154647	92	L1
CETGSNTE	9.79893977879	-1.32905590894	605	L2
VEAAVMAV	-6.76739853765	-1.30167083314	663	L2
TEAVSQVE	-0.889356841358	-1.27249797964	657	L2
KAGDILSG	-11.3841517174	-1.15908916465	19	
RQLVSQLK	-19.4581817129	-1.06816889539	304	CC
GHHAVNIE	-4.73977210317	-1.02697375132	1054	L2
TETATLIE	1.54697170598	-0.860920963179	691	L2
TQEGTLSP	-13.9599543325	-0.818970409638	950	L2
TSVETNSV	-1.05044857819	-0.438858110393	545	L2
STPVTNVS	-4.70577279974	-0.435791779311	254	L1
RVKDINSS	-2.08347749921	-0.327383726473	728	L2

>KANK1-210 peptide: E

Supplementary Table 1. LC8 binding motifs in KANK1 (on the right**)** Listed are 68 LC8 binding motifs withing full-length KANK1 predicted by the LC8Pred algorithm.

5

Differences between KANK1 and KANK2 and their role in cell migration

York-Christoph Ammon[1], Christie Wolzak[1], Anna Akhmanova[1]

unpublished data

1 Cell Biology, Neurobiology and Biophysics, Department of Biology, Faculty of Science, Utrecht University, Utrecht, The Netherlands

Abstract

The cortical microtubule stabilizing complex anchors and stabilizes microtubules in close proximity to integrin-mediated cell-matrix adhesions. Microtubules play an essential role in the regulation and especially in the turnover of cell-matrix adhesions, which in turn is crucial for proper cell migration. KANK family proteins 1 and 2 can both bind to the major adhesion adaptor protein talin and thereby directly connect the cortical microtubule stabilizing complex to cell-matrix adhesions. Despite their similar structure and domain composition, KANK1 and KANK2 show distinct subcellular localizations. However, the factors responsible for these different localizations are unknown. Here, we show that the localization of both KANKs is talin-dependent. Moreover, by using wound healing assays we examined the role of both KANK proteins in cell migration. We found that KANK2 depletion negatively affects migration speed in a cell-type-specific manner. Yet, the exact mechanism how cell motility is affected requires further investigation.

5

Introduction

Cell migration is one of the essential cell functions. In multicellular organisms, it is required for fundamental processes such as embryonic development, immune responses to infections, tissue repair and renewal (Ridley et al., 2003; Vicente-Manzanares and Horwitz, 2011). Yet, cell migration can also be involved in pathological processes like inflammatory diseases or cancer, in particular cancer metastasis which accounts for 90% of all cancer-related deaths (Bravo-Cordero et al., 2012). Most animal cells migrate in an integrin-dependent manner thereby the precise spatiotemporally regulated formation and disintegration of the integrin-mediated adhesions is crucial (Ladoux and Nicolas, 2012). Integrin-dependent cell migration process consists of four steps that are constantly repeated: i) Formation of cell protrusions at the leading edge of the cell. This process is mediated by actin filaments, which polymerize at the leading edge and thereby push the plasma membrane (PM) out (Pollard and Cooper, 2009). ii) The protruded PM adheres to the extracellular matrix (ECM) via integrin receptors spanning through the PM (Bachir et al., 2014; Barczyk et al., 2010). iii) After the cell-matrix adhesions have been stabilized the cell body is translocated in the direction of migration through actin-myosin II- (actomyosin-) dependent contraction (Vicente-Manzanares and Horwitz, 2011). iv) Finally, at the rear of the cell the old cell-matrix adhesions have to detach to allow the cell to move forward.

The life cycle of integrin-mediated cell-matrix adhesion complexes begins with the heterodimeric α/β-integrin receptors (integrins). These integrins cluster into small short-lived nascent adhesions (NAs) at the leading edge of the cell and bind to ECM components such as fibronectin (Bachir et al., 2014). In a force-dependent (actomyosin-dependent) manner a portion of these NAs evolves into mature integrin-mediated cell-matrix adhesion complexes, the so-called focal adhesions (FAs) (Vicente-Manzanares et al., 2007; Wolfenson et al., 2009). With their cytosolic tails, integrins bind to FA adaptor proteins such as talin (Geiger and Yamada, 2011; Parsons et al., 2010). Talin connects the integrins with the actin cytoskeleton thereby functioning as molecular clutch of the cell that transduces forces (Case and Waterman, 2015). Besides the mature FAs that can mostly be found at the cell periphery there exist another group of mature adhesion complexes, the so called fibrillar adhesions (FBs). These FBs are enriched in tensin, another adaptor protein, and α5/β1-integrins (Pankov et al., 2000). They usually appear as elongated stretches or arrays of dots in the central part of the cell (Geiger and Yamada, 2011; Zaidel-Bar et al., 2004). FBs derive from the distal end of FAs and translocate in an actomyosin-dependent manner towards the cell center (Zamir et al., 1999; Zamir et al., 2000).

The microtubule (MT) cytoskeleton plays an important role in regulating the dynamics of cell-matrix adhesion complexes (Etienne-Manneville, 2013). MTs can serve as molecular tracks for the intracellular transport of "building material" to and away from FAs (Stehbens and Wittmann, 2012). Besides, they can influence the actin-FA interplay by regulating Rho GTPase signaling (Seetharaman and Etienne-Manneville, 2019). MT plus ends are usually anchored and stabilized in close proximity to FAs by the CLASPs (CLASP1 and 2), ELKS, liprins and LL5β-containing cortical MT stabilizing complex (CMSC) (Lansbergen et al., 2006; Mimori-Kiyosue et al., 2005; van der Vaart et al.,

5

2013).

Recently, two members of the kidney ankyrin repeat domain-containing (KANK) protein family have been identified as novel binding partners of the FA adaptor protein talin that can connect FAs and the CMSC (Bouchet et al., 2016; Sun et al., 2016). The KANK protein family consists of four human homologs (KANK1 – 4) (Zhu et al., 2008). All four human KANK proteins share a specific structure with three distinct domains (Figure 1). At their N-terminus, all KANKs contain the so-called KANK N-terminal (KN) domain which mediates binding to talin (Bouchet et al., 2016; Sun et al., 2016). At their C-terminus, they possess the highly conserved ankyrin repeat domain which mediates binding to the kinesin-4 KIF21A (Guo et al., 2018; Pan et al., 2018; van der Vaart et al., 2013; Weng et al., 2018). Located in the central region of the KANK proteins, between the KN and the ankyrin repeat domain, are the coiled coil (CC) domains. There exist four conserved CC domains (CC1 – 4) among the KANK family, the composition and number of which vary among the family members (Zhu et al., 2008). Van der Vaart et al. have shown that the CC1 domain binds to liprins, mainly liprin-β1, thereby bringing KANKs to the cortex (van der Vaart et al., 2013). Besides their role as linker between FAs and the CMSC, KANKs have been described as potential tumor suppressors in various types of cancer (Fan et al., 2020; Gu and Zhang, 2018; Guo et al., 2014; Kim et al., 2018; Sarkar et al., 2002).

In the present study, we focus on the differences between (human) KANK1 and KANK2, their subcellular localization and their involvement in cell migration. We show that KANK2 is predominantly located at elongated central adhesions in a talin-dependent manner. When KANK2 binding to talin is perturbed, KANK2 is retained at the cell periphery. Furthermore, we observed that loss of KANK2 in the breast cancer cell line SUM159PT leads to reduced migration velocity and diminished wound closure whereas the depletion of both KANK1 and KANK2 in HeLa cells does not affect cell migration.

Results

KANK2 localizes to central (elongated) adhesions in a talin-dependent manner

Despite their similar domain organization, endogenous KANK1 and KANK2 are distinct in their subcellular localization in various cell lines such as HeLa cells (cervical adenocarcinoma) and SUM159PT cells (anaplastic breast carcinoma). KANK1 predominantly localizes to the cell periphery where it clusters around FAs. Nonetheless, to a small degree it can also be found at central adhesion structures (Figure 1B-C). On the other hand, KANK2 is predominantly located in the central area of the cell, where it forms elongated structures that colocalize with (elongated) talin-positive adhesions. This localization in elongated stretches is strongly pronounced in SUM159PT cells where KANK2 structures can extend to several micrometers in length (Figure 1C). Yet, KANK2 can also be found in the cell periphery where it clusters around FAs, like KANK1 (Figure 1C).

To better understand what determines the localization of KANK2 to central adhesion structures, several KANK2 mutants were generated that were lacking distinct domains such as the KN or the coiled coil domains. These N-terminally bioGFP-tagged KANK2
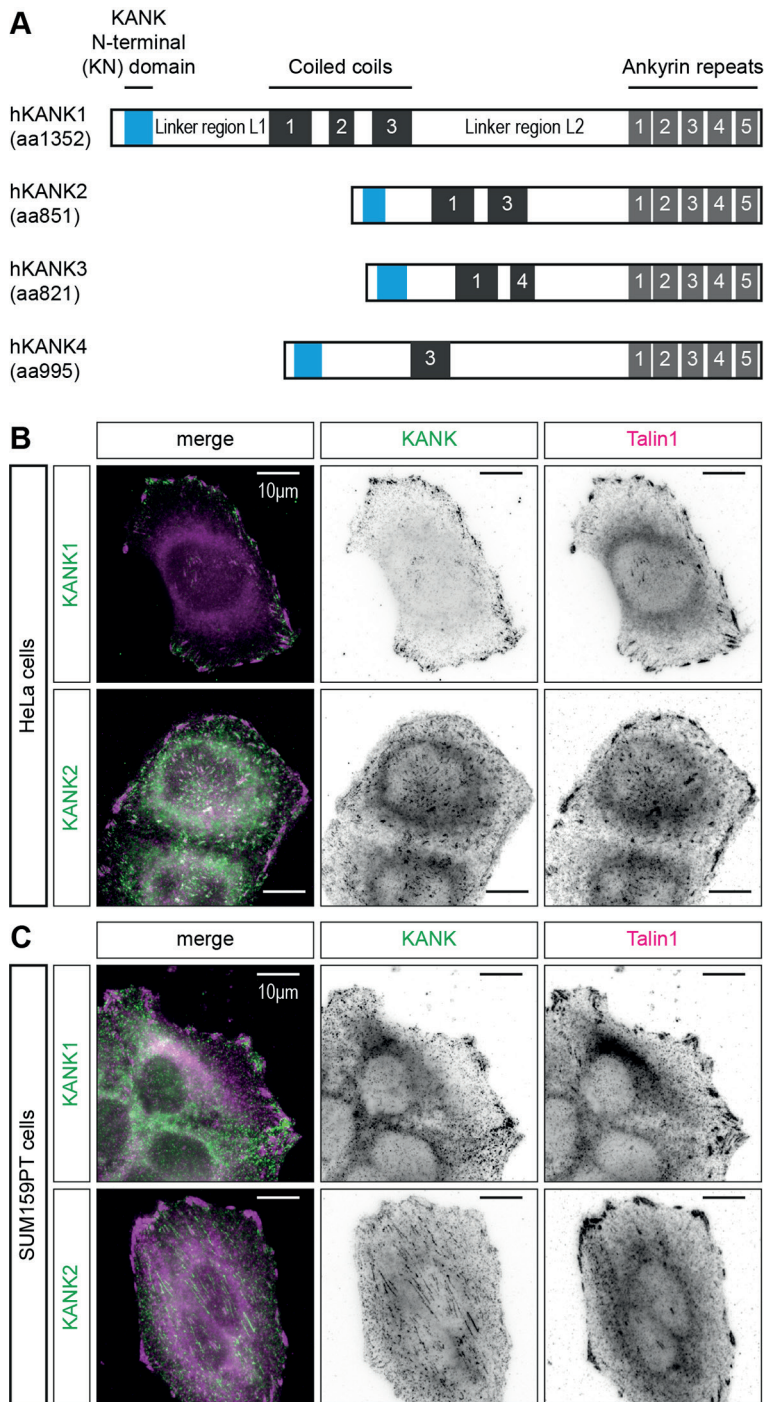
Figure 1. Human KANK family proteins an overview and the subcellular localization of KANK1 and KANK2 in human cellsnxzc

(**A**) Schematic overview of the four human KANK proteins. All four human KANK homologs possess at the N-terminus a highly conserved KANK N-terminal (KN) domain (blue). In the central region there are

the coiled coil domains (black). There are four conserved CC domains (CC1 – 4), the composition and number of which vary among the KANK family members. At the C-terminus, there is the highly conserved ankyrin repeat domain which consists of five ankyrin repeats (grey). (**B-C**) Subcellular localization of endogenous KANK1 and KANK2 (both green) together with endogenous talin1 (magenta) in HeLa (B) and SUM159PT (C) cells.

constructs were expressed in HeLa cells that were depleted of endogenous KANK2 by CRISPR/Cas9-mediated knockout (HeLa-K2-KO cells) as described previously (Yu et al., 2019). Like endogenous KANK2, overexpressed full-length KANK2 (K2-FL-wt) localized to talin-positive central adhesion structures and to the cell periphery (Figure 2B). Interestingly, it seemed that peripheral localization was more pronounced with overexpressed GFP-K2-FL-wt compared to endogenous KANK2. This might suggest that endogenous KANK1 and KANK2 compete for the peripheral binding sites around FAs.

The deletion of the KN domain from KANK2 (K2-ΔKN) led to more diffuse distribution of the construct throughout the cytoplasm. Moreover, the K2-ΔKN structures that could be found were exclusively located at the cell periphery (Figure 2D). In these patches K2-ΔKN strongly colocalized with liprin-β1, to which KANK family proteins can bind via the KANK CC1 domain (Supplementary Figure S1). On the other hand, the removal of the two coiled coil domains of KANK2, either separately or simultaneously, did not affect the localization of KANK2 to central adhesions (Figure 2E-G). Yet, it seemed that the removal of the CC domains affected the clustering of KANK2 around the peripheral FAs (Figure 2E-G; see also Chapter 4). Loss of the CC1 domain or both CC1 and CC3 resulted in tight clustering around the FA rim and these constructs did not colocalize with liprin-β1 anymore (Supplementary Figure S1). Yet, the deletion of the CC3 domain alone (K2-ΔCC3) also led to more tight clustering around peripheral FAs, and even partial overlap with the FAs (Figure 2F). Nonetheless, the K2-ΔCC3 construct could still colocalize with liprin-β1 as it still possessed the CC1 domain (Supplementary Figure S1).

These results suggested that the localization of KANK2 to central adhesion structures depends on the KN domain and thus likely on binding to talin. Therefore, another KANK2 construct was generated carrying a mutation in the KN domain (K2-FL-4A: 42-LDLD-45 = 42-AAAA-45). It was shown previously that mutation of the LDLD motif of the KN domain perturbs the talin-KANK interaction (Bouchet et al., 2016). Like the K2-ΔKN construct, the K2-FL-4A construct localized exclusively to the cell periphery but was more dispersed than KANK2 constructs with an unimpaired KN domain (Figure 2H). At the periphery, K2-FL-4A strongly colocalized with liprin-β1-containing patches (Supplementary Figure S1). Interestingly, in contrast to the KANK2 construct lacking the KN domain, K2-FL-4A showed less diffuse distribution throughout the cytoplasm. Using pulldown assays with the bioGFP-tagged KANK2 constructs as bait we tested whether they could bind to talin and found that this was the case for all KANK2 constructs, except for the K2-ΔKN (Figure 2I). The K2-FL-4A construct was not included in this pulldown (Supplementary Figure S5), yet since its subcellular distribution mimics that of K2-ΔKN it is likely that the mutation of the LDLD motif abolished binding to talin.

Concluding from these data, it appears that the localization of KANK2 to talin-positive central adhesion complexes is mediated by its interaction with talin. Furthermore, it seems likely that KANK2 is not required for the formation of these central adhesions
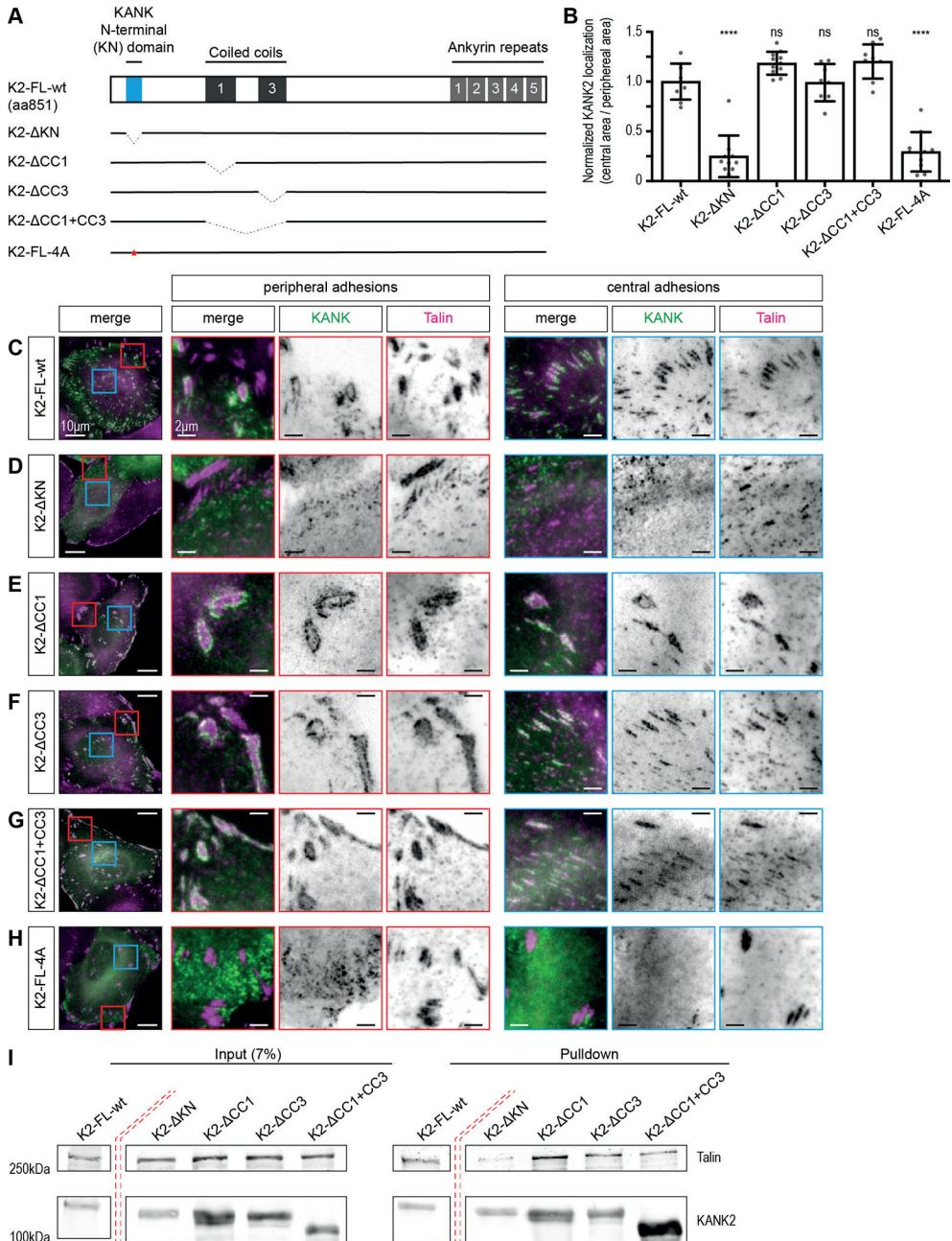
Figure 2. Subcellular localization of KANK2 and different KANK2 mutants in HeLa KANK2-KO cells
(**A**) Schematic overview of full-length KANK2 and the different KANK2 mutants. (**B**) Quantification of the KANK2 localization in HeLa-KANK2-KO cells. The KANK2 localization is represented as a ratio of the GFP-KANK2 signal in the central part of the cell divided by the KANK2 signal at the cell periphery (first 5 μm). The results were plotted as fraction of the control condition (K2-FL-wt) average value The results are represented as mean ± SD; ns, not significant; **** $p < 0.0001$ (Ordinary One-Way-ANOVA (Dunnett's Multiple Comparison Test) (8 – 11 cells were analyzed per condition). (**C-H**) Localization of the indicated KANK2 constructs in HeLa KANK2-KO cells. Cells were transiently transfected with GFP-

tagged KANK2 constructs (green). Subsequently, cells were fixed and stained for the endogenous FA protein talin (magenta). The red insets represent peripheral adhesion complexes whereas the blue insets represent central areas of the cell. (**I**) Pulldown assay using bioGFP-tagged KANK2 constructs as bait to pull down talin from HEK293 cells. The red dashed double line indicates where a lane was cut out (for the original membranes/gels see Supplementary Figure S5).

since they can still be found in cells knockout for KANK2 that are expressing KANK2 constructs that cannot bind to talin (Figure 2D and 2H).

Disruption of the MT cytoskeleton causes re-localization of KANK2 at the cell periphery

For a long time, it has been known that MTs play an essential role in the regulation of FA dynamics and especially in the disassembly of FAs (Stehbens and Wittmann, 2012). Further, it has been described that MT plus-ends are anchored and stabilized in the vicinity of FAs (Lansbergen et al., 2006; Mimori-Kiyosue et al., 2005; van der Vaart et al., 2013). Moreover, it has been shown that nocodazole-induced depolymerization of MTs leads to increased FA assembly (Ren et al., 1999) whereas the re-growth of MTs after depolymerization results in accelerated FA disassembly (Ezratty et al., 2005).

Since MTs are so important to FAs and as KANKs link FAs to the CMSC, we were interested in how the MT cytoskeleton affects the localization of KANK2 to central adhesion structures. To address this question, nocodazole washout experiments were performed. HeLa cells were first incubated with nocodazole for 3 hours and afterwards the cells were either directly fixed (no washout) or the nocodazole-containing medium was removed and the cells were incubated in normal medium for 5, 15 or 45 minutes and then fixed. Subsequently, fixed cells were stained for endogenous KANK2 and talin (Figure 3). A control staining for α-tubulin to verify the effect to the nocodazole treatment was also performed. The non-treated control HeLa cells showed a normal radial MT network (Figure 3). KANK2 localized predominantly to talin-positive central adhesions and also clustered around peripheral FAs (Figure 3B), as described above. On the other hand, nocodazole treatment caused a complete loss of the MT network, and this led to an increase in FA size in these cells (Figure 3C). Interestingly, these cells possessed hardly any talin-positive central adhesions. In line with this observation, KANK2 could only be found clustered around the peripheral FAs and was almost completely absent from the central region of the cell (Figure 3). Removal of the nocodazole resulted in MT (re-) polymerization. Already 5 minutes after the washout, the first MTs could already be seen. At 15 minutes after washout the MT network was almost comparable to that in the non-treated control situation and 45 minutes after washout the MT network was completely restored. Corresponding to the recovery of the MT cytoskeleton, KANK2 and talin-positive adhesions re-appeared in the central region of the cell (Figure 3). In contrast to KANK2, the subcellular localization of KANK1 was not affected by the nocodazole-induced depolymerization of MTs (Supplementary Figure S2).

Concluding from these data, it appears that the localization of KANK2 at central adhesions is MT-dependent. Yet, it has been shown that the disruption of the MT cytoskeleton leads to dramatic changes in the composition and maturation of FAs. Depolymerization of MTs leads to the release of the Guanine Nucleotide Exchange Factor H1 (GEF-H1) which is usually bound to the MT lattice and inactive (Krendel et al., 2002; Ren et al., 1998). Free
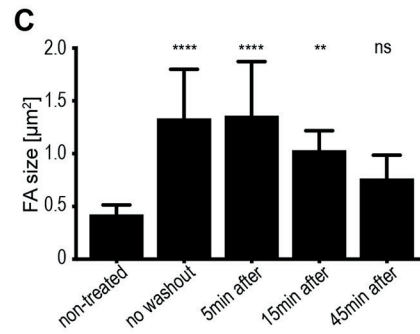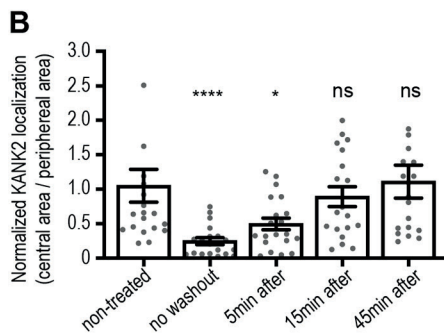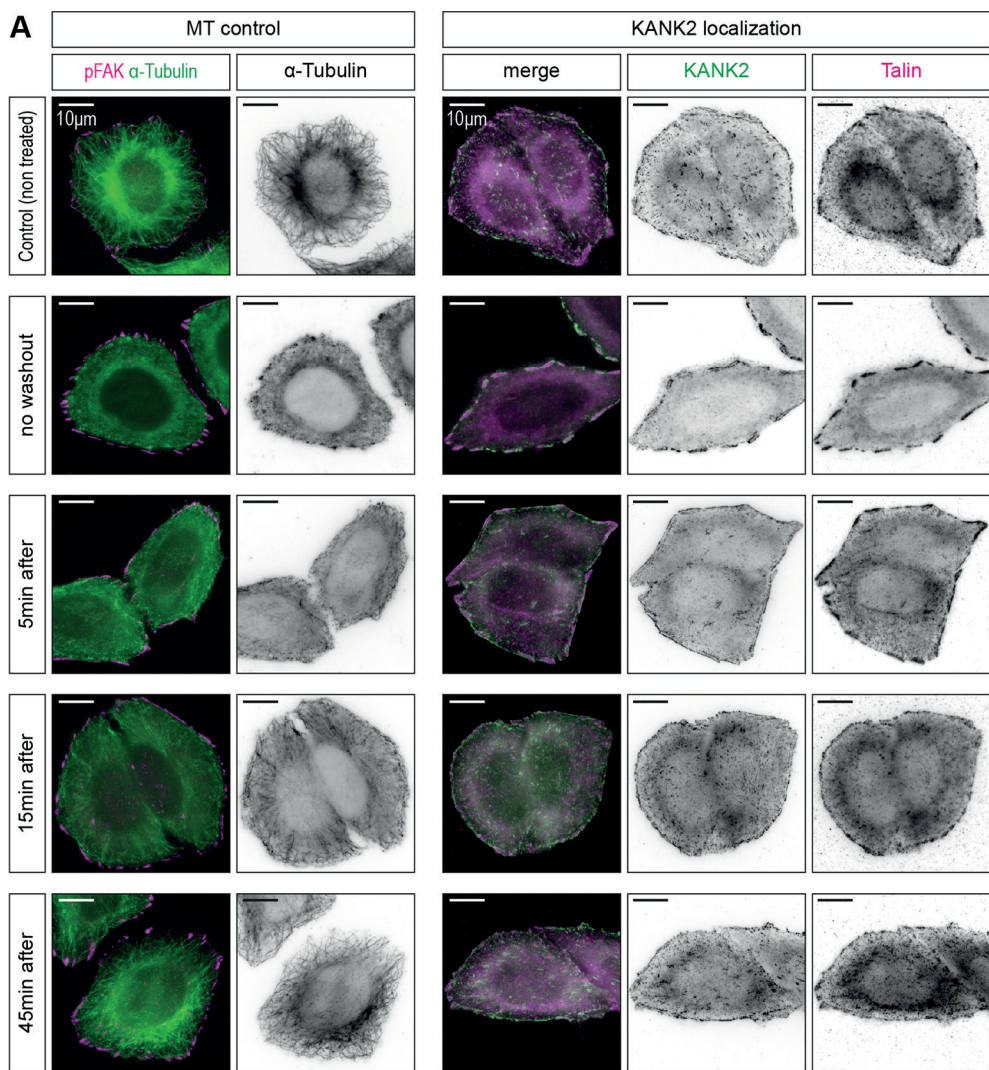
Figure 3. Nocodazole washout experiments in HeLa cells.
(**A**) Localization of endogenous KANK2 in HeLa cells treated with nocodazole (10 µM for 3 hours). After the incubation with nocodazole, the cells were either directly fixed (no washout) or the nocodazole-

containing medium was removed and the cells were incubated in normal medium and subsequently fixed at the indicated timepoints (5, 15, or 45 minutes) after nocodazole removal. The left panel shows cells stained for the FA marker phospho-FAK (magenta) and alpha-tubulin (green) to verify the effect of the nocodazole treatment on the MT network. The right panel shows cells stained for endogenous KANK2 (green) and talin (magenta). (**B**) Quantification of the KANK2 localization in HeLa cells. The KANK2 localization is represented as a ratio of the KANK2 signal in the central part of the cell divided by the KANK2 signal at the cell periphery (first 5 μm). The results were plotted as fraction of the control condition (non-treated) average value. The results are represented as mean ± SEM; ns, not significant; **** $p < 0.0001$; * $p < 0.05$ (Ordinary One-Way-ANOVA (Dunnett's Multiple Comparison Test)) (19 – 20 cells were analyzed per condition). (**C**) FA size represented as mean ± SD; ns not significant; **** $p < 0.0001$; ** $p < 0.01$ (Ordinary One-Way-ANOVA (Dunnett's Multiple Comparison Test)) (108 - 444 FAs in 6 - 11 cells were analyzed per condition).

GEF-H1 can locally activate the Rho GTPase RhoA, which in turn results in strongly increased actomyosin contractility and thereby causes a change of the intracellular forces (Chang et al., 2008). Ng et al. have shown that these intracellular force changes lead to a switch in the maturation state of adhesion complexes thereby favoring FAs over FBs (Ng et al., 2014). They could demonstrate that nocodazole treatment caused α5/β1 integrins, integrins that are usually enriched at the centrally located FBs, to redistribute to peripheral FAs (Ng et al., 2014). This change in the composition and distribution of adhesion complexes might explain the low abundance of talin-positive adhesions in the cell center of our HeLa cells, especially as the central adhesions in HeLa cells were always small puncta instead of pronounced elongated FBs that can be found in fibroblast-like cells such as SUM159PT. Thus, it is possible that the redistribution effect is so strong in HeLa cells that there are hardly any talin-positive central adhesions left in nocodazole-treated cells. Yet, further research needs to be done to fully understand the role of the MT cytoskeleton on the localization of KANK2 and the appearance of talin-positive central adhesions.

Knockdown of KANK2 but not KANK1 leads to reduced wound healing and migration speed in SUM15PT cells

Recently, it has been shown that KANK1 plays an important role as linker between FAs and the CMSC and that removal of KANKs or the perturbation of the talin-KANK interaction leads to dispersion of the CMSC at the cortex as well as MT overgrowth. Yet, despite these effects on MTs and the CMSC a direct effect of KANK depletion on FAs in HeLa cells, such as changes in their size or number, has not been overserved by us (Bouchet et al., 2016). Nonetheless, Sun et al. have described that depletion of KANK2 led to increased migration velocity in mouse fibroblasts (Sun et al., 2016) whereas Gee et al. have reported that depletion of KANK2 in cultured mouse podocytes resulted in reduced migration velocity (Gee et al., 2015). Therefore, we wanted to examine how the depletion of KANK1 and 2 affects cell migration in the human cell lines we study. To analyze this, we performed wound healing assays using HeLa cells that were depleted of KANK1 or KANK2 or both via siRNA-mediated knockdown. After applying the wound, the HeLa cells were allowed to migrate for 24 hours and afterwards they were fixed and stained with phalloidin and DAPI to delineate the cell outlines and nuclei and to measure which part of the wound area was covered by cells. After the initial experiment, it seemed that single depletions of either KANK1 or KANK2 in HeLa cells did not affect wound healing. On the other hand, it seemed that the simultaneous double knockdown of both
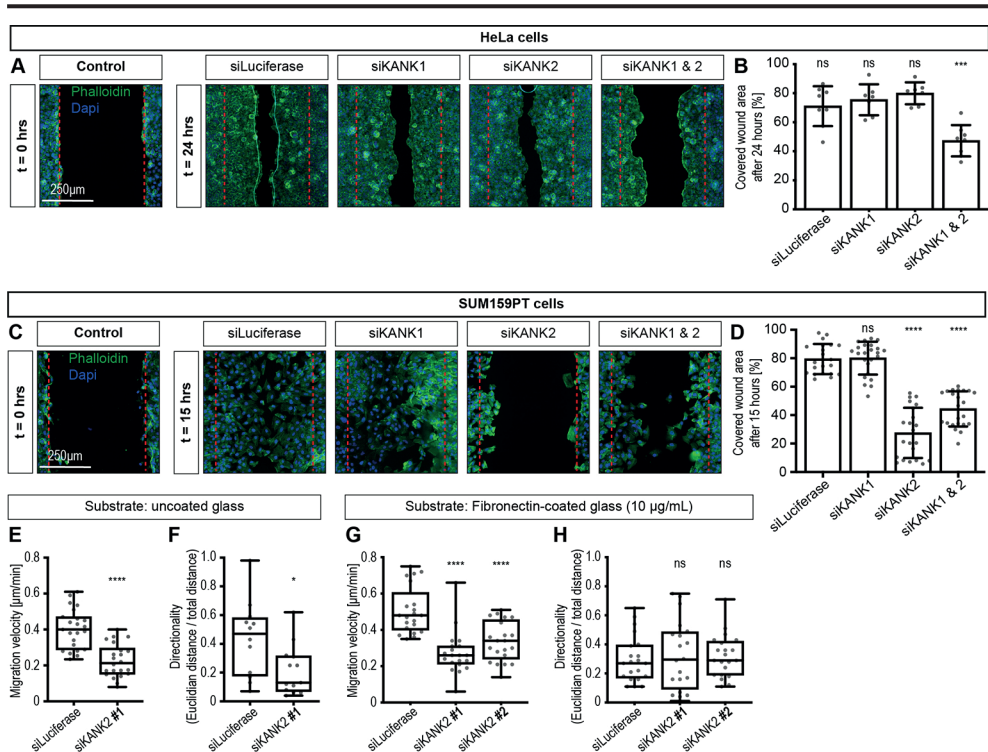
Figure 4. Effects of KANK1 and 2 depletion on cell migration in HeLa and SUM159PT cells
(**A**) Wound healing assay using HeLa cells. HeLa cells were either transfected with control siRNA (siLuciferase) or with siRNAs against KANK1 (siKANK1) or KANK2 (siKANK2) or both (siKANK1 & 2). The application of the wound was timed so that cell migration occurred 48 - 72 hours after siRNA transfection. The cells were allowed to migrate for 24 hours. Subsequently, the cells were fixed and stained with phalloidin (green) and DAPI (blue) to delineate the cell outlines and nuclei. The control panel on the left shows the wound area directly after applying the wound (t = 0 hours). The panels on the right show representative wound areas 24 hours after monolayer wounding (t = 24 hours). Dotted red lines represent the boarders of the wound area. (**B**) Quantification of the covered wound area after 24 hours. Covered wound area is represented as mean ± SD; ns, not significant; *** $p < 0.001$ (Ordinary One-Way ANOVA (Dunnett's Multiple Comparison Test)) (7 – 8 wound areas were analyzed per condition). (**C**) Wound healing assay using SUM159PT cells. The SUM159PT cells were treated as HeLa cells in (A); yet, SUM159PT cells were already fixed 15 hours after applying the wound. The control panel shows control cells that were directly fixed after applying the wound (t = 0 hours). The panels on the right show representative wound areas 15 hours after applying the wound. Dotted red lines represent the boarders of the wound area. (**D**) Quantification of the covered wound area after 24 hours. Covered wound area is represented as mean ± SD; ns, not significant; **** $p < 0.0001$ (Ordinary One-Way ANOVA (Dunnett's Multiple Comparison Test)) (21 – 24 wound areas were analyzed per condition). (**E**) Migration velocity of SUM159PT cells that were either transfected with control siRNA (siLuciferase) or with siRNA against KANK2 (siKANK2). Cells were sparsely seeded on uncoated glass coverslips and allowed to migrate freely; **** $p < 0.0001$ (unpaired t-test) (22 – 23 cells were analyzed per condition). (**F**) Quantification of the directionality of migration of SUM159PT cells migrating on uncoated glass and treated as in (E). The directionality is the ratio of the Euclidian distance between the start and end point of the migration track divided by the total length of the migration track; * $p < 0.05$ (unpaired t-test) (12 - 13 cells were analyzed per condition). (**G**) Migration velocity of SUM159PT cells treated as in (E) and migrating on Fibronectin- (FN-) coated glass coverslips; **** $p < 0.0001$ (Ordinary One-Way ANOVA (Dunnett's Multiple Comparison Test)) (20 – 21 cells were analyzed per condition). (**H**) Quantification of the directionality of the migration of SUM159PT cells migrating on FN-coated glass and treated as in (E); ns, not significant (Ordinary One-Way ANOVA (Dunnett's Multiple Comparison Test)) (20 - 21 cells were analyzed per condition). The migration velocity and directionality are shown as box and whiskers plots (box represents 25th – 75th percentiles; whiskers represent Min and Max; the line represents the median).

KANKs significantly reduced wound closure (Figure 4A-B). However, in a follow-up experiment there was no difference in wound closure between control cells and double knockdown cells (Supplementary Figure S3). Since HeLa cells are not an optimal model system for studying cell migration, we decided to switch to the more motile SUM159PT breast cancer cell line.

Monolayer wound healing experiments were repeated with the SUM159PT cells. Knockdown of only KANK1 in SUM159PT cells did not affect wound healing. Yet, depletion of KANK2, either alone or in combination with KANK1, caused a significant decrease in wound closure (Figure 4C-D). This effect could be reproduced in several follow-up experiments as well as when using two different siRNAs against KANK2 (Supplementary Figure S3). Thus, it seemed that knockdown of KANK2 negatively affected cell migration. Next, SUM159PT cells were seeded sparsely on uncoated glass coverslips to freely migrate overnight, and every 5 minutes an image was taken; afterwards, the tracks of single migrating cells were analyzed. Depletion of KANK2 indeed reduced the migration velocity of single cells compared to the control cells (Figure 4E). Moreover, when looking at the directionality of the cell migration by comparing the total length of the migration track to the Euclidean distance between the starting and end point of the migration track, cells depleted of KANK2 migrated along a less straight path compared to control cells (Figure 4F). However, it is known that the substrate can have a strong impact on cell-matrix adhesions and the cellular behavior (Fusco et al., 2015). Therefore, the glass coverslips were coated with fibronectin (FN) to study the influence of the substrate on cell migration in KANK2-depleted cells. The overall migration velocity was increased for SUM159PT cells migrating on FN-coated glass. Yet, the loss of KANK2 still led to a significant reduction of the migration speed compared to control cells (Figure 4G). Interestingly, there was no difference in the directionality of migration on FN-coated glass (Figure 4H).

Taken together, these results indicate that removal of KANK2 negatively affects cell migration in SUM159PT cells whereas removal of KANKs does not seem to affect cell motility in HeLa cells. Further, single cell migration experiments showed that the loss of KANK2 in SUM159PT cells leads to reduced migration velocity. The effect of KANK2 depletion on directionality was less clear, as it appeared substrate-dependent.

Depletion of KANK2 does not affect FAs nor the formation of the CMSC in SUM159PT cells

Next, we wanted to understand how the depletion of KANK2 causes reduced migration speed in SUM15PT cells. Since the migration speed was reduced upon removal of KANK2 it seemed possible that the disassembly of FAs might be negatively affected by knockdown of KANK2. Therefore, we analyzed the size and number of FAs in KANK2-depleted SUM159PT cells, but observed no significant changes (Figure 5E-F). This is in line with our previous findings on the removal of both KANK1 and 2 in HeLa cells (Bouchet et al., 2016). The interaction between KANK1 and talin is required for proper formation of the CMSC around FAs (Bouchet et al., 2016). To test whether the formation of the CMSC was affected by removal of KANK2 in SUM159PT cells, we analyzed the clustering of the CMSC proteins CLASP2 and liprin-β1 at the cell periphery (cell edge) and found no differences between KANK2-depleted and control cells (Figure 5A-D).
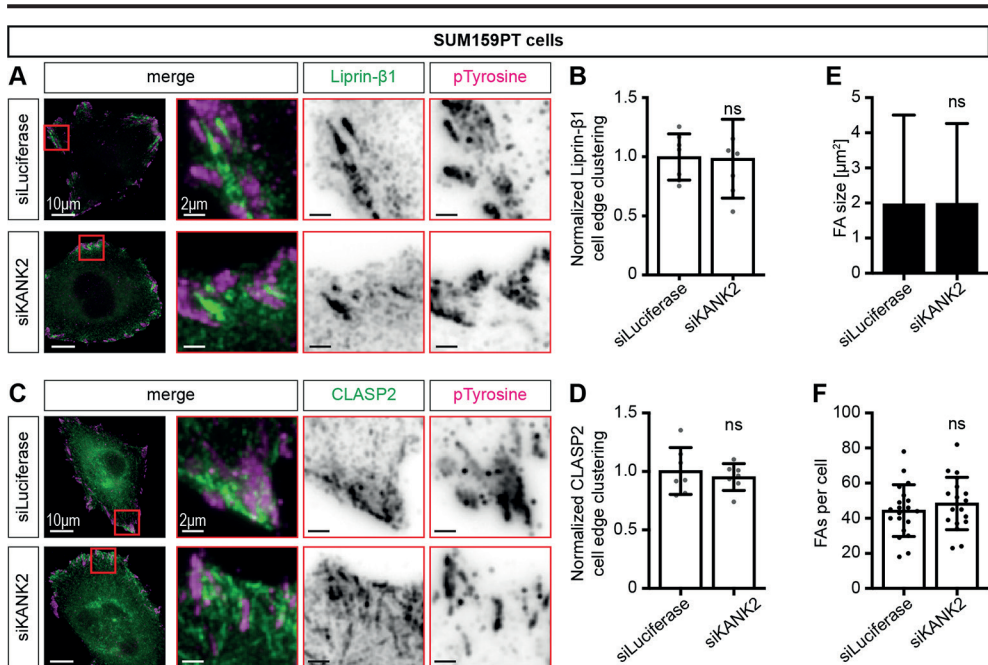
Figure 5. Loss of KANK2 does not affect FAs nor the CMSC in SUM159PT cells
SUM159PT cells were either transfected with control siRNA (siLuciferase) or with siRNA against KANK2 (siKANK2). The cells were fixed 48 – 72 hours after siRNA transfection and stained for endogenous liprin-β1 (**A**) or CLASP2 (**C**) (both green) and the FA marker phospho-tyrosine (magenta). (**B**) Quantification of peripheral clustering of liprin-β1 in cells treated as in (A). The peripheral clustering is the ratio of the liprin-β1 signal at the cell periphery (first 5 µm) divided by the liprin-β1 signal in the adjacent cell area (second 5 µm). The results were plotted as fraction of the control condition (siLuciferase) average value (7 cells were analyzed per condition). (**D**) Quantification of peripheral clustering of CLASP2 in SUM159PT cells treated as in (C). The peripheral clustering of CLASP2 has been quantified as in (B) (7 cells were analyzed per condition). (**E**) Size of FAs in SUM159PT cells either transfected with control siRNA (siLuciferase) or with siRNA against KANK2 (siKANK2) (886 – 992 FAs in 19 – 20 cells were analyzed per condition). (**F**) Number of FAs per cell in SUM159PT cells treated as in (E) (19 – 20 cells were analyzed per condition). All values are presented as mean ± SD; ns, not significant (unpaired t-test).

Concluding from these data, it seems that the removal of KANK2 from SUM159PT cells does not affect FAs nor the formation of the CMSC. Thus, it is likely that the reduction of migration speed upon KANK2 depletion does not result from a direct effect on FAs and their disassembly.

Discussion

In this study, we have looked at the differences between KANK1 and KANK2 with a particular interest in KANK2 and its predominant localization to (talin-positive) central adhesion structures. We found that this localization is mediated by binding to talin and that disruption of this interaction leads to re-localization of KANK2 to the CMSC at the cell periphery. Interestingly, we saw that when overexpressing full-length KANK2 in HeLa K2-KO cells the localization of full-length KANK2 around peripheral FAs was more pronounced compared to endogenous KANK2 (Figure 2B). Usually, KANK1 is the predominant KANK family member located at the cell periphery around FAs whereas

KANK2 is more concentrated at central adhesions. Previously, it has been shown by us that clustering of KANK1 around peripheral FAs is also mediated by binding to talin. Furthermore, by using fluorescence polarization assays we could demonstrate that the highly homologous KN domains of both KANK1 and 2 bind equally well to talin rod domain R7 (Bouchet et al., 2016). Thus, it is likely that the different subcellular localizations of KANK1 and 2 are caused by hitherto unknown interaction partners or other factors. It is known that the composition of FAs and central FBs differs, for example FBs are supposed to be enriched in tensin and α5/β1-integrins and poor in tyrosine-phosphorylated proteins whereas peripheral FAs are rich in αV/β3 integrins and tyrosine-phosphorylated proteins (Geiger and Yamada, 2011; Ng et al., 2014; Pankov et al., 2000). Therefore, it could be that KANK2 interacts with FB proteins, such as tensin, that are less abundant at peripheral FAs (Supplementary Figure S4). Another possibility might be that the two distinct talin isoforms (talin1 and 2) are responsible for the segregation of KANK1 and 2, as it appears that talin2 is slightly more concentrated in the cell center in HeLa cells compared to talin1 (Supplementary Figure S4). Nonetheless, this seems less plausible since endothelial cells, such as HUVECs, only express talin1 and KANK2 is strongly accumulated at the thin elongated central adhesions in HUVEC cells (see Chapter 6 General Discussion). Another factor that might contribute to distant subcellular localizations of KANK1 and 2 are differences in intracellular forces at the distinct cell-matrix adhesions. It has been shown that talin(1) is under less tension in central adhesions compared to peripheral adhesions (Kumar et al., 2016). More recently, it has been shown that the interaction between talin's rod domain R7 and the KN domain of KANK1 is force-regulated. Yu et al. have demonstrated that the R7/KN interaction can withstand forces in the pN range and that under shear-force geometry the interaction becomes more stable with increasing force until a maximum is reached (catch-bond behavior) (Yu et al., 2019). Thus, it is possible that intracellular forces might play a role in the subcellular distribution of KANK1 and KANK2.

Further, we saw that the removal of the coiled coil domains from KANK2 did not affect its localization to central adhesions but caused more tight clustering around peripheral FAs, and even partial overlap with them, as we have seen with KANK1 (see Chapter 4). Morea over, we still found talin-positive central adhesions in HeLa K2-KO cells that were expressing KANK2 constructs that could not bind to talin anymore. Consequently, we assume that KANK2 is not essential for the formation of these central adhesions.

The MT network is a crucial element for regulating the dynamics of FAs (Stehbens and Wittmann, 2012); especially for their disassembly as studies have demonstrated that the nocodazole-induced depolymerization of the MT cytoskeleton perturbs FA disassembly and usually leads to an increase in FA size (Ezratty et al., 2005). Our nocodazole washout experiments with HeLa cells have demonstrated that upon disruption of the MT network KANK2 could almost exclusively be found at the cell periphery around FAs. Interestingly, also the appearance of the talin-positive central adhesions seemed to be affected by the nocodazole treatment as we could only find few of them in nocodazole-treated HeLa cells. Yet, as we mentioned above, this reduction of central talin-positive adhesions is probably due to the RhoA-mediated hyperactivation of myosin II which leads to massive changes in the intracellular forces at adhesions (Chang et al., 2008). The nocodazole-induced disruption of the MT cytoskeleton leads to the release of the

MT-associated GEF-H1, which activates RhoA (Chang et al., 2008; Krendel et al., 2002; Ren et al., 1998). Furthermore, it has been demonstrated by Ng et al. that the changes in intracellular forces result in a switch in the maturation state of adhesion complexes favoring FAs and subsequently to redistribution of adhesion components (Ng et al., 2014), thereby likely causing the re-location of talin to the cell periphery.

Cell migration is a fundamental cellular process that is required for various aspects of animal life such as embryonic development, immune responses, tissue renewal and repair. Yet, perturbed cell migration is often associated with pathological processes such as inflammatory diseases or cancer, especially metastasis of cancer (Ridley et al., 2003; Vicente-Manzanares and Horwitz, 2011). FAs play an essential role in cell migration since their formation at the leading edge and their breakdown at the rear end of the cell require fine spatiotemporal coordination of dozens of proteins (Friedl and Wolf, 2010). Recently, it has been shown that KANK2 can affect cell migration. Sun et al. showed that depletion of mouse KANK2 in mouse fibroblasts led to accelerated cell migration (Sun et al., 2016); whereas Gee et al. have described that loss of mouse KANK2 in cultured mouse podocytes leads to reduced cell migration (Gee et al., 2015). More recently, it was shown that knockdown of KANK2 in the melanoma cell line MDA-MB-435S negatively affected cell migration (Paradžik et al., 2020). In our wound healing experiments, we saw that removal of both KANK1 and KANK2 did not affect migration of HeLa cells. Yet, when using the more motile breast cancer cell line SUM159PT, we observed that depletion of KANK2 caused reduced wound closure. In single cell migration experiments, we could confirm that cell migration velocity was reduced in KANK2-depleted SUM159PT cells compared to control cells. Yet, how exactly the removal of KANK2 reduces migration velocity remains unclear. We never observed any significant effects on FAs, neither in size nor number which is in line with the observations of Sun et al. and Paradzik et al. who also did not see any effects on FA size or number upon KANK2 depletion (Paradžik et al., 2020; Sun et al., 2016). Further, the removal of KANK2 from SUM159PT cells did not affect the formation and clustering of the CMSC components such as liprin-β1 or CLASP2 around FAs. Therefore, KANK2 likely affects cell migration via a heretofore unidentified mechanism. As mentioned previously, Sun et al. have reported that depletion of KANK2 led to more cell migration. Since they also saw that KANK2 mediates FA sliding, a process in which mature FAs slide towards the center of the cell and which has been associate with reduced migration speed (Smilenov et al., 1999), they suggested that the positive effect on cell migration resulted from reduced FA sliding upon KANK2 depletion (Sun et al., 2016). Yet, we did not see any effects of KANK2 removal on the formation of central adhesions (see also Chapter 6 General Discussion). In contrast to Sun et al., two other aforementioned studies showed that loss of KANK2 reduced cell migration (Gee et al., 2015; Paradžik et al., 2020). However, both studies were not able to decipher how exactly KANK2 engages with cell migration. Paradzik et al. solely suggested that probably KANK2's association with αV/β5-integrins, the main type of integrin receptors present in FAs in MDA-MB-435S cells, might be important since the knockdown of KANK2 mimicked the same effects on migration as removal of αV integrins (Paradžik et al., 2020).

Taken together, the exact mechanisms underlying the effects of KANKs (KANK2) on cell migration remains obscure. Due to the contradicting data on the effects of KANK

5

family proteins on cell migration it is likely that there is more than one mechanism through which KANK proteins could affect cell motility. Moreover, it also seems likely that these mechanisms are cell type specific. Thus, further research needs to be done to clarify these open questions also with regard to the different roles that different KANK family members might play.

5

Experimental Procedures

Cell culture and DNA/siRNA transfections

HeLa cells were cultured in DMEM medium; SUM159PT cells were cultured in RPMI 1640 medium; and HEK293T cells were cultured in DMEM/F10 (1:1; v/v) medium. For the KANK2 rescue experiments the same HeLa KANK2-knockout cell line was used as described previously (Yu et al., 2019), this cell line was cultured in DMEM medium. All media were supplemented with 10 % (v/v) fetal calf serum and with Penicillin/ Streptomycin (100 units/mL penicillin and 100 μg/mL streptomycin). All cell lines were grown at 37 °C in humidified incubators at 5 % CO_2 atmosphere. The cell lines were routinely checked for mycoplasma contamination using the Mycoalert assay (Lonza, LT07-518).

Transfection of DNA and siRNA into HeLa cells and of DNA into Hek293T cells was performed as previously described (van der Vaart et al., 2013). HeLa cells were transfected with siRNAs using HiPerFect (Qiagen). SUM159PT cells were transfected with siRNAs using Lipofectamin RNAiMAX (ThermoFisher) following the instructions of the manufacturer. The siRNA-transfected cells were analyzed 48 – 72 hours after transfection. HeLa and SUM159PT cells were both transfected with DNA constructs using FuGene6 (Promega). The cells were analyzed 24 hours after the transfection. Hek293T cells were transfected with DNA using polyethyleneimine (PEI). The cells were harvested for pulldown assays 24 hours after the transfection.

DNA constructs and siRNAs

The BioGFP-tagged KANK2 fusion constructs were made using PCR-based amplification of different KANK2 fragments, pBioGFP-C1 vector and Gibson Assembly mix (New England Biolabs) as described previously (Bouchet et al., 2016). The same siRNAs against KANK1 and KANK2 were used as described previously (Bouchet et al., 2016): control siRNA (siLuciferase) GTGCGTTGCTAGTACCAAC; siKANK1 CAGAGAAGGACATGCGGAT; siKANK2 #1 ATGTCAACGTGCAAGATGA; siKANK2 #2 TCGAGAATCTCAGCACATA.

Antibodies and Immunofluorescence staining

Cell fixation and staining were performed as previously described (van der Vaart et al., 2013). In brief, cells seeded on (12 mm) glass coverslips for immunofluorescence staining were allowed to attach overnight. The following day, the cells were either fixed with 4 % PFA in PBS for 15 minutes at room temperature (phalloidin staining) or with ice-cold methanol for 7 minutes at -20 ºC (staining for KANK1; KANK2; liprin-β1; CLASP2, phosphor-tyrosine; and talin). After one-time washing with PBS, the cells were permeabilized for 4 minutes at room temperature (RT) using permeabilization buffer (0.2 % TritonX-100 (Sigma) in PBS). Thereafter, the cells were blocked in blocking buffer (0.05 % Tween-20 (Sigma) and 2 % BSA (Carl Roth) in PBS) for 1 hour at RT. After blocking, the cells were incubated with primary antibodies diluted in blocking buffer for 1 hour at RT. After incubation, the cells were washed 5-times for 2 minutes with wash buffer (0.05 % Tween-20 in PBS); followed by 1 hour incubation with the fluorescently labeled secondary antibodies diluted in blocking buffer. The cells were washed 5-times

5

for 2 minutes with wash buffer and afterwards, dehydrated using first 70 % and then 100 % ethanol (the dehydration step was left out in case of phalloidin staining). Finally, the cells/coverslips were mounted on glass slides using Vectashield mounting medium (Vector laboratories, H-1000) or DAPI-containing Vectashield mounting medium (Vector laboratories, H-1200) for the wound healing assays.

Commercially available antibodies against alpha-tubulin (Sigma, T5168), KANK1 (Atlas antibodies, HPA005539), KANK2 (Atlas antibodies, HPA015643), phosphotyrosine (Sigma, PT-66), talin (clone 8d4, Sigma, SAB4200694); Talin1 (clone 97H6, BioRad, MCA4770), Talin2 (clone 68E7, Abcam, ab105458) and tensin1 (Sigma, SAB4200283) were used. The rabbit antibody against liprin-β1 was self-made (van der Vaart et al., 2013). The CLASP2 antibody was described before (Lansbergen et al., 2006). Alexa-405, Alexa-488 and Alexa-594 conjugated goat antibodies against rabbit and mouse IgG were purchased from Invitrogen.

Coating 2-well-chambered cover glasses with fibronectin

For the live-cell migration experiments, 2-well-chambered cover glasses (LabTek, 155380) were coated with human fibronectin (FN, PromoCell, C-43060) using a FN/PBS solution (10 μg FN per mL). Of the FN/PBS solution, 250 μL were added to each chamber of the cover glasses. The cover glasses were gently shaken to evenly distribute the FN/PBS solution. Subsequently, they were incubated at 37 °C and 5 % CO_2 in a humidified incubator for 3 hours. After incubation, the remainder of the FN/PBS solution was carefully removed, and the chambers were washed 4-times by gently rinsing them with PBS. Subsequently, the FN-coated cover glasses were directly used for seeding cells in them.

KANK2 rescue experiments

HeLa cells knockout for KANK2 (HeLa-K2-KO cells) were seeded on 12 mm glass coverslips (10,000 – 15,00 cells per coverslip) and allowed to attach overnight. The following day, the medium was refreshed, and the cells were transfected with DNA (0.5 μg DNA/well) using FuGene6 (Promega) transfection reagent. The cells were incubated with the DNA/FuGene6 mixture overnight. The following day (~24 hours after the DNA transfection), the cells were fixed for immunofluorescence staining.

Nocodazole washout experiments

HeLa cells were seeded on 12 mm glass coverslips (10,000 – 15,000 cells per coverslip) and allowed to attach overnight. The following day, the medium was removed, subsequently the cells were either incubated in fresh medium containing nocodazole (10 μM) or normal medium (non-treated control situation) for 3 hours at 37 °C in 5 % CO_2. After incubation, the cells were either directly fixed (non-treated control and no washout condition), or the nocodazole-containing medium was removed and the cells were washed 5-times with cold PBS on ice (to prevent premature re-polymerization of MTs). Afterwards, normal medium was added, and the cells were incubated at 37 °C in 5 % CO_2 for 5, 15 or 45 minutes. Subsequently, the cells were fixed for immunofluorescence staining.

Wound healing assays

HeLa and SUM159PT cells were trypsinized and ~150,000 cells per well were seeded in 6-well culture plates and transfected using 20 nM per siRNA per well using HiPerfect (HeLa cells, Qiagen) or Lipofectamin RNAiMAX (SUM159PT cells, Thermo Fisher) transfection reagent and adding the siRNA/transfection reagent mix to the cell suspension. The cells were allowed to attach and to incubate in the siRNA/transfection reagent-containing medium overnight. The following day, the cells were washed 2-times with PBS and trypsinized. For the wound healing migration assay silicone-made culture-inserts 2 well (ibidi, # 80209) were used. The inserts were placed on 18 mm glass coverslips. The coverslips with the inserts were placed in 6-well culture plates. Subsequently, the trypsinized cells (~24 hours after siRNA transfection) were added to each of the two wells of the insert: 47,000 cells per well for SUM159PT cells and 50,000 cells per well for HeLa cells. The cells were allowed to attach overnight at 37 °C and 5 % CO_2 in a humidified incubator. The following day, the inserts were carefully removed, and the cells were washed 2-times by gently rinsing the wells of the 6-well culture plate with PBS. Afterwards, 2mL of appropriate cell culture medium were added to each of the wells. The cells (~48 hours after siRNA transfection) were then allowed to migrate for 15 hours (SUM159PT cells) or for 24 hours (HeLa cells) at 37 °C and 5 % CO_2 in a humidified incubator. Except for the control cells, the control cells were immediately fixed for immunostaining after removal of the culture-inserts and used as reference for the wound area. After incubation, the cells were directly fixed for immunofluorescence staining. The cells were stained for phalloidin and with DAPI to delineate the cell outlines and nuclei respectively.

Live-cell migration experiments

SUM159PT cells were transfected with siRNA as described above. The following day (24 hours after siRNA transfection, the cells were washed 2-times with PBS, then fresh cell culture medium was added, and the cells were allowed to incubate for another 24 hours at 37 °C and 5 % CO_2 in a humidified incubator. Subsequently, the cells (48 hours after siRNA transfection) were trypsinized and sparsely seeded in 2-well-chambered cover glasses (LabTek, 155380); 20,000 cells were added per well. The cover glasses were either uncoated or coated with FN as described above. Then, the cells were allowed to attach for 6 – 8 hours. Thereafter, the 2-well-chambered cover glass was placed on the phase contrast microscope as described below and every 5 minutes an image was taken of the cells overnight (~12 hours).

Microscopy and image analysis

Images of fixed cells were either collected with a Nikon Eclipse Ni upright wide field fluorescence microscope and a Nikon DS-Qi2 CMOS camera (Nikon), using Plan Apo Lambda 100x N.A. 1.45 oil objective (Nikon) and Nikon NIS (Br) software (Nikon). Alternatively, images were collected with a Nikon Eclipse 80i upright wide field fluorescence microscope and a CoolSnap HQ2 CCD camera (Photometrics) using a Plan Apo VC 100x 100x N.A. 1.40 oil objective, a Plan Fluor 10x N.A. 0.30 objective, or a Plan Fluor 4x N.A. 0.13 objective (all Nikon) and Nikon NIS (Br) software. Nikon Intensilight C-HGFI was used as a light source. For imaging of blue, green and red

fluorescence the filter sets ET-BFP2 (49021), ET-GFP (49002), and ET-mCherry (49008) (all Chroma) were used respectively.

Phase-contrast live cell imaging of migrating SUM159PT cells was performed on a Nikon Ti microscope equipped with a perfect focus system (Nikon), a super high pressure mercury lamp C-SHG1 (Nikon), a Plan Fluor DLL 10x NA 0.3 (Ph1), a CoolSNAP HQ2 CCD camera (Photometrics), a motorized stage MS-2000-XYZ with Piezo Top Plate (ASI) and a stage top incubator model INUBG2E-ZILCS (Tokai Hit) to keep cells at 37 ˚C and 5 % CO2 atmosphere. The microscope setup was controlled by Micro-manager 1.4 software (Edelstein et al., 2014).

For presentation, images were adjusted for brightness and contrast using ImageJ 1.50b (NIH).

For analysis of FA size and number, the FA images were reduced for background (rolling ball radius 20 pixels), subsequently the FA outlines were obtained by thresholding (default setting) and using Analyze Particles in ImageJ (only FAs bigger than 0.25 µm2 were included in the analysis). Statistical analyses were performed using Prism 7 software (GraphPad).

For analysis of KANK2 localization (rescue and nocodazole washout experiments), and cell edge clustering of CLASP2 and liprin-β1, background reduction was applied (rolling ball radius 20 pixels) and images were adjusted for brightness and contrast. The KANK2 localization was quantified as ratio of the integrated density of the (GFP-)KANK2 signal at the center of the cell (cell outline shrunken by 5 um) to the integrated density of the (GFP-)KANK2 signal at the cell periphery (first 5 um). The results were plotted as fraction of the control condition average value. The cell edge clustering of CLASP2 and liprin-β1 were calculated as ratio of the integrated density of the CLASP2/liprin-β1 signal at the cell periphery (first 5 µm) to the integrated density of the signals at the adjacent cell area (second 5 µm) as described before (Bouchet et al., 2016). The results were plotted as fraction of the control condition (siLuciferase) average value. The cell outline was defined by applying Gaussian Blur (ball radius 5 pixels) and thresholding. Statistical analyses were performed using Prism 7 software (GraphPad).

For analysis of the wound healing assays, the control situation (directly fixed after insert removal) was used to create a mask of the uncovered wound area with the adjacent cell areas. To analyze what percentage of the wound area was covered by cells, a Gaussian blur (ball radius 2 pixels) was applied to the images of the other conditions (15 or 24 hours after insert removal), afterwards the images were thresholded, and subsequently the mask of the wound area was fitted on the images and the percentage of wound area covered by cells was calculated. Statistical analyses were performed using Prism 7 software (GraphPad).

For analysis of the live-cell migration assays, the plugin MTrack J for ImageJ (Meijering et al., 2012) was used to track and analyze the migration path of single cells. Statistical analyses were performed using Prism 7 software (GraphPad).

Pulldown assay using bioGFP-tagged KANK2 constructs
Streptavidin-based pulldown assays of biotinylated KANK2 constructs expressed using bioGFP-tagged-KANK2 in HEK293T cells was performed as previously described (van der Vaart et al., 2013). In brief, HEK293T cells were seeded in 10 cm plastic culture dish

to ~80% confluence, the cells were allowed to attach overnight. The following day, the cells were transfected with the bioGFP-tagged KANK2 constructs, biotin-ligase BirA, and GFP-tagged Talin1 (5 µg DNA per construct) using PEI. The DNA/PEI suspension was added to the cells dropwise. Thereafter, the cells were incubated for 24 hours at 37 °C in 5% CO2 atmosphere in humidified incubators. After incubation, the cells were harvested on ice using ice-cold PBS and a spatula to scrape them from the dishes. The harvested cells were pelleted and subsequently lysed using a non-ionic detergent-based lysis buffer (50 mM HEPES pH 7.4, 150 mM NaCl, 1 mM EDTA, protease inhibitor cocktail (Roche), 1 % Triton-X100) for 10 minutes on ice. Afterwards, the suspension was centrifuged at 13,200 rpm at 4 °C for 15 minutes. The streptavidin beads (ThermoFisher, 11206D) were blocked in lysis buffer supplemented with 5% chicken egg white (Sigma) for 30 minutes at RT. Thereafter, the lysates were incubated with the streptavidin beads for 2 hours at 4 °C, except for 7 % of each lysate that was kept as "input" control. DTT-containing SDS-PAGE protein sample buffer was added to the input control. After incubation of the lysates with the streptavidin beads, the beads were washed 5 times using the lysis buffer and a magnetic "DynaMag" rack (ThermoFisher, 12321D). Thereafter, DTT-containing SDS-PAGE protein sample buffer was added to the beads.

The following SDS-PAGE and Western blot analysis were performed according to standard procedures. A commercially available antibody against GFP (Abcam, ab6556) was used. For the detection, near infrared fluorescence technology was used (Li-Cor Biosciences, Odyssey system), using infrared dye conjugated goat antibodies against mouse and rabbit (Li-Cor Biosciences).

5

References

Bachir, A.I., J. Zareno, K. Moissoglu, E.F. Plow, E. Gratton, and A.R. Horwitz. 2014. Integrin-associated complexes form hierarchically with variable stoichiometry in nascent adhesions. Curr Biol. 24:1845-1853.

Barczyk, M., S. Carracedo, and D. Gullberg. 2010. Integrins. Cell Tissue Res. 339:269-280.

Bouchet, B.P., R.E. Gough, Y.C. Ammon, D. van de Willige, H. Post, G. Jacquemet, A.M. Altelaar, A.J. Heck, B.T. Goult, and A. Akhmanova. 2016. Talin-KANK1 interaction controls the recruitment of cortical microtubule stabilizing complexes to focal adhesions. Elife. 5.

Bravo-Cordero, J.J., L. Hodgson, and J. Condeelis. 2012. Directed cell invasion and migration during metastasis. Curr Opin Cell Biol. 24:277-283.

Case, L.B., and C.M. Waterman. 2015. Integration of actin dynamics and cell adhesion by a three-dimensional, mechanosensitive molecular clutch. Nature Cell Biology. 17:955.

Chang, Y.C., P. Nalbant, J. Birkenfeld, Z.F. Chang, and G.M. Bokoch. 2008. GEF-H1 couples nocodazole-induced microtubule disassembly to cell contractility via RhoA. Mol Biol Cell. 19:2147-2153.

Edelstein, A.D., M.A. Tsuchida, N. Amodaj, H. Pinkard, R.D. Vale, and N. Stuurman. 2014. Advanced methods of microscope control using µManager software. 2014.

Etienne-Manneville, S. 2013. Microtubules in Cell Migration. Annual Review of Cell and Developmental Biology. 29:471-499.

Ezratty, E.J., M.A. Partridge, and G.G. Gundersen. 2005. Microtubule-induced focal adhesion disassembly is mediated by dynamin and focal adhesion kinase. Nat Cell Biol. 7:581-590.

Fan, H., H. Tian, X. Cheng, Y. Chen, S. Liang, Z. Zhang, Y. Liao, and P. Xu. 2020. Aberrant Kank1 expression regulates YAP to promote apoptosis and inhibit proliferation in OSCC. J Cell Physiol. 235:1850-1865.

Friedl, P., and K. Wolf. 2010. Plasticity of cell migration: a multiscale tuning model. J Cell Biol.

188:11-19.

Fusco, S., V. Panzetta, V. Embrione, and P.A. Netti. 2015. Crosstalk between focal adhesions and material mechanical properties governs cell mechanics and functions. Acta Biomater. 23:63-71.

Gee, H.Y., F. Zhang, S. Ashraf, S. Kohl, C.E. Sadowski, V. Vega-Warner, W. Zhou, S. Lovric, H. Fang, M. Nettleton, J.Y. Zhu, J. Hoefele, L.T. Weber, L. Podracka, A. Boor, H. Fehrenbach, J.W. Innis, J. Washburn, S. Levy, R.P. Lifton, E.A. Otto, Z. Han, and F. Hildebrandt. 2015. KANK deficiency leads to podocyte dysfunction and nephrotic syndrome. J Clin Invest. 125:2375-2384.

Geiger, B., and K.M. Yamada. 2011. Molecular architecture and function of matrix adhesions. Cold Spring Harb Perspect Biol. 3.

Gu, Y., and M. Zhang. 2018. Upregulation of the Kank1 gene inhibits human lung cancer progression in vitro and in vivo. Oncol Rep. 40:1243-1250.

Guo, Q., S. Liao, Z. Zhu, Y. Li, F. Li, and C. Xu. 2018. Structural basis for the recognition of kinesin family member 21A (KIF21A) by the ankyrin domains of KANK1 and KANK2 proteins. Journal of Biological Chemistry. 293:557-566.

Guo, X., W. Fan, X. Bian, and D. Ma. 2014. Upregulation of the Kank1 gene-induced brain glioma apoptosis and blockade of the cell cycle in G0/G1 phase. Int J Oncol. 44:797-804.

Kim, I., J. Kang, H.Y. Gee, and J.W. Park. 2018. A novel HIF1AN substrate KANK3 plays a tumor-suppressive role in hepatocellular carcinoma. Cell Biol Int. 42:303-312.

Krendel, M., F.T. Zenke, and G.M. Bokoch. 2002. Nucleotide exchange factor GEF-H1 mediates cross-talk between microtubules and the actin cytoskeleton. Nat Cell Biol. 4:294-301.

Kumar, A., M. Ouyang, K. Van den Dries, E.J. McGhee, K. Tanaka, M.D. Anderson, A. Groisman, B.T. Goult, K.I. Anderson, and M.A. Schwartz. 2016. Talin tension sensor reveals novel features of focal adhesion force transmission and mechanosensitivity. J Cell Biol. 213:371-383.

Ladoux, B., and A. Nicolas. 2012. Physically based principles of cell adhesion mechanosensi-

tivity in tissues. Rep Prog Phys. 75:116601.

Lansbergen, G., I. Grigoriev, Y. Mimori-Kiyosue, T. Ohtsuka, S. Higa, I. Kitajima, J. Demmers, N. Galjart, A.B. Houtsmuller, F. Grosveld, and A. Akhmanova. 2006. CLASPs attach microtubule plus ends to the cell cortex through a complex with LL5beta. Dev Cell. 11:21-32.

Meijering, E., O. Dzyubachyk, and I. Smal. 2012. Methods for cell and particle tracking. Methods Enzymol. 504:183-200.

Mimori-Kiyosue, Y., I. Grigoriev, G. Lansbergen, H. Sasaki, C. Matsui, F. Severin, N. Galjart, F. Grosveld, I. Vorobjev, S. Tsukita, and A. Akhmanova. 2005. CLASP1 and CLASP2 bind to EB1 and regulate microtubule plus-end dynamics at the cell cortex. J Cell Biol. 168:141-153.

Ng, D.H., J.D. Humphries, A. Byron, A. Millon-Frémillon, and M.J. Humphries. 2014. Microtubule-dependent modulation of adhesion complex composition. PLoS One. 9:e115213.

Pan, W., K. Sun, K. Tang, Q. Xiao, C. Ma, C. Yu, and Z. Wei. 2018. Structural insights into ankyrin repeat-mediated recognition of the kinesin motor protein KIF21A by KANK1, a scaffold protein in focal adhesion. J Biol Chem. 293:1944-1956.

Pankov, R., E. Cukierman, B.Z. Katz, K. Matsumoto, D.C. Lin, S. Lin, C. Hahn, and K.M. Yamada. 2000. Integrin dynamics and matrix assembly: tensin-dependent translocation of alpha(5)beta(1) integrins promotes early fibronectin fibrillogenesis. J Cell Biol. 148:1075-1090.

Paradžik, M., J.D. Humphries, N. Stojanović, D. Nestić, D. Majhen, A. Dekanić, I. Samaržija, D. Sedda, I. Weber, M.J. Humphries, and A. Ambriović-Ristov. 2020. KANK2 Links αVβ5 Focal Adhesions to Microtubules and Regulates Sensitivity to Microtubule Poisons and Cell Migration. Front Cell Dev Biol. 8:125.

Parsons, J.T., A.R. Horwitz, and M.A. Schwartz. 2010. Cell adhesion: integrating cytoskeletal dynamics and cellular tension. Nat Rev Mol Cell Biol. 11:633-643.

Pollard, T.D., and J.A. Cooper. 2009. Actin, a Central Player in Cell Shape and Movement. Science. 326:1208-1212.

Ren, X.D., W.B. Kiosses, and M.A. Schwartz.

1999. Regulation of the small GTP-binding protein Rho by cell adhesion and the cytoskeleton. Embo j. 18:578-585.

Ren, Y., R. Li, Y. Zheng, and H. Busch. 1998. Cloning and characterization of GEF-H1, a microtubule-associated guanine nucleotide exchange factor for Rac and Rho GTPases. J Biol Chem. 273:34954-34960.

Ridley, A.J., M.A. Schwartz, K. Burridge, R.A. Firtel, M.H. Ginsberg, G. Borisy, J.T. Parsons, and A.R. Horwitz. 2003. Cell migration: integrating signals from front to back. Science. 302:1704-1709.

Sarkar, S., B.C. Roy, N. Hatano, T. Aoyagi, K. Gohji, and R. Kiyama. 2002. A novel ankyrin repeat-containing gene (Kank) located at 9p24 is a growth suppressor of renal cell carcinoma. J Biol Chem. 277:36585-36591.

Seetharaman, S., and S. Etienne-Manneville. 2019. Microtubules at focal adhesions - a double-edged sword. J Cell Sci. 132.

Smilenov, L.B., A. Mikhailov, R.J. Pelham, E.E. Marcantonio, and G.G. Gundersen. 1999. Focal adhesion motility revealed in stationary fibroblasts. Science. 286:1172-1174.

Stehbens, S., and T. Wittmann. 2012. Targeting and transport: How microtubules control focal adhesion dynamics. Journal of Cell Biology. 198:481-489.

Sun, Z., H.Y. Tseng, S. Tan, F. Senger, L. Kurzawa, D. Dedden, N. Mizuno, A.A. Wasik, M. Thery, A.R. Dunn, and R. Fassler. 2016. Kank2 activates talin, reduces force transduction across integrins and induces central adhesion formation. Nat Cell Biol. 18:941-953.

van der Vaart, B., W.E. van Riel, H. Doodhi, J.T. Kevenaar, E.A. Katrukha, L. Gumy, B.P. Bouchet, I. Grigoriev, S.A. Spangler, K.L. Yu, P.S. Wulf, J. Wu, G. Lansbergen, E.Y. van Battum, R.J. Pasterkamp, Y. Mimori-Kiyosue, J. Demmers, N. Olieric, I.V. Maly, C.C. Hoogenraad, and A. Akhmanova. 2013. CFEOM1-associated kinesin KIF21A is a cortical microtubule growth inhibitor. Dev Cell. 27:145-160.

Vicente-Manzanares, M., and A.R. Horwitz. 2011. Cell migration: an overview. Methods Mol Biol. 769:1-24.

5

Vicente-Manzanares, M., J. Zareno, L. Whitmore, C.K. Choi, and A.F. Horwitz. 2007. Regulation of protrusion, adhesion dynamics, and polarity by myosins IIA and IIB in migrating cells. J Cell Biol. 176:573-580.

Weng, Z., Y. Shang, D. Yao, J. Zhu, and R. Zhang. 2018. Structural analyses of key features in the KANK1.KIF21A complex yield mechanistic insights into the cross-talk between microtubules and the cell cortex. J Biol Chem. 293:215-225.

Wolfenson, H., Y.I. Henis, B. Geiger, and A.D. Bershadsky. 2009. The heel and toe of the cell's foot: a multifaceted approach for understanding the structure and dynamics of focal adhesions. Cell Motil Cytoskeleton. 66:1017-1029.

Yu, M., S. Le, Y.C. Ammon, B.T. Goult, A. Akhmanova, and J. Yan. 2019. Force-Dependent Regulation of Talin-KANK1 Complex at Focal Adhesions. Nano Lett. 19:5982-5990.

Zaidel-Bar, R., M. Cohen, L. Addadi, and B. Geiger. 2004. Hierarchical assembly of cell-matrix adhesion complexes. Biochem Soc Trans. 32:416-420.

Zamir, E., B.Z. Katz, S. Aota, K.M. Yamada, B. Geiger, and Z. Kam. 1999. Molecular diversity of cell-matrix adhesions. J Cell Sci. 112 (Pt 11):1655-1669.

Zamir, E., M. Katz, Y. Posen, N. Erez, K.M. Yamada, B.Z. Katz, S. Lin, D.C. Lin, A. Bershadsky, Z. Kam, and B. Geiger. 2000. Dynamics and segregation of cell-matrix adhesions in cultured fibroblasts. Nat Cell Biol. 2:191-196.

Zhu, Y., N. Kakinuma, Y. Wang, and R. Kiyama. 2008. Kank proteins: a new family of ankyrin-repeat domain-containing proteins. Biochim Biophys Acta. 1780:128-133.

5
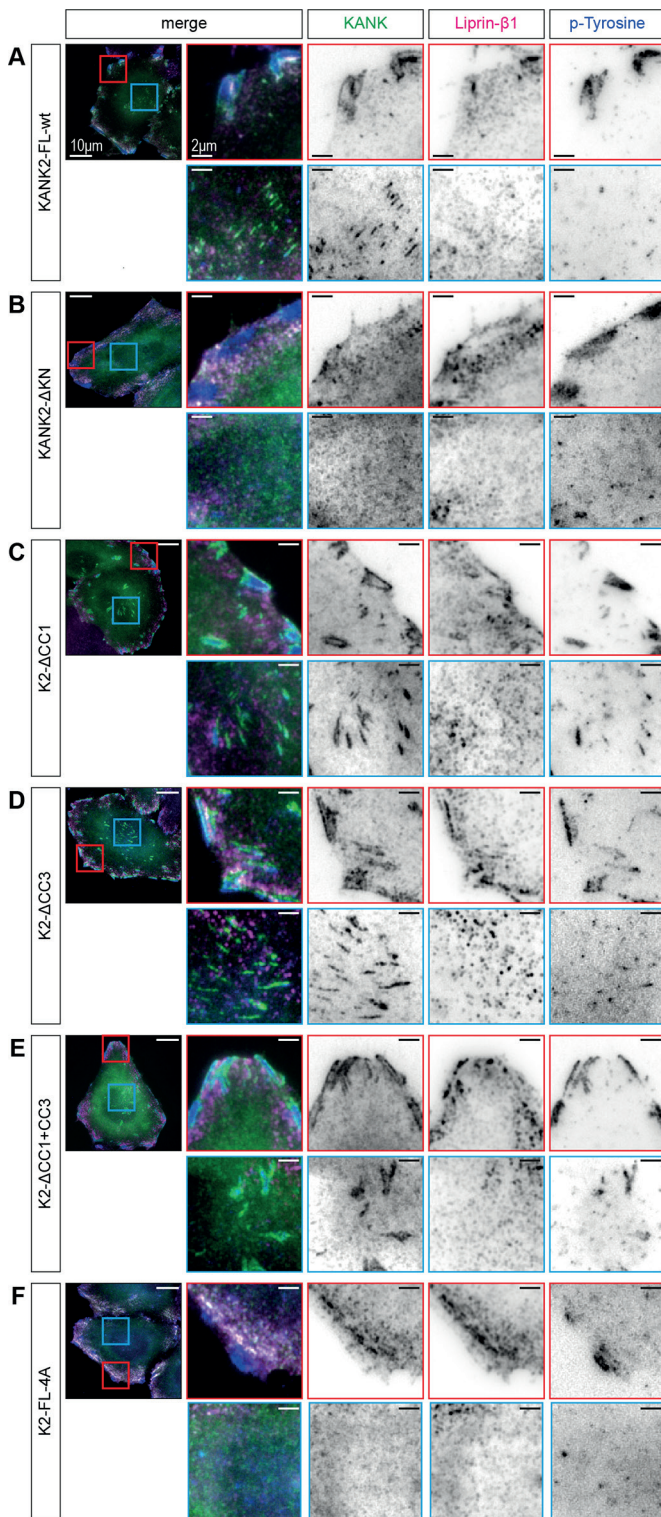
Supplementary Figures

Supplementary Figure S1, related to Figure 2.

(A-F) HeLa cells knockout for KANK2 (HeLa-K2-KO cells) were transiently transfected with same GFP-tagged KANK2 constructs (green) as used in Figure 2. The cells were fixed 24 hours after the DNA transfection and stained for endogenous liprin-β1 (magenta) and the FA marker phospho-tyrosine (blue). The red insets represent peripheral adhesion complexes whereas the blue insets represent central areas in the cell.

5
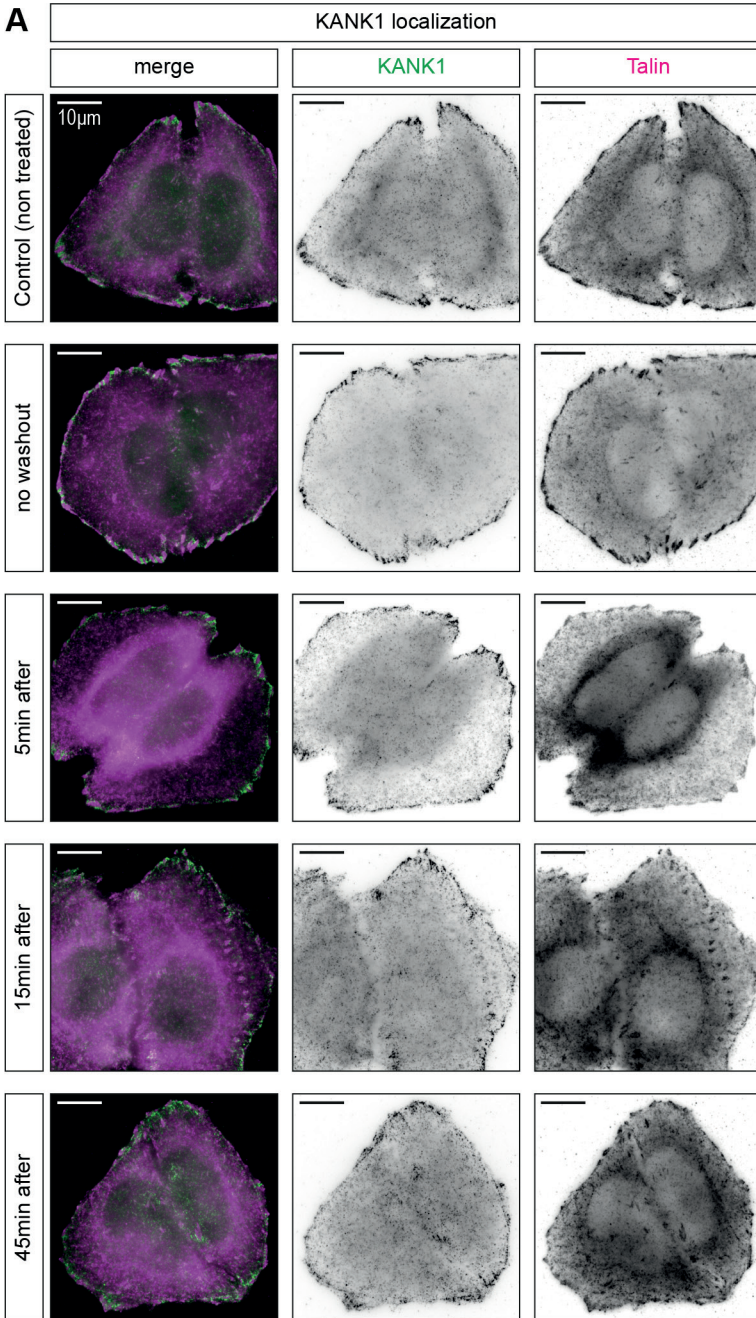
Supplementary Figure S2, related to Figure 3. Disruption of the MT cytoskeleton by nocodazole does not affect the subcellular localization of KANK1

(A) HeLa cells were treated as in Figure 3. The fixed cells were stained for endogenous KANK1 (green) and talin (magenta).
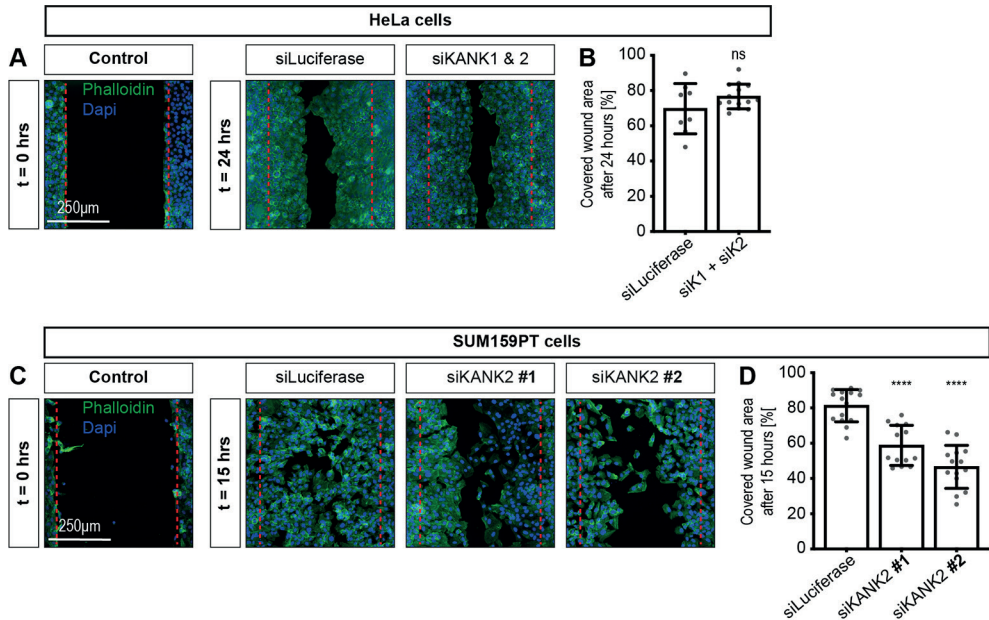
Supplementary Figure S3, related to Figure 4. Control wound healing assays using HeLa and SUM159PT cells

(**A**) Follow-up wound healing experiment using HeLa cells that were either transfected with control siRNA (siLuciferase) or with siRNAs against KANK1 and KANK2 (siKANK1 & 2). The same procedure was followed as in (Figure 4-A) and the fixed cells were stained for phalloidin (green) and DAPI (blue) to visualize the cell outlines and nuclei. The control panel on the left shows the wound area directly after applying the wound (t = 0 hours). The panels on the right show representative wound areas 24 hours after applying the wound (t = 24 hours). Dotted red lines represent the boarders of the wound area. (**B**) Quantification of the covered wound area; ns not significant (unpaired t-test) (8 – 14 wound areas were analyzed per condition). (**C**) Control wound healing experiment using SUM159PT cells and using two different siRNA against KANK2 (siKANK2 #1 and siKANK2 #2). The same procedure was followed as in (Figure 4-C) and fixed cells were stained for phalloidin (green) and DAPI (blue). Dotted red lines represent the boarders of the wound area. (**D**) Quantification of the covered wound area 15 hours after applying the wound; **** $p < 0.0001$ (Ordinary One-Way ANOVA (Dunnett's Multiple Comparison Test)) (13 – 15 wound areas were analyzed per condition). All covered wound areas are presented as mean ± SD.

5
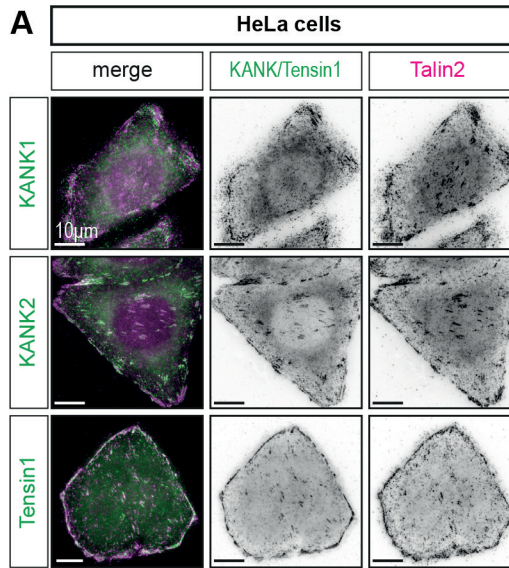
Supplementary Figure S4. Subcellular localization of endogenous KANKs, tensin1 and talin2 in HeLa cells

(**A**) HeLa cells were fixed and stained for endogenous KANK1, KANK2 or tensin1 (green) and endogenous talin2 (magenta). Tensin1 is thought to be mainly concentrated at central (fribrillar) adhesions. However, in HeLa cells it shows strong co-localization with talin2, both at the cell periphery and in the cell center.

A

B
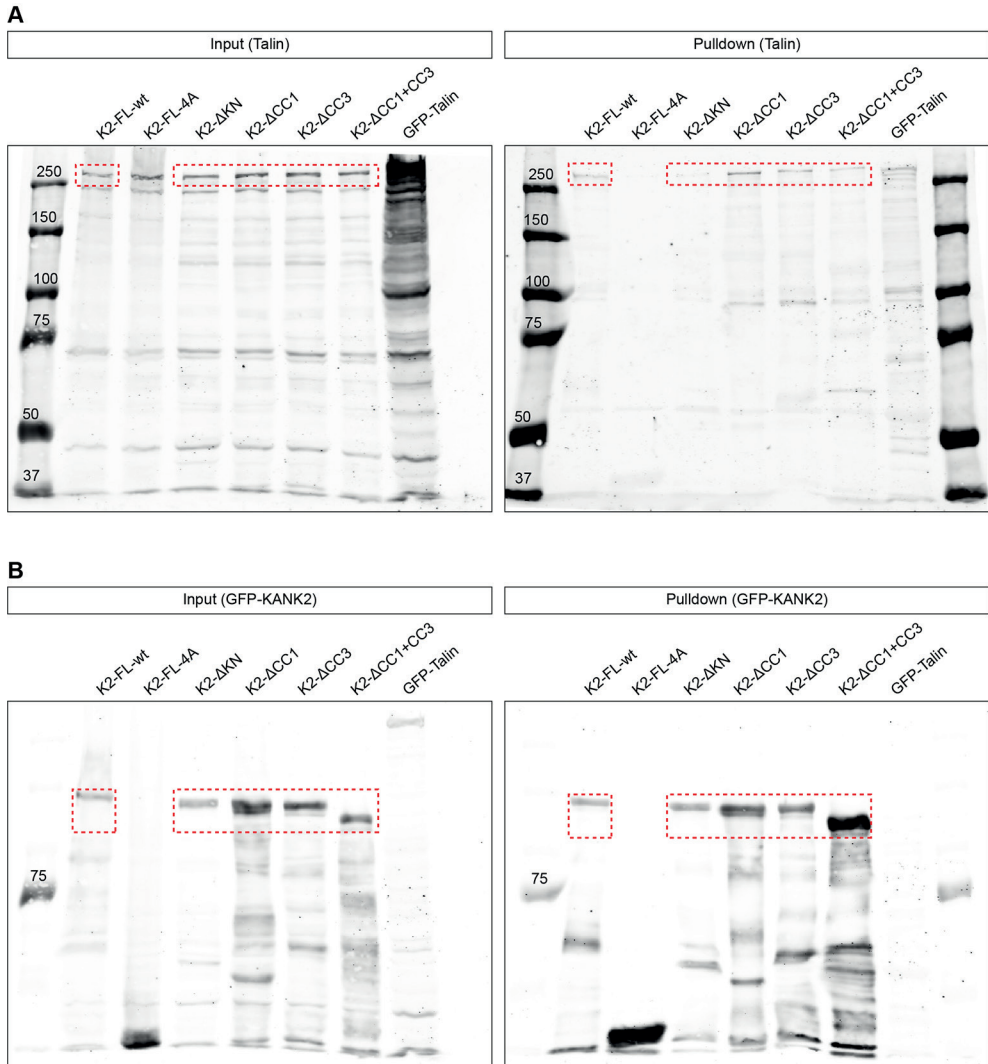
Supplementary Figure S5, related to Figure 2I. Original membranes of bioGFP-KANK2-Talin pulldown.
(**A**) Original blots of the Talin membranes/gels. The dashed red boxes indicate the bands that are shown in Figure 2I. (**B**) Original blots of the membranes/gels of the bioGFP-KANK2 constructs. The dashed red boxes indicate the bands that are shown in Figure 2I. In both (A) and (B), the lane of KANK2-FL-4A was not included since it seems that the cells did not express the bioGFP-K2-FL-4A construct properly. The band of KANK2-FL-4A should be at the same height as bioGFP-KANK2-FL-wt. Yet, neither in the input nor in the pulldown such a band can be seen.

6

General discussion

York-Christoph Ammon[1]

1 Cell Biology, Neurobiology and Biophysics, Department of Biology, Faculty of Science, Utrecht University, Utrecht, The Netherlands

General Discussion

In this thesis, we tried to gain more insight on the KANK family proteins and their role as mediators of the cross-talk between microtubules (MTs) and integrin-mediated cell-matrix adhesions. In Chapter 1, we provided an overview of the current literature about KANK family proteins. In Chapter 2, we established KANK1 as novel binding partner of the adhesion protein talin. Moreover, we could show that the talin-KANK1 interaction is essential for the correct formation of the cortical MT stabilizing complex around focal adhesions and the stabilization and growth inhibition of MTs at the cortex (Chapter 2). Subsequently, we looked at the talin-KANK1 interaction in more detail (Chapter 3). We could demonstrate that the talin-KANK1 interaction is force-regulated. In Chapter 4, we tried to identify what factors/domains recruit KANK1 to the periphery of focal adhesions and prevent them from overlapping with focal adhesions. We showed that the long linker region L2 of KANK1 can sequester the talin-binding KN domain of KANK1 to the adhesion periphery. Moreover, we established the dynamic hub protein dynein light chain LC8 as new interaction partner of KANK1 (Chapter 4). Last but not least, we tried to better understand the differences between KANK1 and KANK2 and what role they might play in cell migration (Chapter 5). In this final chapter, we will discuss our findings, put them in a broader context and make some suggestions for future experimental work.

KANK proteins: new talin binding partners and mediators of microtubule – focal adhesion cross-talk

The tight connection of cells to the extracellular matrix (ECM) is crucial for multicellular organisms as it contributes to tissue integrity (by keeping cells in place) but also to cell motility (by allowing cells to transduce forces and translocate). Cells usually use the heterodimeric α/β-integrin transmembrane receptors (integrins) to bind to the ECM (Bachir et al., 2014; Barczyk et al., 2010; Winograd-Katz et al., 2014). In the five decades since the first description of cell-matrix adhesions, more than 180 proteins have been identified as components of the so-called integrin adhesome (Winograd-Katz et al., 2014). The most well-characterized integrin-mediated cell-matrix adhesion structures are focal adhesions (FAs). The actin cytoskeleton in combination with myosin II (actomyosin) and the forces generated by them are of great importance for the formation, maturation and maintenance of adhesions (Burridge and Guilluy, 2016). Nonetheless, MTs are as essential for cell-matrix adhesions as the actomyosin network (Garcin and Straube, 2019). MTs are hollow cylindrical structures consisting of 11 – 15 laterally organized protofilaments depending on the cell type and species (Aher and Akhmanova, 2018). These protofilaments consist of α/β-tubulin heterodimers that are longitudinally arranged in head-to-tail fashion thereby creating intrinsic polarity of the protofilaments and consequently of the whole MT (Akhmanova and Steinmetz, 2015). This intrinsic polarity of MTs results in two distinct ends of MTs: the fast-growing highly dynamic plus end (β-tubulin is exposed) and the slow-growing minus end (α-tubulin is exposed) (Akhmanova and Steinmetz, 2015; Desai and Mitchison, 1997). Two diverse groups of proteins affect and regulate the dynamics of MTs: i) The MT-associated proteins (MAPs) can bind to the MT lattice or track and concentrate at the growing MT plus end (plus

end-tracking protein, +TIPs). A unique MAP is the Guanine Nucleotide Exchange Factor H1 (GEF-H1) which is usually bound to the MT lattice and thereby inactive (Ren et al., 1998). GEF-H1 is released and activated upon MT disruption, it can then activate the GTPase RhoA (Chang et al., 2008). ii) Motor proteins, such as kinesins and dyneins, walk along the MT lattice towards either the plus end (mainly kinesins) or the minus end (mainly dyneins). Thereby, the motor proteins transport cargo vesicles along their way (Bachmann and Straube, 2015). Besides, motor proteins can also directly affect the dynamics and stability of MTs. For example, members of the kinesin-8 family, such as KIF19A, have been known to depolymerize MTs from their plus ends (Niwa et al., 2012). On the other hand, motor proteins such as kinesin-4 family member KIF21A, can inhibit MT growth (van der Vaart et al., 2013).

It has been shown that MTs play a crucial role in FA turnover (Stehbens and Wittmann, 2012). By using live-cell fluorescence microscopy it could be demonstrated that MTs are targeting FAs in migrating fibroblasts (Kaverina et al., 1999; Kaverina et al., 1998). Moreover, it was shown that nocodazole-induced MT depolymerization leads to increased FA and actomyosin fiber assembly (Ren et al., 1999) whereas the re-growth of MTs leads to massive FA disassembly (Ezratty et al., 2005). The CLIP-associated proteins 1 and 2 (CLASP1 and 2) accumulate at and stabilize the MT plus ends at the leading edge of migrating fibroblasts (Akhmanova et al., 2001). Later, it was found that CLASPs also attach MT plus ends to LL5β- and ELKS-containing patches at the cell cortex in the vicinity of FAs (Lansbergen et al., 2006; Mimori-Kiyosue et al., 2005). Almost a decade later, it was shown that liprins (liprin-α1 and β1) as well as kinesin-4 KIF21A are also components of these cortical MT stabilizing complexes (CMSCs) (van der Vaart et al., 2013). Besides, the study also revealed that KANK1 and KANK2 are also accumulated in the CMSC by binding to liprins (mainly liprin-β1). It was also shown that the KANKs recruit KIF21A to the CMSC via their ankyrin repeat domain. KIF21A inhibits MT growth thereby preventing MT overgrowth at the cortex (van der Vaart et al., 2013). Yet, the link connecting the CMSC to FAs was still missing.

Through combination of pulldown assays and mass spectrometry analysis, we were able to identify KANK1 as new binding partner of the FA protein talin (Chapter 2) (Figure 1). Moreover, we showed that KANK1 binds via its KN domain to the talin rod domain R7. Around the same time, another group discovered the same binding mode for KANK2 (Sun et al., 2016). The talin-KANK1 interaction is required for proper assembly of the CMSC around FAs. We could show that the disruption of this interaction, either by siRNA-mediated depletion of KANK1 and KANK2 or by point mutations in the KN domain or in the rod domain R7, caused dispersion of the CMSC components at the cell cortex and MT overgrowth with MTs growing parallel to the plasma membrane (PM) (Chapter 2).

Does KANK depletion affect FAs?

As mentioned before, it has been reported that MT targeting of FAs is associated with increased rates of FA disassembly (Ezratty et al., 2005; Kaverina et al., 1999; Krylyshkina et al., 2003). Therefore, one would think that the disruption of the CMSC would affect cell-matrix adhesion complexes. As MTs are no longer anchored in close proximity to FAs and since their growth is not inhibited anymore, one would likely assume that the
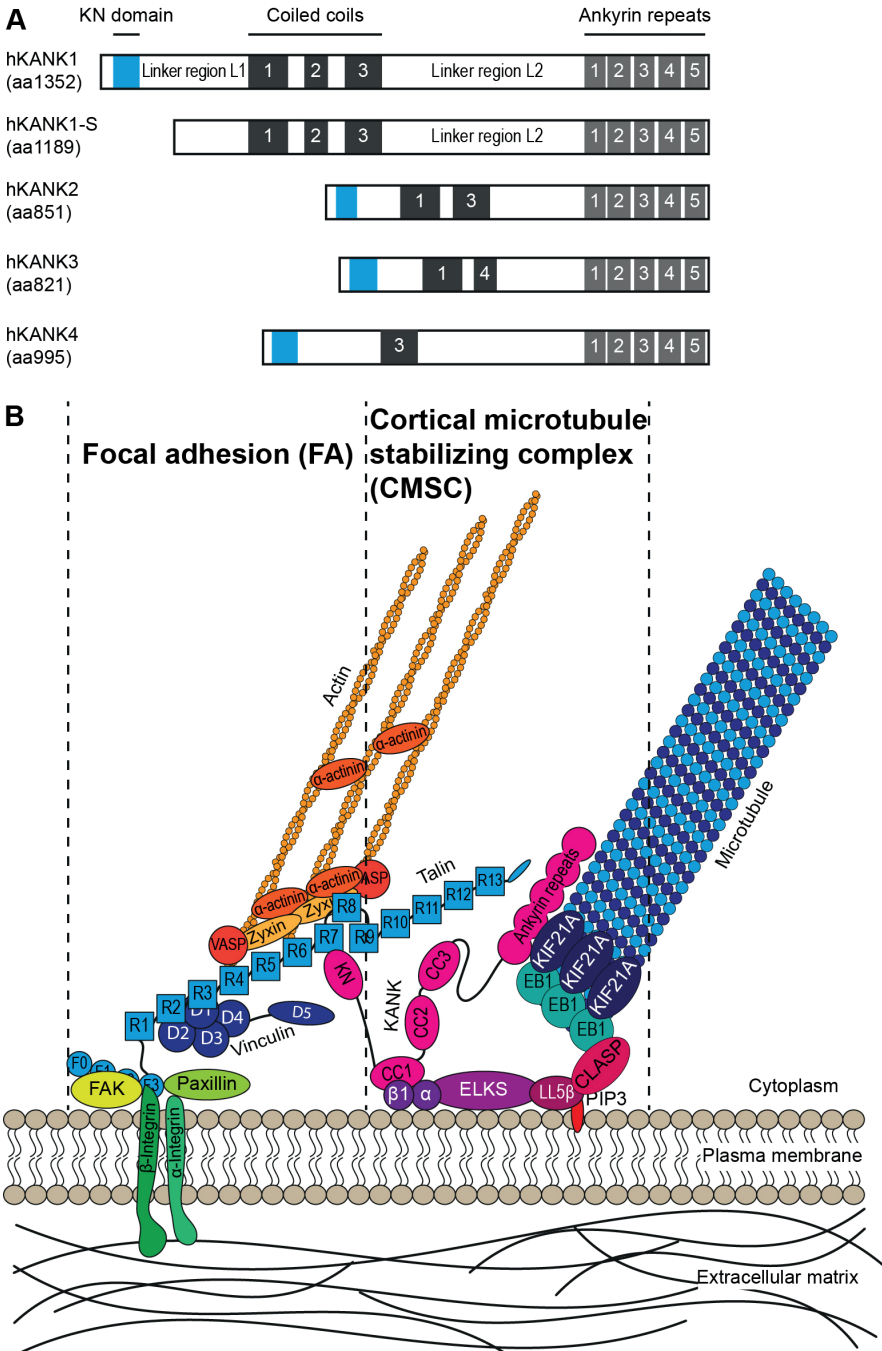
Figure 1. The KANK family proteins and the relationship between the CMSC and FAs at the cell cortex

(**A**) Schematic overview of the four human KANK homologs. All four human KANK proteins possess a similar structure with three distinct domains. At the N-terminus, there is the KANK N-terminal (KN) domain (blue). In the central region there are the coiled coil domains (black). There are four conserved CC domains (CC1 – 4), the composition and number of which vary among the family members. At the

C-terminus, there is the highly conserved ankyrin repeat domain, which consists of five ankyrin repeats (grey). (**B**) Schematic overview of the CMSC in close proximity to a FA at the cortex, reproduced from Chapter 1 Figure 4. Plus ends of MTs are anchored at the plasma membrane by CLASPs (CLASP1 and CLASP2), ELKS, liprins (α1 and β1, dark violet), and LL5β-containing plaques of the CMSC. CLASPs stabilize MT plus ends. KIF21A inhibits MT growth and thereby prevents overgrowth of MTs at the plasma membrane. KANK family proteins link the CMSC to FAs by directly binding to the FA protein talin and by binding to CMSC components such as liprins. Moreover, KANKs recruit KIF21A to the CMSC.

disassembly of adhesion complexes must be perturbed. Yet, we never saw any direct effects on FAs (nor in their size nor number) when depleting KANK family proteins in different cell types (see also Chapter 3 and Chapter 5). This is in line with findings of other groups that also did not observe any significant effects on FAs upon depletion of KANK proteins (Paradžik et al., 2020; Sun et al., 2016). In contrast to that, a recently published study reported that the removal of KANK family proteins (KANK1 and KANK2) did affect FAs. Rafiq et al. showed that depletion of KANK1 and KANK2 in the fibrosarcoma cell line HT1080 mimicked the effects of nocodazole-induced MT depolymerization on FAs leading to bigger FA. Moreover, they reported that these effects on FAs were caused by the release of GEF-H1 from MTs upon KANK removal in HT1080 and HUVEC cells as they observed less decoration of MTs with GEF-H1 (Rafiq et al., 2019). As mentioned previously, free active GEF-H1 (e.g. released due to nocodazole-induced MT depolymerization) stimulates RhoA activity, thereby promoting actomyosin contractility which in turn affects FAs (Chang et al., 2008). However, we were not able to reproduce these findings in our different cell lines, among them HT1080 and HUVEC cells as used by Rafiq et al. In our KANK-depleted cells, the MT integrity was not affected by the loss of KANK family proteins (except for the overgrowth at the cortex) which is in line with the observations of Rafiq et al. Yet, in contrast to their work, we did not see a significant displacement of GEF-H1 from MTs upon KANK depletion (Figure 2). They suggested that the uncoupling of MTs from adhesion complexes (by removal of KANK family proteins and thereby perturbing the talin-KANK interaction) might change MT dynamics: For example, MT plus end could exhibit higher frequencies of catastrophes and rescues thereby causing a higher turnover of GEF-H1. This increased turnover of GEF-H1 would consequently lead to higher GEF-H1 activity and stimulation of cell contractility. Yet, there have been no reports to support this hypothesis so far. Therefore, further research needs to be done to gain more insight into the effect of KANK family proteins on the activity of GEF-H1.

6

Is there redundancy among KANK family proteins?

One point that we did not address in Chapter 2 was whether there is redundancy among the KANK family proteins and whether other KANK homologs such as KANK2 – 4 could rescue the connection to talin as well as the formation of the CMSC.

From our studies, we know that the potential candidate needs to fulfill three requirements to be suitable to substitute KANK1 and rescue the CMSC localization to the vicinity of FAs. First, it should bind to talin. From our work and from that of others, it is known that KANK1 (Chapter 2 and Chapter 3) and KANK2 (Sun et al., 2016) bind to talin via their KN domains. All four human KANK homologs possess the KN domain which is highly conserved (Zhu et al., 2008). Moreover, sequence analysis revealed that the LDLD-motif which is required for the binding to talin is conserved among the KANK family members
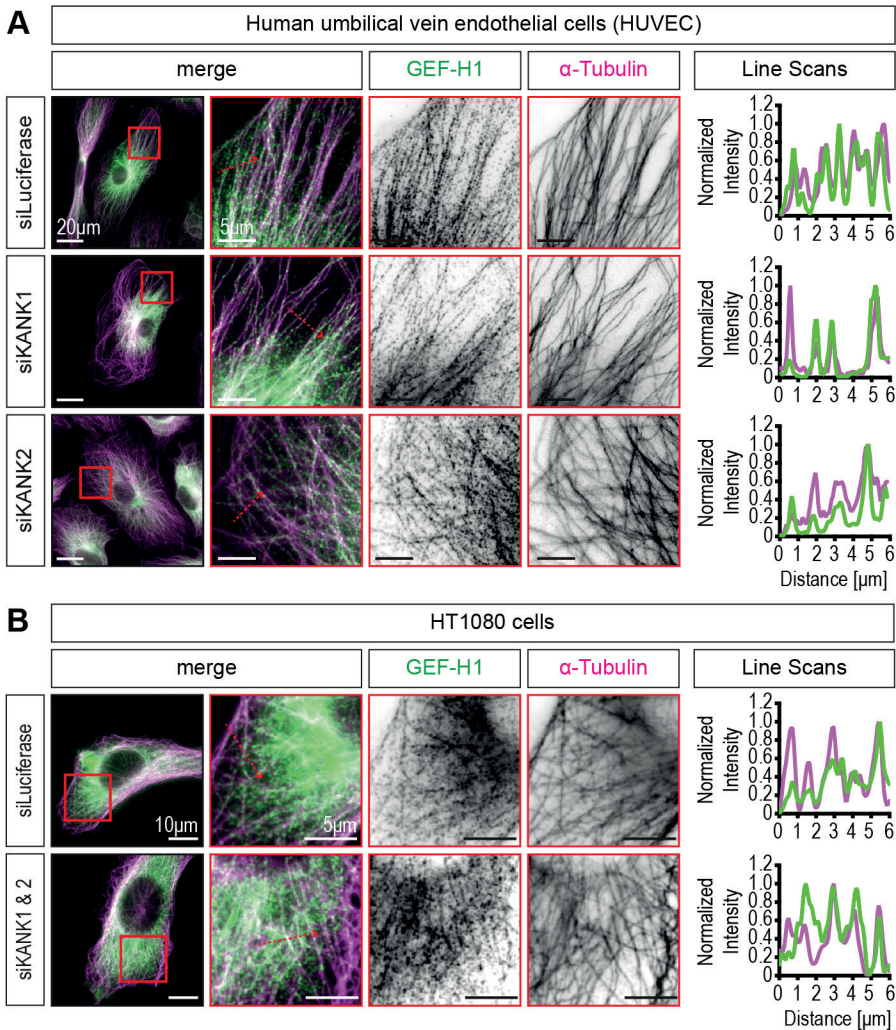
Figure 2. Endogenous GEF-H1 in different cell lines that are depleted of KANK proteins
(**A**) Immunofluorescence staining of endogenous GEF-H1 (green) and α-tubulin (magenta) in HUVEC cells. (**B**) Immunofluorescence staining of endogenous GEF-H1 (green) and α-tubulin (magenta) in HT1080 cells. The right panels in (A) and (B) show the plotted fluorescence intensities of the GEF-H1 (green) and α-Tubulin (magenta) along the line indicated by the dashed red arrow in the inset. The fluorescence intensities were normalized to the maximum intensity of the corresponding channel.

(Figure 3). Therefore, it is highly likely that all four KANKs can bind to talin.
Second, the proteins should bind to liprins in order to provide a scaffold for recruiting the other CMSC proteins such as ELKS and LL5β. In a previous study by our lab, it was shown that binding to liprins is mediated via the KANK coiled coil domain 1 (CC1) (van der Vaart et al., 2013). There are four different coiled coil domains (CC1 – 4) conserved among the KANK family of which the number and composition vary (Zhu et al., 2008). Yet, the important CC1 domain can only be found in KANK1 – 3. Thus, it is likely that KANK4 , which only contains the CC3 domain, cannot substitute KANK1 and rescue the CMSC as it is unlikely that it can function as scaffold to recruit ELKS and LL5β.

```
KANK1-KN (30-68) PYFVETPYGYQLDLDFLKYVDDIQKGNTIKRLNIQKRRK
KANK2-KN (31-69) PYSVETPYGYRLDLDFLKYVDDIEKGHTLRRVAVQRRPR
KANK3-KN (33-74) PYSVETPYGFHLDLDFLKYIEELERGPAARRAPGPPTSRRPR
KANK4-KN (24-62) PYSVETPYGFHLDLDFLKYVDDIEKGNTIKRIPIHRRAK
```

Figure 3. Sequence alignment of the KN domains of all four human KANK proteins
The LDLD motif (bold) which mediates binding to talin is conserved among all four human KANK proteins.

Third, a useful though perhaps not an essential function is binding to KIF21A to prevent MT overgrowth at the cortex. It was shown by our group that this recruitment happens via the highly conserved ankyrin repeat domain (van der Vaart et al., 2013). In addition to that, several groups have extensively studied the KIF21A-KANK-ankyrin repeat interaction. They found that the KIF21A-binding domain is conserved in both KANK1 and KANK2 and that both can bind to KIF21A (Guo et al., 2018; Pan et al., 2018; Weng et al., 2018). On the other hand, the corresponding regions in KANK3 and KANK4 contain some substitutions that make them less negatively charged at the interface which is important for interaction with KIF21A. Moreover, by using *in vitro* binding assays Weng et al. found that the ankyrin repeat domains of KANK3 and KANK4 could not bind to the KANK-binding peptide of KIF21A (Weng et al., 2018). Taken together, it seems less likely that KANK3 or KANK4 could rescue all the CMSC functions as they probably cannot recruit KIF21A to the cortex. Since only KANK2 fulfills all three aforementioned requirements, it is possible that KANK2 could substitute KANK1 and thereby recue the CMSC. This is supported by the fact, that we and others have picked up KANK2 as interaction partner of "integrin adhesome" proteins (Paradžik et al., 2020; Sun et al., 2016; van der Vaart et al., 2013). Besides, we and others have observed KANK2 clustering around FAs at the cell periphery. However, it predominantly localizes at central (fibrillar) adhesions – which will be discussed later (see also Chapter 5).

All in all, with our work we have provided the missing link between cell-matrix adhesions and cortical MT attachment complexes. However, more research needs to be done to decipher the exact mechanisms and functions of KANK family proteins as mediators of the cross-talk between MTs and FAs and to understand whether KANK proteins affect the activity of GEF-H1.

KANK proteins: the force-regulated interaction with talin and distinct subcellular localizations

Cell-matrix adhesions are not only responsible for anchoring cells to the ECM and keeping them in place; but they also have to transmit forces from the cell to the ECM and vice versa. In line with that, it has been known for a long time that forces play an essential role in the formation, maturation and maintenance of adhesions (Burridge and Guilluy, 2016). At the beginning of the life cycle of adhesions, when the nascent adhesions (NAs) consist of only a few clustered integrins, the so-called retrograde flow is the main force driving adhesion formation and maturation. This retrograde flow is mainly caused by (Arp2/3-driven) actin polymerization at the leading edge of cells (Yamashiro and Watanabe, 2014). During the maturation of adhesions, NAs evolve and become FAs, which are attached to actin filaments through talin which binds to integrins. Myosin II crosslinks the actin filaments thereby forming the contractile actomyosin
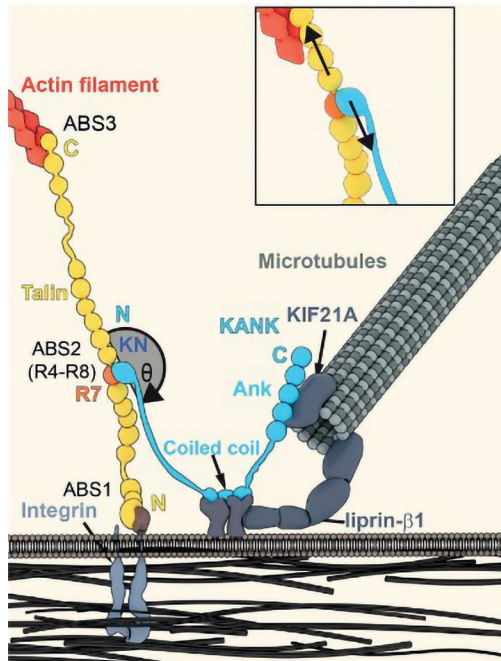
Figure 4, reproduced from Chapter 3 Figure 1A. Schematic overview of the geometry between talin rod domain R7 and KANK1 KN domain at the cell cortex.

KANK (blue) binds to rod domain R7 (orange) of talin (yellow) via its KN domain. At the same time, KANK is bound to liprins via its coiled coil domain. Consequently, KANK is anchored to the plasma membrane (PM). The FA protein talin is also bound to the PM by binding to integrins with its N-terminal talin head domain. Moreover, the talin rod is connected to contractile actin (actomyosin) filaments (red) that exert pulling forces on talin. Thereby, R7-KN interaction is subjected to force as well. The θ represents the possible range of angles that could exist for the R7-KN interaction. With two possible extreme geometries: θ = 90° would be a so-called zipping geometry which represents the weakest interaction, whereas θ = 180° would be the so-called shear-force geometry representing the strongest interaction. The inset at the top is an enlargement of the R7-KN interaction.

cables (Pollard and Cooper, 2009). The forces generated by the actomyosin network are the crucial factor driving adhesion maturation and maintenance (Carlier et al., 2015; Case and Waterman, 2015; Pollard and Cooper, 2009). It has been shown that treatments that interfere with the actomyosin-driven contractility stimulate FA disassembly (Bershadsky et al., 1996). Besides, several adhesion proteins, such as talin and vinculin, are known to be mechanosensitive, with talin being the best well-described example (Atherton et al., 2016; Goult et al., 2018). Talin, the major focal adhesion adaptor protein, binds via its talin head domain to the cytosolic β-integrin tails (Calderwood et al., 1999). The talin rod, which consist of 13 rod domains (R1 – R13), contains two actin binding sites (ABS) (Gough and Goult, 2018; Hemmings et al., 1996). Moreover, the talin rod mediates binding to various other proteins among them vinculin. In total, there are eleven vinculin-binding sites (VBS) in the talin rod. However, these VBS are all buried within the different talin rod domains, which themselves are bundles of 4 – 5 α helices and are not accessible if no force is applied to the molecule (del Rio et al., 2009; Goult et al., 2013). It has been shown that when talin is engaged with integrins and actomyosin, actomyosin cables exert pulling forces on talin. These pulling forces stretch talin and

thereby cause conformational changes in the talin rod leading to the partial unfolding of the rod domains. Consequently, the hidden VBS become accessible and vinculin can bind to talin. This vinculin binding to talin is known to further strengthen talin-actin interaction (del Rio et al., 2009; Goult et al., 2013). Therefore, mechanical forces applied to FAs are essential for the maturation of the adhesion complex since they can lead to conformational changes of adhesion proteins thereby promoting the recruitment of new interaction partners. In Chapter 2, we showed that KANK1 and talin interact with each other via their KN and R7 rod domain respectively. Since talin is subjected to force due to actomyosin contractility and since KANK1 is anchored to the PM by binding to liprins via its CC1 domain, it seemed likely that the talin rod domain R7 – KANK1-KN (R7-KN) interaction is exposed to mechanical force when actomyosin is pulling on the talin rod (Figure 4).

By using magnetic tweezers and a novel single molecule detector, comprised of the talin rod domain R7 and the KN domain of KANK1, we could show that under shear-force geometry a single R7/KN complex can withstand pulling forces of up to 10 pN (Chapter 3). Moreover, these *in vitro* experiments revealed that the R7-KN interaction follows a complex catch-to-slip bond switching behavior. The lifetime of the R7/KN complex increases with increasing force (catch-bond behavior) until a maximum lifetime is reached around forces of 6 pN. Thereafter, the R7/KN lifetime decreases with increasing force (slip-bond behavior). For our cellular experiments, we used a fusion construct of the KN domain fused via the KANK1 linker domain to the membrane-anchoring CAAX-motif of GTP Ras (KN-L1+CAAX). We reasoned that the attachment of the KN domain to the PM could mimic shear force geometry at FAs. Thereby, we observed enrichment of the KN-L1+CAAX constructs at the FA rim. These data support our hypothesis that KANK proteins might accumulate at areas of FAs where the stability of the R7-KN interaction is maximized. Moreover, when using the ROCK inhibitor Y27632, which inhibits actomyosin contractility and thus ablates the pulling forces exerted on talin, we saw that both full-length KANK1 and the KN-L1+CAAX construct were re-distributed to the FA center. This was in line with previous observations of cells treated with ROCK inhibitor expressing full-length KANK1 (see Chapter 2) (Bouchet et al., 2016a). All in all, this study showed that the talin-KANK1 interaction can withstand forces in the physiological range for several seconds to minutes, thereby bolstering the interaction between talin and KANK1 at the periphery of FAs. Furthermore, the cellular experiments supported our hypothesis from previous studies suggesting that there might be a force-regulated component in the talin-KANK interaction that could affect the subcellular localization of KANK family proteins.

Are mechanical forces responsible for the distinct subcellular localizations of KANK1 and KANK2?
In Chapter 5, we looked closer at the differences between KANK1 and KANK2. We observed that both proteins showed distinct subcellular localization despite great similarity in their domain composition. We saw that KANK1 was mainly localized at the cell periphery, where it clustered around FAs. On the other hand, KANK2 was predominantly localized at the center of the cell where it co-localized with talin-positive (thin and elongated) adhesion complexes, which are likely fibrillar adhesions that will

6

be discussed later (see below). Yet, KANK2 could also be found at the cell periphery clustering around FAs. We found that this subcellular localization of KANK2 was likely mediated by talin binding since a KN-depleted KANK2 construct was exclusively enriched at the cell periphery in KANK2-depleted cells. At the cell periphery, KANK2 strongly co-localized with liprins while it was more dispersed around FA. These observations are in line with the observations of others (Sun et al., 2016) and they are similar to our observations of KANK1 constructs lacking the KN domain, which also showed more diffuse localization at the cell periphery (Chapter 2). Deletion of the coiled coil domains caused KANK1 and KANK2 to accumulate strongly at the rim of peripheral adhesions (Chapter 2, Chapter 4 and Chapter 5). Yet, it did not affect the localization of KANK2 at central adhesions (Chapter 5). The nocodazole-induced depolymerization of MTs led to the re-distribution of KANK2 to the cell periphery. Moreover, in the nocodazole treated cells, we could hardly find any talin-positive central adhesions. Nonetheless, as we already discussed in Chapter 5, this re-localization of talin could be due to the massive changes of the intracellular forces that were caused by the nocodazole-induced MT depolymerization. GEF-H1 is released upon MT depolymerization. Consequently, this results in a strong increase of cell contractility (Chang et al., 2008). This in turn leads to intracellular re-distribution of several adhesion proteins as the change in intracellular forces causes a switch in the FA maturation favoring FAs over fibrillar adhesions (Ng et al., 2014). Since we did not follow this further, we cannot be sure whether this change in intracellular forces is the cause of the talin re-localization. However, it would explain the enrichment of KANK2 at the cell periphery upon nocodazole treatment. From our experiments, we could only conclude that binding to talin is important for the subcellular localization of both KANK1 and KANK2. Yet, which other factor(s) might be responsible for the different preferences of the two KANK proteins remains obscure. Yet, with regard to our findings in Chapter 3 that the talin-KANK1 interaction is force regulated and that binding to talin first becomes more stable with increasing force until a maximum is reached, one could think of a force-dependent mechanism for the subcellular localizations of KANK1 and KANK2. It was shown that talins at peripheral adhesions are subjected to much higher tensile forces compared to talins in central adhesions (Kumar et al., 2016). Thus, it could be possible that KANK2, for example, binds preferentially to talin molecules that are exposed to less force (at the cell center) compared to KANK1 that might bind preferably to talins that are subjected to higher tension (at the cell periphery). In case of loss of the binding to talin, for example in KN-depleted KANK constructs, the constructs become enriched at the cell periphery due to their binding to liprins via their CC1 domain.

Does KANK1 self-association contribute to KANK1 clustering around FAs?
In our previous studies, we saw that the KN domain alone strongly overlapped with the FA signal whereas full-length KANK1 clustered broadly around FAs. Interestingly, we also saw that removal of the coiled coil domains led to more tight clustering of KANK1 around FAs (at the FA rim). In Chapter 4, we tried to gain further inside in how the different domains of KANK proteins affect the localization of KANK1 around FAs. To our surprise, we discovered that neither the coiled coil nor the ankyrin repeat domains were responsible for keeping KANK1 protein out of FAs. We found that the hitherto

poorly described linker region L2 of KANK1 carries the potential to prevent the KN domain from penetrating into FAs. A KANK1 construct lacking both the coiled coil and the ankyrin repeat domains still clustered tightly around FAs. Moreover, we could show the same clustering at the FA rim with a fusion construct of the KN domain fused to the linker region L2 (KN+L2 construct). Interestingly, the linker region of KANK2 was not able to recruit the KN domain to the FA rim. Moreover, the linker region L2 of KANK1 alone localized diffusely in the cytoplasm. We were not able to decipher the exact mechanism underlying the ability of the linker region L2 to promote the recruitment of KANK1 to the FA rim. Yet, we were able to show that the linker region L2 (of KANK1) can bind and thereby likely recruit and oligomerize KANK1. This observation is in accordance with a study from Medves et al. They have reported that a fusion gene of KANK1 and PDGFRβ formed oligomers through a region of KANK1 that is located in the long linker region L2 which they termed KANK oligomerization domain (KOD) (Medves et al., 2011). Moreover, for many years, it has been hypothesized by other groups that KANK proteins (mainly KANK1) are probably forming dimers or oligomers most likely mediated by their coiled coil domains (Kakinuma et al., 2009; Zhu et al., 2008). However, we tested several different KANK1 constructs for their ability to bind to full-length KANK1. Surprisingly, the coiled coil domains were not able to bind to full-length KANK1. On the other hand, the constructs containing the linker region L2 were able to bind to KANK1. While we tried to understand how the linker region L2 keeps KANK1 out of the central part of FAs, we also identified a novel binding partner of KANK1: the dynamic hub protein dynein light chain LC8 (LC8). LC8 binds to the linker region L2 exactly in the KOD region. Nonetheless, LC8 is not required to recruit KANK1 to the FA rim as a KN+L2 construct in which all potential LC8 binding motif had been mutated was still able to cluster the KN domain at the FA rim. Another possibility was that the linker region L2 (of KANK1) might behave like an intrinsically disordered protein/region (IDP/R) and mediate the enrichment of KANK1 at the FA rim via phase separation. Yet, bioinformatical sequence and structural analyses showed that L2 displays more characteristics of an ordered protein region than of an intrinsically disordered protein. The analyses even indicated the existence of potential coiled coil in the L2 region. This potential coiled coil in the linker region L2 was also mentioned by Medves et al. It is located C-terminally of the KOD region and in their study, it seemed not to be involved in the oligomerization of the *KANK1:PDGFRβ* gene product (Medves et al., 2011). Yet, this is the current object of our ongoing research to further characterize the L2 region and to understand the exact mechanism that would explain how it recruits KANK1 to the FA rim and to find out whether the predicted coiled coil domain does play a role in this process.

Model of both mechanical forces and KANK1 self-association regulating the localization of KANK1 around FAs

Considering these findings showing the ability of the long linker region L2 of KANK1 to recruit KANK1 to the FA periphery (Chapter 4) and the findings that the talin-KANK1 interaction is force regulated (Chapter 3), it is possible that both factors are contributing to the localization of KANK1 at FAs. It is likely this localization is both force-dependent and due to self-association/clustering leading to steric hinderance with actin fibers. It is
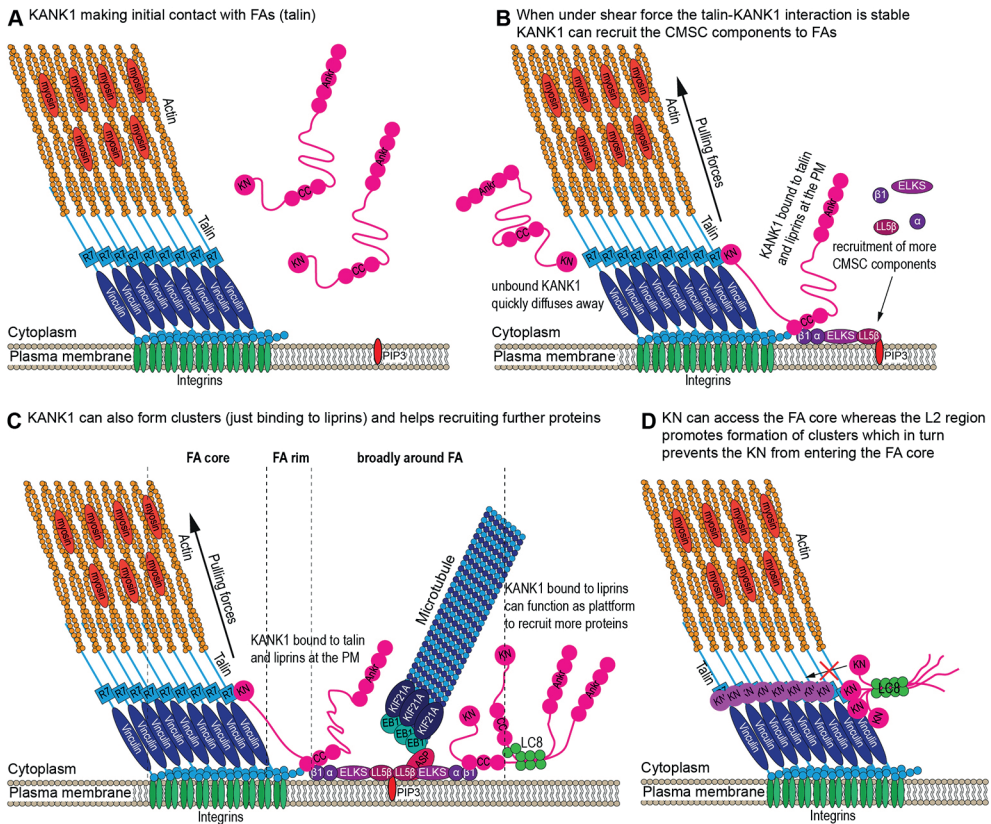
6

Figure 5, reproduced from Chapter 4 Figure 6. Model illustrating different KANK1 subpopulations at FAs and how the KANK1 L2 region could prevent the KN domain from entering the FA core (**A**) KANK1 proteins can interact with talin at FAs. (**B - C**) KANK1 proteins that are bound to both talin and liprins are likely subjected to mechanical forces which have a certain stabilizing effect on the talin-KANK1 interaction. Consequently, these KANK1 proteins can dwell at FAs longer. Thereby, they can promote the recruitment and assembly of the CMSC. Moreover, some KANK1 proteins may not be subjected to mechanical forces that are located more broadly around FAs where they interact with other CMSC proteins such as liprins without interacting with talin. These 2nd layer KANK1 proteins likely function as a scaffold to recruit further proteins to the cell cortex. (**D**) Model how the KANK1 linker region L2 could prevent the KN domain from penetrating into the FA center. Due to its size and the absence of long-lasting interactions, the KN domain alone can easily access the tightly packed FA core and bind to talin proteins located at the FA center. On the other hand, when the KN domain is fused to the linker region L2, it is possible that the L2 region promotes the association and clustering with other L2 regions of other KANK1 proteins. Consequently, the KANK1 proteins or their KN+L2 deletion mutants form clusters which in turn could be too bulky (steric hinderance) and thereby sequester the KN domain at the FA rim. It is possible that the hub protein LC8 (green circles) helps to stabilize the KN+L2 self-association.

possible that different subpopulations of KANK1 proteins exist at FAs: First, KANK1 proteins that are bound to talin rod domain R7 and that are attached to the PM by binding to liprins via their CC1 domain. These KANK1 proteins would be force regulated and kept at the rim of FAs due the force-dependent interaction. One could think that these KANK1 proteins bind more firmly and longer to talin than KANK1 proteins that are freely diffusing and are not bound to the PM via liprins (Figure 5A-B). These "force-stabilized" KANK1 proteins would function as a bridge to recruit the whole CMSC

complex to the vicinity of FAs (Figure 5B-C). Second, KANK1 proteins that are not bound to talin but that are engaged with liprins and/or KIF21A and cluster somewhat further away from the FA complex. These KANK1 proteins could function as scaffold to recruit the bulk of (CMSC) proteins to the cortex. Moreover, via their long linker region L2, they could recruit more KANK1 to the cortex consequently further increasing CMSC accumulation (Figure 5C). One could even imagine that the dynamic hub protein LC8 might be involved in this process. Even though we have seen that LC8 is not essential to enrich KANK1 at the FA rim, it could still be possible that LC8 helps to stabilize the KANK1 clusters. These KANK1 proteins would be mainly kept out of FAs due to their interactions with other proteins (Figure 5C). With regard to the KN+L2 constructs, they could interact with talin via their KN domain and get thereby recruited to FAs. The linker region L2 could cluster other KN+L2 constructs, as well as LC8 which in turn could further stabilize these clusters. Consequently, a big protein cluster would be created that is sterically excluded from the highly organized FA center (Figure 5D). In contrast to that, the KN domain alone and the KN+β-galactosidase chimera do not form clusters that are sterically excluded from the FA center. This likely allows them to penetrate into the FA core and engage with talin molecules at the FA center.

Nonetheless, so far, we have not looked at what happens to the KN+L2 localization at FAs when the pulling forces exerted on talin are relieved, for example by using the ROCK inhibitor Y27632. One could imagine that these constructs will probably start to overlap with the FA center like full-length KANK1. It is known that perturbing the forces exerted on FA causes dramatic changes in the FA organization and consequently promotes their disassembly (Bershadsky et al., 1996). These changes likely render the FA center more accessible and thereby allow KANK proteins to re-distribute to the FA center.

Besides, further research needs to be done on the role of KANK1 self-association and in particular the role of the linker region L2. It would be interesting to abolish L2's ability to bind other KANK1 protein via mutational changes and see how this affects the clustering at FAs.

6

KANK proteins: role in cell migration and as tumor suppressors

According to the World Health Organization (WHO), cancer is the second leading cause of death worldwide with an estimated 9.6 million deaths in 2018 (World Health Organization, 2018). The majority (~90%) of cancer-related deaths are due to metastasis, the spreading of cancer and formation of new (secondary) tumors (Bravo-Cordero et al., 2012). Metastasis is closely linked to cell migration as cancer cells have to leave the tumor, migrate and invade into other tissues to spread and form new tumors (Hanahan and Weinberg, 2011). Therefore, identifying and understanding the factors contributing to cell migration is crucial as it could provide new approaches to treat cancer and to prevent cancer metastasis.

Since KANK proteins link MTs to FAs, we were interested whether they might play a role in cell motility. Besides looking at the different subcellular localizations of KANK1 and KANK2 in Chapter 5, we also performed wound healing assays to study their effects on cell migration. We found that depletion of both KANK1 and KANK2 in HeLa cells did not affect the wound closure. Yet, when we used the more motile breast cancer cell

line SUM159PT, we observed a strong negative effect of KANK2 depletion on cell migration. Wound closure was significantly decreased in KANK2-depleted SUM159PT cells compared to control or KANK1-depleted cells. In single cell migration experiments, we could confirm that removal of KANK2 led to reduced migration speed. As the migration velocity was reduced, one could think that FAs (especially their disassembly) might be affected by the loss of KANK2. Yet, we did not see any effects on FAs nor on the assembly of the CMSC at the cell cortex. However, as mentioned previously, these observations are in line with several other reports that also did not observe any changes in FAs upon KANK removal. Despite this consent regarding the effects on FAs among the different studies, there are striking differences regarding the effects on cell migration. We and others saw reduced cell migration when KANK2 was removed (Gee et al., 2015; Paradžik et al., 2020), whereas Sun et al. observed an increase in cell migration upon loss of KANK2 (Sun et al., 2016). It is important to mention that all studies used different cell types, such as different mouse or human cell lines, for their migration experiments. More importantly, none of the aforementioned reports, including ours, could identify the exact mechanism by which KANK2 was affecting cell migration. The first report on KANK proteins (actually KANK1-S, lacking the KN domain) described KANKs as potential tumor suppressors. Sarkar et al. showed that overexpression of KANK1-S in HEK293 cells that were implanted in mice perturbed the growth of this primary tumor and prevented the formation of secondary tumors whereas mice transplanted with control HEK293 cells suffered from tumor growth and metastases (Sarkar et al., 2002). Over the past 20 years, several other studies bolstered the idea of KANK proteins as tumor suppressors (Chen et al., 2017; Gu and Zhang, 2018; Guo et al., 2014; Kim et al., 2018). Therefore, one could argue that our findings that depletion of KANK2 reduces cell migration would contradict the general notion of KANK proteins having a tumor suppressive potential. However, these aforementioned reports have focused primarily on anti-proliferation and pro-apoptotic effects of KANK1 overexpression in various cancer cells and did not include cell migration experiments. Besides, most of these studies focused on KANK1 and did not test the roles and effects of the other KANK family members. Thus, it seems likely that KANK proteins could suppress cell growth but also promote migration, especially since there are four KANK homologs. They (KANK1/KANK1-S) could indeed have the tumor suppressive effects by stimulating apoptosis as described in various report (Chen et al., 2017; Gu and Zhang, 2018; Guo et al., 2014). In contrast, other KANK family members (KANK2) could affect cell migration.

Moreover, concluding from our data and that of others, it is likely that the effects of KANK proteins on cell migration might by cell type dependent. Yet, more research needs to be done to decipher the mechanism(s) how KANK proteins engage with cell motility. It could also be interesting to change the cell culture system and move from classical 2D migration experiments to 3D migration using soft 3D matrices in which the cells are embedded. There have been multiple studies arguing that migration of cells through (soft) 3D matrices is more likely to mimic the actual physiological circumstances than migration experiment on (stiff) 2D surfaces (Petrie and Yamada, 2012; Yamada and Sixt, 2019). The 3D environment could be very interesting with regard to the role of KANK proteins as linkers between MTs and cell-matrix adhesions. Previously, it has been shown by our group that MTs, especially their stability, play a distinct role in 3D cell migration.

Bouchet and Noordstra have demonstrated that the inhibition of catastrophes of the plus ends of MTs is critical to withstand compression at the pseudopod tip and thereby prevent the retraction of pseudopods of cells migrating through a soft 3D matrix (Bouchet et al., 2016b). Thus, having a look at KANK proteins in a 3D cell culture system could provide new insights on their role in cell motility and their interaction with MTs.

KANK proteins in fibrillar adhesions

As mentioned previously cancer is the second leading cause of death worldwide according to the WHO (World Health Organization, 2018). Apart from forming metastasis, another hallmark of cancer cells is the ability to stimulate growth and expansion of the vascular network (angiogenesis) (Hanahan and Weinberg, 2011). Angiogenesis is essential for tumor growth as it provides the tumor with oxygen and nutrients (Folkman, 1971). It has been shown that in the absence of a vascular network, or when angiogenesis is perturbed, tumor growth is limited and tumor cells can become apoptotic (Holmgren et al., 1995; Parangi et al., 1996). Thus, control of angiogenesis seems to be a promising target for the treatment of cancer in addition to the common therapy strategies. The extracellular matrix (ECM) is of special interest in the process of forming vascular networks as it strongly affects and influences this process (Pickup et al., 2014). It has been shown that remodeling of the ECM is essential for the formation of a (new) vascular network and that these two processes are closely coupled to one another (Cseh et al., 2010; Pickup et al., 2014; Zhou et al., 2008).

One aspect of KANK family proteins that we have not looked at in Chapter 5 was the role or function that KANK proteins, especially KANK2, might play at the elongated central adhesions. These central KANK2-positive structures are especially pronounced in fibroblast-like cells such as the breast cancer cell line SUM159PT (Chapter 5) and endothelial cells such as human umbilical vein endothelial cells (HUVECs) (Figure 6A). When we stained HUVECs for endogenous KANK proteins, we saw that besides KANK2, the two family members KANK1 and KANK3 could also be detected. Interestingly, KANK3 was mainly concentrated at the long elongated talin-positive adhesions, just like KANK2, whereas endogenous KANK1 was predominantly localized at the cell periphery (Figure 6A) (Immunofluorescence stainings and image acquisition were performed as described previously (van der Vaart et al., 2013)). In contrast to its localization in HeLa or SUM15PT cells, endogenous KANK1 did not cluster tightly around peripheral adhesions but showed more dispersed distribution at the cell periphery (Figure 6A). This localization resembled the spread-out distribution of talin-binding deficient KANK1. Thus, it is likely that HUVEC cells are expressing the short KANK1 isoform (KANK1-S) which misses the first 158 amino acids of the long KANK1 isoform at its N-terminus, including the KN domain (Wang et al., 2005) (Figure 6B). To test this idea, we transiently transfected HUVECs with GFP-tagged KANK1-S and KANK1-L. Overexpression of GFP-tagged KANK1-S resembled the diffuse distribution of endogenous KANK1 in HUVECs whereas the GFP-tagged KANK1-L construct strongly accumulated at the thin elongated talin-positive central adhesions, like KANK2 and 3 (Figure 6C). Hence, it appears that HUVECs are mainly expressing the short KANK1 isoform.

The thin elongated (talin-positive) central adhesions appeared to be so-called fibrillar adhesions (FBs). FBs are cell-matrix adhesions that appear as elongated stretches or
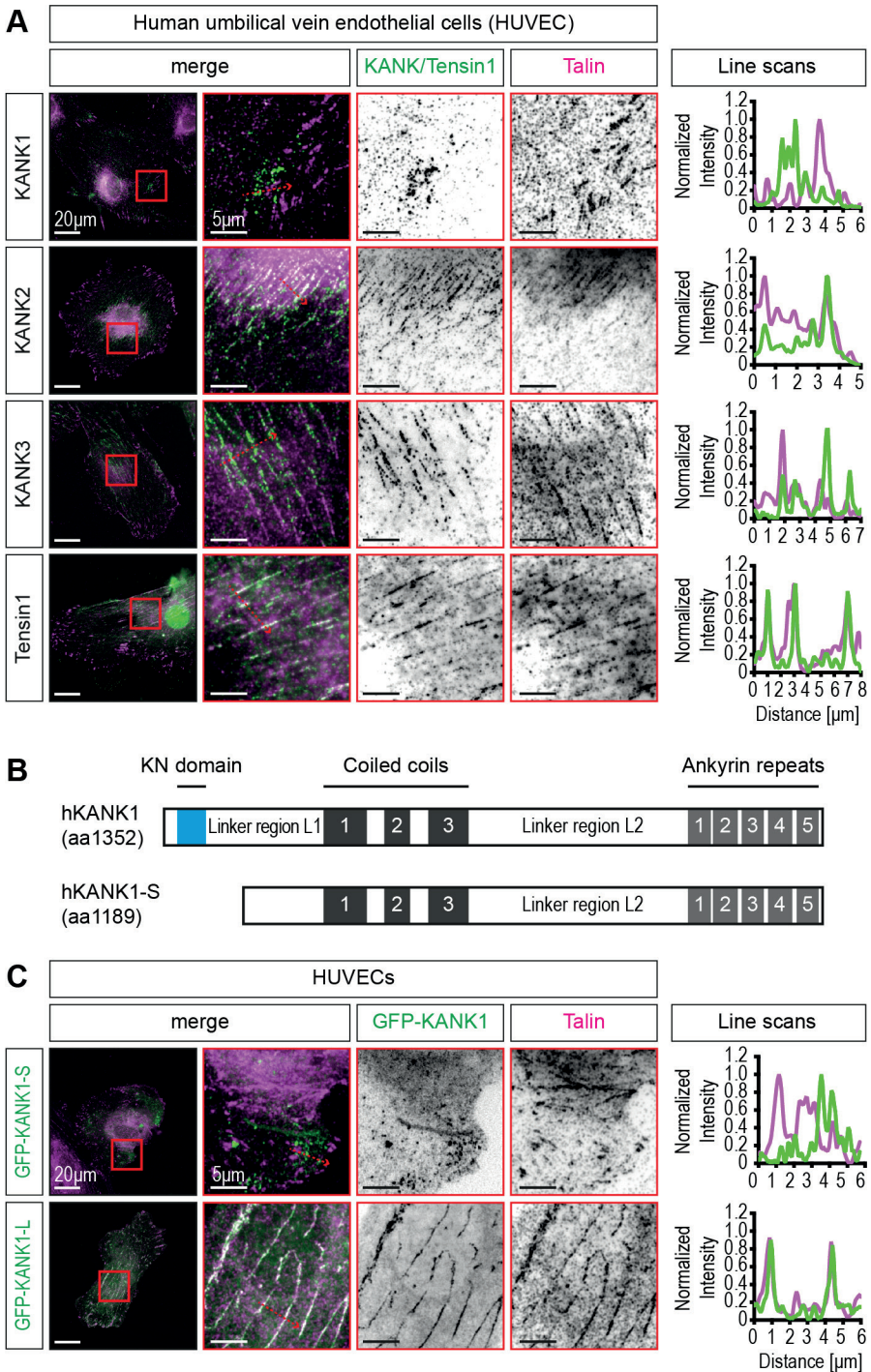
6

181

Figure 6. Figure 6. Endogenous KANK proteins and tensin1 together with talin in HUVECs
(**A**) Subcellular localization of endogenous KANK1 – 3 and tensin1 (all green) together with talin (magenta) in HUVECs. The right panel shows the plotted fluorescence intensities of the KANK/Tensin1 (green) and

talin (magenta) along the line indicated by the dashed red arrow in the inset. The fluorescence intensities were normalized to the maximum intensity of the corresponding channel. (**B**) Schematic overview of the two KANK1 isoforms. The short KANK1 isoform (KANK1-S, upper panel) is missing the first 158 amino acids, including the KN domain, at its N-terminus. (**C**) Subcellular localization of GFP-tagged KANK1-S (upper panel) and KANK1-L (lower panel) (both green) expressed in HUVECs stained for endogenous talin (magenta). The right panel shows the plotted fluorescence intensities of the GFP-KANK (green) and talin (magenta) along the line indicated by the dashed red arrow in the inset. The fluorescence intensities were normalized to the maximum intensity of the corresponding channel.

arrays of dots in the central part of the cell (Geiger and Yamada, 2011; Zaidel-Bar et al., 2004). FBs originate from the distal end of mature FAs, where they evolve into the thin elongated FBs by translocating centripetally to the cell center in an actomyosin-dependent manner (Pankov et al., 2000; Zamir et al., 1999; Zamir et al., 2000). Tensins are a group of FA adaptor proteins that are highly conserved in mammals. It has been shown that tensins are the main regulators of FB formation (Bernau et al., 2017; Georgiadou et al., 2017). The tensin protein family consists of four family members (tensin1 – 3 and C-terminal tensin-like protein (CTEN)). The tensin proteins possess a phosphotyrosine-binding (PTB) domain at their C-terminus which mediates binding to the cytoplasmic tail of β-integrins. Besides, tensins1 – 3 can also bind to the actin cytoskeleton with their N-terminal actin-binding domain (ABD), which is missing in CTEN (Lo, 2017). Tensin and talin both compete for the same binding site at β-integrins, the NPXY motif; yet, talin has a 100-fold higher binding affinity compared to tensin (McCleverty et al., 2007). Thus, under normal conditions talin is the major binding partner of β-integrins. It has been shown that talin binds to the unphosphorylated NPXY motif (Calderwood et al., 1999). However, the phosphorylation of the tyrosine (Y) residue of the NPXY motif strongly alleviates talin's affinity for β-integrin whereas tensin's binding affinity is not affected by tyrosine phosphorylation (McCleverty et al., 2007; Oxley et al., 2008). Therefore, it seems that the talin – tensin switch at β-integrins is regulated by a phosphorylation switch (McCleverty et al., 2007; Oxley et al., 2008). Furthermore, FBs and especially their actomyosin-dependent translocation to the cell center has been linked to remodeling of the ECM, in particular to fibronectin (FN) fibrillogenesis. The α5/β1-integrin-tensin complexes move extracellular dimeric FN and unfold it and thereby organize it into FN fibrils (Pankov et al., 2000). More recently, it was shown that tensins are negatively regulated by the AMP-activated protein kinase (AMPK) and that depletion of AMPK leads to higher levels of tensin1 and 3. This in turn results in increased activation of β1-integrins and consequently to more FBs (Georgiadou et al., 2017). In HUVECs stained for endogenous tensin1, we saw that it was mainly located at the central FBs where it co-localized with talin (Figure 6B).

KANK depletion in HUVECs does not affect the formation of tensin-positive FBs nor FN fibrils but could affect endothelial migration

When we stained HUVECs for endogenous KANKs (KANK1 – 3), tensin1 and FN, we saw strong overlap of KANK2, KANK3 and tensin1 together with FN fibrils (Figure 7A). To test whether KANK2 and KANK3, the two endogenous KANK proteins in HUVECs that are present at FBs, play are role in FN fibrillogenesis, we depleted them and also KANK1 via siRNA-mediated knockdown (Figure 7C). Around 48 hours after siRNA transfection, the transfected cells were trypsinized and re-seeded on uncoated
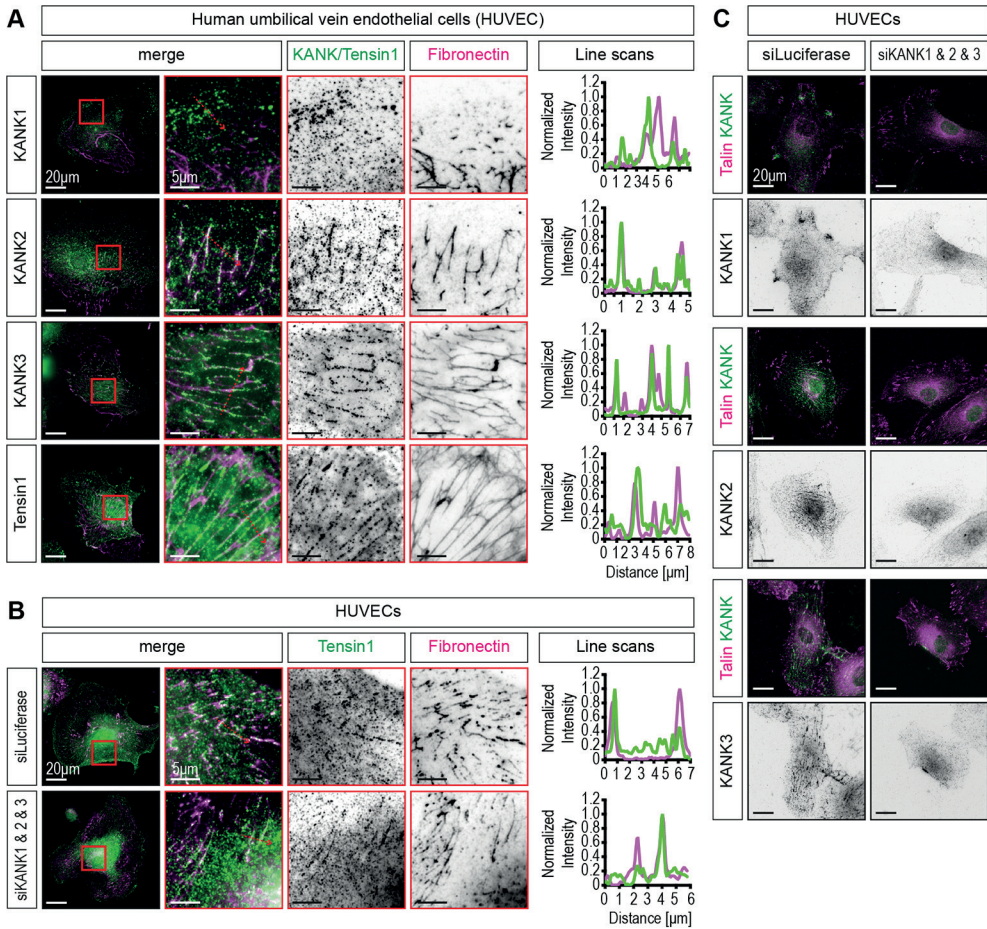
6

Figure 7. Knockdown of endogenous KANK proteins in HUVECs
(**A**) Immunofluorescence staining of endogenous KANK1 – 3 and tensin1 (all green) together with fibronectin (magenta) in HUVECs. (**B**) Staining of endogenous tensin1 (green) and fibronectin (magenta) in control HUVECs that were transfected with siRNA against Luciferase (siLuciferase, upper panel) and in KANK1-3-depleted HUVECs (siKANK1&2&3, lower panel). The right panel shows the plotted fluorescence intensities of the KANK/Tensin1 (green) and fibronectin (magenta) along the line indicated by the dashed red arrow in the inset. The fluorescence intensities were normalized to the maximum intensity of the corresponding channel. (**C**) Control staining of endogenous KANK1-3 (green) together with talin in control HUVECs and KANK1-3-depleted HUVECs to confirm the knockdown.

glass coverslips and allowed to attach for 2 hours. By doing this, we wanted to prevent analyzing FN fibrils that were already made by the cells before the knockdown became effective. After the 2-hour incubation, cells were fixed and stained for endogenous tensin1 and FN. Yet, the removal of all three endogenously expressed KANK proteins did not affect the formation of FN fibrils in the KANK-depleted HUVECs compared to control HUVECs (Figure 7B). Despite these negative results with HUVECs cultured in 2D, we decided to test whether removal of KANK2 and KANK3 affects endothelial migration in soft 3D matrices, as it has been suggested by a study that KANK proteins might play an evolutionary conserved role in mammalian vascular development (Hensley

et al., 2016). Therefore, we performed so-called spheroid-based sprouting assays using KANK2- and 3-depleted HUVECs embedded in a soft 3D matrix made of collagen I as described previously (Martin et al., 2013). Interestingly, in a first pilot experiment, we found that the length of individual sprouts was not affected in KANK-depleted spheroids compared to control spheroids. However, the number of (primary) sprouts emerging from the spheroids was reduced in the KANK-depleted spheroids compared to the control spheroids. Consequently, this led to reduced cumulative sprout length of the KANK-depleted spheroids (Figure 8). Nonetheless, it is important to mention that this was only a first pilot experiment and that further experiments are required to confirm whether the effect on sprout formation was a specific KANK-related effect, and not an unspecific side effect caused by the treatment of the cells with siRNAs and transfection reagents.
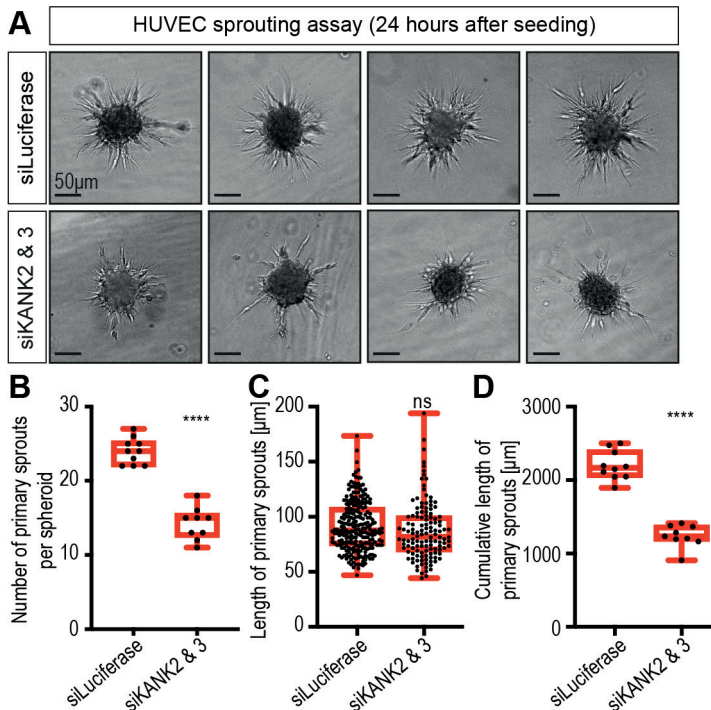

Figure 8. Spheroid-based sprouting assay in a soft 3D collagen I gel
(**A**) Examples of HUVEC spheroids 24 hours after seeding them in a soft 3D collagen I gel. The upper panel shows spheroids made of control HUVEC cells that were transfected with siRNA against Luciferase (siLuciferase). The lower panel shows spheroids made of KANK2- and 3-depleted HUVECs (siKANK2 & 3). (**B**) Number of primary sprouts per spheroid. (**C**) Length of primary sprouts. (**D**) Cumulative length of primary sprouts. All values are shown as box and whiskers plot (box represents 25th – 75th percentiles; whiskers represent Min and Max; the line represents the median). ns not significant; **** $p < 0.0001$ (unpaired t-test) ((9 – 10 spheroids were analyzed per condition).

Taken together, we conclude that in HUVECs KANK2 and KANK3 are strongly enriched at FBs. The recruitment of KANK2 and 3 to FBs is likely due to binding to talin as we showed in Chapter 5 for KANK2 in HeLa cells. Moreover, this is supported by the observation that the short isoform of KANK1 which lacks the first 158 amino acids, including the KN domain, cannot be found at FBs but is dispersed at the cell periphery.

In contrast to that, when overexpressing GFP-KANK1-L, which can bind to talin, we see strong accumulation of KANK1 at FBs just like endogenous KANK2 and 3. Nonetheless, the function of the KANK family proteins at FBs remains obscure, as the depletion of (all) endogenous KANK proteins did not affect the formation of talin-/tensin1-positive FBs nor the formation of FN fibrils. Yet, a first trial experiment with spheroid sprouting assays in collagen I-made 3D gel matrices suggested that removal of KANK2 and 3 might affect sprouting. Yet, this needs to be investigated more thoroughly to rule out unspecific side effects caused by the treatment of the cells with siRNAs and transfection reagents. However, with regard to the work of Hensley et al. who suggested that KANK proteins might have an evolutionarily conserved function in vascular development (Hensley et al., 2016), this seems to be an interesting lead worth to follow further.

Concluding remarks

In this thesis, we have combined biochemical and cellular experiments to gain more insight into the biochemistry of KANK family proteins and their role at the interface of cortical microtubule attachment complexes and integrin-mediated cell-matrix adhesions. We demonstrated that KANK1 directly binds to the adhesion protein talin and thereby recruits the cortical microtubule stabilizing complex to the vicinity of FAs. In addition to that, we also showed that the talin-KANK1 interaction is force regulated and that this interaction can withstand pulling forces in the physiological range for several seconds to minutes. Furthermore, we found that other factors, like the linker region L2 of KANK1, are contributing to the subcellular localization of the KANK proteins. Thus, it seems likely that the clustering of KANK proteins around FAs is likely regulated by both force and self-association/clustering of KANK1 proteins and binding partners. Besides, in our cell migration experiments we saw that KANKs proteins can also affect cell motility. All in all, the combined data from our studies emphasize the role of KANK family proteins (especially KANK1) as mediators of the cross-talk between MTs and FAs and as a scaffold for recruiting other proteins to the cell cortex to FAs. Yet, several open questions remain about KANK family proteins especially regarding their role in cell migration and the contradicting data on this. Moreover, it also remains to be resolved whether KANK proteins and their removal have a direct effect on FAs and whether they affect the activity of GEF-H1. Therefore, this thesis, with our insights on the interaction between talin and KANK proteins, should be seen as foundation for further research to better understand the interplay between cell-matrix adhesion (dynamics) and the MT cytoskeleton.

References

Aher, A., and A. Akhmanova. 2018. Tipping microtubule dynamics, one protofilament at a time. Curr Opin Cell Biol. 50:86-93.

Akhmanova, A., C.C. Hoogenraad, K. Drabek, T. Stepanova, B. Dortland, T. Verkerk, W. Vermeulen, B.M. Burgering, C.I. De Zeeuw, F. Grosveld, and N. Galjart. 2001. Clasps are CLIP-115 and -170 associating proteins involved in the regional regulation of microtubule dynamics in motile fibroblasts. Cell. 104:923-935.

Akhmanova, A., and M.O. Steinmetz. 2015. Control of microtubule organization and dynamics: two ends in the limelight. Nature Reviews Molecular Cell Biology. 16:711.

Atherton, P., B. Stutchbury, D. Jethwa, and C. Ballestrem. 2016. Mechanosensitive components of integrin adhesions: Role of vinculin. Exp Cell Res. 343:21-27.

Bachir, A.I., J. Zareno, K. Moissoglu, E.F. Plow, E. Gratton, and A.R. Horwitz. 2014. Integrin-associated complexes form hierarchically with variable stoichiometry in nascent adhesions. Curr Biol. 24:1845-1853.

Bachmann, A., and A. Straube. 2015. Kinesins in cell migration. Biochem Soc Trans. 43:79-83.

Barczyk, M., S. Carracedo, and D. Gullberg. 2010. Integrins. Cell Tissue Res. 339:269-280.

Bernau, K., E.E. Torr, M.D. Evans, J.K. Aoki, C.R. Ngam, and N. Sandbo. 2017. Tensin 1 Is Essential for Myofibroblast Differentiation and Extracellular Matrix Formation. Am J Respir Cell Mol Biol. 56:465-476.

Bershadsky, A., A. Chausovsky, E. Becker, A. Lyubimova, and B. Geiger. 1996. Involvement of microtubules in the control of adhesion-dependent signal transduction. Curr Biol. 6:1279-1289.

Bouchet, B.P., R.E. Gough, Y.C. Ammon, D. van de Willige, H. Post, G. Jacquemet, A.M. Altelaar, A.J. Heck, B.T. Goult, and A. Akhmanova. 2016a. Talin-KANK1 interaction controls the recruitment of cortical microtubule stabilizing complexes to focal adhesions. Elife. 5.

Bouchet, B.P., I. Noordstra, M. van Amersfoort, E.A. Katrukha, Y.C. Ammon, N.D. Ter Hoeve, L. Hodgson, M. Dogterom, P.W.B. Derksen, and A. Akhmanova. 2016b. Mesenchymal Cell Invasion Requires Cooperative Regulation of Persistent Microtubule Growth by SLAIN2 and CLASP1. Dev Cell. 39:708-723.

Bravo-Cordero, J.J., L. Hodgson, and J. Condeelis. 2012. Directed cell invasion and migration during metastasis. Curr Opin Cell Biol. 24:277-283.

Burridge, K., and C. Guilluy. 2016. Focal adhesions, stress fibers and mechanical tension. Exp Cell Res. 343:14-20.

Calderwood, D.A., R. Zent, R. Grant, D.J. Rees, R.O. Hynes, and M.H. Ginsberg. 1999. The Talin head domain binds to integrin beta subunit cytoplasmic tails and regulates integrin activation. J Biol Chem. 274:28071-28074.

Carlier, M.F., J. Pernier, P. Montaville, S. Shekhar, S. Kuhn, D. Cytoskeleton, and g. Motility. 2015. Control of polarized assembly of actin filaments in cell motility. Cell Mol Life Sci. 72:3051-3067.

Case, L.B., and C.M. Waterman. 2015. Integration of actin dynamics and cell adhesion by a three-dimensional, mechanosensitive molecular clutch. Nature Cell Biology. 17:955.

Chang, Y.C., P. Nalbant, J. Birkenfeld, Z.F. Chang, and G.M. Bokoch. 2008. GEF-H1 couples nocodazole-induced microtubule disassembly to cell contractility via RhoA. Mol Biol Cell. 19:2147-2153.

Chen, T., K. Wang, and X. Tong. 2017. In vivo and in vitro inhibition of human gastric cancer progress by upregulating Kank1 gene. Oncol Rep. 38:1663-1669.

Cseh, B., S. Fernandez-Sauze, D. Grall, S. Schaub, E. Doma, and E. Van Obberghen-Schilling. 2010. Autocrine fibronectin directs matrix assembly and crosstalk between cell-matrix and cell-cell adhesion in vascular endothelial cells. J Cell Sci. 123:3989-3999.

del Rio, A., R. Perez-Jimenez, R. Liu, P. Roca-Cusachs, J.M. Fernandez, and M.P. Sheetz. 2009. Stretching single talin rod molecules activates vinculin binding. Science. 323:638-641.

Desai, A., and T.J. Mitchison. 1997. Microtubule polymerization dynamics. Annu Rev

6

Cell Dev Biol. 13:83-117.

Ezratty, E.J., M.A. Partridge, and G.G. Gundersen. 2005. Microtubule-induced focal adhesion disassembly is mediated by dynamin and focal adhesion kinase. Nat Cell Biol. 7:581-590.

Folkman, J. 1971. Tumor angiogenesis: therapeutic implications. N Engl J Med. 285:1182-1186.

Garcin, C., and A. Straube. 2019. Microtubules in cell migration. Essays Biochem. 63:509-520.

Gee, H.Y., F. Zhang, S. Ashraf, S. Kohl, C.E. Sadowski, V. Vega-Warner, W. Zhou, S. Lovric, H. Fang, M. Nettleton, J.Y. Zhu, J. Hoefele, L.T. Weber, L. Podracka, A. Boor, H. Fehrenbach, J.W. Innis, J. Washburn, S. Levy, R.P. Lifton, E.A. Otto, Z. Han, and F. Hildebrandt. 2015. KANK deficiency leads to podocyte dysfunction and nephrotic syndrome. J Clin Invest. 125:2375-2384.

Geiger, B., and K.M. Yamada. 2011. Molecular architecture and function of matrix adhesions. Cold Spring Harb Perspect Biol. 3.

Georgiadou, M., J. Lilja, G. Jacquemet, C. Guzmán, M. Rafaeva, C. Alibert, Y. Yan, P. Sahgal, M. Lerche, J.B. Manneville, T.P. Mäkelä, and J. Ivaska. 2017. AMPK negatively regulates tensin-dependent integrin activity. J Cell Biol. 216:1107-1121.

Gough, R.E., and B.T. Goult. 2018. The tale of two talins - two isoforms to fine-tune integrin signalling. FEBS Lett. 592:2108-2125.

Goult, B.T., J. Yan, and M.A. Schwartz. 2018. Talin as a mechanosensitive signaling hub. J Cell Biol. 217:3776-3784.

Goult, B.T., T. Zacharchenko, N. Bate, R. Tsang, F. Hey, A.R. Gingras, P.R. Elliott, G.C. Roberts, C. Ballestrem, D.R. Critchley, and I.L. Barsukov. 2013. RIAM and vinculin binding to talin are mutually exclusive and regulate adhesion assembly and turnover. J Biol Chem. 288:8238-8249.

Gu, Y., and M. Zhang. 2018. Upregulation of the Kank1 gene inhibits human lung cancer progression in vitro and in vivo. Oncol Rep. 40:1243-1250.

Guo, Q., S. Liao, Z. Zhu, Y. Li, F. Li, and C. Xu. 2018. Structural basis for the recognition of kinesin family member 21A (KIF21A) by the ankyrin domains of KANK1 and KANK2 proteins. Journal of Biological Chemistry. 293:557-566.

Guo, X., W. Fan, X. Bian, and D. Ma. 2014. Upregulation of the Kank1 gene-induced brain glioma apoptosis and blockade of the cell cycle in G0/G1 phase. Int J Oncol. 44:797-804.

Hanahan, D., and R.A. Weinberg. 2011. Hallmarks of cancer: the next generation. Cell. 144:646-674.

Hemmings, L., D.J. Rees, V. Ohanian, S.J. Bolton, A.P. Gilmore, B. Patel, H. Priddle, J.E. Trevithick, R.O. Hynes, and D.R. Critchley. 1996. Talin contains three actin-binding sites each of which is adjacent to a vinculin-binding site. J Cell Sci. 109 (Pt 11):2715-2726.

Hensley, M.R., Z. Cui, R.F. Chua, S. Simpson, N.L. Shammas, J.Y. Yang, Y.F. Leung, and G. Zhang. 2016. Evolutionary and developmental analysis reveals KANK genes were co-opted for vertebrate vascular development. Sci Rep. 6:27816.

Holmgren, L., M.S. O'Reilly, and J. Folkman. 1995. Dormancy of micrometastases: balanced proliferation and apoptosis in the presence of angiogenesis suppression. Nat Med. 1:149-153.

Kakinuma, N., Y. Zhu, Y. Wang, B.C. Roy, and R. Kiyama. 2009. Kank proteins: structure, functions and diseases. Cell Mol Life Sci. 66:2651-2659.

Kaverina, I., O. Krylyshkina, and J.V. Small. 1999. Microtubule targeting of substrate contacts promotes their relaxation and dissociation. J Cell Biol. 146:1033-1044.

Kaverina, I., K. Rottner, and J.V. Small. 1998. Targeting, capture, and stabilization of microtubules at early focal adhesions. J Cell Biol. 142:181-190.

Kim, I., J. Kang, H.Y. Gee, and J.W. Park. 2018. A novel HIF1AN substrate KANK3 plays a tumor-suppressive role in hepatocellular carcinoma. Cell Biol Int. 42:303-312.

Krylyshkina, O., K.I. Anderson, I. Kaverina, I. Upmann, D.J. Manstein, J.V. Small, and D.K. Toomre. 2003. Nanometer targeting of

6

microtubules to focal adhesions. J Cell Biol. 161:853-859.

Kumar, A., M. Ouyang, K. Van den Dries, E.J. McGhee, K. Tanaka, M.D. Anderson, A. Groisman, B.T. Goult, K.I. Anderson, and M.A. Schwartz. 2016. Talin tension sensor reveals novel features of focal adhesion force transmission and mechanosensitivity. J Cell Biol. 213:371-383.

Lansbergen, G., I. Grigoriev, Y. Mimori-Kiyosue, T. Ohtsuka, S. Higa, I. Kitajima, J. Demmers, N. Galjart, A.B. Houtsmuller, F. Grosveld, and A. Akhmanova. 2006. CLASPs attach microtubule plus ends to the cell cortex through a complex with LL5beta. Dev Cell. 11:21-32.

Lo, S.H. 2017. Tensins. Curr Biol. 27:R331-r332.

Martin, M., I. Geudens, J. Bruyr, M. Potente, A. Bleuart, M. Lebrun, N. Simonis, C. Deroanne, J.C. Twizere, P. Soubeyran, P. Peixoto, D. Mottet, V. Janssens, W.K. Hofmann, F. Claes, P. Carmeliet, R. Kettmann, H. Gerhardt, and F. Dequiedt. 2013. PP2A regulatory subunit Bα controls endothelial contractility and vessel lumen integrity via regulation of HDAC7. Embo j. 32:2491-2503.

McCleverty, C.J., D.C. Lin, and R.C. Liddington. 2007. Structure of the PTB domain of tensin1 and a model for its recruitment to fibrillar adhesions. Protein Sci. 16:1223-1229.

Medves, S., L.A. Noel, C.P. Montano-Almendras, R.I. Albu, H. Schoemans, S.N. Constantinescu, and J.B. Demoulin. 2011. Multiple oligomerization domains of KANK1-PDGFRbeta are required for JAK2-independent hematopoietic cell proliferation and signaling via STAT5 and ERK. Haematologica. 96:1406-1414.

Mimori-Kiyosue, Y., I. Grigoriev, G. Lansbergen, H. Sasaki, C. Matsui, F. Severin, N. Galjart, F. Grosveld, I. Vorobjev, S. Tsukita, and A. Akhmanova. 2005. CLASP1 and CLASP2 bind to EB1 and regulate microtubule plus-end dynamics at the cell cortex. J Cell Biol. 168:141-153.

Ng, D.H., J.D. Humphries, A. Byron, A. Millon-Frémillon, and M.J. Humphries. 2014. Microtubule-dependent modulation of adhesion complex composition. PLoS One. 9:e115213.

Niwa, S., K. Nakajima, H. Miki, Y. Minato, D. Wang, and N. Hirokawa. 2012. KIF19A is a microtubule-depolymerizing kinesin for ciliary length control. Dev Cell. 23:1167-1175.

Oxley, C.L., N.J. Anthis, E.D. Lowe, I. Vakonakis, I.D. Campbell, and K.L. Wegener. 2008. An integrin phosphorylation switch: the effect of beta3 integrin tail phosphorylation on Dok1 and talin binding. J Biol Chem. 283:5420-5426.

Pan, W., K. Sun, K. Tang, Q. Xiao, C. Ma, C. Yu, and Z. Wei. 2018. Structural insights into ankyrin repeat-mediated recognition of the kinesin motor protein KIF21A by KANK1, a scaffold protein in focal adhesion. J Biol Chem. 293:1944-1956.

Pankov, R., E. Cukierman, B.Z. Katz, K. Matsumoto, D.C. Lin, S. Lin, C. Hahn, and K.M. Yamada. 2000. Integrin dynamics and matrix assembly: tensin-dependent translocation of alpha(5)beta(1) integrins promotes early fibronectin fibrillogenesis. J Cell Biol. 148:1075-1090.

Paradžik, M., J.D. Humphries, N. Stojanović, D. Nestić, D. Majhen, A. Dekanić, I. Samaržija, D. Sedda, I. Weber, M.J. Humphries, and A. Ambriović-Ristov. 2020. KANK2 Links αVβ5 Focal Adhesions to Microtubules and Regulates Sensitivity to Microtubule Poisons and Cell Migration. Front Cell Dev Biol. 8:125.

Parangi, S., M. O'Reilly, G. Christofori, L. Holmgren, J. Grosfeld, J. Folkman, and D. Hanahan. 1996. Antiangiogenic therapy of transgenic mice impairs de novo tumor growth. Proc Natl Acad Sci U S A. 93:2002-2007.

Petrie, R.J., and K.M. Yamada. 2012. At the leading edge of three-dimensional cell migration. J Cell Sci. 125:5917-5926.

Pickup, M.W., J.K. Mouw, and V.M. Weaver. 2014. The extracellular matrix modulates the hallmarks of cancer. EMBO Rep. 15:1243-1253.

Pollard, T.D., and J.A. Cooper. 2009. Actin, a Central Player in Cell Shape and Movement. Science. 326:1208-1212.

Rafiq, N.B.M., Y. Nishimura, S.V. Plotnikov, V. Thiagarajan, Z. Zhang, S. Shi, M. Natarajan, V. Viasnoff, P. Kanchanawong, G.E. Jones, and A.D. Bershadsky. 2019. A mechano-signalling network linking microtubules, myosin IIA filaments and

6

integrin-based adhesions. Nature Materials. 18:638-649.

Ren, X.D., W.B. Kiosses, and M.A. Schwartz. 1999. Regulation of the small GTP-binding protein Rho by cell adhesion and the cytoskeleton. Embo j. 18:578-585.

Ren, Y., R. Li, Y. Zheng, and H. Busch. 1998. Cloning and characterization of GEF-H1, a microtubule-associated guanine nucleotide exchange factor for Rac and Rho GTPases. J Biol Chem. 273:34954-34960.

Sarkar, S., B.C. Roy, N. Hatano, T. Aoyagi, K. Gohji, and R. Kiyama. 2002. A novel ankyrin repeat-containing gene (Kank) located at 9p24 is a growth suppressor of renal cell carcinoma. J Biol Chem. 277:36585-36591.

Stehbens, S., and T. Wittmann. 2012. Targeting and transport: How microtubules control focal adhesion dynamics. Journal of Cell Biology. 198:481-489.

Sun, Z., H.Y. Tseng, S. Tan, F. Senger, L. Kurzawa, D. Dedden, N. Mizuno, A.A. Wasik, M. Thery, A.R. Dunn, and R. Fassler. 2016. Kank2 activates talin, reduces force transduction across integrins and induces central adhesion formation. Nat Cell Biol. 18:941-953.

van der Vaart, B., W.E. van Riel, H. Doodhi, J.T. Kevenaar, E.A. Katrukha, L. Gumy, B.P. Bouchet, I. Grigoriev, S.A. Spangler, K.L. Yu, P.S. Wulf, J. Wu, G. Lansbergen, E.Y. van Battum, R.J. Pasterkamp, Y. Mimori-Kiyosue, J. Demmers, N. Olieric, I.V. Maly, C.C. Hoogenraad, and A. Akhmanova. 2013. CFEOM1-associated kinesin KIF21A is a cortical microtubule growth inhibitor. Dev Cell. 27:145-160.

Wang, Y., Y. Onishi, N. Kakinuma, B.C. Roy, T. Aoyagi, and R. Kiyama. 2005. Alternative splicing of the human Kank gene produces two types of Kank protein. Biochem Biophys Res Commun. 330:1247-1253.

Weng, Z., Y. Shang, D. Yao, J. Zhu, and R. Zhang. 2018. Structural analyses of key features in the KANK1.KIF21A complex yield mechanistic insights into the cross-talk between microtubules and the cell cortex. J Biol Chem. 293:215-225.

Winograd-Katz, S.E., R. Fässler, B. Geiger, and K.R. Legate. 2014. The integrin adhesome: from genes and proteins to human disease. Nature Reviews Molecular Cell Biology. 15:273-288.

World Health Organization. 2018. Fact sheets on cancer. Vol. 2020.

Yamada, K.M., and M. Sixt. 2019. Mechanisms of 3D cell migration. Nat Rev Mol Cell Biol. 20:738-752.

Yamashiro, S., and N. Watanabe. 2014. A new link between the retrograde actin flow and focal adhesions. J Biochem. 156:239-248.

Zaidel-Bar, R., M. Cohen, L. Addadi, and B. Geiger. 2004. Hierarchical assembly of cell-matrix adhesion complexes. Biochem Soc Trans. 32:416-420.

Zamir, E., B.Z. Katz, S. Aota, K.M. Yamada, B. Geiger, and Z. Kam. 1999. Molecular diversity of cell-matrix adhesions. J Cell Sci. 112 (Pt 11):1655-1669.

Zamir, E., M. Katz, Y. Posen, N. Erez, K.M. Yamada, B.Z. Katz, S. Lin, D.C. Lin, A. Bershadsky, Z. Kam, and B. Geiger. 2000. Dynamics and segregation of cell-matrix adhesions in cultured fibroblasts. Nat Cell Biol. 2:191-196.

Zhou, X., R.G. Rowe, N. Hiraoka, J.P. George, D. Wirtz, D.F. Mosher, I. Virtanen, M.A. Chernousov, and S.J. Weiss. 2008. Fibronectin fibrillogenesis regulates three-dimensional neovessel formation. Genes Dev. 22:1231-1243.

Zhu, Y., N. Kakinuma, Y. Wang, and R. Kiyama. 2008. Kank proteins: a new family of ankyrin-repeat domain-containing proteins. Biochim Biophys Acta. 1780:128-133.

6

6

&
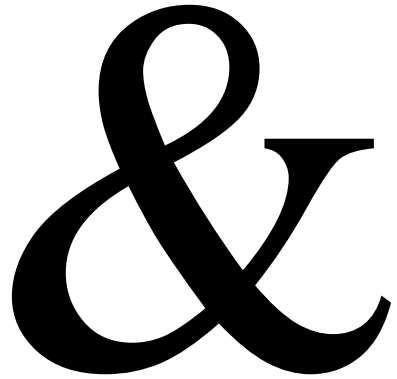
Addendum

- Summary

- Nederlandse samenvatting

- Curriculum vitae

- List of publications

- Acknowldgement

Summary

In animals (multicellular organisms), the contact between cells and the extracellular matrix (ECM) is mediated through cell-matrix adhesion complexes. These complexes are essential for the integrity of tissues as they keep cells in their places. Yet, they are also important for cell motility. Thereby, cell-matrix adhesion complexes transduce the mechanical forces generated by the cell to the ECM and vice versa. As a result of that they promote movement of the cell.

Cell-matrix adhesions consist primarily of heterodimeric alpha/beta integrins, the adaptor protein talin and the cytoskeletal protein actin. Integrins span through the cell membrane and bind with their extracellular part to ECM proteins such as fibronectins or collagens. Inside the cell, integrins bind to talin which in turn binds to actin. Thereby, talin connects the ECM with the cytoskeleton and functions as a "molecular clutch". Talin can change its conformation depending on the mechanical forces that are applied to it. Through these conformational changes other proteins can bind to talin and thereby be recruited to cell-matrix adhesions.

Microtubules, which are another part of the cytoskeleton, are built of alpha/beta-tubulin dimers. These tubulin dimers associate with one another (head-tail interactions) and form protofilaments. Several protofilaments together form a hollow microtubule. Microtubules are polarized with a fast growing plus end and a slow growing minus end. Microtubules play an important role in the regulation of the formation and break down of cell-matrix adhesions. Furthermore, microtubules can function as transport tracks for building material and signaling molecules.

The plus ends of microtubules are anchored and stabilized at the cell membrane in close proximity to cell-matrix adhesion complexes by another specialized protein complex, the cortical microtubule-stabilizing complex (CMSC). The CMSC is formed by several proteins including KANK proteins. Especially KANK1 plays a crucial role in CMSCs. So far there are four KANK proteins (KANK1-4) known in humans. All KANK family proteins share the same structure: at their N-terminus the conserved KANK N-terminal (KN) domain can be found. At the C-terminus are five highly conserved ankyrin repeats (ANKR1-5) located. In the middle of the protein sit the coiled coil (CC) domains. In total there exist four different CC domains among the KANK family of which the composition and number can vary among the KANK proteins. Between the KN domain and the CC domains sits a short linker region L1 and a longer linker region L2 is located between the CC domains and the ankyrin repeats.

In this thesis, we analyzed the role of KANK proteins (mainly KANK1) in the interaction between cell-matrix adhesions and microtubules. We showed that KANK1 can directly bind to the cell-matrix adhesion protein talin and thereby link cell-matrix adhesions and the CMSC with one another. The talin-KANK1 interaction is required for the correct formation of CMSCs in the vicinity of adhesion complexes. Moreover, the loss of KANK proteins perturbs the organization of microtubules in the periphery of cells. Without KANK the CMSC is not formed as a result of that microtubules do not stop growing in the vicinity of adhesions but keep on growing (Chapter 2).

Furthermore, we discovered that the interaction between talin and KANK1 is regulated by mechanical forces. Using a molecular tweezer, we have demonstrated that the

&

connection between talin and the KANK1 KN domain gets stronger with increasing pulling forces. This connection reaches it most stable point at pulling forces of 6 pN. Thereafter, the talin-KANK1 interaction gets weaker when the applied pulling forces increase further. With our experiments in cells we could show that this force regulation affects the localization of KANK1 in cells. KANK1 proteins that are bound to talin and that are exposed to mechanical (pulling) forces show a strong preference for the rim of cell-matrix adhesion complexes (Chapter 3).

Another aspect that we looked at was which other factors might affect the localization of KANK proteins in cells, especially around adhesion complexes. We were able to show that the long linker region L2 of KANK1 plays an important role in recruiting KANK proteins to the rim of cell-matrix adhesion complexes. Yet, the exact mechanism how the L2 regions does this remains elusive. Besides, we were able to identify a new binding partner of KANK1, the dynein light chain protein LC8 (LC8) which binds to the linker region L2. However, the KANK1-LC8 interaction is not necessary to recruit KANK proteins to the rim of adhesion complexes. It rather appears that some sort of self-association mechanism of KANK1 proteins is responsible for the rim localization (Chapter 4).

Finally, we studied the differences between KANK1 and KANK2. We saw that KANK1 localizes preferentially at the cell periphery around cell-matrix adhesion complexes whereas KANK2 can be mainly found at the central part of the cell. The factors that are responsible for the different distributions of KANK1 and KANK2 have not been discovered yet. Moreover, we analyzed the role of KANK1 and KANK2 in cell motility which seems to be cell line specific. In HeLa cells, we observed that the removal of both KANK proteins barely affected cell motility. Yet, when we removed KANK2 in the breast cancer cell line SUM159PT we saw a strong negative effect on cell migration whereas the removal of KANK1 did not (Chapter 5).

In this thesis, we have shown that KANK proteins, especially KANK1, can interact with several different proteins, such as the adhesion protein talin, through their different domains and regions. Hereby, our studies underline the complexity of the molecular mechanisms and physical forces which regulate the interaction between talin and KANK and in a broader sense between cell-matrix adhesion complexes and microtubules.

&

Nederlandse samenvatting

In meercellige organismen is contact tussen cellen en de extracellulaire matrix (ECM) gefaciliteerd door aanhechtingscomplexen. Deze cel-matrix aanhechtingscomplexen zijn essentieel voor de integriteit van weefsels, doordat ze cellen op hun plaats houden. Ook zijn ze belangrijk voor de cel-motiliteit. Dit doen ze door mechanische krachten door te geven van de cel naar de ECM en andersom, en bevorderen hiermee verplaatsing van de cel.

Cel-matrix aanhechtingscomplexen bestaan voornamelijk uit de heterodimere α/β-integrines, het eiwit talin en het cytoskelet-onderdeel actine. Integrines zitten in de celmembraan en steken aan de buitenkant van de cel uit, waar ze aan ECM-eiwitten kunnen binden (bijvoorbeeld aan fibronectines of collagenen). Aan de binnenkant van de cel binden ze aan talin, die vervolgens aan actine bindt. Zo brengt talin de ECM samen met het cytoskelet en werkt het als een "moleculaire koppeling". Afhankelijk van de mechanische krachten die op talin werken kan het zijn conformatie veranderen. Door deze conformatie veranderingen kunnen andere eiwitten aan talin binden en zo gerekruteerd worden naar cel-matrix aanhechtingscomplexen.

Microtubuli, die onderdeel zijn van het cytoskelet, bestaan uit α/β-tubuline dimeren. Deze tubuline dimeren zijn met elkaar geassocieerd (kop-staart interacties) en vormen protofilamenten. Meerdere protofilamenten samen vormen een microtubule. Microtubuli zijn gepolariseerd met een snelgroeiend plus-eind en een langzaam groeiend min-eind. Microtubuli spelen een belangrijke rol in de regulatie van de vorming en de afbraak van cel-matrix aanhechtingscomplexen. Daarnaast kunnen MT ook als spoor gebruikt worden voor het transport van bouwmateriaal en signaalmoleculen.

De plus-einden van MT worden door een ander eiwitcomplex, het corticale microtubule-stabilisatie complex (CMSC), gestabiliseerd en in de buurt van aanhechtingscomplexen aan de celmembraan gehecht. Het CMSC worden gevormd door verschillende eiwitten, waaronder KANK-eiwitten. Met name KANK1 speelt hierbij een belangrijk rol. In mensen zijn er voor zover bekend vier verschillende KANK-eiwitten (KANK1-4) gevonden. Alle KANK-eiwitten hebben dezelfde opbouw: aan de N-terminus zit het geconserveerde KANK N-terminale (KN) domein. Aan de C-terminale einden zijn de vijf ankyrin herhalingen (ANKR1-5) sterk geconserveerd en in het midden van het eiwit zittten nog coiled coil (CC) domeinen. In totaal bestaan er in de KANK-eiwitten vier verschillende "coiled coil" (CC) domeinen, waarvan de samenstelling sterk kan verschillen. Tussen het KN-domein en de CC-domeinen zit nog een L1 verbindingsstuk en een langer L2 verbindingsstuk tussen de CC-domeinen en ankyrin herhalingen.

In dit proefschrift hebben we de rol van KANK-eiwitten (vooral KANK1) en de interactie tussen cel-matrix aanhechtingen en microtubuli onderzocht. We laten zien dat KANK1 direct aan het aanhechtingscomplex-eiwit talin bindt en zo kan KANK1 de aanhechtingscomplexen en CMSCs aan elkaar koppelen. De talin-KANK1 interactie is nodig voor de juiste vorming van CMSCs in de buurt van cel-matrix aanhechtingen. Bovendien leidt het weghalen van KANK1 tot een verstoorde organisatie van microtubuli in de periferie van de cel. Zonder KANK1 wordt het CMSC-complex niet meer gevormd waardoor de groei van microtubuli niet kan worden gestopt en de microtubuli door blijven groeien (hoofdstuk 2).

Wat we nog meer hebben ontdekt is dat de interactie tussen talin en KANK1 door mechanische krachten gereguleerd wordt. Met een moleculaire pincet hebben we laten zien dat de verbinding tussen het KN-domein van KANK1 en talin met toenemende trekkracht sterker wordt. Bij een trekkracht van 6 pN bereikt deze interactie zijn sterkste punt. Daarna wordt de talin-KANK1 verbinding zwakker als de trekkracht verder toeneemt. Met cellulaire experimenten hebben we aangetoond dat deze mechanische regulatie de lokalisatie van KANK-eiwitten beïnvloed. KANK-eiwitten die aan talin binden en waarop mechanische krachten werken, hebben een sterke voorkeur voor de buitenrand van de cel-matrix aanhechtingscomplexen (hoofdstuk 3).

Een ander aspect wat we hebben onderzocht is welke andere factoren de lokalisatie van KANK-eiwitten in cellen kunnen beïnvloeden, met name in de omgeving van aanhechtingscomplexen. Hierbij hebben we ontdekt dat het verbindingsstuk L2 van KANK1 een belangrijke rol speelt om KANK-eiwitten naar de buitenrand van aanhechtingscomplexen te rekruteren. Het exacte mechanisme hoe L2 dit doet is nog niet bekend. Wel hebben we gezien dat een nieuwe bindingspartner van KANK1, het dynein "light-chain"-eiwit LC8 (LC8), aan L2 kan binden. Deze interactie tussen LC8 en het KANK1-verbindingsstuk L2 is echter niet noodzakelijk om KANK-eiwitten naar de buitenrand van aanhechtingscomplexen te brengen. Zo blijkt dat een zelf-associatie mechanisme van KANK1-eiwitten hiervoor verantwoordelijk is (hoofdstuk 4).

Tot slot hebben we ook het verschil tussen KANK1 en KANK2 bestudeerd. We hebben gezien dat KANK1 zich voornamelijk aan de rand van de cel bevindt en KANK2 vooral in het midden. De exacte factoren die verantwoordelijk zijn voor de verschillende distributie van KANK1 en KANK2 hebben we nog niet kunnen identificeren. Verder hebben we gekeken naar het effect van KANK-eiwitten op cel-motiliteit en dit lijkt sterk afhankelijk te zijn van de cellijn. In HeLa-cellen heeft het weghalen van KANK1 en KANK2 weinig invloed, maar in SUM159PT borstkankercellen heeft een verlies aan KANK2 een negatief effect op de cel-motiliteit. Het weghalen van KANK1 heeft hier verder geen invloed op (hoofdstuk 5).

In dit proefschrift hebben we laten zien dat KANK-eiwitten, en met name KANK1, door hun verschillende domeinen en verbindingsstukken met verschillende eiwitten kunnen samenwerken, zoals met het aanhechtingseinwit talin. Onze studie onderstreept hiermee de complexiteit van de moleculaire mechanismen en fysieke krachten, die de interactie reguleren tussen talin en KANK en in de bredere zin tussen cel-matrix aanhechtingscomplexen en microtubuli.

&

Curriculum vitae

York-Christoph Ammon was born on November 27th, 1988 in Braunschweig, Germany. In 2008 he obtained his A-level (Abitur) from the Wilhelm-Remy Gymnasium in Bendorf, Germany. After serving his mandatory year in the military and civil service, he started his bachelor studies in Molecular Biomedicine at Bonn University, Germany, in 2009. After obtaining his bachelor's degree in 2012, he stayed at Bonn University to continue with his master studies in Drug Research. He did his master thesis research internship in the Pharmaceutical Institute in the group of Prof. dr. Christa Müller. During his internship he was involved in establishing proximity ligation assays in order to study receptor-receptor interaction. He graduated in 2015 with distinction.

At the beginning of 2016, York joined the lab of Prof. dr. Anna Akhmanova at Utrecht University, The Netherlands. During his PhD studies he focused on trying to understand the role of KANK family proteins in the interplay between cell-matrix adhesions and microtubules. The results of this research are described in this thesis.

&

List of publications

Force-Dependent Regulation of Talin-KANK1 Complex at Focal Adhesions
Yu, M.*, S. Le*, **<u>Y. C. Ammon</u>***, B. T. Goult, A. Akhmanova and J. Yan.
Nano Lett 19(9): 5982-5990 (2019)

Systematic identification of recognition motifs for the hub protein LC8
Jespersen, N., A. Estelle, N. Waugh, N. E. Davey, C. Blikstad, **<u>Y. C. Ammon</u>**, A. Akhmanova, Y. Ivarsson, D. A. Hendrix and E. Barbar.
Life Sci Alliance 2(4) (2019)

Adenosine A2A receptor ligand recognition and signaling is blocked by A2B receptors
Hinz, S., G. Navarro, D. Borroto-Escuela, B. F. Seibt, **<u>Y. C. Ammon</u>**, E. de Filippo, A. Danish, S. K. Lacher, B. Cervinkova, M. Rafehi, K. Fuxe, A. C. Schiedel, R. Franco and C. E. Muller.
Oncotarget 9(17): 13593-13611 (2018)

Mesenchymal Cell Invasion Requires Cooperative Regulation of Persistent Microtubule Growth by SLAIN2 and CLASP1
Bouchet, B. P.*, I. Noordstra*, M. van Amersfoort, E. A. Katrukha, **<u>Y. C. Ammon</u>**, N. D. Ter Hoeve, L. Hodgson, M. Dogterom, P. W. B. Derksen and A. Akhmanova.
Dev Cell 39(6): 708-723 (2016)

Talin-KANK1 interaction controls the recruitment of cortical microtubule stabilizing complexes to focal adhesions
Bouchet, B. P., R. E. Gough, **<u>Y. C. Ammon</u>**, D. van de Willige, H. Post, G. Jacquemet, A. M. Altelaar, A. J. Heck, B. T. Goult and A. Akhmanova.
Elife 5 (2016)

* these authors contributed equally

&

Acknowledgement

After almost five years of hard work this journey has come to an end. Even though it might appear from the outside that a PhD is mostly an individual effort – it is more like a great team effort and without the support from many amazing colleagues, friends and my family this would not have been possible and I would not be standing where I am right now. Therefore, this section is dedicated to all people that supported me during my PhD. Yet, I am also aware that during five years you encounter many great people and there is always the danger of forgetting someone during the acknowledgement. Therefore, I already would like to apologize in case that I missed someone.

First, I would like to thank my supervisor and promotor Anna Akhmanova. Anna, thank you so much that you gave me the opportunity to do my PhD in your lab. Over the past five years, you have guided me through the ups-and-downs of a PhD project. You always knew the right things to say to keep me motivated and to go for the extra mile. This ability of you to lead and manage a lab of so many different people and to find the right words to motivate each one of us is truly impressive. Moreover, your passion for science, your dedication to your work and your vast knowledge about biology amazed me. I wish you and the lab all the best of luck for the future and I hope that you keep your passion and dedication for your work so that many more aspiring young researchers can be inspired by it.

Lukas, I have always experienced you as an enthusiastic, dedicated and funny person. Moreover, I have always appreciated your critical insights about my projects during work discussions. I wish you and your group all the best for the future. And of course, many thanks for being on my thesis committee and taking the time to evaluate my thesis. Sander, also many thanks to you for being a member of my thesis committee and evaluating my thesis. I have always welcomed your insightful comments on my work during work discussions and seminars. Besides, I really appreciated our conversations during dinner at PolarNet meetings. I wish you and the rest of your group all the best of luck for the future.
Moreover, I also would like to express my gratitude towards the other members of my thesis committee, Madelon Maurice, Arnoud Sonnenberg and Willem Stoorvogel. Thank you for your commitment of time and effort to be on this committee and to evaluate my thesis.

During my PhD, I have had the great opportunity to be part of multiple collaboration projects with several groups and PIs outside the UU.
First, I would like to thank Jie Yan and his mechanobiology group in Singapore. Especially, I would like to thank Shimin Le and Miao Yu for giving me the opportunity to be a co-first author on your amazing work about the mechanical regulation about the talin-KANK1 interaction. I really appreciated working with you, and I wish you all the best for your future (scientific pursuits).
Moreover, I have to thank Elisar Barbar and her group at Oregon State University, especially Nathan Jespersen and Aidan Estelle. Thank you for all your insights about

&

dynein light chain LC8 and our joint project to analyze what LC8 and KANK1 are doing together.

Last but not least, I would like to express my gratitude towards Ben Goult and his group at Kent University. Ben, you and the collaborative projects about the talin-KANK interaction have basically accompanied from the beginning of my PhD. I really enjoyed our email conservations about KANK and talin. Thereby, I enjoyed especially your down-to-earth attitude which I could see in our conversations that were not about science but about family, dogs and football. I wish you and your family all the best for the future. I truly hope that we can hit the links together one day.

Over the years, I have had many great colleagues at the Akhmanova lab. First and foremost, I would like to thank Peter Jan (PJ). We both started around the same time with our PhDs and ever since our first meeting at the sushi restaurant [with the other lab members, where the both of us were struggling miserably using chopsticks :-)] I felt this special connection. Since then, we have been through the ups-and-downs of a PhD together and I really appreciated that you always had an open ear and time for a quick chat when things were not going smoothly or when there were things to celebrate. Moreover, you were a real inspiration to me: I was and I am still amazed how well you managed all the things that came upon you during your PhD; yet, you never lost your smile nor your friendly attitude towards your colleagues and you were always willing to help. This is really one of your great strengths and I hope that you keep this wonderful ability no matter what things may come in your future. Besides, I am really happy that we both can finish our journey together and I feel honored to be your paranymph during this special day and that you agreed to be one of my paranymphs. I wish you and Rosanna all the best and luck in the world for your future and I hope that we manage to keep in touch after finishing our PhDs. By the way, thanks for teaching me most of the Dutch swearwords!!! ;-)

Besides PJ there was another companion who traveled with me from the start till the end of my time at Cell Biology: Chiung-Yi. You started one month after me with your PhD and as foreigners we both went through the same struggles at the beginning (like waiting for a BSN number or learning Dutch). Like PJ, you were another great partner in conversations about the ups-and-downs during a PhD and about the future after a PhD. For the future, I wish you and your soon-to-be husband George all the best.

A little bit later another great colleague joined our lab and my office, Cyntha. Thank you very much for convincing me to give top-rope climbing a try – you were totally right it is amazing, and I personally find it much better than bouldering (sorry Boris, Kyle and Milena). Moreover, thank you for all the cookies that I could "borrow" from you and for being such a great Dutch teacher :-) And thank you for all our talks about the ordering and organizational things in the lab that were not always running that smoothly and last but not least that you agreed to be my other paranymph. I wish you for the rest of your PhD all the best and some nice publications.

The same goes for Dipti, the latest addition to our office. When you started you had some big shoes to fill in (Amol's) – yet, I would say that you managed perfectly and since then you have been amazing us with your hard dedication and crazy working hours :-) As Cyntha, I wish you the best of luck and some nice publications for the rest of your PhD.

Ivar, you were one of the senior PhDs when I joined the lab in 2016. I was so impressed how well you handled all your work and extracurricular activities in the lab and still you managed to have a great work-life-balance while performing with your band in the weekends or preparing for a triathlon. I wish you and your wife Lilian all the luck of the world and a great time in Australia (be careful of all the poisonous animals!). Amol, my film buddy. You were another senior PhD when I joined the lab, and as with Ivar, I was so amazed how you owned you projects and how much you knew about microtubule-related topics and beyond. Yet, I was even more impressed by your enthusiasm about movies and series. I really enjoyed our conversations about Game of Thrones and other series during our daily walks to the UMC canteen. I wish you a great time at Big Apple and all the luck for your future (scientific endeavors). By the way, I finally watched "The Wire"! You were right! It is an amazing series. Chao, our EB expert and the biggest FC Utrecht supporter from our department that I know. I have to thank you for all our great discussions and post-game analyses of football (mostly Champions League) games. I wish you and your small family all the luck for the future. Ankit, your kindness, your calm approach to all your projects and work in the lab always intrigued me. I enjoyed our talks about India, and I press my thumbs for you and your family that you find a nice position in India closer to your families. Ilya, lord of the microscopes, thank you for your funny introductions and all your help with the microscopes (especially during my FRAP experiments). I really enjoyed our conversations about Russia and Germany and your special kind of humor. Eugene, the other master of the microscopes, thank you for all your help with the microscopes and the analyses. I really enjoyed our conversations about (ice) hockey and the Pittsburgh Penguins. I wish you and your wife Desiree all the best for the future and lots of joy with your house. Maud, like Ben (Bouchet) you taught me many things about culturing cells and especially how to take care of HUVECs. Thank you for all your support during my PhD and I am so happy that you found a nice position in Belgium close to your family. Milena, our organoid and keratin expert. For the remainder of your PhD I wish you all the best and I hope that you get some nice publications out of your organoid work. Hugo, already when you were PJ's master student I was impressed by your enthusiasm about research and you drive to try new ways to analyze your (image) data. Lately, as a PhD student you have astonished us with your formidable expansion microscopy work. I wish you all the best for the future and that you can enjoy your house. Emma, the latest PhD to join our lab. Thank you for taking over the shipping of constructs from our lab into the world. I wish you all the best for this work and that the FedEx account numbers are always correct and that your dry-ice packages never get stuck at customs. And of course, I wish you all the best for your PhD. Ruben, I always enjoyed your presentations about your work on spindle positioning with the breathtaking movies of optogenetically controlled mitotic spindles. I am glad that you got a permanent position as research assistant in Mike's lab. Boris and Joyce, my top-rope climbing buddies in the beginning. I will never forget the thrill when we were stopped by the police coming back from climbing for making an illegal U-turn to catch Joyce's train on time ;-). I wish the two of you all the best for your future and I really enjoyed our chats and going climbing together. Kyle, the latest post-doc to join our lab. Thanks for making me aware of the twitter feed of the "Bash brother" José and our conversations about gerrymandering. I hope that your girlfriend liked the "Bash

brother experience" and is not completely put off by baseball now. Babet, thank you very much for taking over my things and the KANK1-self-association project. I really enjoyed working with you and especially our conversations about the organizational things in the lab that were not always going that smoothly. Besides, I wish you lots of luck for the future and less stress with the organization of the lab. Funso, you have my greatest respect for following your passion for science and making the sacrifice of being so far away from your family. Yet, you never seem to lose your optimism and your faith that good and hard work will eventually pay off. I hope that you keep this good spirit no matter what may come and that your hard work pays off with some great publications. Jingchao, Qingyang, Rudi, Kai and Sasha, project-wise we never worked together. Yet, I really enjoyed working alongside you in the lab. I was especially impressed by Kai's and Sasha's dedication and work ethic and I am more than happy that it worked out for you and that you could start your own group at Wuhan University.

Last but not least, I would like to thank Ben (Bouchet). Ben, for the first six months of my PhD you were my (daily) supervisor and you introduced me to the KANK family proteins. Moreover, from you I learned most about working with cells and being meticulous about them and everything that has to do with them. Besides, you taught me how to perform IFs (my bread and butter during my PhD). But most importantly, you taught how important it is to label my stuff in the lab. I think that I can say that the apprentice has become the master (several generations of new PhD students will probably encounter things carrying a label from me long after I have left the lab). I really appreciated working together with you and that you gave me the opportunity to be a co-author on two of your publications. Besides, I totally enjoyed our shit-chats on Friday afternoons.

During my five-year tenure, I also had the pleasure of supervising my master students Maxime, Christie and Miquel and my bachelor students Maxime, Benjamin, Jelle and Maryse. I really enjoyed working with you guys and I myself learned a lot from you as well. I wish all of you the best of luck for the future.

Besides, I encountered so many nice and interesting colleagues at Cell Biology. Like my fellow PhD students (some of you already finished your PhDs and left): Robin, Lisa, Liu, Lotte, Malina, Klara, Daphne, Robbelien, Feline, Vida, Mai Dan, Nazmiye, Xingxiu, Carlijn, Nicky, Manon, Katarina, Cátia, Marta, Dieudonnée, Anne, Elske, Ate, Wouter, Giel, Thomanai, Jian, Sybren, Marijn, Jelmer, Yujie, Bas, Max, Hai Yin, Riccardo, Roderick and Dennis. I wish you all the best (for the rest of your PhD) and for your future endeavors. And the post-docs: Anna, Mithila, Amélie, Yolanda, Lena, Elena, Gabriela, Eliana, Olga, Inês, Martin, Arthur, Max, Wilco, Josiah and Eitan. Hereby, I would like to thank especially Wilco for all your critical input during seminars and work discussions and all the thoughts that you put into how KANK proteins might be regulated at focal adhesions. I wish all of you lots of luck and many nice publications. I also wish Corette's, Florian's, Ginny's, Harold's, Paul's and Sabrina's groups all the best for the future.

Last but not least, there are two more persons that I would like to thank from the department of Cell Biology: Bart and Phebe. Many thanks to the both of you for your organizational work in the labs. Without you the labs would not be running that well.

&

For the first four years (or almost first four years), I have had the privilege of being part of the Marie Sklodowska-Curie Actions Innovative Training Network "PolarNet". Being part of this network was an awesome experience and I will definitely not forget the great PolarNet meetings that we had in Utrecht, London, Nice, Dresden and Utrecht again. Moreover, it gave me the opportunity to visit the lab of Trevor Dale at Cardiff University for a whole month. Hereby, I would like to express my gratitude towards Trevor Dale and my fellow PolarNet PhDs Eider and Nuria for your hospitality during my visit in Cardiff. Moreover, I would like to thank my other fellow PolarNet PhDs: Victoria Yan, Rukshala, Yamini, Shailaja, Eric, Charlie and Filippos. I really enjoyed the meetings and the extracurricular activities with you, and I will never forget sharing a hotel room with Eric and Filippos in Nice :-). In particular I would like to thank my PolarNet fellows from Utrecht Victoria, Sara, Janine and Amalia. Thank you for all the fun that we had together in Utrecht when we were shooting videos for the PolarNet website (yet, somehow only my video ended up there). I would like to thank especially Sara, my fellow German, for all the great conversations that we had when traveling to the PolarNet meetings. I wish you all the best of luck for your future. Of course, I also would like to thank Mike (Boxem) for being such a great program coordinator and all your critical input during the PolarNet meetings.

Of course, there were not only my dear colleagues who supported me during my journey but also my friends and family. First, I would like to thank my dear friend Mario. Thank you for all your support and funny memes that you kept sending me over the past years. I am glad that despite the distance and the border between us our friendship prevailed and even got stronger. Also, my gratitude towards Smiddy (a.k.a. Rechtsanwalt Furch) thanks for all our funny, hour-long phone calls and the great winter and summer vacations together.

Moreover, I would like to thank my soon-to-be family in law. I am forever grateful for the kindness and warmth with which you welcomed me into your middle. And thank you for all your support during my PhD.

I also have to thank my own family, especially my parents. Mama und Papa, you were incredible. Since I was a child, you have always supported me during all my endeavors (from driving me to friends and sport competitions to financing my studies). Without you behind me, I would not have been able to be where I am today. Thank you so much!

And finally! Elodie, my soon-to-be wife. Words can hardly express how much I have to thank you for being by my side for the past four years. You helped me tremendously to carry on with my research even when I was going through the darkest valleys during my PhD. You always knew how to pick me up and put me back on my feet to keep on going. I am so glad that you said YES and I am looking forward to the years to come together with you and Ollie…

&

&